

The Development and Evaluation of Small Molecule Inhibitors of the MDM2-p53 Interaction

By

Junfeng Liu

Supervisors: Prof. John Lunec & Dr Ian Hardcastle

**The thesis submitted in part requirement for
the Doctor of Philosophy Programme**

June 2010

Northern Institute for Cancer Research

Medical School, Framlington Place,

Newcastle University

Newcastle upon Tyne, NE2 4HH



Declaration

I declare that this thesis represents my own unaided work, except where acknowledged otherwise in the text.

This work has not been submitted previously, in whole or in part at any other institutions.

Studies involving collaboration with the University of Oxford and DePPICT project collaborators have been cited and acknowledged in the text.

Junfeng Liu

30th Sep 2010

Abstract

As a principal gatekeeper, p53 is inactivated mutationally in over 50% of human cancer (1). However, in approximately 7% of tumours, especially of the glia, bone, and soft tissues, loss of wild-type p53 function results from amplification and over-expression of the MDM2 gene, causing transformation and uncontrolled tumour growth (2-7). Several research reports have revealed that p53 and MDM2 proteins form an auto-regulatory feedback loop (8-10). Inhibition of the p53-MDM2 interaction has been validated as an attractive target for anti-cancer therapy.

Several different scaffold small-molecule inhibitors have been discovered by both structure-based design and compound library screening (11-16).

The first chapter of this thesis contains a general overview of research carried out that lead to the discovery and optimization of published potent p53-MDM2 interaction inhibitors, together with an overview of the p53-MDM2 antagonists development project carried out in our group, the progress obtained so far and future directions.

After the presentation of general materials and methods of experiments applied in my thesis in chapter two, four chapters are formed for presenting the research results I obtained within more than three years laboratory work.

Chapter three demonstrates the evaluation (ELISA) and optimization of the *in vitro* activity of isoindolin-1-one compounds, which is a group of potent lead small-molecule inhibitors of the MDM2-p53 interaction developed by our research group in Newcastle. The results indicate the impressive progress of this series of compounds, from NU8260 ($IC_{50}=2.4\pm0.2\ \mu M$) to the most recently developed lead compound, NCL-00016149 ($IC_{50}=15.8\pm2.6\ nM$), which is about 150-fold more potent.

The followed chapter (chapter 4) presents the evaluation (Western blot, SRB and Caspase-Glo 3/7 assay) of cellular activity of potent isoindolin-1-one compounds, especially the comparison of pure enantiomers, by using Nutlin-3 as the positive control. The result show that isoindolin-1-one compounds can induce p53 and its down stream target MDM2 and p21 accumulation and activation, corresponding to their *in vitro* potencies; both the *in vitro* and cellular activities presented are mainly for the potent enantiomer.

Chapter five is aimed at obtaining a better understanding of MDM2/MDMX inhibitor design and screening procedures. As part of the FP6 DePPICT project, more than 3800 compounds that were selected as possible MDM2 and/or MDMX inhibitors by *in silico* screening millions of commercially available compounds, together with some in-house pyrrole scaffold compounds and p53 peptides analogs were evaluated by ELISA. A number of lead compounds showed dose-dependent activity, and 7 scaffold series were selected for further SAR exploration by using synthetic chemistry technology.

With the progress of the isoindolin-1-ones and the development of Nutlin-3 and MI-63 series of MDM2 antagonists, several drug candidates may enter clinical trials soon. As a result, relapse caused by drug resistance may need to be considered as early as possible. Therefore, in chapter six, the research of MDM2 antagonists resistant cell clones is demonstrated. Several resistant cell clones were selected by treating SJSA-1 and NGP tumour cell lines with Nutlin-3 and MI-63. Resistance mechanisms were explored by using a range of bioassays, and one of the key mechanisms was confirmed to be p53 dysfunctional missense mutation.

Finally, the achievements and future work of my research are discussed in chapter seven.

Acknowledgements

First of all, I would like to take this opportunity to thank my supervisor Professor John Lunec. I shall forever be indebted for his expert advice and guidance that has enabled me to have enjoyed the whole experience of my PhD study. I am truly grateful for the support and help that he has provided throughout the past four years. Moreover, I believe his passion, dedication and enthusiasm for science and research has and will continue to give me positive influence through my research career.

Special thanks go to the Medicinal Chemistry Section (ADDI group) and the Northern Institute for Cancer Research (Drug Development Group), especially my two assistant supervisors Dr Ian Hardcastle and Dr Xiaohong Lu, for their technical guidance and support; sincere thanks to Dr Anna Watson, Dr Eric Valeur and Dr Karen Haggerty, without whom I could not have turned the compound structures in my mind to be the test samples on my bench; thanks also to Dr Yan Zhao, Dr Claire Hutton, Dr Catherine Drummond, Dr Jennifer Jackson, Dr Karim Bennaceur and Miss Qing Xu, with whom I have enjoyed most of my laboratory experiences and achievements. Great thanks also go to Professor Herbie Newell, Professor Bernard Golding and my two internal assessors Professor Hilary Calvert and Professor Roger Griffin, for their valuable advice throughout the progress of my PhD study. I would like to also add my thanks to our extended collaborators at the University of Oxford, Professor Martin Noble, Dr Jane Endicott and Dr Jan Gruber, as well as our collaborators within the DePPICT project.

Finally, I will thank Cancer Research UK for providing me with the research funding, UK/China Postgraduate Research Scholarships-Scholarships for Excellence for funding my tuition fees and China Scholarship Council for supporting me with living expenses. Thank you, my dear mam and dad, my dear wife Junfeng Zan and daughter Yiran Liu, for your full support and sacrifice during this four years.

Contents

The Development and Evaluation of Small Molecule Inhibitors of the MDM2-p53 Interaction	1
Declaration	I
Abstract	II
Acknowledgements.....	IV
Contents	V
List of Figures	XI
List of Tables	XVII
Abbreviations.....	XIX
Chapter One.....	1
Introduction	1
1.1 Literature Review	1
1.1.1 p53, a Vital Tumour Suppressor Gene	1
1.1.2 p53 Restoration as a Cancer Therapy	8
1.1.3 MDM2 Plays a Pivotal Role in Restraining p53	9
1.1.4 Rescue of p53 Function by Disrupting the p53–MDM2 Interaction	13
1.1.5 MDMX as a druggable target for p53 reactivation	28
1.2 Research Project	35
Chapter Two	37
General Materials and Methods	37
2.1 ELISA Assay.....	38
2.1.1 Experiment Design	38
2.1.2 Plasmid DNA Preparation	42
2.1.3 Compound Sample Preparation	47
2.1.4 ELISA Protocol.....	48
2.2 Tissue Culture.....	54
2.2.1 Cell Lines.....	54
2.2.2 Cell Culturing	55
2.2.3 Sub-culturing	55
2.2.4 Counting Cells.....	56

2.2.5	Cell Storage and Cryopreservation.....	56
2.2.6	Thawing Cells.....	57
2.2.7	Plating out cells	57
2.3	Western Blotting	57
2.3.1	Basic Principles of Western Blotting Assay	58
2.3.2	Cell Seeding into Culture Plates and Drug/IR Treatment.....	59
2.3.3	Collecting Cell Lysate	61
2.3.4	Protein Estimation.....	61
2.3.5	Gel Electrophoresis of Protein (SDS-PAGE)	63
2.3.6	Protein Transfer.....	63
2.3.7	Immunodetection.....	65
2.3.8	Enhanced chemiluminescence (ECL) detection	66
2.3.9	Densitometry analysis	67
2.4	Sulphorhodamine B (SRB) Assay	68
2.4.1	Basic Principles of SRB Assay	68
2.4.2	96-well Plate Preparation for Growth Curve Evaluation.....	68
2.4.3	96-well Plate Sample Preparation for GI ₅₀ Value Evaluation	69
2.4.4	Plate Fixation, SRB Staining and Data Collection	71
2.5	Caspase-Glo [®] 3/7 Assay.....	72
2.5.1	Basic Principles of Caspase-Glo [®] 3/7 Assay	72
2.5.2	Cell Seeding	73
2.5.3	Drug Treatment	74
2.5.4	Caspase-Glo [®] 3/7 Assay	75
2.5.5	Data Analysis	75
2.6	Cell Cycle Analysis Using FACscan	76
2.6.1	Basic principles of fluorescence activated flow cytometry.....	76
2.6.2	Apply Flow Cytometry for Cell Cycle Analysis	78
2.6.3	Protocol of cell cycle analysis assay	79
2.7	PCR	81
2.7.1	Principle of Polymerase Chain Reaction (PCR).....	81
2.7.2	DNA extraction and purification for PCR.....	83
2.7.3	PCR method	85
2.7.4	Agarose Gel Method.....	86
2.7.5	PCR product purification for Sequencing	87
2.8	FISH Assay	88

2.8.1	Principle of Fluorescent <i>in situ</i> Hybridization (FISH) Assay	88
2.8.2	FISH Protocol	89
2.9	Computational QSAR.....	93
2.9.1	Principle of Quantitative Structure-Activity Relationship (QSAR) Analysis	93
2.9.2	Online Resources and Softwares Applied for Computational QSAR Analysis	94
Chapter Three		96
Isoindolin-1-one Compounds: Structure-Activity Relationship Analysis		96
3.1	Introduction	96
3.2	ELISA for Isoindolin-1-one Compound <i>in vitro</i> Activity Evaluation.....	97
3.2.1	Isoindolin-1-one Compound Potency Evaluation as MDM2/p53 Inhibitors	97
3.2.2	IC ₅₀ Comparison of MI-63, Nutlin-3, (-)-Nutlin-3 and potent isoindolin-1-ones as MDM2/p53 Inhibitors	110
3.2.3	Screening of isoindolin-1-ones as MDMX/p53 Inhibitors	113
3.3	Structure-activity Relationships for the analysis of ELISA IC ₅₀ data	121
3.3.1	Isoindolin-1-one compounds side-chain comparison	121
3.3.2	Isoindolin-1-one compounds as MDMX/p53 interaction inhibitors	138
Chapter Four		140
Isoindolin-1-one Compounds: Evaluation of Cellular Activity.....		140
4.1	Introduction	140
4.2	Western Blotting for Cellular Activity Evaluation and Comparison of Isoindolin-1-one Compounds	143
4.2.1	Western Blot Result for Stage 1 Isoindolin-1-one Compounds	143
4.2.2	Western Blot Comparison of MDM2/p53 Inhibitors and X-ray Irradiation Time Course Cellular Effects.....	148
4.2.3	Western Blot Analysis of the Cellular Effects of Potent Stage 2 and 3 Isoindolin-1-one Compounds	156
4.2.4	Potency Comparison of Isoindolin-1-one Enantiomers	160
4.3	The Growth Inhibitory Activity (GI ₅₀) of Isoindolin-1-one Compounds compared with Nutlin-3 and MI-63.....	169
4.3.1	Background.....	169
4.3.2	Materials and Methods	169
4.3.3	Results	169
4.4	Apoptotic Effect of Isoindolin-1-one Compounds in SJSA-1 Cells	172
4.4.1	Background.....	172

4.4.2	Results	172
4.5	Conclusion and Discussion	177
4.5.1	The Cellular Effects of the Lead Isoindolin-1-ones are Comparable to Nutlin-3 Treatment.....	177
4.5.2	The Mechanism of p53 Pathway Activation by MDM2-p53 Binding Antagonists differs from that of X-ray irradiation.....	179
4.5.3	Comparison of Isoindolin-1-one Enantiomers	180
4.5.4	The Cellular Activity Comparison of MDM2 Antagonists.....	181
Chapter Five.....		183
Alternative Scaffold Compounds as MDM2/p53 and MDMX/p53 Interactions		
Inhibitors		183
5.1	Introduction	183
5.2	Materials and methods of ELISA for <i>in vitro</i> activity evaluation	184
5.3	Results	187
5.3.1	DePPICT compound screening	187
5.3.2	DePPICT compound screening as MDM2/MDMX inhibitors	199
5.3.3	Threshold value determination of DePPICT compounds	204
5.3.4	Pyrrole Compounds as MDM2/p53 and/or MDMX/p53 Inhibitors ...	205
5.3.5	Comparison of Peptide Inhibitors against both MDM2 and MDMX Targets	210
5.4	Conclusion and Discussion	218
5.4.1	The DePPICT project as a successful attempt to use virtual screening technology.....	218
5.4.2	DePPICT compound SEN0040028 binding mode prediction.....	219
5.4.3	Cellular evaluation of SEN0040028 and potential drug design direction	221
5.4.4	The possible reason for marked negative percentage inhibition values in the binding assay	222
5.4.5	Pyrrole scaffold compounds as a potent MDM2 and MDMX inhibitor lead compounds	224
Chapter Six.....		225
Generation and Characterization of MDM2/p53 Inhibitor Resistant Cell Lines....		
6.1	Introduction	225
6.2	Overview of resistant cell line selection and characterization	226
6.3	Characterization Stage I selected resistant cell lines	229
6.3.1	Resistant potency evaluation	229

6.3.2	Measurement of p53, MDM2 and p21 ^{WAF1} expression.	233
6.3.3	DNA Sequencing of p53 in Stage I Resistant Cell Clones.....	235
6.4	Further developed resistant cell clones: characterization and analysis of potential mechanism.....	243
6.4.1	Growth curve comparison.....	243
6.4.2	Resistance evaluation for stage II resistant cell clones.....	246
6.4.3	Western blotting assay for protein expression determination.....	249
6.4.4	Cell cycle studies.....	253
6.4.5	Caspase-Glo [®] 3/7 Assay for apoptosis analysis	256
6.4.6	DNA Sequencing of p53.....	259
6.4.7	Comparison of p53 Specific PCR Amplification of DNA from Resistant Cell Clones and parental SJSA-1 Cell line.....	260
6.4.8	Low level p53 Mutation Detection in SJSA-1 parental cell line DNA extracts	262
6.4.9	SJSA-1 parental and resistant cell clones comparison using fluorescence <i>in situ</i> hybridization (FISH) to test for allelic loss of the p53 gene	265
6.5	Conclusion and Discussion	268
Chapter Seven		270
Further Discussion and Future Work.....		270
7.1	Further Discussion.....	270
7.1.1	Summary of Achievements	270
7.1.2	“See-saw Theory” generation based on the development of MDM2/p53 and MDMX/p53 antagonists	272
7.1.3	“Parachute Analogy” generation based on MDM2/p53 antagonists development	274
7.1.4	“Bridge Effect Theory” based on screening data analysis of the DePPICT compounds and suggestions for future <i>in silico</i> screens.....	276
7.1.5	“Predictable vs. unpredictable”, the lesson learnt from MDM2/p53 antagonists resistant mechanism research.....	277
7.2	Future Work	278
7.2.1	Possible plan for MDM2/p53 antagonists design and development.	278
7.2.2	Possible plan for MDMX/p53 antagonists design and development	279
7.2.3	Further research on MDM2/p53 antagonists resistant cell clones ...	280
References		282
Appendix I.....		297

Potent Isoindolin-1-one compounds and MDM2 protein binding mode prediction	297
Background.....	297
Results	298
1. MDM2 protein structures selection and docking software training	298
2. MDM2 and isoindolin-1-one compounds binding mode prediction and comparison	302
Appendix II.....	319
Western Blotting Reagents and Equipment.....	319
Cell Culture Reagents	320
Sulphurhodamine B (SRB) colourimetric assay Reagents	321
Polymerase chain reaction assay Reagents	321
Polymerase chain reaction assay procedure for sequence amplification.....	322

List of Figures

Chapter 1

Figure 1. 1 The schematic view of the functional domain structure of p53 together with relative mutation frequency in human cancer bar chart according to the table of 'p53 mutation distribution' in The TP53 Web Site (http://p53.free.fr/Database/p53_database_distr.html).	2
Figure 1. 2 p53 Tumour Suppression	5
Figure 1. 3 Crystal structure of DNA bind with p53 core domain.	7
Figure 1. 4 The schematic view of the human MDM2 protein primary structure (96).	11
Figure 1. 5 Regulation of p53 by MDM2. (102)	12
Figure 1. 6 Structure aspect of p53-MDM2 Interaction.....	16
Figure 1. 7 The crystal structure of p53 peptide binding with MDM2 protein (116).20	
Figure 1. 8 MDM2-Nutlin-2 binding image.....	24
Figure 1. 9 Structure-based design produced small molecule antagonists of MDM2-p53 binding interaction by mimicking Phe19, Trp23, Leu26 and Leu22 residues in p53 (133).	25
Figure 1. 10 Chemical structures of potent spirooxindole MDM2 inhibitors (146)...26	
Figure 1. 11 Primary strucutre comparison of human MDM2 and human MDMX proteins.	28
Figure 1. 12 Surface representations of human MDMX (the left side) and two human MDM2 structures (the right side) (168).	34

Chapter 2

Figure 2. 1 Procedure of ELISA for MDM2/MDMX antagonists screening in A) single well and B) a 96-well plate	40
Figure 2. 2 Plate arrangements for IC ₅₀ value determination	41
Figure 2. 3 The ELISA Flow Chart for MDM2 Inhibitors Screening.....	50
Figure 2. 4 Sample plate placing area for X-ray irradiation treatment	60
Figure 2. 5 Plate arrangements for BCA assay	62
Figure 2. 6 Western blot cassette order illustration in transfer procedure.....	64
Figure 2. 7 Chemiluminescent Peroxidase Substrates for protein band detection ...	67
Figure 2. 8 SRB structure and SRB assay plate for growth curve determination.....	69
Figure 2. 9 SRB structure and SRB assay plate arrangement for GI ₅₀ evaluation	70
Figure 2. 10 The reactions and mechanisms of Caspase-Glo® 3/7 Assay	72
Figure 2. 11 The plate arrangements for Caspase-Glo® 3/7 Assay	73
Figure 2. 12 FACscan optical configuration with the common fluorochromes list for each detector.	77
Figure 2. 13 A schematic of the cell cycle and cytometric components of each phase.	78

Figure 2. 14 The exponential amplification of the gene in PCR.	81
Figure 2. 15 Three steps of a Polymerase Chain Reaction.	82
Figure 2. 16 Purification of total DNA from cells by using DNeasy Blood & Tissue Kit	84
Figure 2. 17 The process of the fluorescence in situ hybridization technique.	88

Chapter 3

Figure 3. 1 Isoindolin-1-one core structure shared by compounds in Table 3.1.	98
Figure 3. 2 Comparison of IC ₅₀ Values for Inhibition of the MDM2-p53 Binding Interaction by Isoindolin-1-ones with Side-chain Variation in the R ₂ position.	109
Figure 3. 3 Structures of MI-63, Nutlin-3, (-)-Nutlin-3 and potent isoindolin-1-ones NU8354A, NU8406A, NCL-00017305 and NCL-00017306 and NCL-00016149.	111
Figure 3. 4 IC ₅₀ comparison of MI-63, Nutlin-3, (-)-Nutlin-3 and potent isoindolin-1-ones as MDM2/p53 inhibitors	112
Figure 3. 5 Three side chains of isoindolin-1-one compounds with the modification to be discussed highlighted in blue	121
Figure 3. 6 NU8354-MDM2 Docking Results Generated by Using Molegro Virtual Docking Software Indicated Different Binding Modes with whether Considering Water Solvation Effects or Not.	128
Figure 3. 7 Modification of the isoindolin-1-one ring based on the NU8260 scaffold	136
Figure 3. 8 Modification on isoindolin-1-one ring based on the NU8354 scaffold.	137
Figure 3. 9 ELISA for isoindolin-1-one compounds as MDMX inhibitors	138

Chapter 4

Figure 4. 1 Progression of isoindolin-1-one scaffold compounds during lead optimisation as MDM2-p53 binding interaction inhibitors	142
Figure 4. 2 Western blotting evaluations of dose-dependent cellular effects of selected stage 1 isoindolin-1-one compounds and Nutlin-3 using the SJSA-1 cell line	145
Figure 4. 3 Densitometry analyses of protein bands densities of MDM2, p53 and p21 ^{WAF1} for the western blotting results in Figure 4.2	146
Figure 4. 4 Western blot analysis of p53, MDM2 and p21 ^{WAF1} for three time points of treatment with NU8354 compared with Nutlin-3 in a) SJSA-1, b) HCT116 _{p53+/+} & c) HCT116 _{p53-/-} cell lines.	147
Figure 4. 5 Western blot time courses of SJSA-1 cellular effects comparing NU8354A with Nutlin-3, MI-63 and X-ray irradiation treatments.	151
Figure 4. 6 Western blot time courses of NGP cellular effects comparing NU8354A with Nutlin-3, MI-63 and X-ray irradiation treatments.	155
Figure 4. 7 Structures, molecular weights and IC ₅₀ values of stage 2 isoindolin-1-one compounds selected for western blot analysis.	156
Figure 4. 8 Western blot result of selected stage 2 isoindolin-1-one compounds compared with Nutlin-3 using the SJSA-1 cell line.	157

Figure 4. 9 Western blot result of selected stage 2 isoindolin-1-one compounds compared with Nutlin-3 using HCT116+/+ & -/- cell lines	157
Figure 4. 10 Structures, molecular weights and IC ₅₀ values of stage 3 isoindolin-1-one compounds selected for western blot analysis.	158
Figure 4. 11 Western blot showing the dose dependent effect of selected stage 3 isoindolin-1-one compounds compared with Nutlin-3 using SJSA-1 cell line.....	159
Figure 4. 12 Resolution of enantiomers of NU8354 by using HPLC and a chiral column.....	160
Figure 4. 13 Resolution of enantiomers of NU8406 by using HPLC and a Prep-chiral column.	161
Figure 4. 14 NU8354 and Related Enantiomer Structures.....	162
Figure 4. 15 IC ₅₀ Comparison of NU8354 Enantiomers.....	163
Figure 4. 16 Western Blot Analysis of the Cellular Response to NU8354 enantiomers.	163
Figure 4. 17 Comparison of the Growth Inhibitory Effect of NU8354 Enantiomers.	164
Figure 4. 18 NU8406 enantiomers structures	165
Figure 4. 19 IC ₅₀ Comparison of NU8406 Enantiomers.....	166
Figure 4. 20 Western Blot Analysis of the Cellular Response to NU8406 enantiomers.	167
Figure 4. 21 Comparison of the Growth Inhibitory Effect of NU8406 Enantiomers.	168
Figure 4. 22 SRB Assay Comparison of the Growth Inhibitory Effects of MDM2/p53 Inhibitors against (A) SJSA-1 and (B) NGP Cell Lines.	171
Figure 4. 23 SJSA-1 Cell Images with 48 hours Antagonist Treatment	173
Figure 4. 24 BCA Assay Showed Marked Protein Concentration Variation of the Cell Lysate Samples in a Dose- and Potency-Dependent Manner	174
Figure 4. 25 Western blot result of SJSA-1 cells treated with MDM2 antagonists for 48 hours.....	175
Figure 4. 26 Caspase-Glo 3/7 assay for SJSA-1 cells treated with MDM2 antagonists for 48 hours indicated the dose-dependent cellular effect of apoptosis induction.	176

Chapter 5

Figure 5. 1 Plate arrangements for MDM2/MDMX inhibitors screening purpose ..	186
Figure 5. 2 Plate for MDM2/MDMX inhibitor dose-dependent activity evaluation	186
Figure 5. 3 a. Inhibitory activity against the MDM2/p53 interaction for the batch 1 compounds screened at 10 μ M final concentration (the most potent one is indicated by a red arrow together with its compound ID); b. Batch 1 compounds screened for inhibitory activity against the MDM2/p53 interaction with 50 μ M final concentration (the most potent one is indicated by a red arrow together with its compound ID).	188
Figure 5. 4 Structures of the batch 1 hit compounds with inhibitory activity against the MDM2/p53 interaction.	190

Figure 5. 5 Inhibitory activity against the MDMX/p53 interaction for the batch 1 compounds screened at 10 μ M final concentration (the most potent one is indicated by a red arrow together with its compound ID); b. Batch 1 compounds screened for inhibitory activity against the MDMX/p53 interaction with 50 μ M final concentration (the most potent one is indicated by a red arrow together with its compound ID).	192
Figure 5. 6 Hit compounds against MDMX/p53 interaction at 50 μ M final concentration	194
Figure 5. 7 Structures of compounds tested for dose dependent activity against MDM2/p53 and/or MDMX/p53 binding interaction.	195
Figure 5. 8 a) Dose-dependent-activity (DDA) of SEN0040028 and SEN0031562 as the MDM2/p53 interaction inhibitors (ELISA); b) dose-dependent-activity of NU8325 and SEN0040028 as the MDMX/p53 interaction inhibitors (ELISA).	197
Figure 5. 9 Images of NGP cells treated with various concentrations of Nutlin-3, MI-63 and SEN0040028 for 24 hours	198
Figure 5. 10 Undissolved compound clusters (surrounded with red circles) observed in 50 μ M SEN0040028 treated NGP cell culture media.	199
Figure 5. 11 Screening of plates 0034879-34887 for compounds with inhibitory activity against the MDM2/p53 interaction at 10 μ M final concentration.	200
Figure 5. 12 Screening of plates 0035091-35099 for compounds with inhibitory activity against the MDM2/p53 interaction at 10 μ M final concentration.	201
Figure 5. 13 Screening of plates 0035110-35113 for Crystax fragment compounds with inhibitory activity against the MDM2/p53 interaction at 250 μ M final concentration.	201
Figure 5. 14 Screening of plates 0035114-35115, 35141-35142, 35476 and 35829 for compounds with inhibitory activity against the MDM2/p53 interaction at 10 μ M final concentration.	201
Figure 5. 15 Screening of plates 0035440-35448 for compounds with inhibitory activity against the MDM2/p53 interaction at 10 μ M final concentration.	202
Figure 5. 16 Screening of batch 4 plates for compounds with inhibitory activity against the MDM2/p53 interaction at 10 μ M final concentration.	202
Figure 5. 17 Screening of batch 4 plates for compounds with inhibitory activity against the MDMX/p53 interaction at 10 μ M final concentration.	202
Figure 5. 18 Screening of plates 0035449-35456 for compounds with inhibitory activity against the MDMX/p53 interaction at 10 μ M final concentration.	203
Figure 5. 19 Screening of plates 0035468-35475 for compounds with inhibitory activity against the MDMX/p53 interaction at 10 μ M final concentration.	203
Figure 5. 20 Frequency distribution of percentage inhibition values for DePPICT compounds screened for activity as MDM2/p53 interaction inhibitors.	204
Figure 5. 21 Potent peptide inhibitors for MDM2-p53 interaction and crystal structure analysis of p53 related peptide bound to the MDM2 protein(12, 125) ..	210
Figure 5. 22 Binding groove comparison of MDM2 1YCR and MDMX 3DAB structure	211

Figure 5. 23 MDM2 and MDMX binding pockets comparison by using 3DAB, 3DAC, 1YCR and 1T4F protein database structures.	213
Figure 5. 24 Comparisons of the binding affinity of three p53 peptide analogues with MDM2 and MDMX by using ELISA method.....	216
Figure 5. 25 Comparisons of peptides binding with MDM2 and MDMX by manual docking.	217
Figure 5. 26 Comparisons of predicted binding mode of SEN0040028 binding with MDM2 and MDMX by manual docking.	220
Figure 5. 27 Example of DePPICT compounds screening results showing lower than -50% MDMX inhibition values and their related compounds structures.	222

Chapter 6

Figure 6. 1 Selection of SJSA-1 and NGP resistant cell clones.....	228
Figure 6. 2 SJSA-1 parental and stage I resistant cell clone GI ₅₀ Comparison.	230
Figure 6. 3 NGP parental and stage I resistant cell clone GI ₅₀ Comparison.	231
Figure 6. 4 Western blot showing p53 pathway activation by Nutlin-3 and MI-63 for the SJSA-1 parental cell line and reduced activation in stage I resistant cell clones.	233
Figure 6. 5 Western blot comparing p53 activation by Nutlin-3 and MI-63 in the NGP parental cell and stage I resistant cell clones.....	235
Figure 6. 6 SJSA-1 parental and resistant cell clones DNA sequencing alignment results of Exon 8 SN primers PCR products showed similar 14522 genomic DNA position point mutation.	238
Figure 6. 7 SJSA-1 parental and resistant cell clones DNA sequencing alignment results of Exon 8 ASN primers PCR products confirming the 14522 p53 genomic DNA point mutation.	239
Figure 6. 8 SJSA-1 parental and resistant cell clones DNA sequencing traces of Exon 8 PCR products confirming the 14522 point mutation corresponding to codon 285, changing GAG to AAG.....	240
Figure 6. 9 NGP parental and resistant cell clones DNA sequencing results	241
Figure 6. 10 NGP parental and resistant cell clones DNA sequencing traces of Exon 5 PCR products confirmed the 13133 point mutation corresponding to codon 152, changing CCG to ACG.	242
Figure 6. 11 Growth curves of SJSA-1 parental cell line and resistant cell clones ...	245
Figure 6. 12 SJSA-1 parental and resistant cell clone GI ₅₀ Comparison.	248
Figure 6. 13 NGP parental and resistant cell clone GI ₅₀ Comparison.....	248
Figure 6. 14 Western blot results showing p53 pathway activation in the SJSA-1 parental cell line by Nutlin-3 and MI-63, but not in the stage II resistant cell lines, with cross resistance effects.	252
Figure 6. 15 Western blot results of the time course response of the SJSA-1 parental cell line and resistant clone S_M6R1 induced by 6.3 Gy X-ray irradiation.	252
Figure 6. 16 Western blot results showing lack of increased p-glycoprotein and/or MRP1 overexpression in the SJSA-1 resistant cell clones tolerant to p53-MDM2 antagonists, compared to the parental SJSA-1 cells.	252

Figure 6. 17 Histogram of cell cycle distribution for the SJSA-1 parental cell line and the two resistant cell clones S_M6R1 and S_N40R1 after 24 hours treatment with Nutlin-3 or MI-63 and 24 hours post-treatment with 6.3 Gy of X-rays, compared with untreated controls.	254
Figure 6. 18 Bar chart of cell cycle distribution for the SJSA-1 parental cell line and the two resistant cell clones S_M6R1 and S_N40R1 after 24 hours treatment with Nutlin-3 or MI-63 and 24 hours post-treatment with 6.3 Gy of X-rays, compared with untreated controls.	255
Figure 6. 19 Caspase 3/7 enzymatic activity in resistant cell clones treated by various concentrations of MI-63 (A) or Nutlin-3 (B) for 48 hours showed little induction compared to the response in SJSA-1 parental cell lines, which increased markedly.	258
Figure 6. 20 Resistant SJSA-1 cell clone S_M6R1 DNA sequencing result showing the point missense mutation in the p53 DNA binding domain. The same point mutation was found in SJSA-1 resistant clones obtained from Nutlin-3 treatment.....	259
Figure 6. 21 PCR products comparison using wild-type and mutation specific p53 sequence primers to amplify DNA from SJSA-1 resistant clones and the parental cell line. NGP parental cell line DNA is included as a additional wild-type p53 positive control.	261
Figure 6. 22 p53 mutation specific and normal PCR products compared for SJSA-1 resistant clones and SJSA-1 and NGP parental cell line DNAs.	262
Figure 6. 23 Direct evidence of resistant cells in the parental SJSA-1 population undergoing single step selection with 5 μ M Nutlin-3	264
Figure 6. 24 FISH images illustrating the different p53 status (red) and chromosome 17 copy number (green) alteration in resistant cell clones S_M6R1 and S_N40R1 compared to SJSA-1 parental cell line.	266

Chapter 7

Figure 7. 1 ‘See-Saw Theory’ based on MDM2/p53 and MDMX/p53 antagonist design	273
Figure 7. 2 Side-chain –R ₂ of idoindolin-1-one compound NU8354 act as a parachute	275

Appendix I

Appendix I Figure 1. Reproduction images of published co-crystal structure of 1YCR, 1RV1, 1T4F and 2GV2.	300
Appendix I Figure 2. Reproduced hydrophobic binding pocket images of MDM2 protein in 1YCR, 1RV1, 1T4F and 2GV2.	301
Appendix I Figure 3. Scatter Charts show the correlation of the Docking Scores with the IC ₅₀ Values of isoindolin-1-one scaffold key compounds.	315

List of Tables

Chapter 1

Table 1. 1 Inhibitors of the p53-MDM2 Interaction.....	18
Table 1. 2 Trp indole C5/C6 substitution SAR of octapeptide-based MDM2 inhibitors.	22
Table 1. 3 C5/C6/N1 SAR of N α -(2-phenoxybenzoyl) tryptophan-based MDM2 inhibitors.....	23

Chapter 2

Table 2. 1 Coupled Transcription/Translation Components	49
Table 2. 2 Original Cell lines applied for the experiments	54
Table 2. 3 Cell lines seeding densities applied for the experiments	59
Table 2. 4 Details of Primary Antibodies Used for Western Blot	66

Chapter 3

Table 3. 1 IC ₅₀ of Isoindolin-1-ones with Side Chains Variation	99
Table 3. 2 Compounds evaluated as MDMX/p53 interaction inhibitors	113
Table 3. 3 Side-chain –R ₁ modification comparison.....	123
Table 3. 4 Side-chain –R ₂ modification comparison.....	132
Table 3. 5 Side-chain –X modification comparison	135

Chapter 4

Table 4. 1 IC ₅₀ and SJSA-1 and NGP Cell Line GI ₅₀ value Comparison of Potent MDM2/p53 Interaction Inhibitors.....	171
Table 4. 2 MDM2/p53 Inhibitors IC ₅₀ value and SJSA-1 and NGP Cell Line GI ₅₀ Standardised Value Comparison	171

Chapter 5

Table 5. 1 Potent compounds in the batch 1 compounds screening results for inhibitory activity against MDM2/p53 interaction.	189
Table 5. 2 Potent compounds in the batch 1 compounds screening results for inhibitory activity against MDMX/p53 interaction.	193
Table 5. 3 Inhibition Potency of Pyrrole Compounds as MDM2/p53 and MDMX/p53 Interaction Antagonists	206
Table 5. 4 Modified peptides made for binding affinity evaluation with MDM2/MDMX.....	214

Chapter 6

Table 6. 1 GI ₅₀ comparison of stage I resistant clones with their parental cell lines	232
Table 6. 2 Comparison of stage II resistant cell clones with their parental cell lines showing marked increases in GI ₅₀	247
Table 6. 3 FISH assay colour coded signal counting results showing marked differences between the three SJSA-1 cell clones	267

Appendix I

Appendix I Table 1. Virtual docking predicted binding modes and scores of the published MDM2 crystal structures of 1YCR, 1RV1, 1T4F and 2GV2 binding with Nutlin-2 and isoindolin-1-one scaffold key compounds.	304
Appendix I Table 2. Virtual docking predicted binding modes and scores of isoindolin-1-one enantiomers binding with the 2GV2 MDM2 structure.....	316

Abbreviations

6ClTrp	6-chlorotryptophan
Ac	Acetyl
Ac₃C	1-amino-cyclopropanecarboxylic acid
Aib	α -aminoisobutyric acid
AP	active peptide (AP-B)
AP-B	Ac-Phe ¹⁹ -Met-Aib-Pmp-(6-Cl)Trp-Glu-Ac ₃ C-Leu ²⁶ -NH ₂
ARF	alternative reading frame
ATM	ataxia-telangiectasia mutated
ATR	ATM and Rad3 related
BAX	Bcl-2 associated X protein
BCA assay	Bicinchoninic acid assay
b-IP3	biotinylated IP3 peptide
Bn	Benzyl
BSA	Bovine Serum Albumin
Bu	Butyl
CBP	CREB-Binding Protein
CDK	cyclin-dependent kinase
Chk	checkpoint kinase
CKII	casein kinase II
Cop1	constitutively photomorphogenic 1
CREB	cAMP Response Element-Binding (a transcription factor)
DAPI	4',6-diamidino-2-phenylindole
DBD	DNA Binding Domain
DDA	Dose Dependent Activity

DePPICT	Designing Therapeutic Protein-Protein Inhibitors for Brain Cancer Treatment
DIPEA	Diisopropylethylamine
DMSO	Dimethylsulfoxide
DNA	Deoxyribose Nucleic Acid
DNA-PK	DNA-dependent protein kinase
dNTPs	deoxyribonucleoside triphosphates
dpc	days postcoitum
dT	doubling Time
E2F	Stands for family of Transcription Factors (TF) in higher eukaryotes
ECL	Enhanced Chemiluminescence
EDTA	Ethylenediaminetetraacetic acid
ELISA	Enzyme Linked ImmunoSorbent Assay
eq	Equivalence
Et	Ethyl
EtBr	Ethidium Bromide
EtOAc	Ethyl acetate
EtOH	Ethanol
FAS	Fatty acid synthase (<i>The most intensely studied member of the death receptor family</i>)
FBS	Fetal Bovine Serum
FISH	Fluorescent <i>in situ</i> Hybridization
Fmoc-	9-fluorenylmethyloxycarbonyl-
FSC	Forward light Scatter
GADD45	growth arrest and DNA-damage inducible gene 45
GI₅₀	the half maximal Growth Inhibitory concentration
GST ELISA	Glutathione S-Transferase Enzyme-Linked ImmunoSorbent Assay
HRP	horseradish peroxidase

IC₅₀	the half maximal inhibitory concentration
IP3	Ac-Met-Pro-Arg-Phe ¹⁹ -Met-Asp-tyr-Trp-Glu-Gly-Leu ²⁶ -Asn-NH ₂
IR	ionizing radiation
ISH	<i>In situ</i> hybridization
IV-MDM2	in vitro translated MDM2 lysate
kD	kilodalton
KI	Knockin
LB	Luria-Bertani Medium
LCMS	Liquid Chromatography Mass Spectrometry
LSCC	Laryngeal Squamous Cell Carcinoma
MBO	Mixed-Backbone Oligonucleotides
mdm2	mouse double minute 2 gene
MDM2	human mdm2 gene
MDM2	mouse double minute 2 protein
MDM4	human mdm4 gene
MDMX (4)	Murine double minute X (4)
Me	Methyl
MeOH	Methanol
MI-63	MDM ₂ Inhibitor 63
MRP	Multidrug-resistance associated protein
MRP1	Multidrug Resistance Protein 1
NLS	Nuclear Localization Signal
NMR	Nuclear Magnetic Resonance
NoLS	Nucleolar Location Signal
NP-40	Nonidet P-40
NRD	Negative Regulatory Domain
OD	Homo-Oligomerization Domain

OPT	<i>O</i> -phthalaldehyde
PARP	Poly (ADP-Ribose) Polymerase
PBS	Phosphate Buffered Saline
PCR	Polymerase Chain Reaction
PDB	Protein Data Bank
P-gp	P-glycoprotein
Ph	Phenyl
PI	Propidium Iodide
Pirh2	p53-induced RING-H2 protein
PMP	phosphonomethylphenylalanine
Pr	Propyl
Pu	Purine base
PUMA	p53 up regulated modulator of apoptosis
Py	Pyrimidine base
QSAR	Quantitative Structure-Activity Relationship
RING	Really Interesting New Gene
RITA	reactivation of p53 and induction of tumour cell apoptosis
RLU	relative luminescence units
RNA	Ribonucleic Acid
RNAi	RNA interference
RNase	Ribonuclease
RPA	Replication Protein A
rpm	Revolutions per minute
rt	Room Temperature
RT	Radiotherapy
SAR	Structure-Activity Relationship
SDS-PAGE	Sodium Dodecyl Sulphate Polyacrylamide Gel Electrophoresis

SE	Standard Error
SH3	Src Homology 3-like domain
shRNA	Short hairpin RNA
siRNA	Small interfering RNA
SRB	Sulphorhodamine B
SSC	Side light Scatter (FACS)/Standard Saline Citrate (FISH)
SV40	Simian Virus 40, a strain that induced development of tumours
TAD	Transcription-Activation Domain
TAFs	TBP Associated Factors
TBE	Tris/Borate/EDTA
TBP	TATA Box binding Protein
TBS	Tris-Buffered Saline
TCA	Trichloroacetic Acid
THF	Tetrahydrofuran
TMA	Tissue MicroArray
Trp	Tryptophan
UV	Ultraviolet
WAF1	Wild type p53-Activated Fragment 1

Chapter One

Introduction

1.1 Literature Review

1.1.1 p53, a Vital Tumour Suppressor Gene

Tumour-suppressor genes are important to prevent the abnormal poliferation of cells. The p53 gene, initially reported in 1979 (17-18), was originally thought to be a target of the simian virus 40 (SV40, a strain of virus that induced development of tumours) DNA large-T antigen. Because of the use of mutated p53 cDNA following purification of tumour cell mRNA, it was initially regarded as a cellular oncogene (19-21). Then p53 was identified to be a tumour-suppressor in 1989 (22-24). It is known as the 'guardian of the genome' owing to its ability to integrate many signals that control life or death (25-26).

1.1.1.1 p53 Structure and Function

In humans, p53 is encoded by the *TP53* gene located on the short arm of chromosome 17 (17p13) (27) and the human p53 protein contains 393 amino acids. Although the amino acid composition of p53 protein varies from species to species (28), the primary structure of the protein, especially the five functional domains, is conserved during evolution.

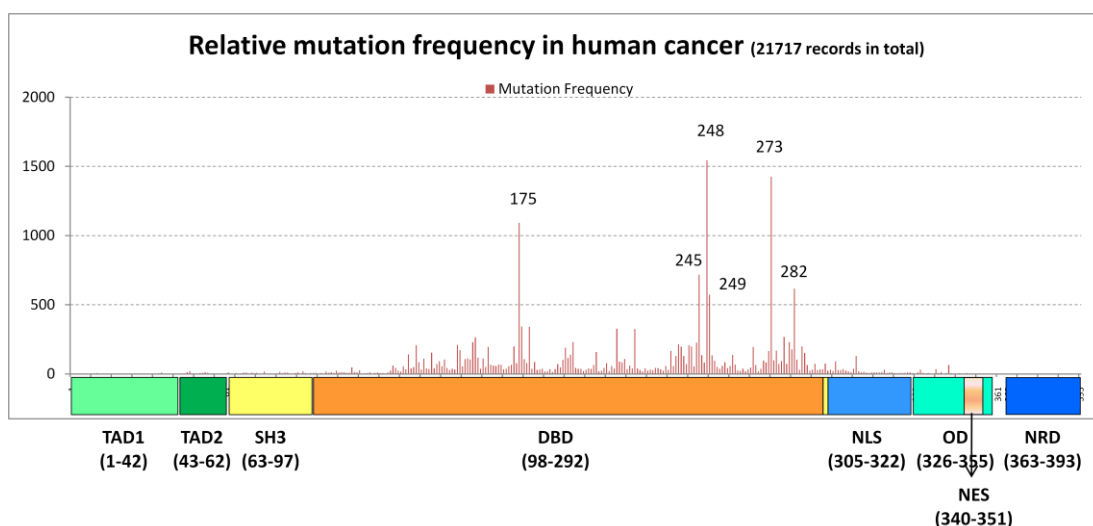


Figure 1. 1 The schematic view of the functional domain structure of p53 together with relative mutation frequency in human cancer bar chart according to the table of 'p53 mutation distribution' in The TP53 Web Site (http://p53.free.fr/Database/p53_database_distr.html).

The 393-residue p53 protein comprises (Figure 1. 1):

1. The N-terminal transcription-activation domain (TAD), contains transactivation domain 1 (TAD1, residues 1-42, light green) and transactivation domain 2 (TAD2, residues 43-62, green). The transactivation domain 1 is required for transcriptional transactivation activity and interacts with its downstream targets, such as its negative regulator MDM2 (murine double minute 2) (29-31), and various transcription factors, such as components of the transcription initiation complex including the TATA box binding protein (TBP) and TBP associated factors (TAFs), which are the components of TF_{II}D (32-33), and the acetyltransferases p300 and CBP that act as co-activators and regulate p53 function by acetylating its C-terminus

(34-36). The transactivation domain 2 is also reported to be important in p53 regulation (37-40).

2. Src homology 3-like (SH3, residues 63-97, yellow) domain is a proline-rich domain required for interaction of p53 with SIN3, which prevents p53 from degradation. It contains SH3-domain binding motifs PXXP, where P designates proline and X for any amino acid, and is suggested to have a regulatory function (41-42). In addition, it has been suggested to have the function of mediating p53 transactivation by binding to p300 (43).
3. A central sequence-specific DNA binding domain (DBD, residues 98-292, orange), which contains several arginine amino acids. It can bind specifically to double-stranded target DNA, which consists of two copies of 10 bp motifs 5'-PuPuPuC(A/T)(T/A)GPyPyPy-3' separated by 0-13 bps (Pu is a purine base, Py is a pyrimidine base) (44). Interestingly, p53 always binds with high affinity to the recognition elements of genes responsible for cell cycle arrest; whereas the lower binding affinity positions are found in genes responsible for apoptosis (45-49). This domain is also the most frequently mutated region that accounts for above 80% of all the p53 mutations found in human tumours (50-53).
4. Nuclear localization signal (NLS, residues 300-323, light blue) (54).

5. Homo-oligomerisation domain (OD, residues 326-355, cyan), enables p53 tetramerization, which makes the sequence-specific binding of p53 to DNA more efficient (55).
6. Nuclear export signal (NLS, residues 340-351, light brown) (56).
7. C-terminal negative regulatory domain (NRD, residues 363-393, blue) that is responsible for down regulation of specific DNA binding and the stability of the p53 protein (57). This region is the target of a number of post-translational modifications (58).

The p53 protein initiates several programmes that arrest proliferation and prevent the generation of genetically-altered cells, and is activated by various types of cellular stress, such as DNA damage and oncogenic stress. Firstly, p53 can mediate cell cycle arrest. It is known that wild type p53 is required for the induction of G1 arrest in response to ionising irradiation (IR) as cell lines that lack p53 activity display a reduced response (59-60). Also, embryonic fibroblasts from p53 null mice lose the ability to undergo G1 arrest in response to IR (61). Another function of p53 is mediating apoptosis. In certain cell types, such as cells of hematopoietic origin, activation of the p53 pathway leads to apoptosis (62-63). Works of Yamamoto *et al.* showed that Huh6 cells underwent apoptotic cell death in response to oxidative stress, which was associated with the nuclear translocation of p53. When the endogenous p53 was knocked down by siRNA, Huh6 cells became resistant to oxidative stress (64). In addition, p53 also influences differentiation. Several studies

have shown that wild-type p53 expressed in undifferentiated cells can result in progression to a more differentiated state (65-66).

In fact, p53 plays a central role in a large network of messengers and effectors that are associated with the G1 and G2 DNA-damage checkpoints, apoptosis and DNA repair (Figure 1. 2) (67).

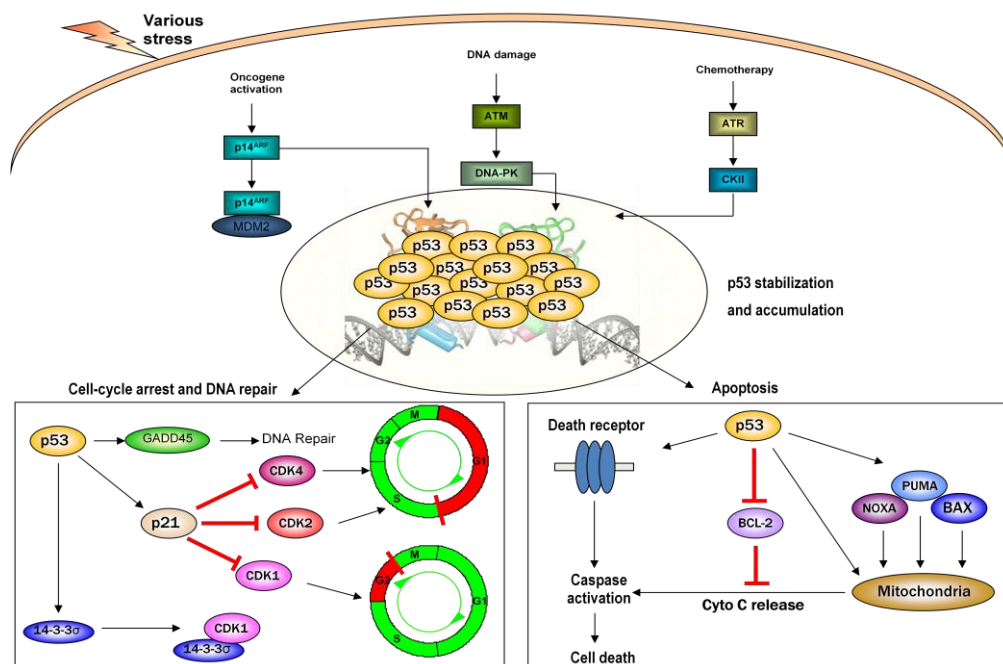


Figure 1. 2 p53 Tumour Suppression

The figure is a combination of two figures (67-68). Various cellular stresses can induce p53 stabilization and accumulation by different pathways to promote anti-proliferative and/or pro-apoptotic cellular effects. For example, deregulated oncogenes induce p14^{ARF} activation, which sequesters one of the key regulator of p53, MDM2, into the nucleolus; DNA damage activates protein kinase ATM, which, through DNA-dependent protein kinase (DNA-PK) phosphorylate the N-terminal of p53 to interrupt the MDM2 binding, and another protein kinase ATR can be activated by chemotherapy, which through casein kinase II (CKII) to phosphorylate the C-terminal of p53 to enhance sequence-specific DNA binding. These factors increase p53 level, which then activates its downstream targets. By activate the transcription of its target gene GADD45, stressed cells may be recovered via DNA repair procedure; 14-3-3 σ and p21 activation can induce cell cycle arrest at the DNA-damage checkpoints G1 and G2 by suppressing the activity of cyclin-dependent protein kinases (CDK1, CDK2 and CDK4) respectively. By acting as a transcription factor, p53 can activate target genes (PUMA, NOXA, BAX, p53AIP) or direct translocation to mitochondria to induce cytochrome c release, and it can also bind to the inhibitors of apoptosis (such as BCL-2 that block the release of cytochrome c from mitochondria) or death receptor, to promote caspase activation and lead to programmed cell death if the DNA can not be repaired properly.

1.1.1.2 p53 Dysfunctional Alteration in Human Cancer

That p53 was considered as a common denominator in human cancer has stimulated lots of investigations since 1989. In fact, p53 is one of the most-frequently altered proteins in human cancer.

It is found that most human cancers contain either mutations in the p53 gene that generate a dysfunctional or absent protein, or have disrupted p53 function induced by altered expression of other gene products (69). In about a half of adult cancers, p53 is inactivated directly as a result of mutations in the p53 gene (69).

In 1994, Cho *et al.* determined the crystal structure of the DNA binding site of p53 core domain at 2.2 Angstroms resolution, based on a complex containing the core domain of human p53 binding with double-stranded cognate DNA (70). The result revealed that the p53 core domain structure consists of a beta sandwich that serves as a scaffold for two large loops and a loop-sheet-helix motif. An even better structure resolution result was presented in the work done by Kitayner et al. (71), which together with the 1994 data enabled us to understand how p53 recognizes target sequences specifically (Figure 1. 3).

However, about half of all cancers retain the ability of expressing a normal p53 protein and many are thought to have inadequate p53 function as a result of abnormal regulation of p53 or defective signalling in the p53 pathway (26, 72).

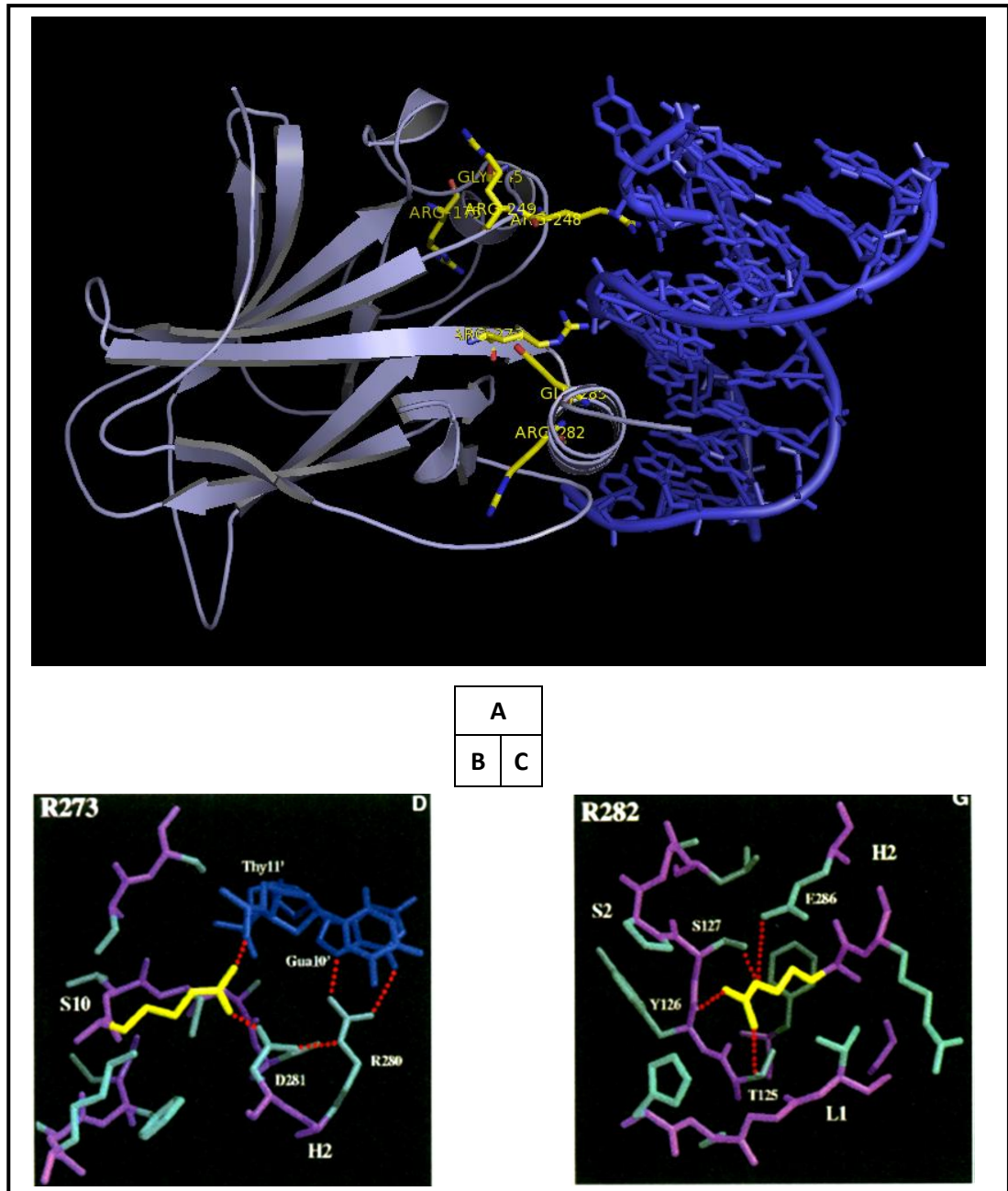


Figure 1. 3 Crystal structure of DNA bind with p53 core domain.

A) The structure of p53 core domain (light blue, ribbon diagram) bound to double-stranded DNA (blue, thick line), with high relative mutation frequency amino acid residues high lighted (yellow, stick model) and labelled, the blue and red spheres indicate nitrogen and oxygen atoms, respectively (PDB ID code 2AHI) (71), this image is generated by using PyMOL (Delano, 2002); B) & C) Detailed view of the two most frequently mutated residues of p53, Arg273 and Arg282 (yellow) and residues surround them ($\leq 7\text{\AA}$). The protein back bone atoms are in purple, amino acid side chains are in cyan, the DNA is in blue and the hydrogen bond and electrostatic interactions that the mutation hotspot residues make with DNA and other side chains are indicated by red-dotted lines (70).

1.1.2 p53 Restoration as a Cancer Therapy

The high frequency of inactivation of p53 in human cancers suggests that restoring p53 function might be an attractive and tumour cell-specific strategy for treating cancers.

Recent papers have supported the hypothesis that restoration of p53 function in established tumours causes regression of tumours *in vivo*.

By using a reversibly switchable p53 knockin (KI) mouse model that permits modulation of p53 status from wild-type to knockout at will, Martins *et al.* found that p53 was spontaneously activated when restored in established *Eμ-myc* lymphomas *in vivo*, leading to rapid apoptosis and a significant increase in survival (73).

Another study used regulatable RNA interference (RNAi) to demonstrate that p53 loss is required for maintenance of aggressive hepatocarcinomas. They have observed that even brief reactivation of endogenous p53 in p53-deficient tumours can produce complete tumour regressions (74).

Restoring endogenous p53 expression also leads to regression of lymphomas and sarcomas arising either spontaneously or induced in p53-null mice, without affecting normal tissues (75).

These observations strongly support efforts to treat human cancers by the method of pharmacological reactivation of p53 (76-77).

1.1.3 MDM2 Plays a Pivotal Role in Restraining p53

A number of ubiquitin ligases have been identified to target the p53 protein for degradation through the proteasome (78). These ubiquitin ligases include MDM2, Pirh2 (p53-induced RING-H2 protein), and Cop1 (constitutively photomorphogenic 1) (79). Although the exact role of some of the more recently described ubiquitin ligases in the regulation of p53 stability is unclear, numerous studies have shown that MDM2 plays a pivotal role in restraining p53.

The murine double minute 2 (*mdm2*) gene was originally identified as one of three genes (*mdm1*, 2, and 3) which were over-expressed greater than 50-fold by amplification in a spontaneously transformed mouse BALB/c cell line (3T3-DM) (80). The amplified *mdm* genes in the 3T3-DM cells were found to be located on small, acentromeric extrachromosomal nuclear bodies, called double minutes, which are retained in cells only if they provide a growth advantage, and *mdm2* is the most important one among them.

The full-length transcript of the *MDM2* gene encodes the human MDM2 protein, which consists of 491 amino acids. This protein contains several conserved functional domains and residues in its primary structure (Figure 1. 4):

1. The N-terminal p53 binding domain (red), residues 18-101, contributes to its binding with the p53 transactivation domain to inhibit the transcription activation function of p53 (10);

2. Nuclear Localization Signal (NLS, light blue), residue 178 and Nuclear Export Signal (NES, brown), residue 192 [\(81-82\)](#);
3. The acidic region(green), residues 237-288. This domain has been suggested to be involved in p53 ubiquitination [\(83-84\)](#);
4. The zinc finger domain(cyan), residue 289-331, which based on missense mutation identified in follicular lymphomas and liposarcomas [\(85-86\)](#), was suggested to have a role in negatively regulating the level of MDM2 [\(87\)](#);
5. The Really Interesting New Gene (RING) finger domain (yellow), residue 436-482, which confers the E3 ubiquitin ligase function to MDM2 protein that is responsible for the proteasomal degradation of p53 and itself [\(88-91\)](#). Moreover, this domain was implicated to be required for p53 nuclear exclusion [\(92-93\)](#);
6. A Nucleolar Location Signal (NoLS, purple), residue 466-473, which is located within the MDM2 RING finger domain [\(82, 94\)](#). Wang *et al.* [\(95\)](#) reported that MDM2 could be acetylated *in vitro* by CREB-binding protein (CBP) and also by p300 to a relatively lesser extent, although not by p300/CPB-associated factor, and only by CBP *in vivo*. Interestingly, they observed that an MDM2 mutant (K466/467Q) mimicking acetylation led to its decreased ability to promote ubiquitination of p53 and itself, as well as inactivating its function of promoting p53 degradation in living cells.

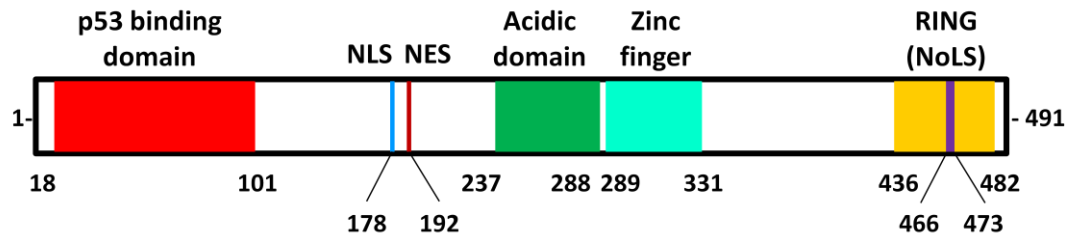


Figure 1. 4 The schematic view of the human MDM2 protein primary structure (96).

MDM2 was shown to bind p53 and form a complex with p53, leading to inhibition of p53-mediated transactivation (10). *MDM2* gene amplification was subsequently observed in many human sarcomas that retained wild-type p53 (3). In Momand's database, information on *MDM2* amplification frequency has been collected from previously published sources on 3889 samples from tumours or xenografts from 28 tumour types. *MDM2* gene amplification was reported to be observed in 19 tumour types, with the highest frequency observed in soft tissue sarcomas (20 %), osteosarcomas (16 %) and oesophageal carcinomas (13 %). In these studies, 29 out of a total of 33 *MDM2* amplification-positive tumours retained wild-type p53 (2). These data were consistent with the previously published overall *MDM2* amplification frequency reported for human tumours (7 %) (2). A large body of research indicates that over-expression of MDM2 is an important factor that can inactivate p53.

Further studies demonstrated that MDM2 is a prominent regulator of p53 stability and activity. The crucial role of MDM2 in p53 regulation is strongly supported by the fact that *mdm2*-null mouse embryos die early after implantation, but are fully rescued if they are co-deficient for p53 (97-98). This indicates the most important

role of MDM2 is in the regulation of p53 function, at least in early development. Meanwhile, MDM2 itself is the product of a p53-transcriptionally regulated gene (99). When nuclear p53 level is elevated, it activates the transcription of the *MDM2* gene, thus raising the level of MDM2 protein. On the other hand, MDM2 binds to p53, which blocks its N-terminal transactivation domain and targets p53 for degradation via the ubiquitin–proteasome system following ubiquitinylation of p53 through the E3 ligase activity of MDM2 (100–101). Thus, p53 and MDM2 form an autoregulatory negative feedback loop so that p53 is maintained at a low level in the absence of stress (Figure 1. 5) (102).

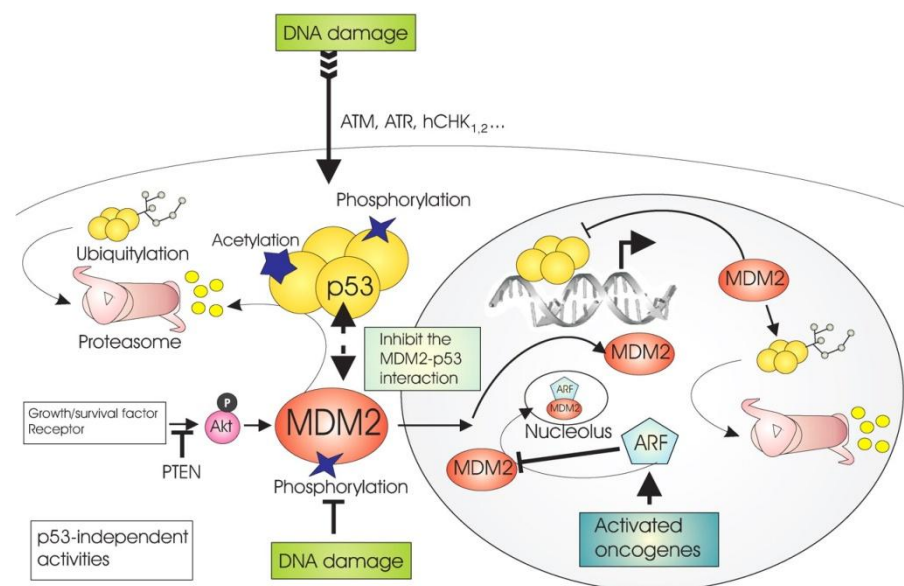


Figure 1. 5 Regulation of p53 by MDM2. (102)

As one of the downstream targets of p53, MDM2 regulate the function of p53 via a autoregulatory feedbackloop mechanism. First, MDM2 can bind to p53 transactivation domain to block its ability of activating transcription; second, MDM2 acts as an E3 ubiquitin ligase that promotes the proteasomal degradation of p53; last, MDM2 is involved in the nuclear export of p53. Moreover, growth/survival signals activate Akt and mediate nuclear import of MDM2 to suppress p53 function. Conversely, various cellular stresses such as DNA damage, oncogene activation can activate p53 via different mechanisms. DNA damage promote p53 and MDM2 phosphorylation and p53 acetylation through the activation of protein kinase pathways, such as ATM, ATR, to interrupt the interaction of MDM2 and p53 and stabilize p53. Activated oncogenes induce p14^{ARF} protein, which prevents p53 degradation by sequestering MDM2 into the nucleolus.

However, this feedback loop is frequently dysregulated in cancer. There is inadequate p53 activation induced by stress in many tumours, leading to inefficient growth arrest and/or apoptosis, as a result of abnormal regulation (26, 72). Therefore, rescue of p53 function by disrupting the MDM2-p53 interaction is considered to be a potential approach for anti-cancer therapy in some circumstances (103).

1.1.4 Rescue of p53 Function by Disrupting the p53–MDM2 Interaction

The rescue of p53 function by disrupting the MDM2-p53 interaction has been explored by several studies using macromolecular tools. A synthetic MDM2-binding mini-protein was reported to bind to the p53-binding pocket on the MDM2 protein (104). When introduced into cells containing low levels of wild-type p53, this protein caused a striking accumulation of the endogenous p53 protein, activation of a p53-responsive reporter gene, and cell cycle arrest which was similar to the effects seen in these cells after exposure to UV or ionising radiation. An octamer synthetic peptide (AP-B) which has been developed by Chene *et al.* from the peptide sequence corresponding to the minimal p53 binding site for MDM2, was shown to be a potent inhibitor of the p53-MDM2 interaction *in vitro*. In cellular assays, this untagged peptide also showed an induction of the accumulation of p53 in tumour cells. Furthermore, the AP-B peptide induced apoptosis in tumour cells over-expressing MDM2 protein (105). These studies suggest that, once released

from MDM2, p53 rapidly accumulates and then activates p53 target genes and the p53 pathway, resulting in cell-cycle arrest and/or apoptosis.

Several strategies have been used to release p53 from MDM2 control, including blocking MDM2 expression, inhibition of MDM2 ubiquitin ligase activity and disruption of MDM2–p53 binding.

1.1.4.1 Blocking MDM2 Expression

Zhang *et al.* described antisense mixed-backbone oligonucleotides (MBO) which specifically inhibited MDM2 expression in a dose- and time-dependent manner, resulting in significant anti-tumour activity *in vitro* and *in vivo* (106). A study by Tortora *et al.* also showed that oligonucleotide anti-sense MDM2 treatment could induce a growth-inhibitory effect and apoptosis in human GEO colon cancer cells and anti-tumour activity *in vivo* (107). Moreover, anti-sense MDM2 was shown to have a co-operative growth-inhibitory and apoptosis-induction effect with different classes of cytotoxic drugs acting by different mechanisms (107). However, the drawback of this strategy is the inefficient delivery of antisense oligonucleotides into cells.

1.1.4.2 Inhibiting MDM2 Ubiquitin Ligase Activity

Inhibiting the ubiquitin ligase activity of MDM2 has also been investigated as a p53-activating strategy, as p53 ubiquitination and degradation is the major component of the negative control of p53 by MDM2 (88-89, 108). Ribosomal

proteins L5, L11, and L23 have been shown to activate p53 by inhibiting MDM2-mediated p53 ubiquitination and thus activate p53 (109-110); other small proteins such as p19ARF (a 19 kDa polypeptide in the mouse, but p14ARF in humans) inhibit p53 degradation and activate p53 by binding to a C-terminal domain of MDM2 and promoting MDM2 degradation, rather than by directly preventing the MDM2/p53 interaction (111-112). In 2004, Yang *et al.* reported the identification of a family of small molecules (HLI98) that inhibit the E3 ligase activity of human MDM2. The compounds were observed to stabilize both p53 and HDM2 proteins and to active p53-dependent transcription and apoptosis in cells (Table 1.1) (113). Three years later, the synthetic route and biological evaluation data for this series of inhibitors (with the 5-deazaflavin scaffold) were disclosed (114) with further optimization to increase their potency, specificity and to eliminate p53-independent off-target activities (68) based on a structure-activity relationship (SAR) analysis. Also in 2007, a series of compounds (PYR-41, Table 1.1) with a different core structure to 5-deazaflavin was identified by the same group, which specifically inhibits the ubiquitin E1 rather than E2 to block protein degradation. Moreover, the results showed that PYR-41 at 20 μ M induced p53 accumulation and downstream target p21 activation (115).

1.1.4.3 Disruption of the p53-MDM2 Interaction

Many studies have concentrated on disrupting the MDM2 and p53 protein-protein interaction, especially after the publication of the co-crystal structure of the

complex between MDM2 protein and a peptide corresponding to p53 residues 17-29, and the revelation of the molecular details of their interface (116). MDM2 and p53 bind to each other via their N-terminal domains (Figure 1. 6). The MDM2 binding site of p53 partially overlaps with its transactivation domain and this is why MDM2 effectively inhibits p53 transcriptional activity (10).

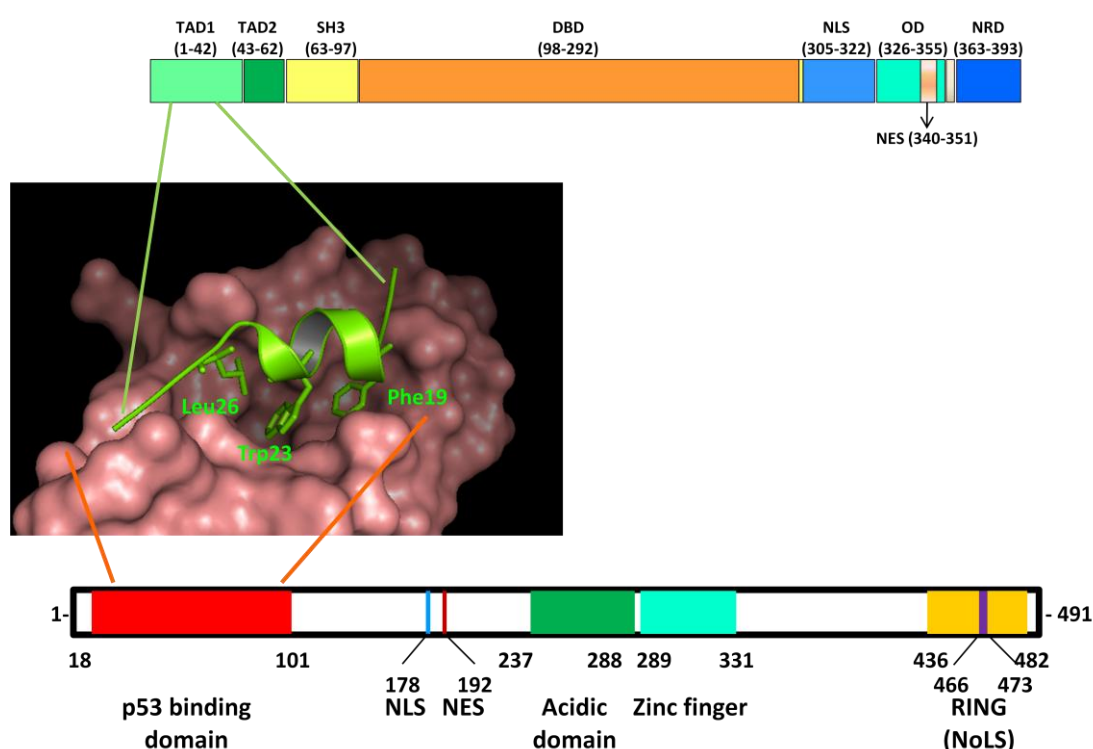


Figure 1. 6 Structure aspect of p53-MDM2 Interaction

The MDM2 protein can inhibit p53 transactivation by binding to the N-terminal transactivation domain of p53 through a well defined p53 binding pocket in its N-terminal binding domain. The co-crystal structure of this binding interaction published in 1996 revealed that three key amino acid residues of the α -helix p53 peptide (green), Phe19, Trp23 and Leu26 insert deeply into the hydrophobic binding groove of the MDM2 protein (light brown). The schematic view of the functional domain structures of p53 and MDM2 are presented above and below the p53-MDM2 binding image respectively (68).

Early studies have shown that p53-derived peptides inhibit the p53-MDM2 interaction, suggesting that they could be used as starting points in the design of inhibitors (105, 117-118). The introduction of non-natural amino acids can further

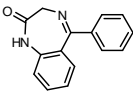
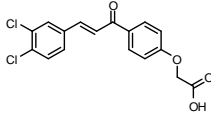
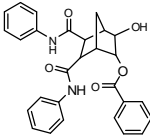
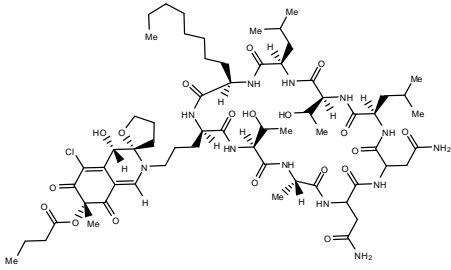
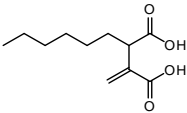
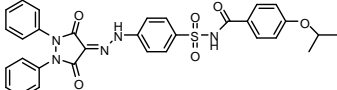
enhance binding and lead to even more potent peptides ([105, 117-119](#)). On the other hand, a retroinverso isomer of the natural N-terminal helical peptide was found to interact with MDM2 using the same hydrophobic residues, Phe19, Trp23, and Leu26, indicating that the retroinverso D-peptide adopts a right-handed helical conformation to mimic the p53 peptide, with key residues maintained in an appropriate conformation to interact with the binding pocket of MDM2, and the potency is enhanced at least two-fold ([120](#)).

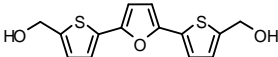
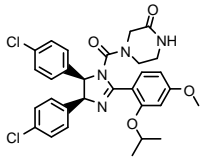
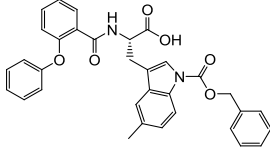
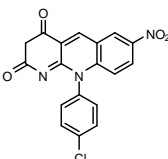
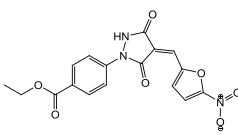
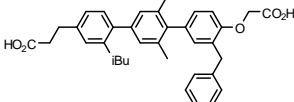
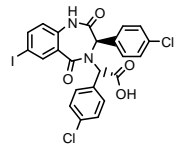
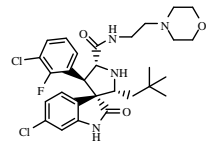
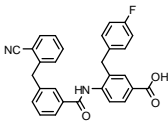
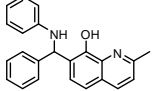
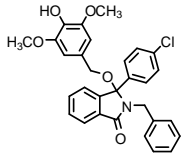
However, since these peptides were macromolecules with low bioavailability, researchers tried to find antagonists from natural products and compound libraries or *via* structure based design.

Although approximately 60% of small molecule drugs on the market are derived from natural products ([121](#)), only three natural products including chalcone-based inhibitors ([122](#)), chlorofusin ([123](#)) and hexylitaconic acid ([124](#)) have been reported to inhibit p53-MDM2 binding ([Table 1. 1](#)).

With the contribution of many researchers focused on the p53-MDM2 interaction, an increasing number of small molecules have been developed to disrupt p53-MDM2 binding interaction ([Table 1. 1](#)).

Table 1. 1 Inhibitors of the p53-MDM2 Interaction

No.	Structure	Evaluation methods	IC ₅₀ (μM)	Type of compounds	Ref.
1	Ac-Gln-Glu-Thr-Phe19-Ser-Asp-Leu-Trp23-Lys-Leu-Leu26-Pro-NH ₂	ELISA (GST)	8.7	Wild-type p53 derived peptide	(125)
2	Ac-Met-Pro-Arg-Phe19-Met-Asp-Tyr-Trp23-Glu-Gly-Leu26-Asn-NH ₂	ELISA (GST)	0.3	Phage-derived peptide	(125)
3	Ac- Phe19-Met-Asp-Tyr-Trp23-Glu-Gly-Leu26-NH ₂	ELISA (GST)	8.9	Truncated phage-derived peptide	(125)
4	Ac-Glu-Thr-Phe19-Aib-Asp-Aib-Trp23-Lys-Aib-Leu26-Aib-glu-NH ₂	ELISA (GST)	5.2	Constrained wild-type p53	(126)
5	Ac-Phe19-Met-Aib-Tyr-Trp23-Glu-Ac ₃ C-Leu26-NH ₂	ELISA (GST)	2.2	Constrained peptide 3	(125)
6	Ac-Phe19-Met-Aib-Pmp-Trp23-Glu-Ac ₃ C-Leu26-NH ₂	ELISA (GST)	0.3	Peptide 5 with a PMP at position 22	(125)
7	Ac-Phe19-Met-Aib-Pmp-6ClTrp23-Glu-Ac ₃ C-Leu26-NH ₂	ELISA (GST)	0.005	Peptide 6 with a 6ClTrp at position 23	(125)
8		Library Docking	ND	[1,4]benzodiazepine-2-one	(127)
9		ELISA (Streptavidin)	117	Chalcone derivative (B-1)	(122)
10		ELISA (detection only)	ND	Polycyclic Compound (syc-7)	(128)
11		DELFI-modified ELISA	4.6	Chlorofusin	(123)
12		ELISA (GST)	ND	Hexylitaconic acid	(124)
13		ELISA (GST)	31.8	Sulfonamide (NSC279287)	(129)

14		Cell line Screening	ND	RITA (binding to p53)	(130)
15		Biacore's Surface Plasmon Resonance Competition Assay	0.09	cis-imidazoline compounds (Nutin)	(77)
16		Fluorescence-Polarization (FP)-based Binding Assay	0.1	N α -(2-phenoxy-benzoyl) tryptophan-based MDM2 inhibitors	(131)
17		Plate-based Assays	20	Deazaflavins HL198C	(113)
18		Plate-based Assays	ND	PYR-41	(115)
19		ELISA (GST)	10	Terphenyl scaffold compounds	(132)
20		ThermoFluor Assay	0.08	Benzodiazepine edione compounds	(11)
21		FP-based Binding Assay	0.003	Spiro-oxindoles	(133)
22		FP-based Binding Assay	12	Proteomimetic library chemisets	(14)
23		FP-based Binding Assay	0.12	Quinolinols (NSC 66811)	(134)
24		ELISA (b-IP3 & Streptavidin)	5.3	Isoindolinone compounds	(15-16)

Compounds 1 to 7 are peptides. Compounds 11, 12 and 14 are natural products. The remained compounds are synthetic molecules. Aib, -amino isobutyric acid; Ac₃C, 1-amino-cyclopropanecarboxylic acid; PMP, phosphonomethylphenylalanine; 6ClTrp, 6-chloro-tryptophan; GST ELISA, Glutathione Transferase ELISA.

Targeting of protein–protein interactions by small molecules is challenging. The factors contributing to the challenge include 1) the general lack of small-molecule starting points for drug design, 2) the typical flatness of the interface, 3) the difficulty of identifying real binding, and 4) the limitation of the size and character of typical small-molecule libraries (135). However, protein–protein interfaces with a α -helix binding groove might be particularly valuable for small-molecule drug discovery (135).

In the case of the MDM2-p53 interaction it involves the binding of a single α -helix (from p53) in a hydrophobic groove formed by three α -helices (from MDM2).

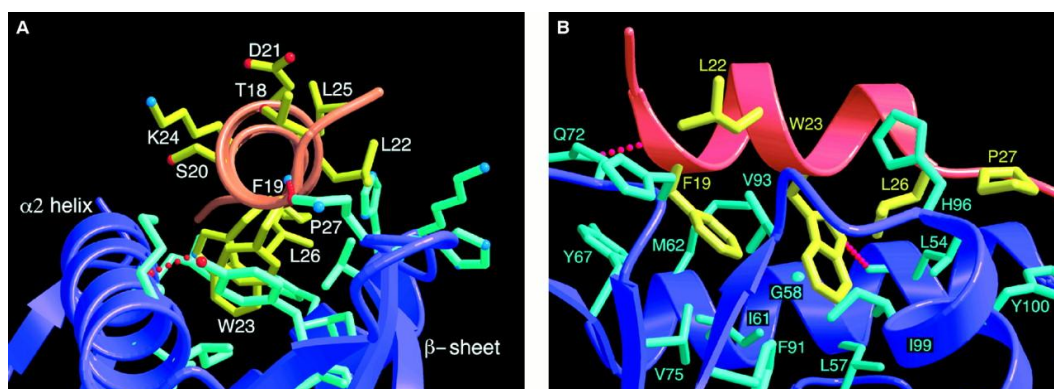


Figure 1. 7 The crystal structure of p53 peptide binding with MDM2 protein (116).

The crystal structure of p53 peptide forms an amphipathic helix (main chain structure in red and side chains in yellow) and binds with the MDM2 protein (main chain structure in blue and side chains in cyan) by inserting its key hydrophobic amino acid residues into the p53 binding groove on MDM2 protein surface. The binding groove is formed by an α 2 helix on one side, and a β -sheet on the other side, and is lined with hydrophobic and aromatic amino acids (or both), the blue and red spheres indicate nitrogen and oxygen atoms, respectively, the key hydrogen bond interactions are shown as red dotted lines. (A) The helical backbond of p53 peptide is shown as a circle-like structure, by presenting the structure view as looking down the helix axis, with all amino acid side chains labelled to emphasize its amphipathic nature. The α 2 helix and β -sheet backbone structure of MDM2 is located below the p53 peptide structure with amino acid sidechains at the interface presented but without label. The two hydrogen bonds at the interface are also emphasized as red dotted lines. (B) View of the interface in an orientation clockwise rotated 90° about the vertical axis of (A), so that the MDM2 α 2 helix is behind the plane of the figure, and its β -sheet is in front of the plane of the figure, with the p53 structure between them two. All the interacting amino acids of both p53 and MDM2 at the interface are shown and labelled.

In fact, as displayed in [Figure 1. 7](#) only a limited number of amino acid residues, just three p53 amino acids – Phe19, Trp23 and Leu26, are crucial for the binding of these two proteins [\(116\)](#). These three amino acid residues are inserted into a deep hydrophobic pocket on the surface of the MDM2 molecule which made designing small molecules to inhibit this interaction possible [\(68\)](#).

Using a cell-proliferation assay to screen the National Cancer Institute (NCI) library of compounds, Issaeva *et al.* identified RITA (reactivation of p53 and induction of tumour cell apoptosis), 2,5-bis(5-hydroxymethyl-2-thienyl)furan, which suppressed the growth of HCT116 cells in a dose-dependent manner as a result of binding with p53 and inducing its accumulation in cells [\(130\)](#). It was observed that RITA binds to the MDM2-p53 transactivation domain-binding cleft [\(136\)](#). However, a recent study report from Krajewski *et al.* argues that RITA does not block the formation of the complex *in vitro* between p53(residues1-312) and the N-terminal p53-binding domain of MDM2(residues 1-118) [\(137\)](#). Although Grinkevich *et al.* attempted to defend their hypothesis by suggesting that the native conformation of p53 may be required for enabling RITA to bind with it, they also admitted that elucidation of the structure-activity relationship of RITA-p53 binding could be important for future research [\(137\)](#).

By using a high-throughput fluorescence polarization binding assay [\(138-139\)](#), Zhang *et al.* have rank ordered a series of small-molecule inhibitors ([Table 1. 2 &](#)

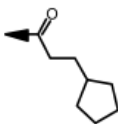
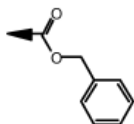
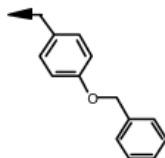
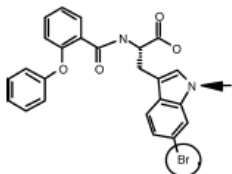
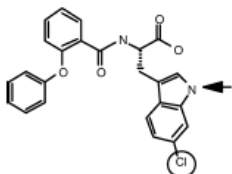
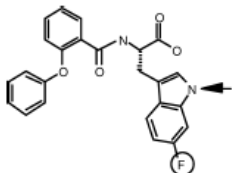
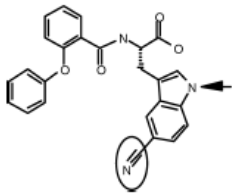
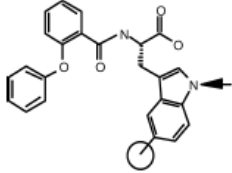
Table 1. 3) that block the binding of MDM2 to a p53-derived fluorescent peptide (131). In their research results, all the octapeptide-based MDM2 inhibitors in Table 1. 2 had K_i values in the nanomolar range of potency, however, most of the tested $N\alpha$ -(2-phenoxybenzoyl) tryptophan-based MDM2 inhibitors in Table 1. 3 exhibited micromolar range potencies. No binding mode analysis or cellular activity evaluation data have been published to date following this report.

Table 1. 2 Trp indole C5/C6 substitution SAR of octapeptide-based MDM2 inhibitors.

Octapeptide											K_i (nM) ^a
1	AC-	Phe-	Lys-	Lys-	Ac6C-	Trp-	Glu-	Glu-	Leu-	NH2	240
2	AC-	Phe-	Lys-	Lys-	Ac6C-	(5-CN)Trp-	Glu-	Glu-	Leu-	NH2	530
3	AC-	Phe-	Lys-	Lys-	Ac6C-	(5-Me)Trp-	Glu-	Glu-	Leu-	NH2	76
4	AC-	Phe-	Lys-	Lys-	Ac6C-	(5-F)Trp-	Glu-	Glu-	Leu-	NH2	45
5	AC-	Phe-	Lys-	Lys-	Ac6C-	(6-Me)Trp-	Glu-	Glu-	Leu-	NH2	120
6	AC-	Phe-	Lys-	Lys-	Ac6C-	(6-F)Trp-	Glu-	Glu-	Leu-	NH2	44
7	AC-	Phe-	Lys-	Lys-	Ac6C-	(6-Cl)Trp-	Glu-	Glu-	Leu-	NH2	1
8	AC-	Phe-	Lys-	Lys-	Ac6C-	(6-Br)Trp-	Glu-	Glu-	Leu-	NH2	0.7
9	AC-	Phe-	Arg-	Dpr-	Ac6C-	(6-Br)Trp-	Glu-	Glu-	Leu-	NH2	2

^a Ac6C-, α -aminocyclohexyl carboxylic acid and its residue; Dpr-, α,β -diaminopropionic acid and its residue; Reported are FP K_i values to Trx-MDM2. The FP assay was performed at room temperature in PBS containing 2.5% DMSO (131).

Table 1. 3 C5/C6/N1 SAR of N α -(2-phenoxybenzoyl) tryptophan-based MDM2 inhibitors.

Indole C5/C6/N1 substitutions	H			
	R1C1 3	R1C2 0.8	R1C3 0.5	R1C4 0.6
	R2C1 6	R2C2 0.8	R2C3 0.6	R2C4 1
	R3C1 20	R3C2 0.4	R3C3 0.8	R3C4 2
	R4C1 10	R4C2 0.6	R4C3 0.6	R4C4 1
	R5C1 10	R5C2 0.2	R5C3 0.1	R5C4 0.6

FP K_i Values are reported in μ M. The compounds are identified by column and row numbers.

Nutlins were identified as the first potent and selective small-molecule antagonists of MDM2 by Vassilev *et al.* (77). X-ray crystallography was used to confirm the specific binding of Nutlins in the p53-binding pocket of MDM2 (Figure 1. 8).

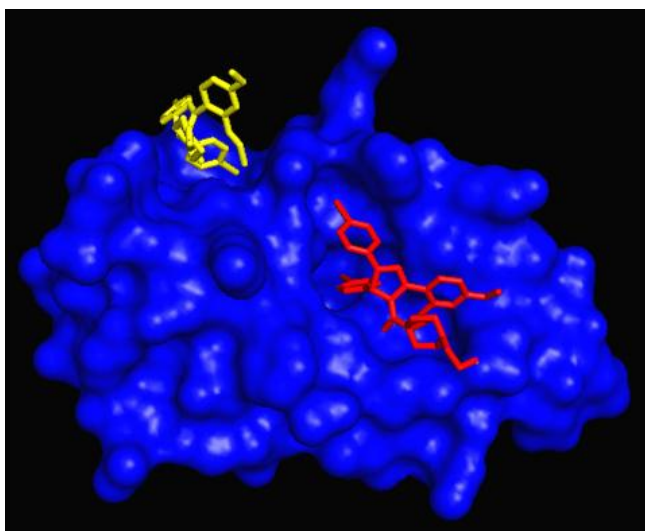


Figure 1. 8 MDM2-Nutlin-2 binding image.

The MDM2-Nutlin-2 co-crystal structure in this figure indicated that one Nutlin-2 (in red) blocked the p53-binding pocket of MDM2 (in blue) and the other Nutlin-2 (in yellow) bound to another position of the MDM2 protein surface (PDB ID code 1RV1 molecule group A) (77). The figure was generated using PyMOL (DeLano, 2002).

With the blocking of the p53-MDM2 binding interaction by Nutlins, the p53 pathway was activated, leading to cell cycle arrest, apoptosis, and growth inhibition of human tumour xenografts in nude mice (77, 140-141). The specificity of Nutlin-3 activation of the p53 pathway was shown by the induction of apoptosis in cells with wild-type p53, but not mutant p53 (141-142). Supportive evidence for Nutlin-3 being a highly selective MDM2 antagonist and p53 inducer has been provided by gene array analysis of Nutlin-induced expression patterns, and also by SJSA-1 and MHM osteosarcoma xenografts *in vivo* (143). Van Maerken *et al.* came to the same conclusion when investigating neuroblastoma cells with wild-type p53 (144). The

discovery of the Nutlin small molecule inhibitors of the p53-MDM2 interaction was suggested to represent the end of the 'peptide era' and beginning of the 'low molecular weight era' of protein-protein interaction antagonists (145).

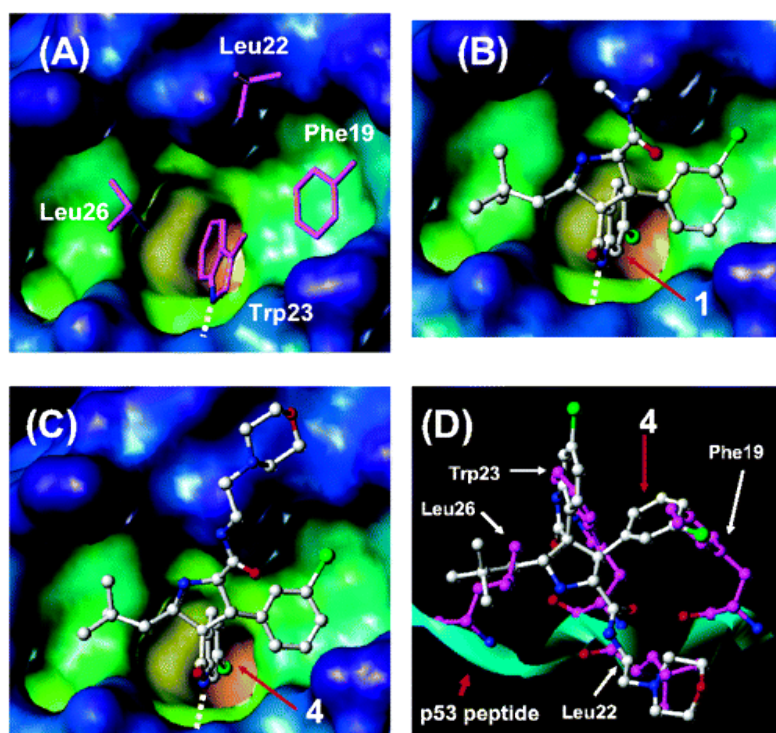


Figure 1. 9 Structure-based design produced small molecule antagonists of MDM2-p53 binding interaction by mimicking Phe19, Trp23, Leu26 and Leu22 residues in p53 (133).

(A) The analysis of X-ray structure of the p53-MDM2 complex indicates that except Phe19, Trp23, and Leu26, Leu22 in p53 has also contributed to the interaction between p53 and MDM2. The MDM2 binding site is colour-coded according to the cavity depth (the binding groove is coded in light green, and solvent-exposed regions are coded in blue). The four key amino acid side-chain residues in p53 are shown as stick model and colour-coded in purple. (B, C) Predicted binding models of two spiro-oxindole complexed with MDM2 binding groove using the GOLD programme. For both of the two compounds (1 and 4 as labelled), carbons are in white, nitrogens in blue, chloride in green, and oxygens in red. Hydrogen bonds interaction between each compound with MDM2 are shown with a dashed yellow line. (D) View of superposition of compound 4 (is colour-coded as illustrated in C) to the p53 peptide (α-helix backbone is shown in light green) conformation in the crystal structure of p53 peptide in complex with MDM2. Four amino acid side-chains, Phe19, Leu22, Trp23, and Leu26, in p53 are labelled and colour-coded in purple.

Using a structure-based design strategy to mimic the Phe19, Trp23, Leu26, and

Leu22 residues in p53, Ding *et al.* have designed a class of small-molecule inhibitors (spirooxindoles) of the MDM2-p53 interaction(Figure 1. 9).

The most potent inhibitor, which was named MI-63 (MDM2 inhibitor 63), has a K_i value of 3 nM for binding to MDM2, and is over 2000-times more potent than the natural p53 peptide (residues 13-29). The study also showed that MI-63 is a highly effective activator of p53 function and inhibitor of LNCaP prostate cancer cell growth, and reported to have minimal toxicity to normal cells (133).

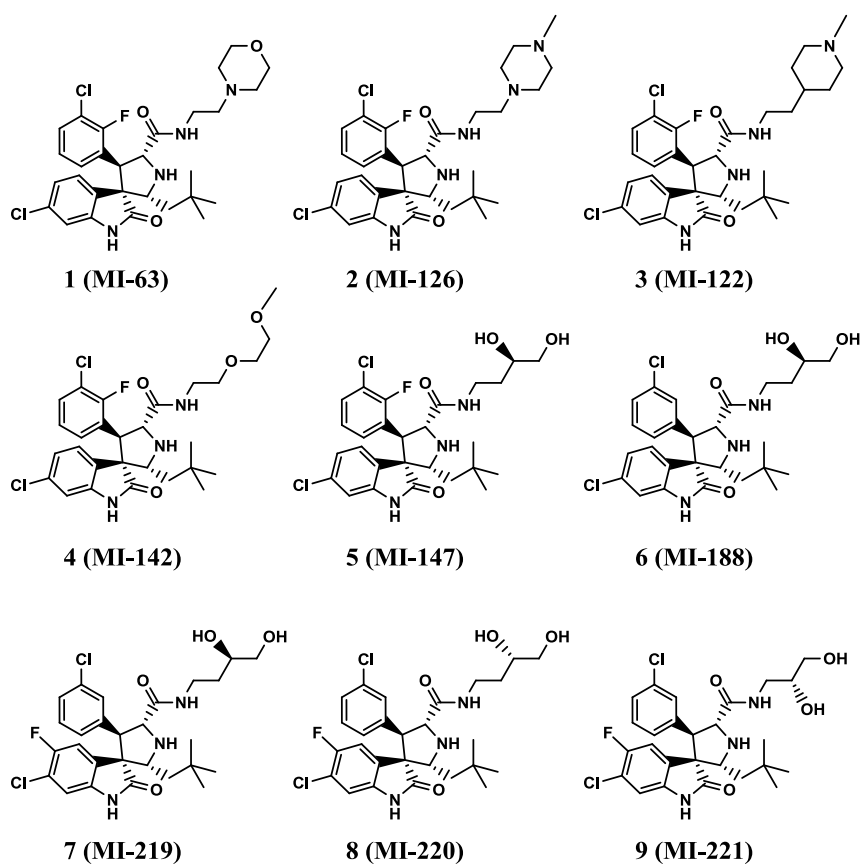


Figure 1. 10 Chemical structures of potent spirooxindole MDM2 inhibitors (146).

With several years of continuous optimization (147-151), a batch of potent and orally active small-molecule inhibitors of the MDM2-p53 interaction were obtained based on the spirooxindole core scaffold (Figure 1. 10). Noticeably, compound 5 binds to MDM2 with a K_i value of 0.6 nM and activates p53 at the concentration as low as 40 nM with a good oral bioavailability (146). These successful

structure-based MDM2 inhibitor design strategies have provided solid evidence that reactivation of p53 using small-molecule inhibitors is a promising new cancer therapeutic strategy (146).

A series of isoindolin-1-ones has been identified as inhibitors of the MDM2-p53 interaction in previous studies by our group, using *in silico* screening and small library synthesis (15-16). As this research was carried out without structural data on the isoindolinone-MDM2 interaction, docking was applied using the published MDM2 crystal structure 1YCR and the easyDock computer programme as a virtual screening method, but a unique binding mode could not be defined with the limited information available. As a result, a combinatorial approach was employed to optimize the activity of a series of compounds, and three side chains were chosen for the first attempt. With a series of SAR analyses, two of the most potent compounds, 2-benzyl-3-(4-chlorophenyl)-3-(3-hydroxypropoxy)-2, 3-dihydroisoindol-1-one ($IC_{50} = 15.9 \mu M$) and 3-(4-chlorophenyl)-3-(4-hydroxy-3, 5-dimethoxybenzyloxy)-2-propyl-2, 3-dihydroisoindol-1-one ($IC_{50} = 5.3 \mu M$) (Table 1. 1), were identified. Bioassay evaluation showed that these two compounds induced p53-dependent gene transcription, in a dose-dependent manner, in the MDM2 amplified SJS human sarcoma cell line (15-16). Further investigations to increase the potency, bioavailability and selectivity, and to evaluate biological effects *in vivo* of these lead compounds has been the priority of this project.

1.1.5 MDMX as a druggable target for p53 reactivation

A cDNA clone encoding MDMX (MDM4) was isolated and identified from a whole mouse cDNA expression library in 1996 and showed the function of inhibiting p53-activated transcription (152). One year later, the human homologue of MDMX was isolated and identified, which contains 490 amino acids and is 90% similar to mouse MDMX (153). The comparison between MDM2 and MDMX proteins (Figure 1. 11) showed marked structural similarity (96).

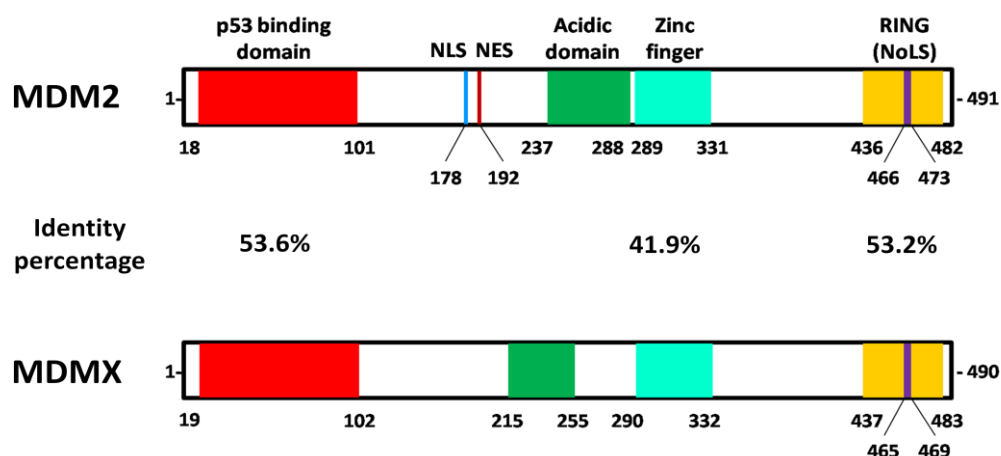


Figure 1. 11 Primary structure comparison of human MDM2 and human MDMX proteins.

In the schematic primary structures of both MDM2 and MDMX proteins, the p53 binding domain (red), Zinc finger domain (cyan) and RING finger domain (yellow) are well conserved, with marked conserved percentage (53.6%, 41.9% and 53.2% correspondingly). It also shows that although both of the two proteins contain high content of acidic amino acids, but no significant similarity between these two domains, which in MDM2 is from 237 to 288, and in MDMX is from 215 to 255. In addition, although a consensus nucleolar location signal (NoLS, purple) is present within the RING domain of both MDM2 and MDMX protein structures, nuclear localization signal (NLS, light blue) and nuclear export signal (NES, brown) present only in MDM2 but not MDMX (96).

The highest similarity of MDM2 and MDMX protein structure is found at the N-terminal region that overlaps the p53-binding domain, which is consistent with the observation that both MDM2 and MDMX can interact with p53, and the amino

acids required for the interaction of p53 with human MDM2 are precisely conserved in human MDMX. Moreover, these amino acids are strictly conserved in all known orthologs of human MDM2 and human MDMX (154).

Using cells deficient in either MDM2 or MDMX, Gu *et al.* (155) demonstrated that MDM2 and MDMX are actually functionally dependent on each other. On the one hand, in the absence of MDMX, MDM2 is quite ineffective in suppressing p53 activity because of the handicap of its very short half-life, i.e. MDMX enhances MDM2 protein stability sufficiently to enable its p53 degradation function thoroughly. On the other hand, as a cytoplasmic protein, MDMX presents no NLS and NES regions, and hence has to rely on MDM2 (155-156) or other shuttles such as p53 (157) to get into the nucleus to inhibit p53 function. When excessively overexpressed, MDMX can inhibit MDM2-mediated p53 degradation by competing with MDM2 for binding to p53 (157).

To study MDMX function *in vivo*, Parant *et al.* generated MDM4-null mice by using a homologous recombination method to delete exon 3-5 of MDM4 that encodes most of the p53 binding domain (amino acids 27-96). This mutation caused the death of MDM4-/- embryos at 7.5-8.5 dpc (days postcoitum) due to loss of cell proliferation but not induction of apoptosis. In addition, by crossing in the Trp53-null allele, they observed complete rescue of MDM4-/- embryonic lethality. Based on these observations, they suggested that MDM4 and MDM2 may regulate p53 function via different pathways *in vivo* (158). By random insertion mutagenesis upstream of the

ATG start codon with a viral insertion mapped in intron 1, Finch *et al.* generated a 2nd MDMX null (mutant) mouse line, which results in midgestational embryo lethality (died between 9.5-10.5 dpc) because of overall growth defects and massive apoptosis in the neuroepithelium (159). Furthermore, this mouse line can be completely rescued by the absence of p53, and mice homozygous for both MDMX and p53 null mutations are viable and appear developmentally normal (159).

Migliorini *et al.* characterized a mutant mouse line with a specific gene trap event in the MDM4 locus. Without the MDM4 expression, the mice embryos died at between 10 and 12 dpc because of overall growth deficiency, anaemia, improper neural tube closure and dilation of lateral ventricles, and this could be rescued by transferring the MDM4 mutation into a Trp53-null background. *In situ* analysis of RNA showed p21 level increasing and decreased levels of Cyclin E, as well as proliferating cell nuclear antigen expression, which suggest a G₁ phase cell cycle arrest of the MDM4 mutant embryo cells. It also demonstrated that MDM4-deficient mouse embryonic fibroblasts showed a marked reduction of proliferative capacity in culture, and p53-dependent cell death was generally detected in the developing central nervous system of MDM4 mutant embryos (160).

In a further mouse model study, Francoz *et al.* generated sophisticated mouse models to demonstrate that both MDM2 and MDM4 are essential for preventing p53 activity in the same type of cells, at either proliferation or differentiation status (30). The data suggest that MDM2 is responsible for preventing p53 protein accumulation, while MDM4 contributes to the overall inhibition of p53 activity

independent of MDM2 (30). They seem to cooperate like 'brothers in arms' (96) to keep p53 in check.

These observations confirmed that MDMX function is critical and synergistic for negative regulation of p53 activity *in vivo* (at least during embryogenesis).

After the confirmation of MDMX as a key down-regulator of p53 function *in vivo*, it was necessary to figure out if MDMX can contribute to tumour formation directly or not. Using retrovirus-mediated MDMX over-expression in primary mouse embryonic fibroblasts, Danovi *et al.* (161) demonstrated that increased and constitutive MDMX expression led to immortalization and neoplastic transformation of the cells, which suggested that the abnormal expression of MDMX could contribute to tumourgenesis. Following this observation, human MDMX mRNA expression levels of hundreds of primary human tumour samples were checked using *in situ* hybridization (ISH) and tissue microarray (TMA) methods, and observed 3-5 fold higher levels of human MDMX expression in 19 % of breast (41 of 218), 19 % of colon (5 of 27) and 18 % of lung (16 of 88) cancers than those in matched controls. In addition, MDMX amplification was observed (defined as more than 6 to 8 copies per cell) in 5 % (8 of 162) of primary breast tumour samples analyzed and all of the tested tumour samples retained wild type p53. Actually, human MDMX over-expression has been reported in around 40 % (13 of 31) of cancer cell lines tested (162). It is amplified in 4 % of glioblastomas (163), and about 60% of retinoblastomas have been reported to have MDMX over-expression or

gene amplification (164). All these data indicated MDMX as a new putative drug target for cancer therapy.

By using an ELISA method and cellular assays, Hu *et al.* (165) demonstrated that Nutlin-3 could inhibit the binding of p53 to MDM2 but not to MDMX. In the experiment, Nutlin-3 inhibited the p53-MDM2 binding interaction with an IC_{50} of about 800 nM, but showed little or no inhibitory activity against p53-MDMX binding at concentrations up to 30 μ M. Following that, JEG3 and MCF7 cell lines that express a high level of endogenous MDMX had been used for confirming the observation. The data suggested a correlation between MDMX level in cell lines with p53 activation and p21 protein induction, as well as with cell cycle and growth arrest effects. In the report of Patton *et al.* (166), isogenic populations of normal human fibroblasts transformed *in vitro* by human MDM2, human MDMX or shRNA to p53 had been applied to determine the effects of Nutlin-3 in cells with wild type p53. The result indicated that Nutlin-3 efficiently induced apoptosis in cells expressing human MDM2, whereas human MDMX-expressing cells and cells with low level of p53 have no significant response. Moreover, for the Nutlin-3 resistance cells overexpressing human MDMX, elimination of MDMX expression by shRNA sensitized them to Nutlin-3 mediated cell cycle arrest or cell death. These findings highlighted the requirement of developing MDMX-specific small molecule inhibitors for research into MDMX function and as therapeutic agents.

Most recently, Bo et al. (167) have validated a subgroup of chronic lymphocytic leukaemia (CLL) cells containing wild type p53, which show a lack of cytotoxic response to *in vitro* treatment with Nutlin-3. Interestingly, by utilizing a qRT-PCR method, they compared the *MDM4* transcript level of a different series of 43 CLL samples to the normal B cells purified from peripheral blood samples of 15 healthy donors and observed that *MDM4* was not only remarkably over-expressed in a subset of CLL cells that contain wild type p53 and lack of cytotoxic response to Nutlin-3 treatment, but also universally over-expressed by CLL cells compared to normal B cells. These observations suggest that *MDM4* could be a potential therapeutic target for CLL.

In 2008, Popowicz *et al.* (168) determined the first co-crystal structure of a peptide derived from human p53 transactivation domain binding with a humanized zebra-fish MDMX and compared the p53 binding pocket of the MDMX crystal structure together with that of two MDM2 (PDB Code: 1YCR & 1T4F) crystal structures (Figure 1. 12). The comparison of these structures indicate that although the principal features of the MDM2-p53 binding interaction are preserved in the MDMX-p53 binding interaction, and the three key residues of p53 (Phe19, Trp23 and Leu26) still contribute to the binding, the central hydrophobic groove of MDMX that the p53 peptide binds is smaller and differently shaped than those of MDM2 proteins. The key amino acid residues that contribute to this difference (Leu53 and Tyr99 in MDMX, and Leu54 and Tyr100 in MDM2) are highlighted in Figure 1. 12.

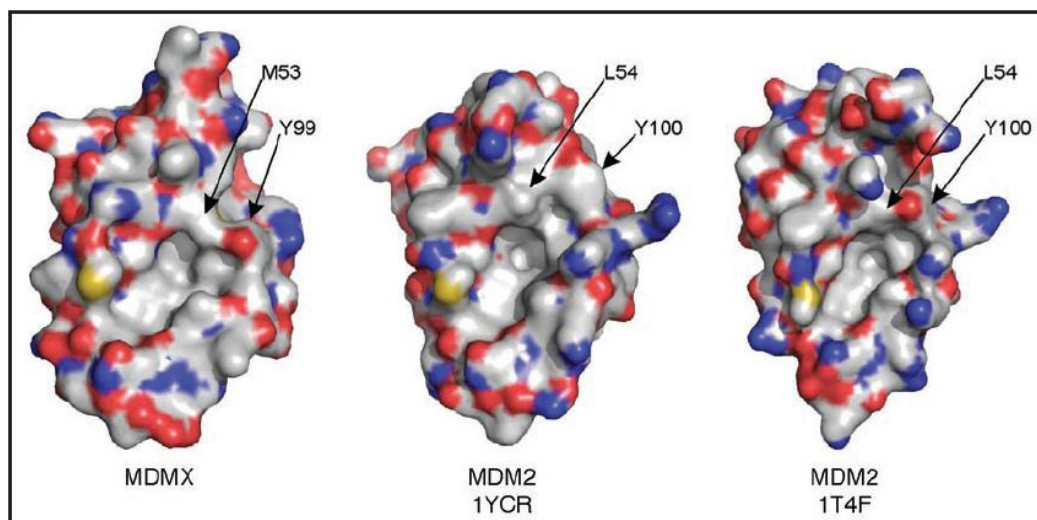


Figure 1. 12 Surface representations of human MDMX (the left side) and two human MDM2 structures (the right side) (168).

Significant differences in the shape of p53 binding pocket are clearly visible. Amino acid residues mainly responsible for the differences in the binding groove are labelled.

Following these observations, several p53 analogue peptide inhibitors were generated (169-173) to explore the p53-MDMX binding interaction and to refine the differences of MDMX-p53 binding with MDM2-p53 binding, which together with the assays developed for evaluating the binding affinity should contribute to speeding up the development of a simple pharmacophore model of cross-selective MDM2-MDMX/p53 inhibitors.

1.2 Research Project

My research project is based on the theories and hypotheses about MDM2/p53 small molecule antagonists design and mentioned above, and the progress our research group has made.

Aims:

1. Continue to optimize the structure of the isoindolin-1-one scaffold compounds, based on the X-ray crystal structure model of the MDM2-p53 binding interaction, and structure/activity analysis to design more potent compounds with good water solubility and bioavailability.
2. Evaluate the activity of newly synthesised isoindolin-1-one scaffold compounds with a sequence of cell-free and intact cell bioassay methods combined with information from NMR and X-ray crystal structure analysis to establish the binding modes of inhibitors with MDM2, so that we can obtain SAR information to inform the continued optimization process.
3. Test the most potent isoindoline-1-one compounds for differential growth inhibition and/or cytotoxicity with a panel of cell lines of defined p53 and MDM2 status, to validate the specificity of the compounds for inhibition of the MDM2-p53 interaction.

4. Establish whether or not the new inhibitors can also bind MDMX, a closely related structural homologue of MDM2, which can also potentially prevent p53 activation after MDM2 has been inhibited.
5. Screen compounds with different core scaffolds in an attempt to obtain alternative scaffold compounds as MDM2/p53 and/or MDMX/p53 small molecule antagonists.
6. Generate MDM2/p53 antagonist-resistant cancer cell lines and explore the possible mechanisms of their resistance.

Chapter Two

General Materials and Methods

During this PhD project, a broad range of techniques have been employed, including synthetic chemistry, biochemistry (ELISA, western blotting, SRB assay, Caspase-Glo 3/7 assay, DNA sequencing, FISH assay) and computational quantitative structure activity relationship (QSAR, for binding mode prediction) analysis for the purpose of developing a better understanding of the p53 pathway and its activation with MDM2/p53 antagonists.

This chapter focuses on the general methods and materials applied during my study, and further specific information for each method will be explained where appropriate in the Results chapters.

2.1 ELISA Assay

Enzyme-Linked Immuno-Sorbent Assay (ELISA) is a technique often employed due to its extreme sensitivity and scale, which enables a rapid detection system suitable for high throughput screens of protein expression and protein interactions with other macromolecules, including protein-protein binding. The original ELISA description was published by Dr Peter Perlmann and Dr Eva Engvall in 1971 (174). After about four decades development, a vast number of applications based on the initial ELISA principal have been published worldwide and all of them typically contain the procedure that an unknown amount of antigen or antibody is tightly affixed to a surface (in a tube or microtiter plate), and then a specific antibody or antigen is applied over the surface so that it can bind to the antigen/antibody, respectively. Then a detection antibody labelled with an enzyme is added, and in the final step a substance is added that the enzyme can convert to some detectable signal, most commonly a colour change or light emission in a chemical substrate.

2.1.1 Experiment Design

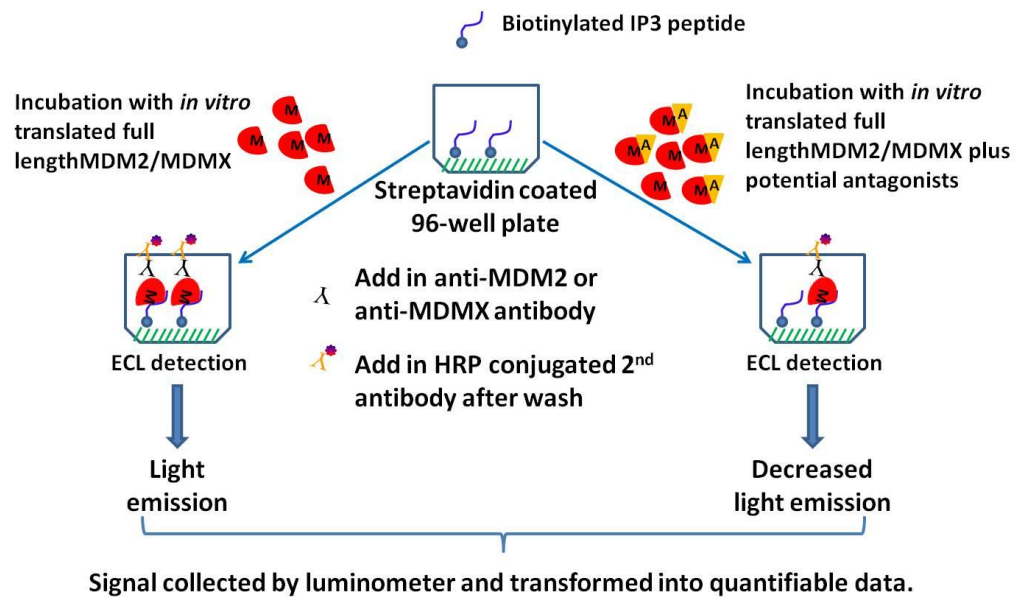
2.1.1.1 Mechanisms of ELISA for MDM2/MDMX Antagonist Screening

An ELISA method, as previously described (16) was used to screen compounds using a 96 well Streptavidin Covalent ScintiPlate (Perkin Elmer), as schematically illustrated in Figure 2. 1.

The plate was coated with streptavidin which formed a complex with the biotinylated IP3 (118) peptide that based on the wild type p53 sequence (b-IP3: Biotin-Met-Pro-Arg-Phe[19]-Met-Asp-Tyr-Trp[23]-Glu-Gly-Leu[26]-Asn-NH₂) when it was added. Samples from a parallel clear plate consisting of *in vitro* translated MDM2/MDMX lysate (IV-MDM2/IV-MDMX) incubated with various concentrations of antagonists was then directly transferred to the IP3 peptide coated binding plate. Since the antagonists and IP3 bind to the same N-terminal region of MDM2/MDMX, the potency of the compound is determined by the amount of IP3-MDM2/IP3-MDMX complex formation; the less complex formation detected by the subsequent procedure, the greater the potency of the compound.

The amount of IP3-MDM2 or IP3-MDMX complex formation was determined by using a primary mouse anti-MDM2 antibody (MDM2-Ab5 from Calbiochem)/rabbit anti-MDMX antibody (BL1258 from Bethyl), as appropriate, followed by a goat anti-mouse secondary horseradish peroxidase (HRP) conjugated antibody for MDM2 primary antibody detection or a goat anti-rabbit secondary horseradish peroxidase (HRP) conjugated antibody for MDMX primary antibody detection. An Enhanced Chemiluminescence (ECL) system was used to detect the amount of HRP bound and hence to quantify the complex formation. By detecting the amount of light produced using a luminometer, the amount of secondary antibody bound to the primary MDM2/MDMX antibody can be inferred.

ELISA screening for MDM2/MDMX-p53 binding antagonists



A

B

ELISA screening for MDM2/MDMX Antagonists (96-well plate)

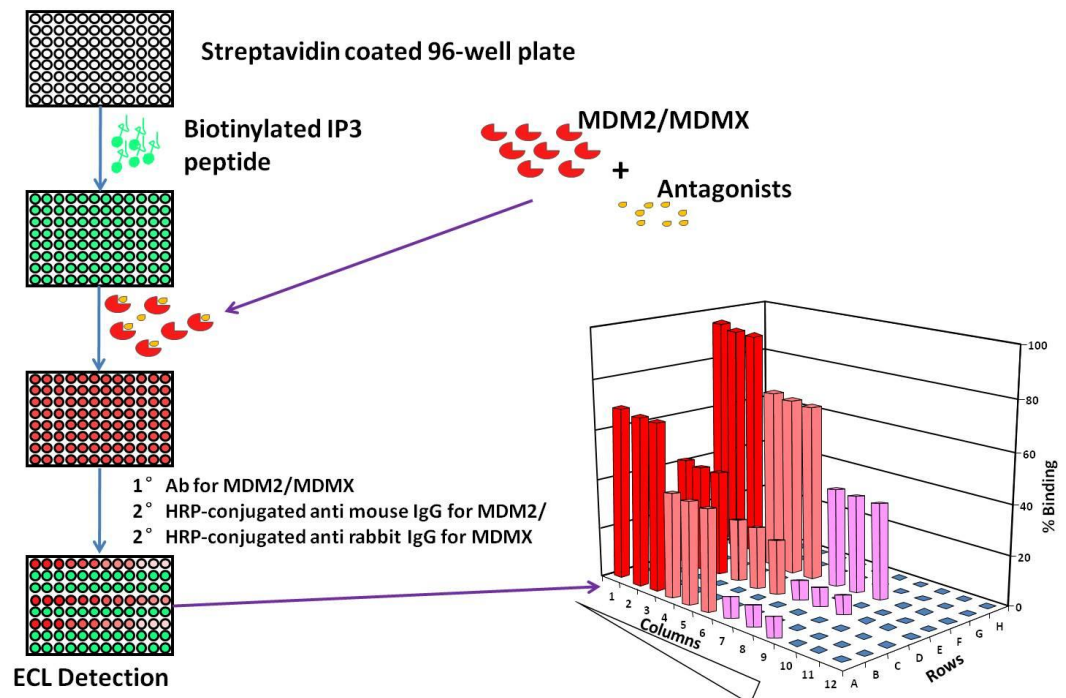


Figure 2. 1 Procedure of ELISA for MDM2/MDMX antagonists screening in A) single well and B) a 96-well plate

2.1.1.2 Plate Arrangement for MDM2/MDMX Antagonists IC_{50} Determination

For evaluation of dose-dependent-activity, the ELISA assays were carried out with the plate arrangement method shown in Figure 2. 2; 7 compounds could be evaluated within one plate. The first three vertical lines of wells were solvent controls and three different concentrations of positive controls (Nutlin-3 at 50, 100, 200 nM for MDM2 inhibitor screening, IP3 peptide at 0.5, 2, 10 μ M for MDMX inhibitor screening) were placed in the top row 9 wells. Each concentration of every compound was plated out in triplicate at three different concentrations.

The 63 wells colour coded as grey can also be individual compounds with the same concentration for high throughput screening.

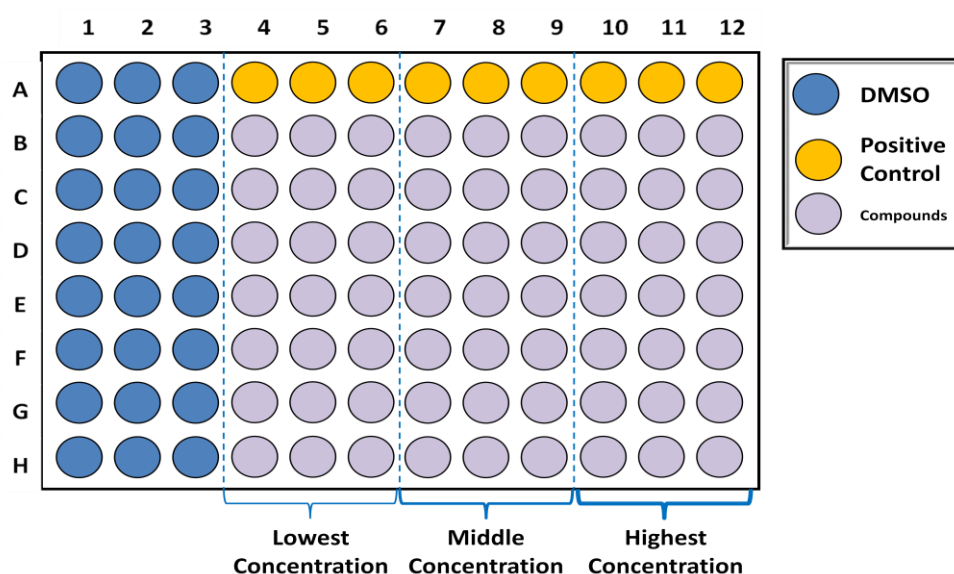


Figure 2. 2 Plate arrangements for IC_{50} value determination

2.1.2 Plasmid DNA Preparation

For the preparation of MDM2/MDMX plasmid DNA, we have produced detailed protocol of 'Plasmid preparation by using QIAGEN tip 2500' based on the QIAGEN tip 2500 supplier's protocol in the QIAGEN Plasmid Purification Handbook.

Day 1

Prepare bacterial culture

For high yields of pure DNA (~2.5mg), 500ml of LB culture are needed for high copy-number plasmids.

LB broth (per Liter): 10 g bacto-tryptone, 5 g Bacto-yeast extract and 10 g NaCl. The mixture of the materials in the list needs to be autoclaved immediately after adding the right amount of water.

Day 2

- 1. Prepare a starter culture** by inoculating 10µl from a bacterial frozen stock stored in 10% DMSO at -70°C (prepared by Dr. Xiaohong Lu) into 2–10 ml LB medium containing the appropriate antibiotic (Ampicillin 50µg/ml). Grow at 37°C for approximately 5 hours with vigorous shaking (~300 rpm).
- 2. Dilute the starter culture 1/500 to 1/1000 into a larger volume of selective LB medium.**

A flask that is at least 5 times the volume of culture will be needed to ensure sufficient aeration.

A larger culture volume than recommended in the protocol should not be used, as it will produce too many cells that will result in inefficient lysis and reduce the quality of the preparation.

3. Grow the culture at 37°C with vigorous shaking (~300 rpm) for 12–16 h.

Growth for 12–16 h corresponds to the transition from logarithmic into stationary growth phase, when cell density is high ($3\text{--}4 \times 10^9$ cells per ml) and RNA content of cells is low.

The growth of cultures is dependent on factors such as host strain, plasmid insert and copy number, and culture medium.

Day 3

1. Harvest the bacterial culture by centrifugation at 6000 x g for 15 min at 4°C.

Remove all traces of the supernatant. The cells will then be ready for the lysis procedure.

The procedure may be stopped at this point and continued later by freezing the cell pellets obtained by centrifugation. The frozen cell pellets can be stored at -20°C for several weeks.

2. Re-suspend the bacterial pellet in 50 ml of Buffer P1.

For efficient lysis it is important to use a vessel that is large enough to allow complete mixing of the lysis buffers.

A 500 ml bottle is recommended for large scale (Mega) preparations.

Ensure that the RNase A has been added to Buffer P1 to give a final concentration of 100 µg/ml. The bacteria should be resuspended completely by vortexing or pipetting up and down until no cell clumps remain.

- 3. Add 50 ml of Buffer P2, mix thoroughly by vigorously inverting 4–6 times, and incubate at room temperature for 5 min.**

Vortexing should be avoided at this stage, as this may result in excessive shearing of bacterial genomic DNA, which may cause difficulties in later separation from plasmid DNA. The lysate should appear viscous. The lysis reaction should not be continued for more than 5 min. After use, the bottle containing Buffer P2 should be closed immediately to avoid acidification of Buffer P2 from CO₂ in the air.

- 4. Add 50 ml of chilled Buffer P3, mix immediately and thoroughly by vigorously inverting 4–6 times, and incubating on ice for 30 min.**

Precipitation is enhanced by using chilled Buffer P3 and incubating on ice. After addition of Buffer P3, a fluffy white material forms and the lysate becomes less viscous. The precipitated material contains genomic DNA, proteins, cell debris, etc. The lysate should be mixed thoroughly to avoid localized potassium dodecyl sulfate precipitation.

- 5. Centrifuge at $\geq 20,00 \times g$ for 30 min at 4°C. Collect supernatant containing plasmid DNA promptly.**

Before loading the centrifuge, the sample should be mixed again. Centrifugation should be performed in 250 ml or 500 ml non-glass tubes (e.g., polypropylene).

Note: Instead of centrifugation, steps 7 and 8 can be applied.

6. The lysate can then be efficiently cleared by filtration using a paper filter (e.g. Whatman Grade 2V 8µm, Cat. 1202-240).

7. Equilibrate a QIAGEN-tip 2500 by applying 35 ml Buffer QBT, and allow the column to empty by gravity flow.

Flow of buffer will begin automatically by reduction in surface tension due to the presence of detergent in the equilibration buffer. Allow the QIAGEN-tip to drain completely. QIAGEN-tips can be left unattended, since the flow of buffer will stop when the meniscus of the solution reaches the upper frit in the column.

8. Apply the supernatant from step 8 to the QIAGEN-tip and allow it to enter the resin by gravity flow.

The supernatant should be loaded onto the QIAGEN-tip promptly. If it is left too long and becomes cloudy due to further precipitation of protein, it must be centrifuged again or filtered before loading to prevent clogging of the QIAGEN-tip.

9. Wash the QIAGEN-tip with a total of 200 ml Buffer QC.

Allow Buffer QC to move through the QIAGEN-tip by gravity flow. The first half of the volume of wash buffer is sufficient to remove all contaminants in the majority of plasmid DNA preparations. The second half is particularly necessary when large culture volumes or bacterial strains producing large amounts of carbohydrates are used.

10. Elute DNA with 35 ml Buffer QF.

Use of polycarbonate centrifuge tubes for collection is not recommended as polycarbonate is not resistant to the alcohol used in subsequent steps.

- 11. Precipitate DNA by adding 24.5 ml (0.7 volumes) room-temperature isopropanol to precipitate the eluted DNA. Mix and centrifuge immediately at $\geq 15,000 \times g$ for 30 min at 4°C. Carefully decant the supernatant.**

All solutions should be at room temperature in order to minimize salt precipitation, although centrifugation is carried out at 4°C to prevent overheating of the sample.

Alternatively, disposable conical bottom centrifuge tubes can be used for centrifugation at $5000 \times g$ for 60 min at 4°C. Isopropanol pellets have a glassy appearance and may be more difficult to see than the fluffy, salt-containing pellets that result from ethanol precipitation. Marking the outside of the tube before centrifugation allows the pellet to be more easily located. Isopropanol pellets are also more loosely attached to the side of the tube, as a result, care should be taken when removing the supernatant.

- 12. Wash DNA pellet twice with 1 ml of room-temperature 70% ethanol, and transfer into an eppendorf tube. Centrifuge at $\geq 15,000 \times g$ for 10 min, then carefully decant the supernatant without disturbing the pellet.**

Alternatively, disposable conical-bottom centrifuge tubes (not supplied) can be used for centrifugation at $5000 \times g$ for 60 min at 4°C. The 70% ethanol removes precipitated salt and replaces isopropanol with the more volatile ethanol, making the DNA easier to be re-dissolved.

- 13. Air-dry the pellet for 10–20 min, and re-dissolve the DNA in a suitable volume of basic buffer (e.g. 1×Tris-EDTA buffer, pH 7.4 or 10 mM Tris-Cl, pH 8.5).**

Re-dissolve the DNA pellet by rinsing the walls to recover the entire DNA, especially if glass tubes have been used. Pipetting the DNA up and down to promote re-suspension may cause shearing and should be avoided. Over drying the pellet will make the DNA difficult to re-dissolve. DNA dissolves better under slightly alkaline conditions; it does not easily dissolve in acidic buffers.

- 14. Determination of yield.**

To determine the yield, DNA concentration should be determined by a nanodrop spectrophotometry at 260 nm. For reliable spectrophotometric DNA quantification, Absorbance reading at 260nm (A_{260}) readings should lie between 0.1 and 1.0; and a ratio of A_{260}/A_{280} should ideally be reach approximately 1.8.

- 15. Dilute plasmid DNA to 1 µg/ml with deionized water and stored at -20°C for ELISA assay.**

Reproduced based on QIAGEN Plasmid Purification Handbook.

2.1.3 Compound Sample Preparation

Due to the limitation of low aqueous solubility of the compounds, they were dissolved in 100 % DMSO to make up an initial stock concentration of 10 mM, and then diluted in DMSO to 2 mM and 400 µM. The compounds were screened at final concentrations of 20 µM, 100 µM and 500 µM, respectively. After calculating the

approximate IC₅₀ range of the antagonists based on the initial three concentrations, three lower concentrations may be determined, which should be around the IC₅₀ value, and the detailed IC₅₀ results can be obtained thereafter.

To make 10 mM concentration compound solution:

Volume (μl) = Weight (mg) x 100 / Molecular Weight of the compound

Then dilute it into the required lower concentration solutions before the experiment and the sample's final concentration is 1/20 of the working stock in each well of the plate.

To make β-IP3 peptide solution:

Dissolve β-IP3 peptide powder in DMSO to make 20 mg/ml Stock.

Add the same volume of phosphate buffered saline (PBS) in above stock and make 10 mg/ml. Store in -80 C.

To make working solution 0.1μg/μl:

Add 10μl of 10 mg/ml stock into 990μl PBS.

2.1.4 ELISA Protocol

For the convenience of describing the ELISA method, the flow chart ([Figure 2. 3](#)) was designed to illustrate the procedure of ELISA for MDM2 antagonists screening, and the procedure for MDMX antagonists screening was almost the same.

2.1.4.1 *In Vitro* Transcription/Translation Reaction

The coupled transcription/translation system using the TNT[®] Rabbit Reticulocyte Lysate system (Promega) was used for the *in vitro* production of the full length MDM2/MDMX protein.

2.1.4.2 Components of TNT[®] Rabbit Reticulocyte Lysate System

The reaction components (Table 2. 1) were put together in a 5 ml universal (Bijou, Sterilin); mixed gently using a vortex and incubated in 100 μ l aliquots in microfuge tubes for 2 hours at 30 °C. The human MDM2/MDMX sequence was cloned in a pCR3 plasmid (Invitrogen) by Iakovos Sigalas (175) and was used at the concentration of 1 μ g/ μ l. Following incubation the microfuge tubes were removed and stored at -20 °C for the ELISA procedure illustrated in the followed flow charts.

Table 2. 1 Coupled Transcription/Translation Components

Components	MDM2 protein preparation		MDMX protein preparation	
	Volume per reaction (μ l)	Volume per Promega pack (μ l)	Volume per reaction (μ l)	Volume per Promega pack (μ l)
T7 Buffer	1.0	80	1.0	80
T7 RNA polymerase	0.5	40	0.5	40
Amino acid mixture	1.0	80	0.5	40
RNasin	0.5	40	0.5	40
Plasmid DNA (1 μ g/ μ l)	2.0	160	0.5	40
Nuclease free water	9.5	750	9.5	760
Reticulocyte Lysate	125	1000	125	1000

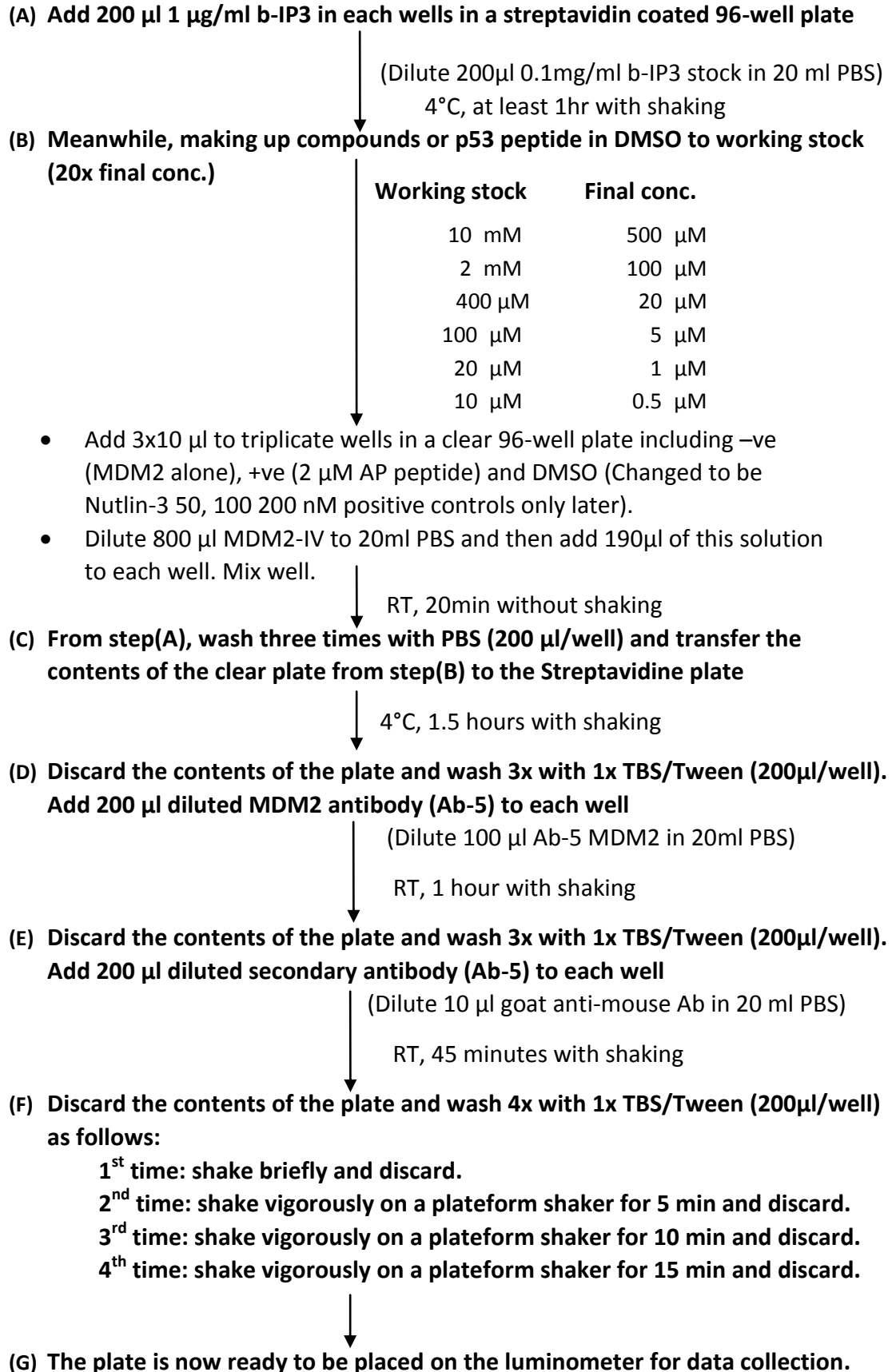


Figure 2. 3 The ELISA Flow Chart for MDM2 Inhibitors Screening

2.1.4.3 Data Analysis

Using Microsoft Office EXCEL software:

The plate layout should already be saved in an Excel file.

1. Cut and paste the RLU results from the luminometer onto the same page as the plate layout.
2. On the same page set out a table with the well contents down the side, as below:

	<u>Mean RLU</u>	<u>SE</u>	<u>% complex formation</u>	<u>% inhibition</u>
5% DMSO				
Positive Control				
NU8354				
NU8355				
.....				

Greater % inhibition = greater compound activity

3. Tools – Data analysis – Descriptive statistics – Highlight cells containing data to be averaged (eg. 4 results for control wells, or 3 results for a specific compound)
– Summary Statistics – Click box for Output range – Press OK twice – Move the Mean RLU and SE results to the correct place in the above table
4. Calculate % complex formation for DMSO using the following equation:

$$= \text{DMSO RLU} / \text{MDM2 RLU} * 100$$

$$\text{eg.} = \text{B2/A2} * 100$$

5. Calculate % complex formation for the compounds as follows:

% complex formation = Compound RLU/type in number for DMSO RLU * 100

Drag this down to calculate all the compound results

6. Calculate % inhibition as follows:

% inhibition = 100 - % complex formation

Drag this down to calculate all the compound results

7. Highlight the columns of results – Format – Cells – Number – 1 decimal place
8. Go to Chart Wizard – Bar chart by rows - Highlight the Mean RLU's & Headings –

Click on each bar in turn – right click – Format data series – Y error bars –

Custom – Highlight SE box in table

This will give a bar chart including error bars

Using GraphPad PRISM v 4.0 statistical software (San Diego, CA, USA):

Point to Point Analysis (for compounds' general IC₅₀ validation based on 3 concentrations evaluation)

1. In the 'X' column enter 0, 20, 100 & 500 (the compound concentrations)
2. In the 'Y' column enter the % inhibition values for the compound at each concentration, as calculated by Excel. Put 50 in the box below this list of values as this is to be calculated
3. Select Analyse – Curves & Regression – Fitspline/LOWESS - OK
4. Select Point to point – Show the table XY co-ordinates – Standard X from Y - OK
5. Select View – Standard curve X from Y. This will show the IC₅₀ value for the compound

Non-linear Regression (for compounds' refined IC₅₀ validation and dose-dependent curve formation based on 8 or 9 concentrations evaluation)

1. In the 'X' column enter the log of the concentrations
2. In the 'Y' column enter the % inhibition values for the compound, but do not include the 50 at the bottom of this column
3. Select Analyse – Non-linear regression – Sigmoidal dose response – Constants, top = 100, bottom = 0 – Unknowns from standard curve - OK
4. This will give a slightly different IC₅₀ from the Point to point analysis.

In brief, the MDM2 inhibition at a given concentration was calculated by taking into account the effect of the DMSO control on the percentage of IP3-MDM2 complex formation, and evaluated using the following formula: (RLU detected in the compound treated sample / RLU of DMSO controls) x 100 and hence the percentage of MDM2 inhibition is 100 minus the value from previous formula.

The IC₅₀ for each isoindolin-1-one compound was calculated from 3 concentrations where each concentration was tested in a triplicate. The quoted IC₅₀ for each compound was calculated by using Prism Graph-pad (point-point analysis). The final IC₅₀ value is the average of three independent experiments, and hence a standard error (SE) was also generated.

2.2 Tissue Culture

2.2.1 Cell Lines

The cell lines used in experiments included the osteosarcoma cell line SJSA-1 with *MDM2* amplification and wt-p53, the neuroblastoma cell line NGP with *MDM2* amplification, wt-p53 and MDMX expression, and the isogenic matched colorectal cancer cell line pair HCT116_{p53+/+} and HCT116_{p53-/-}.

All cell lines used in this study were previously confirmed as being *mycoplasma* negative using the Mycoalert Elisa Method (carried out by Mrs Elizabeth Matheson).

All tissue culture was carried out using aseptic technique in class II containment hoods (Biomat, Medair Technologies). The growth media was made in a sterile environment and PBS was made up using sterile filtered H₂O and autoclaved prior to use. All surfaces and equipment were swabbed with 70 % Ethanol. The *MDM2*, p53 status and doubling times of all the cell lines used in the current study are summarized in [Table 2. 2](#).

Table 2. 2 Original Cell lines applied for the experiments

Cell line	MDM2 status	P53 status	Doubling time (hours)	Reference	Extra information
SJSA-1	Amplified	WT	24	(3)	
NGP	Amplified	WT	53	(176)	Express MDMX
HCT116+/+	None-amplified	WT	24	(177-178)	
HCT116-/-	None-amplified	Knock out	24	(179)	

2.2.2 Cell Culturing

The NGP, HCT116_{+/+} and HCT116_{-/-} cell lines were grown in RPMI 1640 medium (Sigma) supplemented with 10 % foetal bovine serum (FBS, Sigma) and the SJSA-1 cell line was also supplemented with a further 1 % (v/v) HEPES buffer (Sigma), 1 % (v/v) sodium pyruvate (Sigma) and 1.25 g/500 ml glucose (Sigma), then all of them were kept in a humid atmosphere at 37 °C containing 5 % carbon dioxide in the incubator (Incu Safe, Sanyo).

Cell lines were maintained in flat-sided flasks (Corning) of various sizes (growth surface areas of 25 cm², 75 cm² and 175 cm²) with appropriate amounts of medium. Cells were sub-cultured once a week into fresh medium.

2.2.3 Sub-culturing

To sub-culture adherent cells, the medium was aspirated and cells washed in PBS to remove any remaining medium. Cells were then treated with a Trypsin-PBS-EDTA solution (see Appendix II) for between 2-5 minutes in 37 °C incubator in order to detach cells from the growth surface. In the case of the HCT116 cell lines, the detached cells were passed through a plastic syringe (Sterilin) with a 23 G needle in order to separate the cells. Then 8 ml fresh growth media was added into the flask to neutralize the trypsin and the cells were counted using a haemocytometer. Cells were then re-cultured, frozen down or used in experiments, keeping a note of the passage number every time.

2.2.4 Counting Cells

A 20 µl solution containing equal amounts of harvested cell suspension and Carnoy's fixative (see Appendix II) was pipetted from the top edge of the chamber of the haemocytometer (Neubauer assistant, BDH), under the coverslip and the cells were counted. The haemocytometer had 2 grids for scoring cells and each grid was 1mm² (area) x 0.1 mm (depth), with a total volume of 0.1 mm³. Cells within each grid were counted under a light microscope (Teitz). The average number of cells scored from the two grids was calculated (n). The concentration of the cells in the solution was equal to 2 (n x 10⁴). This takes into account the 1:2 dilution of the cell suspension with Carnoy's solution.

2.2.5 Cell Storage and Cryopreservation

The cells were trypsinised and counted as described in the previous section. The cells were initially made into pellets by centrifugation at 1,000 rpm in a Beckman-Coulter Allegra X-12R benchtop centrifuge at 23 °C for 5 minutes, followed by aspirated of the medium and then re-suspended in freezing medium composed of 8 ml of full culture medium (10 % FBS), 1 ml of cryoprotective agent DMSO (Sigma, Tissue culture grade, 10 % final concentration), and 1 ml FBS (20 % final concentration). Approximately about 5 x 10⁵ cells were aliquoted into a cryo-vial (1-1.5 ml). The vials were initially stored at -20 °C and then transferred into a -80 °C freezer or even liquid nitrogen for long-period storage.

2.2.6 Thawing Cells

Freezing vials were removed from liquid nitrogen and thawed in a 37 °C water bath for less than 30 seconds. The thawed cell suspension was then transferred into a sterile universal tube (Sterilin) containing 5 ml of pre-warmed medium. The cells were then collected into a pellet by centrifugation for 3-5 minutes at 1,500-2,000 rpm and the supernatant was removed by aspirating. Finally, the cells were then re-suspended in 5 ml of fresh medium, transferred to a 25 cm² culture flask (Corning) and kept in humid atmosphere at 37 °C containing 5 % carbon dioxide in the incubator (Incu Safe, Sanyo).

2.2.7 Plating out cells

Adherent cells were trypsinised and counted as described above. For irradiation experiments, 28 cm² tissue culture dishes were used (Corning). 5x 10⁵ cells were plated per dish with 5 ml of growth media. Cell plates were then incubated for 48-72 hours until 70% confluent before irradiation experiments.

2.3 Western Blotting

Western blotting is a technique by which a sample of proteins is separated by gel electrophoresis and then transferred to a binding membrane (immobilizing matrix) enabling characterization, identification and quantification of the proteins of interest.

2.3.1 Basic Principles of Western Blotting Assay

Western blotting determines the level of protein expression in a sample and comprises 3 main steps: 1) electrophoresis using sodium dodecyl sulphate polyacrylamide gel electrophoresis (SDS-PAGE) to separate proteins according to size; 2) transfer to a nitrocellulose membrane; and 3) antibody detection of the immobilised proteins.

The electrophoresis step separates proteins depending on molecular weight. Proteins are completely denatured during this process through boiling the protein lysate with detergent (SDS) and the reducing agent β -mercaptoethanol. The reducing agent is used to break disulphide bonds within the protein. The use of reducing conditions means that proteins are separated only on size but not on the size/charge ratio that occurs under non-denaturing conditions. On the SDS gel, when an electric field is applied, smaller proteins move faster than bigger ones. In these experiments, protein sizes ranged from 14 KDa to 110 KDa and 4-20 % acrylamide tris-glycine gradient gels were used to give good separation and resolution across the range of protein sizes.

The separated proteins were then transferred onto a nitrocellulose membrane electrophoretically.

Proteins were detected using primary antibodies that recognize specific proteins.

Secondary antibodies were conjugated to horseradish peroxidase (HRP) for use with

the enhanced chemiluminescence (ECLTM) detection kit (Amersham) and then visualized by using an X-ray film.

2.3.2 Cell Seeding into Culture Plates and Drug/IR Treatment

2.4.2.1 Plating out Cells

To seed plates for drug treatment or irradiation, cells were taken from a 3 day old flask, which were exponentially growing, and adherent cells were trypsinised and counted as described in Section 2.3. Then the cells were plated into 28 cm² tissue culture dishes (Corning) with a final volume of 5 ml in growth media with the concentration displayed in [Table 2. 3](#).

Table 2. 3 Cell lines seeding densities applied for the experiments

Cell line	Seeding density
HCT116 & HCT116-/-	5 x 10 ⁵
NGP & NGP MDM2 Antagonists Resistant Clones	5 x 10 ⁵
SJSA-1 & SJSA-1 MDM2 Antagonists Resistant Clones	2 x 10 ⁵

Cell plates were then incubated for 48-72 hours until 70 % confluent before experiments.

2.4.2.2 Drug Treatment

Compounds were taken forward for intact cell studies if the IC₅₀ in the cell-free ELISA was <1μM. For evidence of intact cell activity by Western blot analysis of p53, MDM2 and p21, the initial dose range tested was 5, 10 and 20μM.

Lower doses were tried subsequently depending on the observed initial effect.

For example, Nutlin-3 was used at final concentrations in dishes of 0.2, 1 and 5 μM in 1 % DMSO, from stock concentrations made up in 100 % DMSO:

0.5 mM 100 % DMSO \longrightarrow 30 μl in 3 ml dish = 5 μM final Concentration at 1 % DMSO.

0.1 mM 100 % DMSO \longrightarrow 30 μl in 3 ml dish = 1 μM final Concentration at 1 % DMSO.

20 μM 100 % DMSO \longrightarrow 30 μl in 3 ml dish = 0.2 μM final Concentration at 1 % DMSO.

2.4.2.3 X-ray Irradiation

After seeding cells into plates and incubating for 48 hours, the sample plates were put into a D3300 X-ray System cabinet and just below the X-ray tube (within the shaded area in [Figure 2. 4](#)) and exposed to 6.3 Gy X-ray irradiation treatment, then put back into an incubator until each time point of testing.

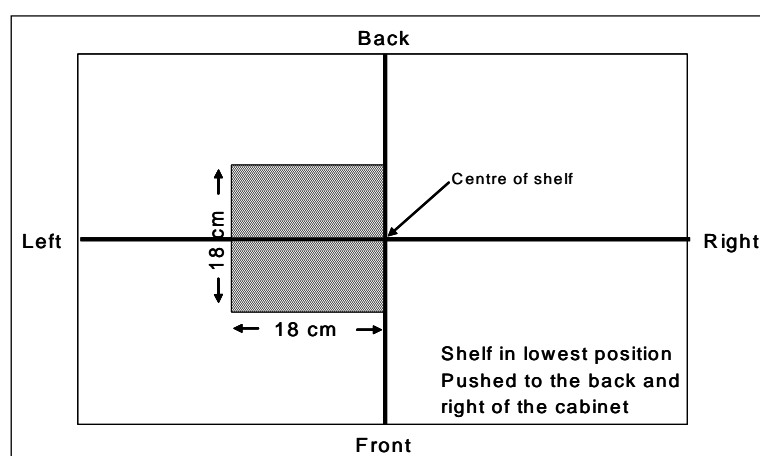


Figure 2. 4 Sample plate placing area for X-ray irradiation treatment

NB: In order to irradiate samples within the cabinet they must be placed below the X-ray tube on the metal shelf. The shelf must be positioned as far to the back and to the right of the cabinet as it will go in. In this position, the cross on the shelf identifies the centre of the cabinet. With the shelf in the lowest position a square area measuring 18 cm x 18 cm receives uniform amounts ($\pm 5\%$) of radiation at all points within this square. The square is positioned to the centre (back to front) and left (as viewed from the front of the cabinet). This area is marked as a hashed square on the shelf (The fact that it is not central is because the X-ray beam is not truly perpendicular).

2.3.3 Collecting Cell Lysate

At each time point, the medium was removed from the dish and the attached cells rinsed with ice cold PBS before adding 50 μ l of a Laemmli lysis buffer (see Appendix II) to the 2 ml plate with approximately 7.5×10^5 cells.

Whole cell extracts were prepared by scraping adherent cells from the bottom of the dishes using cell scrapers (Sterilin) and lysis buffer, then pipette into 0.5 ml eppendorf tubes. The samples were then boiled for 10 minutes at 100 °C before sonicating for 3 x 15 seconds at maximum power. The protein lysate samples were then stored at -20 °C.

2.3.4 Protein Estimation

The protein estimation assay was carried out on the lysates to calculate and decide the amount of protein to load on the gel. Generally, for SJSA-1 cells 20-30 μ g was loaded per sample track, and for other cell lines 35-50 μ g was loaded.

The protein concentrations of the cell lysates were estimated using a protein concentration estimation assay with a BCA kit (Pierce) in a 96-well plate format (Figure 2. 5).

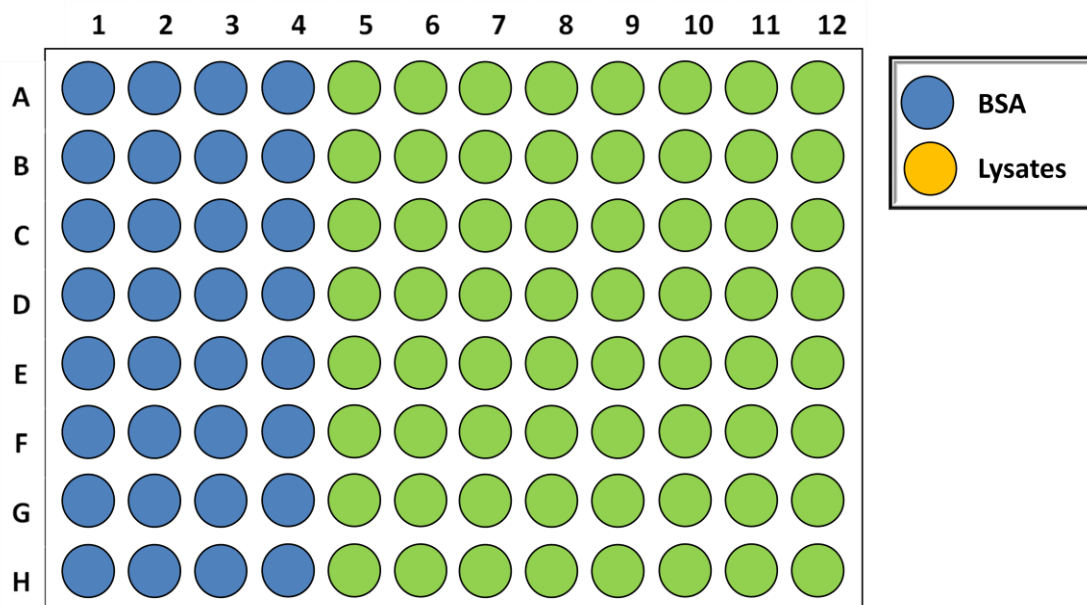


Figure 2. 5 Plate arrangements for BCA assay

Bovine Serum Albumin (BSA) was used as a reference standard at 0.2, 0.4, 0.6, 0.8, 1.0, 1.2 and 2.0 mg/ml were used. Samples were diluted from 2 mg/ml using double distilled H₂O (*ddH*₂O) and plated out in 10 µl volumes in quadruplets along with a *ddH*₂O blank into a 96 well plate to produce a standard curve that the concentration of the lysates samples would fall on. The cell lysates were diluted 1:10 with *ddH*₂O and plated out in quadruplicate.

BCA Reagent A and B were combined in a ratio of 50:1 and 190 µl of the mixture added to each well and mixed on a plate shaker for 1 minute at room temperature.

The plate was then covered in cling film and incubated at 37 °C for 30 minutes followed by absorbance reading at 562 nm on a Spectra Max Pro 400 plate spectrophotometer (Molecular Devices). The protein concentration of each sample was calculated from the standard curve using Genesis life software.

2.3.5 Gel Electrophoresis of Protein (SDS-PAGE)

Sodium Dodecyl Sulphate Polyacrylamide Gel Electrophoresis (SDS-PAGE) is a technique used for the analysis of proteins which enables both an estimation of polypeptide molecular mass as well as high-resolution analysis of a complex mixture of proteins.

Following protein estimation, 20-50 µg of protein was diluted in SDS loading buffer (if non-ionic detergent was used to lyse cells, see Appendix) or a 1:1 ratio of bromophenol blue and beta-mercaptoethanol (if SDS buffer was used) and made up to a maximum volume of 25 µl, which was suitable for 1.5 mm, 15 wells, pre-cast 4-20 % gradient tris-glycine Polyacrylamide gel (Invitrogen). This mixture was then heated at 100 °C for 10 minutes, followed by brief centrifugation before loading onto the gel. 10 µl of SeeBlue™ (Invitrogen) pre-stained protein molecular weight standards were run on each gel in parallel to the test cell lysate samples. Gel electrophoretic separation was carried out in a Novex XL tank (Invitrogen) containing 1 x electrophoresis buffer containing SDS at 180 V for 90 min.

2.3.6 Protein Transfer

Western-blotting was performed by filling a BioRad mini-blot electrophoresis tank (Novex) with transfer buffer (see Appendix II).

Two pieces of glass fibre pads, two pieces of filter papers (the same size as the gel, Whatman 3MM Chr) and a piece of Hybond-C nitrocellulose membrane

(Amersham) was soaked in the transfer buffer. The following items were then assembled in order starting from the black side of the cassette as was illustrated in [Figure 2. 6](#): fibre pad, filter paper, gel, Hybond membrane, filter paper and fibre pad.

Then the entire apparatus will be placed into the chamber of the transfer tank that filled with transfer buffer by making the black side of the cassette face the black anode side. The transfer step was carried out at 30 V overnight or at 65 V for 1-1.5 hours.

One key thing needs to remember is to make sure there are no air bubbles between the gel and membrane when setting up the transfer cassette, as a result, this procedure can be carried out in a glass pan filled with transfer buffer or add some transfer buffer onto the surface of the gel then put the membrane onto it and push gently to remove air bubbles with excessive transfer buffer.

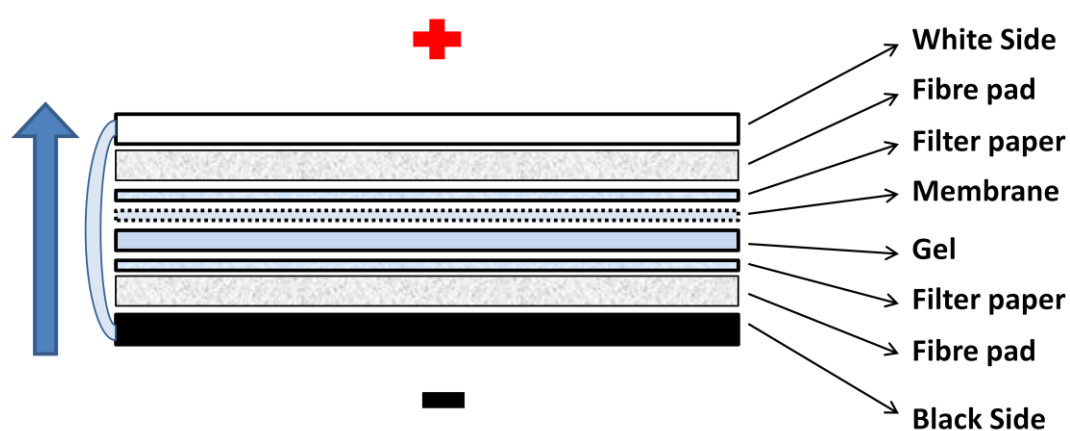


Figure 2. 6 Western blot cassette order illustration in transfer procedure

2.3.7 Immunodetection

The levels of various proteins including p53, MDM2 and p21^{WAF1}, etc. were measured using western blot analysis.

After the transfer procedure, the Hybond-C membrane was removed from the blotting cassette and incubated in 5 % non-fat milk TBS-Tween (PBST-M) solution (Appendix II) on a platform shaker for one hour at room temperature, followed by washing the membrane three times with 1 x TBS-Tween (15 minutes per wash). Then it was cut into three strips at 64 and 36 KDa based on the position to which protein molecular weight standards had migrated.

Then the primary antibodies ([Table 2. 4](#)) were diluted in 3 ml 5 % skimmed milk-TBS-Tween in a 50 ml Falcon tube. The membrane strips then been transferred into the tubes containing the appropriate primary antibodies. After that, these tubes were left on a roller for 1 hour at room temperature or overnight at 4°C. Every western blot membrane was probed with α -tubulin or β -actin as a control of sample loading and transfer.

The membrane was then washed three times with 1 x TBS-Tween (5 minutes per wash), at the same time, the secondary antibodies: HRP conjugated goat anti mouse IgG (Dako) or HRP conjugated goat anti rabbit IgG (Dako) were diluted 1:1000 in 3 ml 5 % skimmed milk-TBS-Tween solution. Then these membrane strips were incubated in 50 ml Falcon tubes containing the appropriate secondary antibody

solution on a roller for 45-60 minutes at room temperature. The final washing procedure of the membrane involves 6 washes with TBST (5 minutes per wash) before Enhanced Chemiluminescence (ECL) detection.

Table 2. 4 Details of Primary Antibodies Used for Western Blot

Protein	1st Antibody (Clone No.)	Type	Dilution	Band size in Western blot	Manufacturer
P53	P53 (DO7)	Mouse	1:1000	53 KDa	Novocastra
MDM2	MDM2 (IF2)	Mouse	1:100	90 KDa	Calbiochem
P21 ^{WAF1}	P21 ^{WAF1} (DF10)	Mouse	1:100	21 KDa	Calbiochem
MDMX	MDMX/MDM4	Rabbit	1:1000	70 KDa	Bethyl
PARP	PARP-1/2 (H-250)	Rabbit	1:1000	116, 85 KDa	Santa Cruz
α -Tubulin	α -Tubulin (DM1A)	Mouse	1:3000	55 KDa	Sigma-Aldrich
β -Actin	β -Actin (AC-40)	Rabbit	1:1000	42 KDa	Sigma-Aldrich
Cleaved Caspase-3	Cleaved Caspase-3 (Asp175)	Rabbit	1:1000	19, 17 KDa	Cell Signaling
PUMA	PUMA	Rabbit	1:1000	23 KDa	Cell Signaling

2.3.8 Enhanced chemiluminescence (ECL) detection

The ECL kit (Amersham) was used for indirectly detecting the amount of proteins by actually detecting secondary antibodies with the conjugated HRP (mechanism is illustrated in [Figure 2. 7](#)). The ECL kit contains solution A and B. They were mixed in a 1:1 ratio just before adding onto the washed membrane strips. The washed membrane strips were dabbed by using blue paper tissue to remove excess TBS-Tween, placed on cling film and then fully covered with the mixed ECL solution. After ~1 minute room temperature incubation, the excessive ECL solutions were removed and the membrane strips were covered with cling film and placed into an

X-ray cassette. Then X-ray film (Kodak or Super RX, Fuji) was used in the dark room by exposing it on the top of the membrane strips for various lengths of time, ranging from seconds to several minutes depending on the strength of the signal. Finally, the X-ray films were developed using a Mediphot 937 film developer (Colenta).

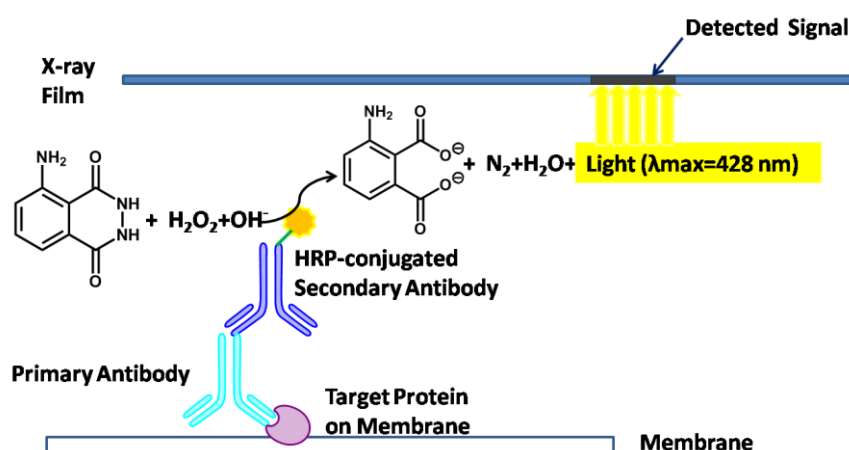


Figure 2. 7 Chemiluminescent Peroxidase Substrates for protein band detection

2.3.9 Densitometry analysis

In order to quantify the protein bands from western blotting, densitometry analysis was performed using Fuji-Las Pro (Fuji) to obtain images of western blot bands from the film. The AIDA image analyser programme software (Raytest) was then applied to estimate the size and densities of each band. The emission value of each protein band was recorded by considering its integrality, area and the background lightness. Obtained data were then normalized to the loading control of corresponding sample. The fold induction of proteins after various treatments were calculated based on untreated sample control for each experiment.

2.4 Sulphorhodamine B (SRB) Assay

The SRB assay was developed by Skehan *et al.* (180) as a simple method to assess the growth rate of cells with various treatments. It is based on the total amount of protein accumulating in the wells of a culture dish over a period of time.

2.4.1 Basic Principles of SRB Assay

Cells growing in a 96-well plate were fixed using trichloroacetic acid (TCA) and then were stained using SRB dye solution. The SRB dye binds to the basic amino acid residues of the fixed cells' proteins. Then the excessive SRB dye was washed away using 1 % acetic acid and air dried samples in the wells of the plates were re-suspended using 10 mM Tris base solution (pH 10.5) and the optical density of SRB bound proteins was evaluated at 564 nm, which gives a measure of the number of cells in each well.

2.4.2 96-well Plate Preparation for Growth Curve Evaluation

To prepare the 96-well cell sample plates for growth curve evaluation purpose, the 70 % confluent adherent cells were trypsinised and cell concentration were determined by cell counts using a haemocytometer (Section 2.2.4).

100 µl of a range of concentrations from 24,000 to 12 cells/well (with half cell density than the previous row for 12 rows) cell suspensions for each SJSA-1 series cell line was added into each well with the lay out shown in Figure 2. 8. 100 µl

medium/well were added into all outskirt wells surrounding the sample wells to prevent the evaporation effect that may affect the edge well samples.

Then the sample plates were incubated in a humidified incubator at 37 °C, 5 % CO₂ until each time point at which the plates were fixed. Plates were fixed at 24 hour intervals for 9 days in the relevant experiments.

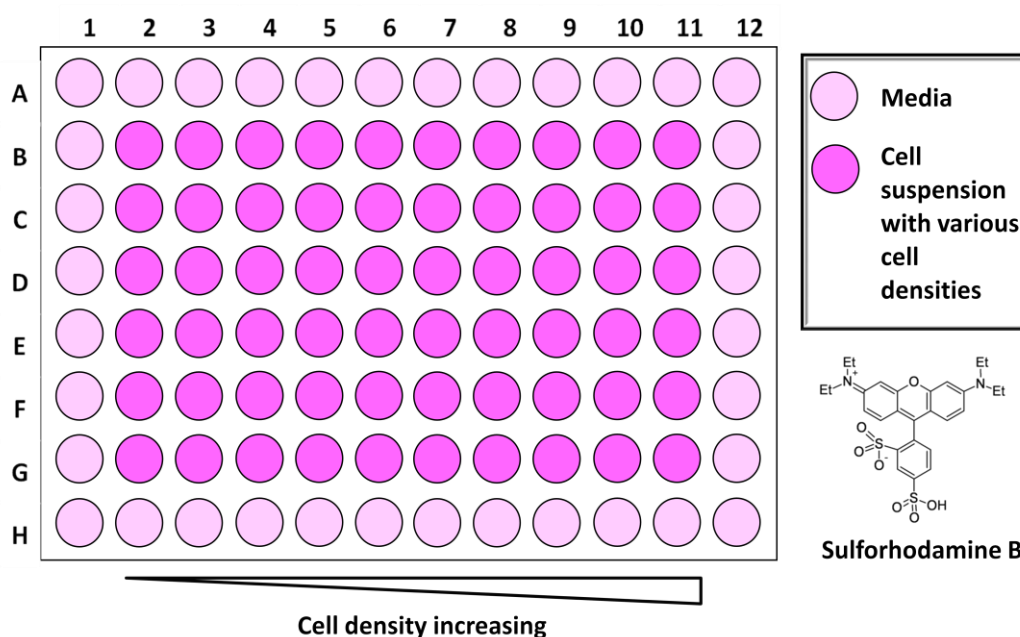


Figure 2. 8 SRB structure and SRB assay plate for growth curve determination

2.4.3 96-well Plate Sample Preparation for GI₅₀ Value Evaluation

To prepare the 96-well cell sample plates for growth curve evaluation, the 70 % confluent adherent cells were trypsinised and cell concentration were determined using a haemocytometer (Section 2.2.4). A 7 ml volume of 2×10^4 cells/ml cell suspension of SJSA-1 cells or 5×10^4 cells/ml cell suspension of NGP cells were prepared in 'Universal' tubes. Then 100 µl of cell suspension was added into each well and 100 µl media was added into each well surrounding the sample wells to

prevent the evaporation effect that can affect the edge well samples. For the Day 0 plate, seed one row of cell suspension and also add medium to the empty wells to avoid edge effects due to evaporation.

Then the sample plates were incubated in a humidified incubator at 37 °C, 5 % CO₂ for 24 hours to allow attachment and start growth, at which point plates would be ready for drug treatment.

After 24 hours incubation, Day 0 plates were fixed. For other plate samples that need 72 hours drug treatment, the medium was removed by vacuum aspiration, using a fine tipped glass pipette to minimize the possibility of losing cells, from the plates. Then 100 µl aliquots of fresh medium containing compound with a range of concentrations were added into each well (Figure 2. 9).

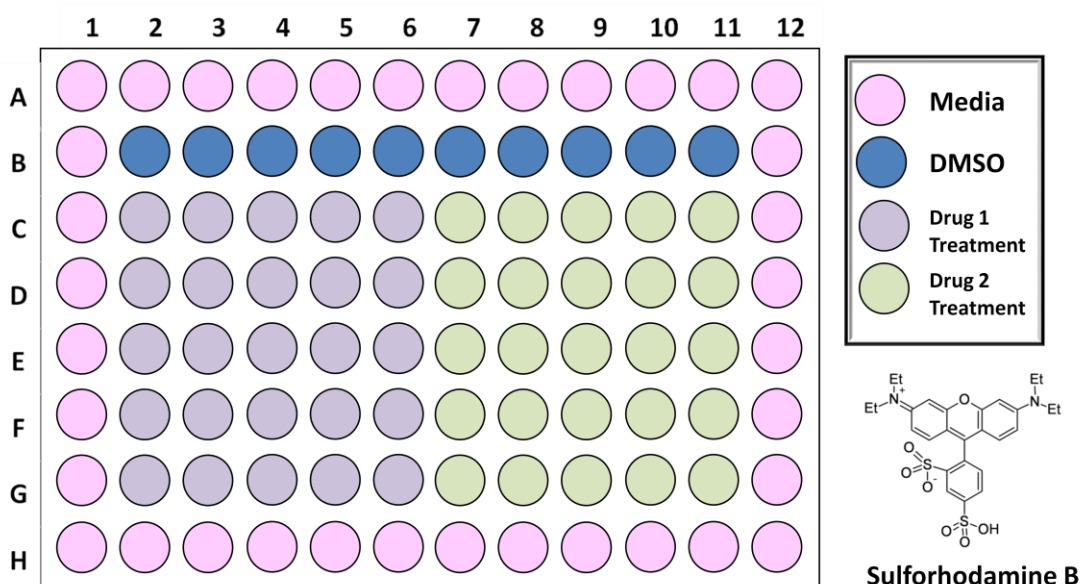


Figure 2. 9 SRB structure and SRB assay plate arrangement for GI₅₀ evaluation

The plates were then put back in the humidified incubator at 37 °C, 5 % CO₂ and incubated for 72 hours, then fixed.

2.4.4 Plate Fixation, SRB Staining and Data Collection

At the time point, plates were fixed *in situ* by adding 25 µl ice cold 50 % trichloroacetic acid (TCA) solution into each well and were stored at 4 °C for at least 1 hour.

Then the plates were put on the bench for 30 minutes to equilibrate to room temperature and the TCA solution was washed away using distilled water (dH₂O) for 5 times.

After air drying the plates, 100 µl SRB dye at 0.4 % (w/v) in 1 % acetic acid solution was added into each well of the plates and incubated at room temperature for 30 minutes.

After staining, unbound dye was removed by washing 5 times with 1% acetic acid and plates were air dried overnight.

Bound stain was solubilized with 10mM Tris base solution (pH 10.5) and absorbance was measured on a Spectra Max Pro 400 plate reader (96-well microtiter) at 570 nm. Data were then exported into an Excel file and analysed using Prism v 4.0 statistical software for GI₅₀ calculation. For growth curve generating, the optical densities were plotted using Microsoft Excel software.

2.5 Caspase-Glo® 3/7 Assay

Caspase-3 and caspase-7 are the members of the cysteine aspartic acid-specific protease (caspase) family that play key effector roles in mammalian cells apoptosis.

2.5.1 Basic Principles of Caspase-Glo® 3/7 Assay

The Caspase-Glo® 3/7 Assay is a luminescent assay that is designed to measure caspase-3 and -7 activities. The assay provides a luminogenic caspase-3/7 substrate, which contains the tetrapeptide sequence DEVD, in a reagent optimized for cell lysis, caspase activation and luciferase activation. By adding a single Caspase-Glo® 3/7 Reagent into an “add-mix-measure” format results in cell lysis, followed by the caspase cleavage of the substrate and the generation of a “glow-type” luminescent signal that produced by luciferase. Luminescence is proportional to the amount of caspase activity (Figure 2. 10).

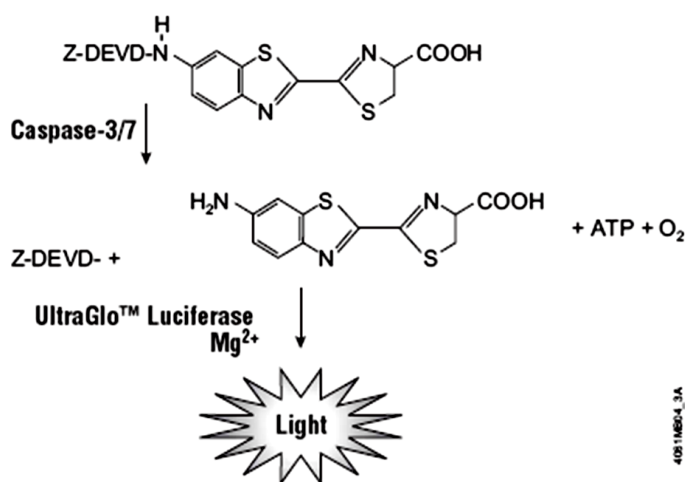


Figure 2. 10 The reactions and mechanisms of Caspase-Glo® 3/7 Assay

(From Technical Bulletin, Promega Part# TB323)

2.5.2 Cell Seeding

To seed plates for drug treatment, cells were taken from 3 day old flasks that were exponentially growing, and adherent cells were trypsinised and counted as described in Section 2.2.

SJSA-1 cells were seeded at 2×10^3 /100 μ l/well and NGP cells at 5×10^3 /100 μ l/well into four 96-well black/white plates (Wallac, PerkinElmer), to allow cells to reach at 25-50 % confluence on the day of drug treatment. To set up blank wells, medium alone was added into the first row of wells (Figure 2. 11).

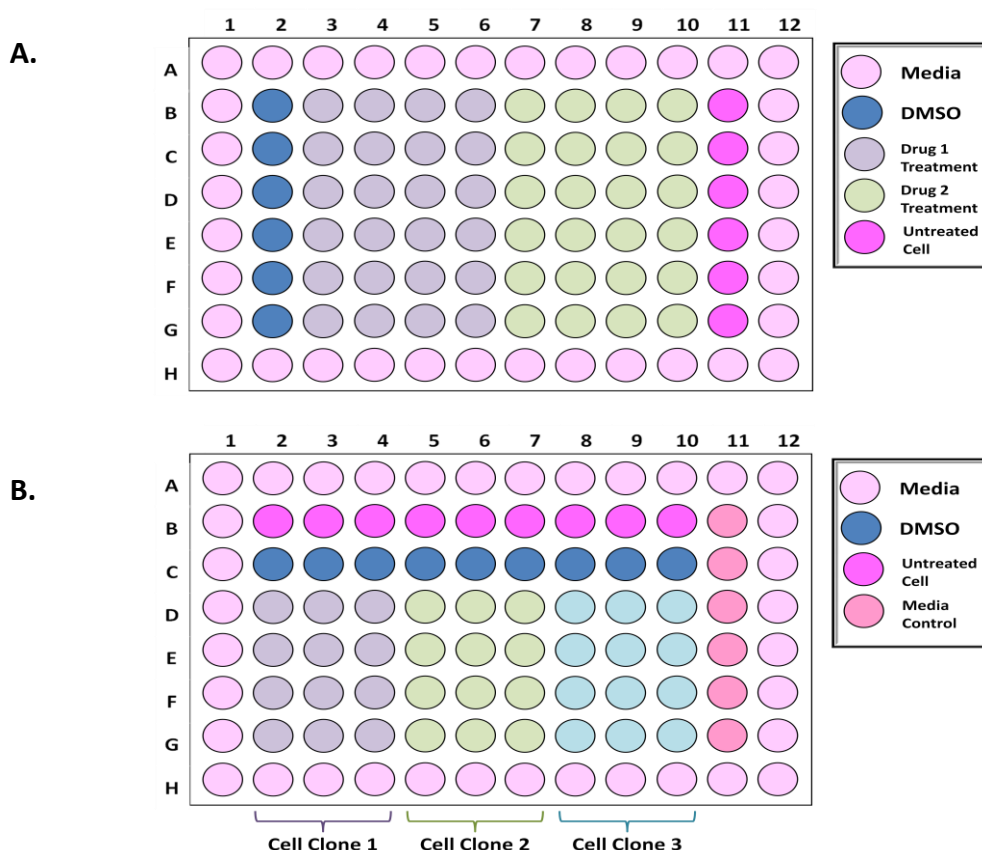


Figure 2. 11 The plate arrangements for Caspase-Glo® 3/7 Assay

(A. is for the comparison of different drugs using one cell line; and B. is for comparison of different cell lines treated with one drug).

2.5.3 Drug Treatment

Working concentrations (100×) were prepared for each compound (eg. Nutlin3, using 0.1 mM, 0.2 mM, 0.5 mM and 1 mM in DMSO):

Working concentration (100×)	Final concentration (1×)	volume
1 mM	40 µl 2 mM+40 µl DMSO 1 0 µM	20 µl in 2 ml medium
0.5 mM	40 µl 1mM+40 µl DMSO 5 µM	20 µl in 2 ml medium
0.2 mM	20 µl 0.5 mM +40 µl DMSO 2 µM	20 µl in 2 ml medium
0.1 mM	10 µl 0.5 mM+40 µl DMSO 1 µM	20 µl in 2 ml medium

For isoindolinone compounds, 100x concentrations of 0.1 mM, 0.5 mM, 1 mM and 2 mM in DMSO were used:

Working concentration (100×)	Final concentration (1×)	volume
2 mM	20 µl10 mM+80 µl DMSO 20 µM	20 µl in 2ml medium
1 mM	40 µl 2 mM+40 µl DMSO 10 µM	20 µl in 2 ml medium
0.5 mM	20 µl 2 mM+40 µl DMSO 5 µM	20 µl in 2 ml medium
0.1 mM	10 µl 0.5 mM+40 µl DMSO 1 µM	20 µl in 2 ml medium

Medium was aspirated from the 96-well plate and drug-containing medium added into the appropriate wells, including 1 % DMSO controls.

2.5.4 Caspase-Glo® 3/7 Assay

The plates were incubated at 37 °C for 48 hours.

At the time point, Caspase-Glo®3/7 Assay was performed by adding equal volumes of buffered Caspase-Glo®3/7 substrate (100 µl), followed by mixing and incubation at room temperature for 30 minutes to 3 hours. Then the luminescence value in each well were collected by using microplate luminometer (MicroLumatPlus LB96V, EG&G Berthold).

2.5.5 Data Analysis

The original data were generated by using Winglow (Berthold technologies) software and transformed into Excel version. Triplicate repeat assays were performed for each compound concentration, which allowed the calculation of an average and standard deviation of the result using Excel.

The average luminometer reading in relative light units (RLU) and standard deviations were used to calculate fold changes by dividing the RLU from drug treatment by the RLU from DMSO control.

2.6 Cell Cycle Analysis Using FACscan

Flow cytometers analyse the fluorescence and light scatter from cells in a flowing fluid stream passed through a fixed laser beam. Several measurements can be made based on the physical characteristics and labelling of the sample cells, which is represented by how the cells scatter light and emit fluorescence. This provides information about the cell size, internal complexity and relative fluorescence intensity. The distribution of cells with respect to their position in the cell growth cycle can be measured by using propidium iodide (PI) as fluorescent DNA stain.

2.6.1 Basic principles of fluorescence activated flow cytometry

The flow cytometer used in this project was a FACscan (Beckton Dickinson).

When samples of cells are analysed on the machine, they are forced into a single stream to pass through the flow chamber. This is achieved by passing a sample in the form of a single cell suspension through the flow chamber, where an argon laser beam excites the fluorescent PI dye that is bound to the DNA. The scattered fluorescent light generated by cells passing through the laser beam is collected by photo-detectors. Dichromatic mirrors at right angles of the laser beam reflect specific wavelength of light onto the detector ([Figure 2. 12](#)). Then this light signal is converted into an electronic signal that can be recorded ([181](#)). The FACscan can measure five parameters including: forward light scatter (FSC), side light scatter (SSC) and three fluorescence wavelengths (FL1, FL2 and FL3). For the cell cycle analysis using the PI staining method, the FSC, SSC and FL2 were used.

FACScan Optical Configuration

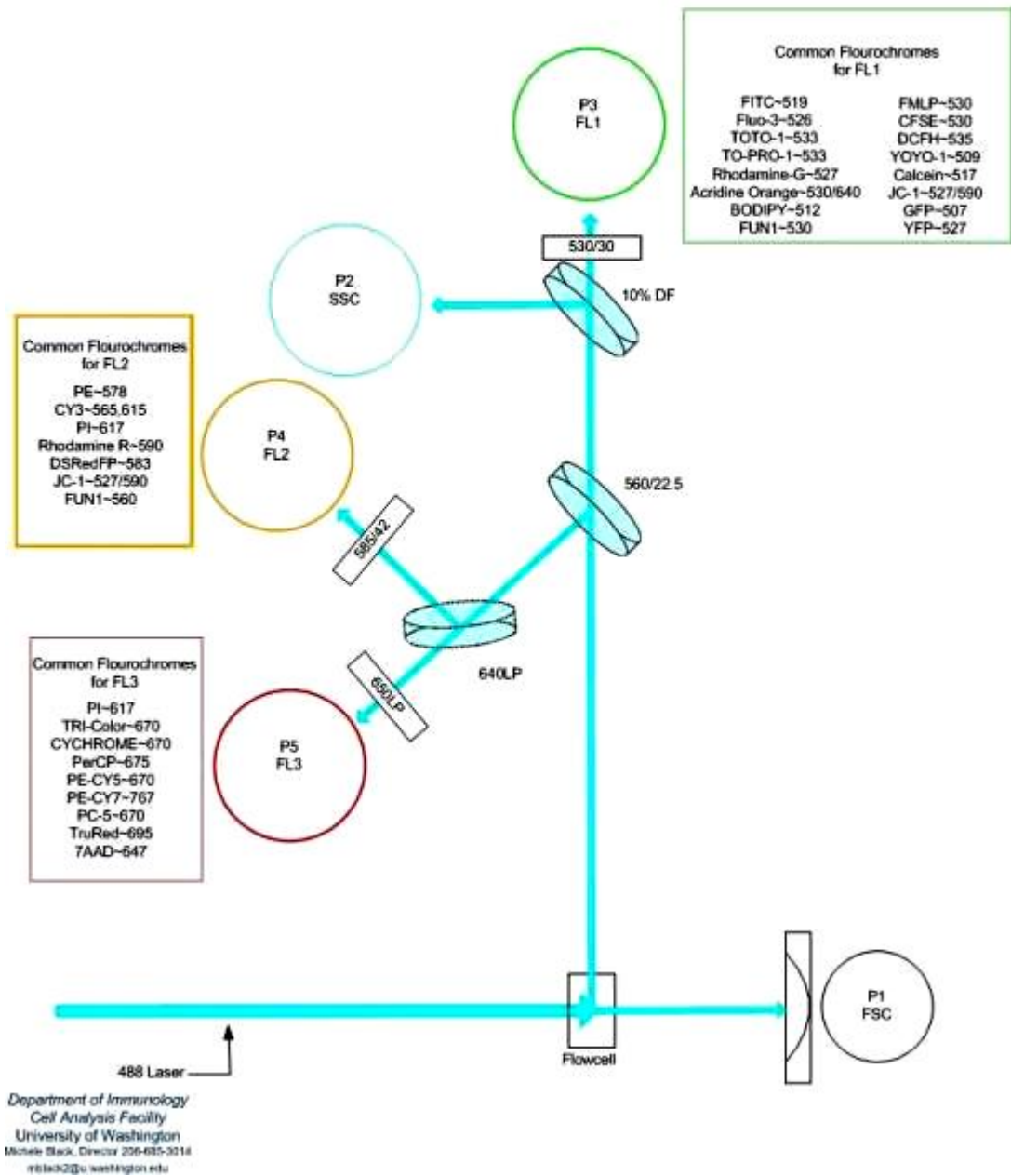


Figure 2. 12 FACscan optical configuration with the common fluorochromes list for each detector.

This figure is from jgc-wiki.igc.gulbenkian.pt/doku.php?id=uic:fl....

2.6.2 Apply Flow Cytometry for Cell Cycle Analysis

The phases of cell cycle are described in Figure 2. 13, cells undergoing mitosis or in G2 phase have doubled the DNA content of cells in G1 phase. Because the DNA is synthesized in the S phase, these cells have DNA content between G1 and G2.

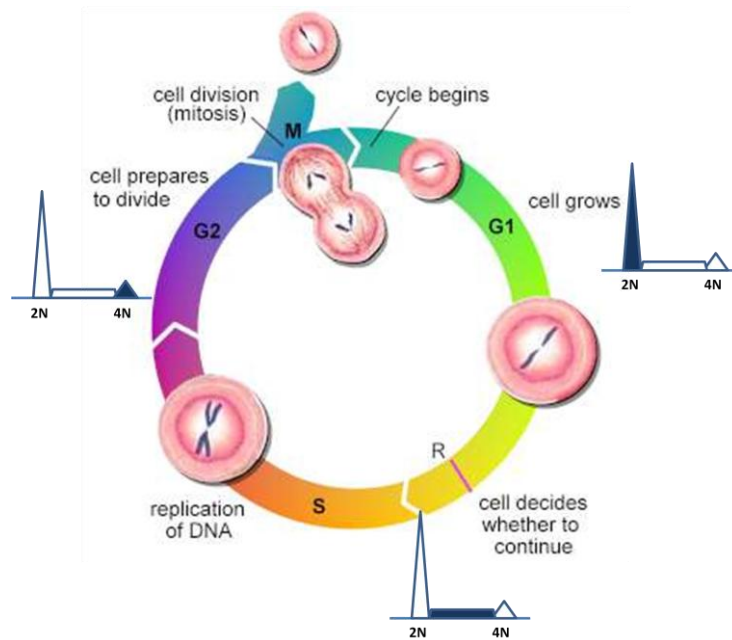


Figure 2. 13 A schematic of the cell cycle and cytometric components of each phase.

The cell cycle cartoon is from teachline.ls.huji.ac.il/.../substance_x/q2a.html. Within the cytometric components images, the component portion corresponding to each phase are highlighted in dark blue.

The DNA of cells undergoing apoptosis becomes fragmented and separates into apoptotic nuclei, which produce signal intensities below those corresponding to G1 phase cell DNA content. This is often referred to as the “sub-G1” peak. The differences in DNA contents can be detected by flow cytometry after PI staining because PI binds to the chromatin of cells by intercalating between the bases in DNA. Since double stranded regions of ribonucleic acid (RNA) can also bind PI, cell samples are treated with RNase to degrade all the RNA before or at the same time

of the PI staining procedure. It is also important to pass cell samples through a fine needle syringe several times to prevent cell clumping. Otherwise, the clumped cells will disturb the signal recording procedure and produce misleading results.

2.6.3 Protocol of cell cycle analysis assay

2.6.3.1 *Sample Preparation*

Cells were plated into 28 cm² tissue culture dishes and incubated for 48-72 hours until 70% confluent. Then they were treated by DMSO, drugs or X-ray irradiation. After 24 hours drug treatment or post irradiation, all cells in each dish were harvested and transferred into a Sterilin tube, spun down at 1,000 × g for 5 minutes, then washed by using ice cold PBS once. Then after spinning down at 1,000 × g for 5 minutes again, the supernatant was removed and cells were resuspended and fixed in 2 ml of ice cold 70 % ETOH/PBS solution and stored at 4° C for at least 2 hours.

2.6.3.2 *PI Staining*

In preparation for running cell samples on the Facscan, the fixed samples were spun at 1,000 × g for 5 minutes to remove the solution, then suspended in 800 µl PBS and passed through a 23 gauge syringe before adding 100 µl of 40 µg/ml PI and 100 µl 0.1 mg/ml RNase A and incubating at 37°C for ~0.5 hour, using aluminium foil to protect the samples from light.

2.6.3.3 Running Samples on FACscan

The measurements were carried out on a FACscan (Beckton Dickinson). To set up the template for a cell line, the control sample was run on the machine firstly. The SSC versus FSC, FL2-A versus FL2-W scatter plots and FL2-A histogram were used to evaluate the data collected. Ideally, the G1 peak was at 200 FL2-A and G2 peak at 400 FL2-A fluorescence intensity channels. The optimized setting for each cell line on the FACscan was saved as the specific named template for each cell line. For each sample, fluorescence data for 10,000 cells in total were collected. Each sample was run at least three times.

2.6.3.4 Data Analysis

FACscan data were analysed using WinMDI 2.8 software (TSRI). G1, S, G2/M and sub G1 populations defined and quantified by the gate method. The gated data were plotted as an FL2-A histogram and the proportion of cells in each phase was determined by defining them as section M1, M2, M3 and M4. Then the statistics function of the software calculated the percentage of cells in each phase.

2.7 PCR

2.7.1 Principle of Polymerase Chain Reaction (PCR)

PCR is a molecular biology technique, invented by Kary Mullis, for enzymatically replicating DNA without using a living organism, such as *E. coli* or yeast. Just like amplification using living organisms, the technique allows a small amount of DNA to be amplified exponentially in a sequence specific manner for a wide range of genetic applications including DNA mutation detection.

The purpose of a PCR is to make a huge number of copies of a gene, as illustrated in [Figure 2. 14](#). As Mullis has written in the Scientific American: "Beginning with a single molecule of the genetic material DNA, the PCR can generate 100 billion similar molecules in an afternoon. The reaction is easy to execute. It requires no more than a test tube, a few simple reagents, and a source of heat."

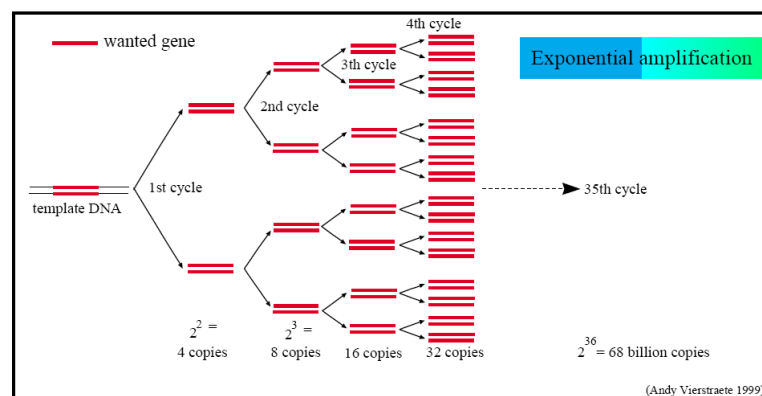


Figure 2. 14 The exponential amplification of the gene in PCR.

This figure is obtained from <http://users.ugent.be/~avierstr/principles/pcr.html>.

The reaction involves target DNA, properly designed sense and antisense primers, the four deoxyribonucleoside triphosphates (dNTPs) and a thermostable DNA

polymerase. There are three major steps in a standard PCR including denaturation, annealing and extension [Figure 2. 15](#), which are repeated for 30 to 40 cycles. This is carried out on an automated cycler that can heat and cool the tubes with the reaction mixture in a very short time.

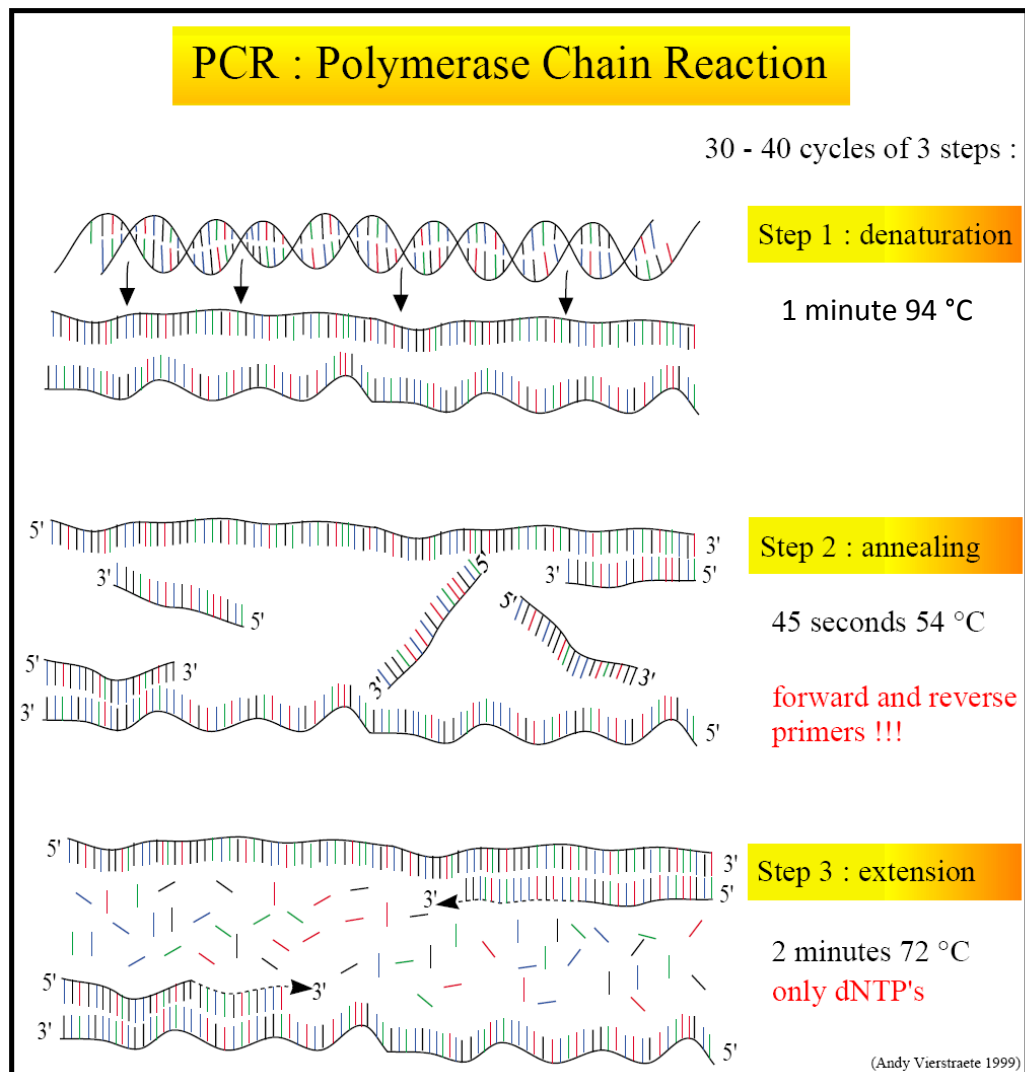


Figure 2. 15 Three steps of a Polymerase Chain Reaction.

This figure is adapted from information on <http://users.ugent.be/~avierstr/pdf/PCR.pdf>.

In the denaturation step, the sample is heated to ~94 °C to denature the double strand DNA into single stranded DNA for replication purpose, all enzymatic

reactions stop. With the temperature rapidly cooled down to ~54 °C, the primers are then annealed to the target DNA single stranded templates by forming ionic bonds with them. Then the polymerase can attach and starts copying the template. Then with the reaction temperature jumps up to ~72 °C, which is the ideal working temperature for the polymerase, the DNA polymerase then elongates the primers on right position of the templates and produces a complementary strand of DNA that is conjugated to the template it attached. On the other hand, primers that are on the positions without exact match, are released again because of the higher temperature and do not give an elongation of the fragment. This process is repeated for 30 to 40 cycles to amplify large amount of target DNA [\(182\)](#).

2.7.2 DNA extraction and purification for PCR

DNeasy Blood & Tissue Mini Kit (QIAGEN) and protocol was applied for cancer cells DNA extraction and purification. The detailed procedure was illustrated as a flow chart in [Figure 2. 16](#).

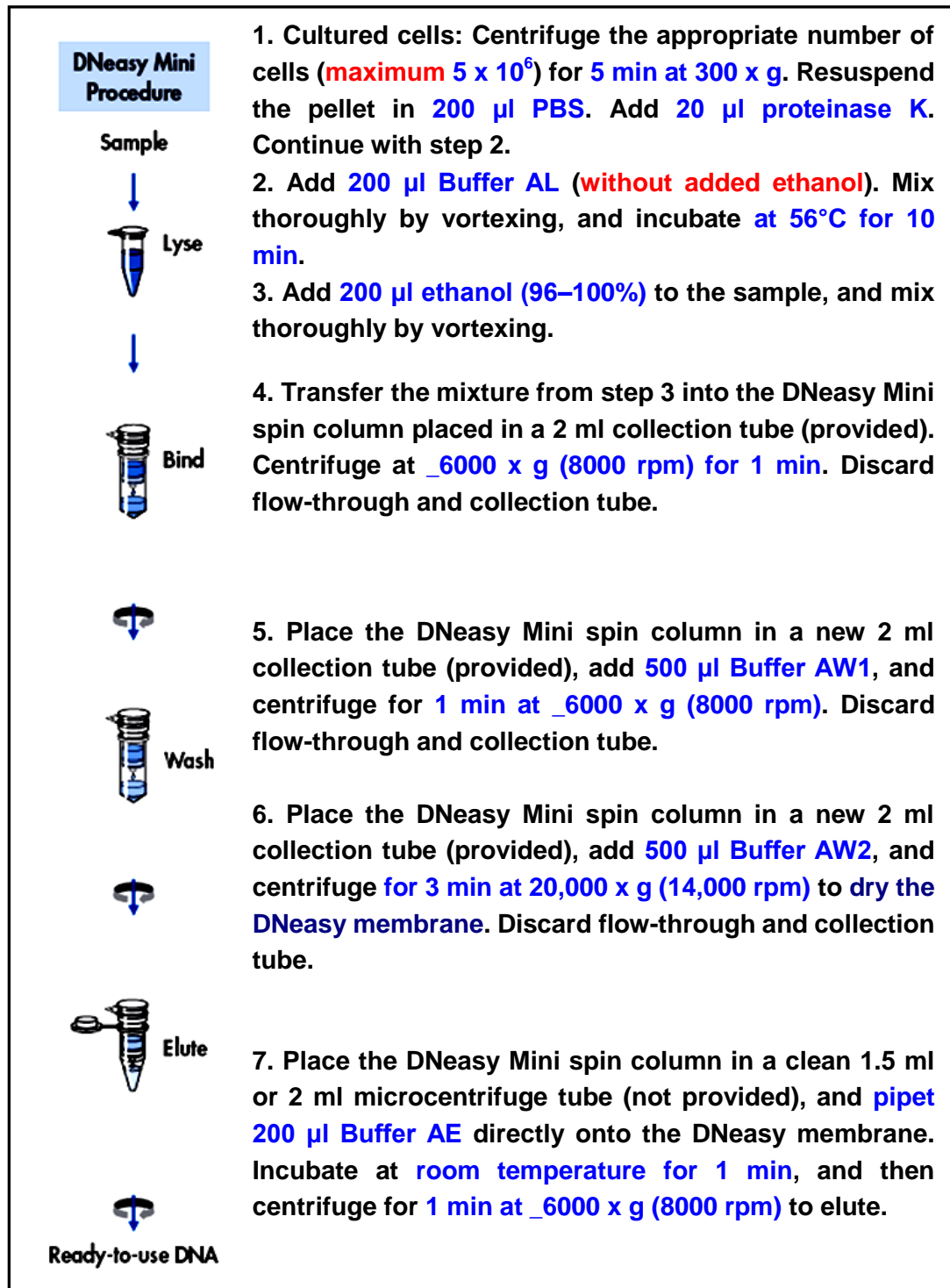


Figure 2. 16 Purification of total DNA from cells by using DNeasy Blood & Tissue Kit

(This flow chart is generated by combine the flow chart with the protocol in the QIAGEN DNeasy Blood & Tissue Kit Handbook)

2.7.3 PCR method

Reagents

DNA samples
Distilled water
10 x Buffer
MgCl₂
dNTP mix (2.5 mM)
Sense Primer (10 µM)
Antisense Primer (10 µM)
Amplitaq Gold

Equipment

Gilson pipettes
sterile filter tips
0.2ml PCR tubes or PCR plate, and lids
1.5ml tube (for making master mix)
Bucket of ice
Thermal Cycler

1. Use the Stratalinker to UV irradiate the tips, Gilsons, PCR tubes, etc to be used in the protocol before proceeding. UV at 200-500 nm. To set: Type in 200, Press Energy, then Start.

(Remember to close tip boxes, tube lids before removing from the stratalinker).
2. Working in the flow hood make up a 'Master Mix' of reagents, enough for all the samples, leaving the enzyme until last.
3. Remove the Amplitaq Gold from -20 °C and keep on ice. Add the enzyme to the 'Master Mix' and vortex to mix thoroughly.
4. Add the appropriate amount of 'Master Mix' to the tubes (23 µl for a standard reaction).
5. No DNA is allowed in the flow hood, so when ready to add the DNA, do this outside of the hood. Add the appropriate amount of DNA to each tube, vortex briefly, and pulse spin. Keep the samples on ice until they are put onto the thermal cycler.
6. For p53 PCRs there are programmes set up on the thermal cyclers. Touchdown 55 is used for Exons 4, 5, 6 and 9. Touchdown 60 is used for Exons 7 and 8. Touchdown 63 is used for codon 285 point mutation detection specific PCR reaction (the detailed information for Touchdown programmes is in appendix II).

Standard PCR Reaction Mix (for one 25ul reaction)

Reagents	Volume μL
DNA samples	2
10 x Buffer	2.5
MgCl ₂	2.5
dNTP mix (2.5mM)	2.5
Sense Primer (10 μM)	1
Antisense Primer (10 μM)	1
Amplitaq Gold	0.25
Distilled water	13.25

(Amounts of DNA and dH₂O can be varied)

2.7.4 Agarose Gel Method

Reagents	Equipment
Agarose	Gilson pipettes
0.5 x TBE	sterile filter tips
Loading buffer	0.2ml PCR tubes or PCR plate, and lids
EtBr (10 mg/ml)	Measuring cylinder
	Microwave
	Gel mould and combs
	Electrophoresis tank and power pack
	Gel doc image capture equipment
	Balance
	Conical flask
	Image analysis system

1. When the PCR run has finished, remove PCR product samples and either store at 4 °C, or prepare to load them onto an agarose gel. For loading onto a gel take 5 μL of the PCR product into a clean tube and add 2 μL loading buffer (Recipe see Appendix II).
2. Make a 2 % agarose gel by weighing out 2 g agarose into a conical flask, and add 100 ml 0.5 x TBE, then heat in a microwave until the agarose has

melted. Cool this solution and add 1 drop (1 μ l) EtBr, swirl to mix. Pour the cooled solution into a gel mould with the combs in place and leave to set.

3. When the gel is set place it into an electrophoresis tank, submerge in electrophoresis buffer (0.5 x TBE) and gently remove the combs. Carefully load a DNA marker (8 μ l) and your prepared samples. Connect the leads and apply a voltage (100-150 V) for approx 1 hr.
4. When the gel has finished the electrophoretic separation procedure, remove it from the tank and place the gel onto the platform of the gel doc equipment. Using 'Quantity One' software position and focus the gel, then close the door and switch on the UV light to visualize the bands your PCR has generated. Save the image and print it to a local printer.

2.7.5 PCR product purification for Sequencing

After the PCR products were confirmed to be the desired products according to size and specificity by agarose gel image, the remaining PCR products were then purified by using PurelinkTM PCR Purification Kit K3100-02 (Invitrogen) following the protocol supplied by the manufacturer.

The purified samples were sent together with their corresponding primers to our colleagues in Durham University (DBS Genomics) for sequencing.

2.8 FISH Assay

2.8.1 Principle of Fluorescent *in situ* Hybridization (FISH) Assay

FISH (fluorescence *in situ* hybridization) is a cytogenetic technique developed by Christoph Lengauer that is used to detect and localize the presence or absence of specific DNA sequences on condensed chromosomes in mitotic cells or in interphase nuclei.

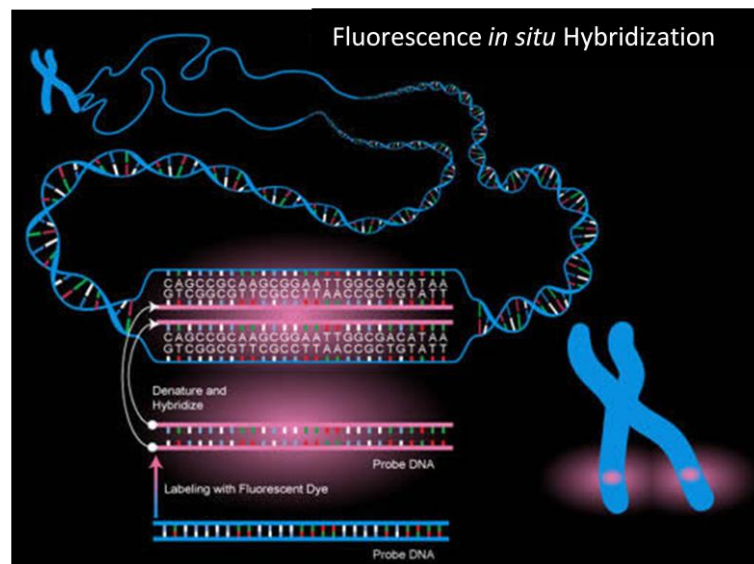


Figure 2. 17 The process of the fluorescence *in situ* hybridization technique.

This diagram is obtained from the National Human Genome Research Institute website

<http://www.genome.gov/10000206>. The FISH technique is dependent upon hybridizing a probe with a fluorescently tagged cloned DNA fragment, complementary in sequence, to a short section of DNA on a target genomic region. The tag and probe are applied to a sample of interest under conditions that allow for the probe to hybridised to the complementary sequence in the specimen if it is present. After the specimen has been treated, excess fluorophore is washed away and the sample can be visualized under a fluorescent microscope. By quantifying the amount of fluorescence with the microscope it can be determined if sequence the probe was designed for is present, and if so, how much of it is present in a sample and its cellular location.

As illustrated in Figure 2. 17, FISH uses fluorescent probes that bind to only those parts of the chromosome with which show a high degree of sequence similarity.

Fluorescence microscopy can be used to visualise the location of the fluorescent probe bound to the chromosomes.

FISH is often used for finding specific features in DNA for use in genetic counselling, medicine, and species identification. FISH can also be used to detect and localize specific mRNAs within tissue samples. In our research project, this technique has been applied for identifying the status of p53 DNA sequences on chromosome 17p in stage I and II resistant cell clones, i.e. to detect p53 locus deletions and their distribution in the cell population.

2.8.2 FISH Protocol

2.8.2.1 *Harvesting Cell Lines for FISH*

Reagents

1 x Trypsin
75 mM KCl
Fixative (Freshly made)
3:1 Methanol : Acetic Acid
Sterilized PBS

Equipment

Centrifuge (1,000 × g for 5 minutes)
15 ml Centrifuge Tubes
Nitrile Gloves
Pasteur pipette
Pipette aid

1. Transfer the media from a 25 cm² flask contain > 70 % confluent cells into labelled 15 ml centrifuge tube, rinse with sterile PBS to remove remaining media by using sterilized PBS, then add 1 x trypsin to the cell culture, incubate in 37 °C incubator to release most of the cells from the bottom of the flask.
2. Suspend the detached cells using the original media, then transfer the cell suspension into the original labelled centrifuge tube.
3. Add ~7 ml 0.075 M KCl , mix thoroughly by inverting.

4. Incubate for 15 min at 37 °C if possible but room temperature is okay.
5. Centrifuge at 1,000 × g for 5 min.
6. Discard the supernatant and re-suspend the pellet thoroughly by vigorous flicking.
7. Add 1ml of fresh 3:1 Methanol:Acetic Acid fixative a few drops at a time with constant flicking to avoid clumping. Add further fixative to a total of 7ml.
8. Centrifuge at 1,000 × g for 5 min.
9. Discard the supernatant
10. Add 7ml of fresh 3:1 Methanol:Acetic Acid fixative
11. Repeat steps 8-10.
12. Store at -20 °C.

2.8.2.2 Slide Preparation

Reagents

Fixative (Freshly made)

3:1 Methanol : Acetic Acid

Equipment

Centrifuge (1,000 × g for 2 minutes)

Phase contrast microscope

Microscope slides (Cleaned)

Pasteur pipette

Procedures

1. Prepare fresh fixative by Mixing methanol and acetic acid 3:1 in a fume hood.
2. Centrifuge the cell samples 5 mins at 1,000 × g.

3. Remove fixative from the sample using a pipette, being careful not to remove the cell pellet at the bottom of the tube.
4. Re-suspend the cell pellet in a small amount of fresh fixative.
5. One slide is required per FISH study. Delineate the FISH area with a glass marker on the reverse of the slide. Label the slides with sample number, storage box position, and the probe to be used.
6. Drop 2-3µl of sample on to a slide and allow it to air dry.
7. Check the slide under a microscope to make sure that there is a good spread of cells.

2.8.2.3 Probe preparation

Reagents

FISH Probes

Hybridisation Solution

Rubber Solution

Equipment

Micro-centrifuge

10 mm Cover slip

Micro pipette

Nitrile Gloves

Forceps

Procedures

1. Defrost the FISH probe and hybridisation buffer at room temperature for 5 minutes.
2. Mix the probe by flicking the tube.
3. Spin in a micro-centrifuge if required for a maximum of 5 seconds.
4. For commercial probes prepare a 1:10 Probe:Hybridisation buffer dilution.
For home-grown probes dilution will be different for each probe.
5. Mix well by flicking.

6. Spin in micro-centrifuge if required for a maximum of 5 seconds.
7. Apply 2 μ l of probe mixture to the slide.
8. Apply 10 mm diameter coverslip and once the solution has spread, seal with rubber solution. Allow to stand for 5 minutes at room temperature.

2.8.2.4 Denaturation and Hybridisation

Reagents

Distilled Water

Equipment

Hybridisation heated block (Hybrite [Temp. set for probe])

Procedures

1. Place the slide, with the coverslip uppermost, onto the pre-warmed Hybrite for the time allocated for that probe. Most commercial probes use 75 °C for 2 minutes and 72 °C for 5 minutes for home-grown probes.
2. Incubate on the Hybrite at 37 °C overnight.

2.8.2.5 Post Hybridisation Wash

Reagents

0.4 × Standard saline citrate (SSC) / 0.3%
Nonidet P-40 (NP-40)
2 × SSC / 0.1 % NP-40
2 × SSC
4',6-diamidino-2-phenylindole
(DAPI)/Antifade Mountant

Equipment

Water Bath at 72 °C

Micro pipetter
Nitrile Gloves
Olympus BX51 microscope
Forceps

Procedures

1. Remove the slides from the hybrite and carefully remove the rubber solution from the coverslips using forceps.
2. Soak in $2 \times \text{SSC}$ to remove coverslips.
3. Soak slides in $0.4 \times \text{SSC} / 0.3 \% \text{NP-40}$ at 72°C for 2 minutes exactly.
4. Transfer immediately to $2 \times \text{SSC} / 0.1 \% \text{NP-40}$ at RT.
5. Tap the slide dry on absorbent paper and wipe dry the underside.
6. Mount with $7 \mu\text{l}$ of DAPI/Antifade Mountant. A 50×25 rectangular cover slip should then be placed on to the slide.
7. Store at 4°C until required.
8. Check the slides and score them using the Olympus BX51 fluorescence microscope (Olympus) equipped with appropriate filters. Images were captured with CytoVision image capture software (Applied Imaging).

2.9 Computational QSAR

2.9.1 Principle of Quantitative Structure-Activity Relationship (QSAR) Analysis

QSAR (quantitative structure-activity relationship) analysis is the process by which molecules with similar chemical structures are quantitatively correlated with a well defined process, such as biological activity, chemical reactivity or docking score (descriptors) produced by using virtual docking software. The last one is also be defined as computational QSAR. The purpose of using QSAR analysis is mainly to

allow the prediction of biological activities or mechanisms (in here, binding mode prediction) of untested or novel compounds to provide insight into relevant and consistent chemical properties or descriptors which defines the biological activity. After a series of predicted models is collected, they can be used for database mining for the identification of novel chemical compounds, particularly, for those having drug-like properties (following Lipinski's Rule of Five) (183) along with suitable pharmacokinetic properties.

2.9.2 Online Resources and Softwares Applied for Computational QSAR Analysis

PDB files of structures of MDM2 protein in complex with either p53 related peptides or small molecule inhibitors were downloaded from 'RCSB Protein Data Bank' website <http://www.pdb.org>, which were then used for docking software training.

ChemBioOffice 2008 software ChemBioDraw Ultra 11.0 and ChemBio3D Ultra 11.0 from <http://www.cambridgesoft.com> were used for generating isoindolin-1-one compound structures and predicting their lowest energy configurations.

PyMOL v0.99 software from Delano Scientific LLC <http://www.PyMOL.org> was applied for re-building isoindolin-1-one compounds structures.

Molegro Virtual Docker software (Free Trial Version) from Bioinformatics Research Center, University of Asrhus (molegro bioinformatics solutions) <http://www.molegro.com> was used for virtual docking, to predict and rank the lowest energy binding modes and to generate final binding mode images.

After binding mode generation, PyMOL v0.99 software was used for detailed visualisation of binding mode structure, including side-chain interactions between the ligand and MDM2 protein. Furthermore, PyMOL v0.99 software was also used to generate docking movies for presentation purposes.

All the methods for using these software packages were based on the manuals and protocols provided by the corresponding companies and programme authors.

Chapter Three

Isoindolin-1-one Compounds: Structure-Activity Relationship Analysis

3.1 Introduction

After reviewing reports of the X-ray crystal structure of the MDM2-p53 complex (116), several structure design research reports based on it (11-12, 14, 133-134), and the SAR (structure-activity relationship) for the isoindolin-1-one scaffold compounds we had already synthesized and tested, a new hypothesis was proposed; that there should be taken into consideration an additional residue of the p53 transactivation domain that binds to the hydrophobic cleft of MDM2, namely residue Leu22, which we had not previously considered in our structure optimization studies before. This may also contribute substantially to the binding activity, and additional interaction should be incorporated in further studies of structure-based design for lead optimisation.

If this hypothesis is correct, it should be possible to design compound structures with improved binding affinity to the target protein MDM2, based on mimicking the four key binding residues of p53 rather than just the three previously assumed. It also argues for an adjustment of the drug design and *in silico* compound library screening methods used to search for potential inhibitors of the MDM2/p53 interaction.

My research aims and analysis presented in this chapter are based on the theories and hypothesis mentioned above, and the progress our research group has made, as explained in detail below:

1. Based on the X-ray crystal structure of the MDM2-p53 binding interaction and the hypothesis mentioned above, to use drug design software to optimize the structure of the isoindolin-1-one scaffold compound.
2. Evaluate the activity of new compounds with a cell-free bioassay method (ELISA) to obtain structure-activity-relationship (SAR) information to inform the continued optimization process.
3. Establish whether or not the new inhibitors can also bind MDMX, a closely related structural homologue of MDM2, which can also potentially prevent p53 activation after MDM2 has been inhibited.

3.2 ELISA for Isoindolin-1-one Compound *in vitro* Activity Evaluation

3.2.1 Isoindolin-1-one Compound Potency Evaluation as MDM2/p53 Inhibitors

The compounds evaluated with the Enzyme-Linked Immuno-Sorbent Assay (ELISA) by me with the collaboration and guidance of Dr. Claire Hutton and Dr. Xiaohong Lu are listed in [Table 3. 1](#) in NU number order, which essentially reflects the order of

successful synthesis. If the compound IC_{50} value could not be obtained, its percentage inhibition at the highest concentration tested was presented in the table. The isoindolin-1-one core structure shared by most of the compounds listed in Table 3. 1 is displayed in Figure 3.1, with the side-chain position labeled corresponding to the side-chain modification in Table 3. 1. The structures of four compounds (NU8433-NU8436) in the table are shown separately because they do not share the core structure.

Each compound was plated out in triplicate at three different concentrations and the experiments were repeated at least three times for confirmation.

IC_{50} results of all compounds were calculated using Prism Graphpad™ software by point-to point analysis.

All the compounds with IC_{50} values lower than 1 μ M are highlighted with light green background (grey background in black & white print version). The most potent compound (NCL-00016149) was labelled with a asterisk (Table 3. 1).

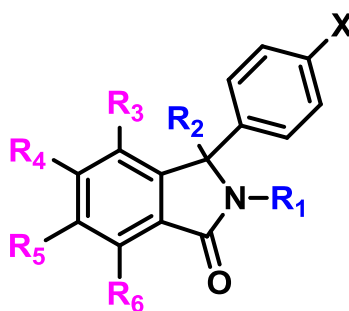
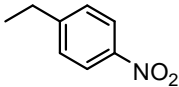
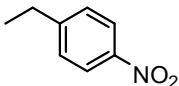
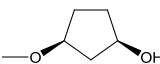
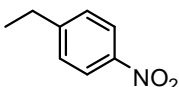
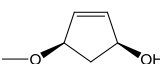
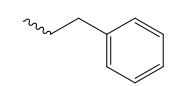
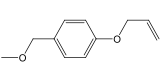
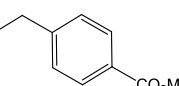
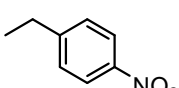
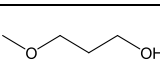
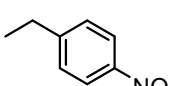
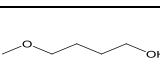
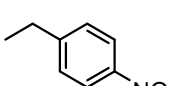
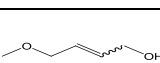
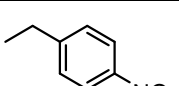

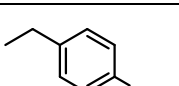
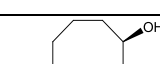
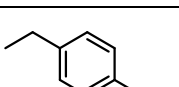
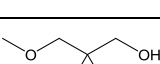
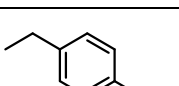
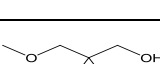
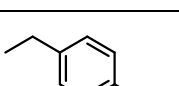
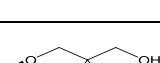
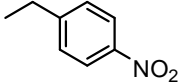
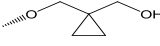
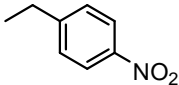
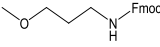
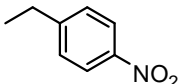
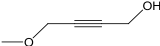
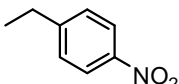
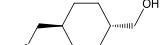
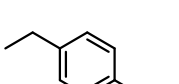

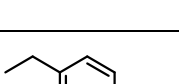

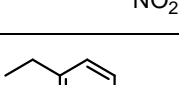
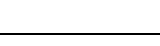
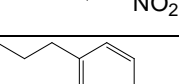
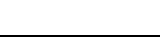

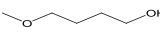
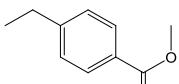
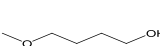
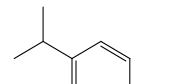
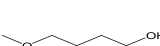
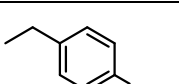
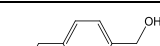
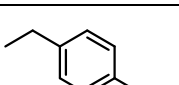
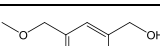
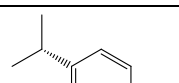

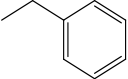

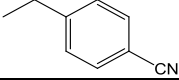

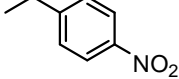
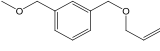
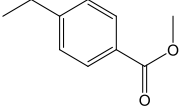

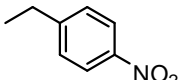
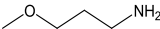
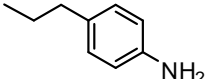
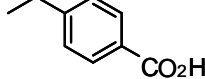
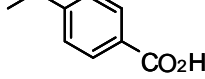
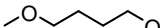
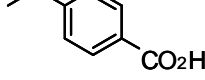

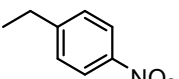
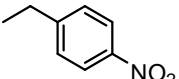
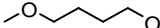
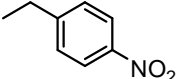

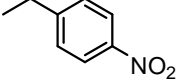
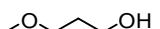
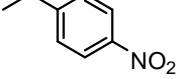


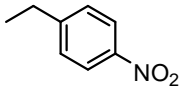
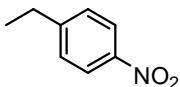
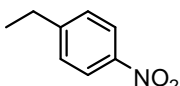
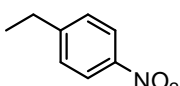
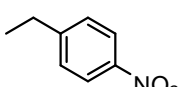
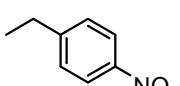

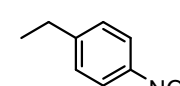

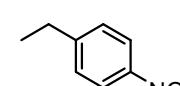

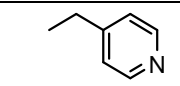
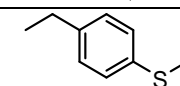

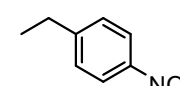

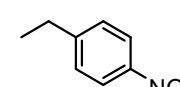

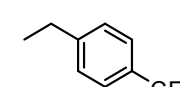
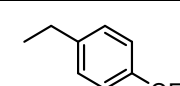

Figure 3. 1 Isoindolin1-one core structure shared by compounds in Table 3.1.

Table 3. 1 IC₅₀ of Isoindolin-1-ones with Side Chains Variation

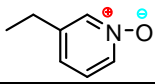
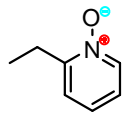
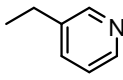

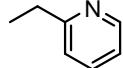

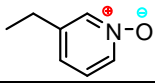

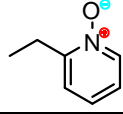

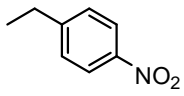
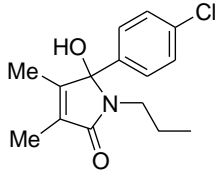
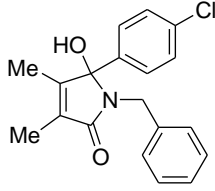
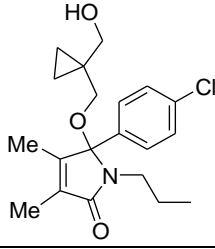
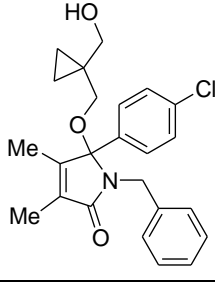
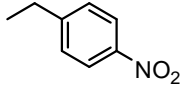
Compound Code	-R ₁	-X	-R ₂	-R ₃	-R ₄	-R ₅	-R ₆	IC ₅₀ μM	SE μM
NU8260		-Cl	-OH	-H	-H	-H	-H	2.4	0.2
NU8296		-Cl		-H	-H	-H	-H	0.4	0.04
NU8297		-Cl		-H	-H	-H	-H	1.9	0.3
NU8332		-Cl		-H	-H	-H	-H	78.4	5.1
NU8346		-Cl	-OH	-H	-H	-H	-H	10.8	3.8
NU8348		-Cl		-H	-H	-H	-H	0.5	0.01
NU8349		-Cl		-H	-H	-H	-H	0.4	0.044
NU8350		-Cl		-H	-H	-H	-H	0.4	0.01
NU8351		-Cl		-H	-H	-H	-H	0.4	0.01
NU8352		-Cl		-H	-H	-H	-H	0.4	0.04
NU8353		-Cl		-H	-H	-H	-H	0.4	0.08
NU8354		-Cl		-H	-H	-H	-H	0.27	0.01
NU8354 A		-Cl		-H	-H	-H	-H	0.16	0.02

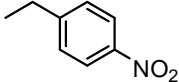
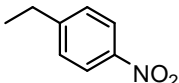

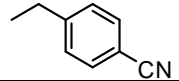
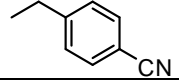
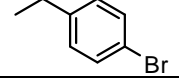
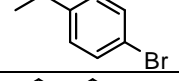
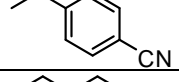
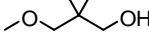
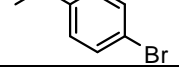
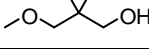
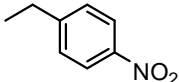

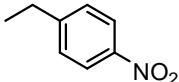

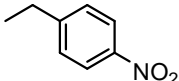

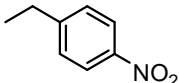
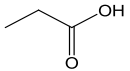
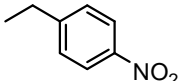

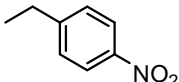
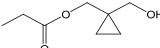
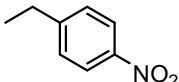
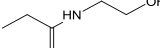
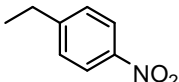
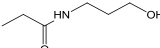
NU8354 B		-Cl		-H	-H	-H	-H	1.33	0.12
NU8355		-Cl		-H	-H	-H	-H	79.8	2.5
NU8357		-Cl		-H	-H	-H	-H	0.66	0.11
NU8358		-Cl		-H	-H	-H	-H	0.58	0.08
NU8359		-Cl		-H	-H	-H	-H	0.57	0.07
NU8360		-Cl		-H	-H	-H	-H	0.39	0.11
NU8361		-Cl		-H	-H	-H	-H	0.31	0.09
NU8362		-Cl		-H	-H	-H	-H	3.2	1.0
NU8363		-Cl		-H	-H	-H	-H	> 10	
NU8364		-Cl		-H	-H	-H	-H	> 10	
NU8365		-Cl		-H	-H	-H	-H	0.87	0.06
NU8366		-Cl		-H	-H	-H	-H	0.98	0.20
NU8367		-Cl		-H	-H	-H	-H	0.73	0.13
NU8368		-Cl		-H	-H	-H	-H	2.5	0.8

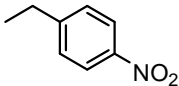
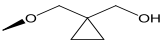
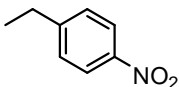
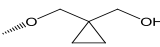
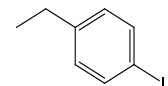
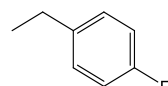
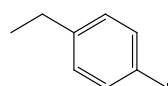

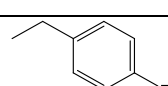
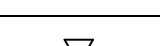
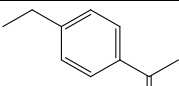

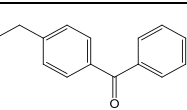
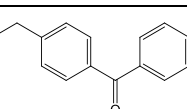
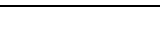
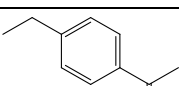
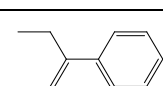
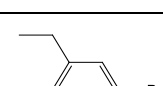
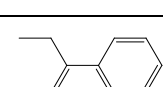
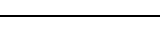
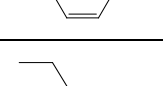
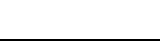
NU8369		-Cl		-H	-H	-H	-H	> 10	
NU8370		-Cl		-H	-H	-H	-H	3.5	1.5
NU8371		-Cl		-H	-H	-H	-H	> 10	
NU8378		-Cl		-H	-H	-H	-H	> 20	
NU8380		-Cl		-H	-H	-H	-H	1.9	0.17
NU8383		-Cl	-OH	-H	-H	-H	-H	15.5	2.5
NU8386		-Cl	-OH	-H	-H	-H	-H	> 100	
NU8387		-Cl		-H	-H	-H	-H	83.8	2.4
NU8388		-Cl		-H	-H	-H	-H	> 10	
NU8389		-Br	-OH	-H	-H	-H	-H	3.1	0.2
NU8390		-Br		-H	-H	-H	-H	0.57	0.06
NU8391		-Br		-H	-H	-H	-H	0.37	0.05
NU8392		-Br		-H	-H	-H	-H	1.4	0.2
NU8393		-Cl	-OH	-Me	-H	-H	-H	2.2	0.3

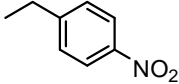
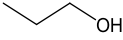
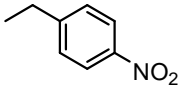
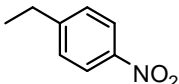
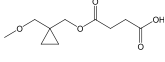
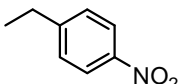
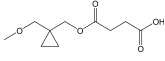
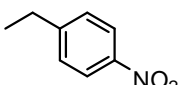
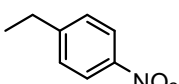
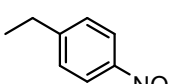

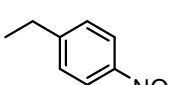
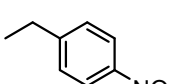
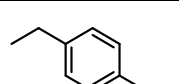
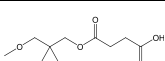
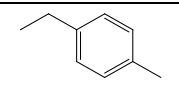

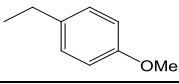
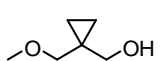
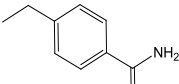

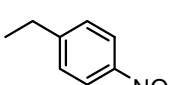
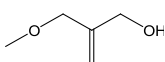
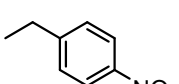

NU8394		-Cl	-OH	-H	-H	-H	-Me	6.9	2.7
NU8395		-Cl	-OH	-H	-Me	-H	-H	5.1	0.7
NU8396		-Cl	-OH	-H	-t-Bu	-H	-H	12.7	1.4
NU8397		-Cl	-OH	-H	-H	-t-Bu	-H	0.84	0.05
NU8398		-Cl	-OH	-Cl	-H	-H	-H	0.50	0.03
NU8399		-Cl		-H	-H	-t-Bu	-H	0.15	0.03
NU8400		-Cl		-H	-t-Bu	-H	-H	0.73	0.03
NU8401		-Cl		-H	-Me	-H	-H	0.49	0.04
NU8402		-Cl	-OH	-H	-H	-H	-H	> 20	
NU8403		-Cl	-OH	-H	-H	-H	-H	> 20	
NU8404	n-pr	-Cl		-H	-H	-H	-H	> 20	
NU8405		-Cl		-Me	-H	-H	-H	0.27	0.04
NU8406		-Cl		-Cl	-H	-H	-H	0.14	0.03
NU8407		-Cl	-OH	-H	-H	-H	-H	433	
NU8408		-Cl		-H	-H	-H	-H	214	

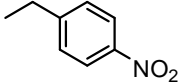
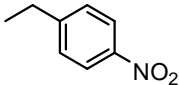

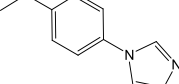

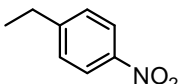
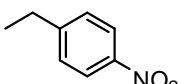

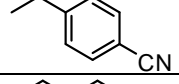
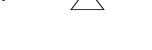
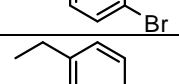

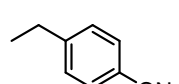
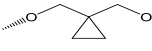
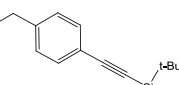
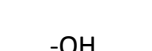
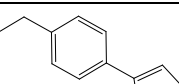
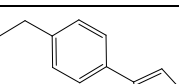
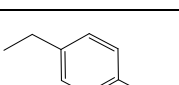
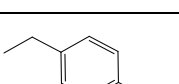
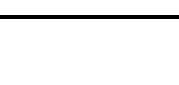

NU8409		-Cl	-OH	-H	-H	-H	-H	> 500	
NU8410		-Cl		-H	-H	-H	-H	175	
NU8411		-Cl		-H	-H	-H	-H	252	
NU8412		-Cl	-OH	-H	-H	-Me	-H	1.5	0.4
NU8413		-Cl	-OH	-H	-H	-Br	-H	5.4	0.5
NU8414		-Cl	-OH	-H	-Br	-H	-H	5.7	0.2
NU8415		-Cl		-H	-H	-H	-H	0.63	0.02
NU8416		-Cl		-H	-H	-H	-H	0.89	0.06
NU8417		-Cl		-H	-H	-H	-H	0.39	0.06
NU8418		-Cl		-H	-H	-H	-H	6.7	0.4
NU8419		-Cl		-H	-H	-H	-H	7.2	1.0
NU8420		-Cl	-OH	-H	-H	-H	-H	> 200	
NU8421		-Cl		-H	-H	-H	-H	> 200	
NU8422		-Cl	-OH	-H	-H	-H	-H	> 200	
NU8423		-Cl	-OH	-H	-H	-H	-H	> 200	
NU8424		-Cl		-H	-Br	-H	-H	0.9	0.1
NU8425		-Cl		-H	-H	-Br	-H	1.0	0.04

NU8426		-Cl	-OH	-H	-H	-H	-H	> 200	
NU8427		-Cl	-OH	-H	-H	-H	-H	> 200	
NU8428		-Cl		-H	-H	-H	-H	28.5	6
NU8429		-Cl		-H	-H	-H	-H	10.6	0.8
NU8430		-Cl		-H	-H	-H	-H	> 200	
NU8431		-Cl		-H	-H	-H	-H	32.9	2.9
NU8432		-Cl	-OH	-H	-Cl	-Cl	-H	35.1	6.8
NU8433								>200	
NU8434								>200	
NU8435								8.9	
NU8436								3.7	
NCL-000 10485		-Cl	-OH	-H	-F	-H	-H	3.8	0.5

NCL-000 10486		-Cl	-OH	-H	-H	-F	-H	5.2	1.5
NCL-000 10487		-Cl		-H	-Cl	-Cl	-H	3.7	1.2
NCL-000 10488		-Cl	-OH	-Cl	-H	-H	-H	1.6	1.0
NCL-000 10489		-Cl	-OH	-H	-H	-H	-Cl	9.0	2.2
NCL-000 10490		-Cl	-OH	-Cl	-H	-H	-H	8.5	0.1
NCL-000 10491		-Cl	-Me	-H	-H	-H	-H	85.3	12.5
NCL-000 10492		-Cl		-Cl	-H	-H	-H	0.19	0.02
NCL-000 10493		-Cl		-Cl	-H	-H	-H	0.17	0.00
NCL-000 10494		-Cl		-H ₂	-H ₂	-H ₂	-H ₂	2.8	0.1
NCL-000 10495		-Cl		-H	-F	-H	-H	0.3	0.1
NCL-000 10496		-Cl		-H	-H	-F	-H	0.9	0.1
NCL-000 10497		-Cl		-H	-H	-H	-H	4.2	0.2
NCL-000 13767		-Cl		-H ₂	-H ₂	-H ₂	-H ₂	3.5	0.01
NCL-000 13768		-Cl		-H	-H	-H	-H	10.5	0.2
NCL-000 13769		-Cl		-H	-H	-H	-H	16.0	1.6
NCL-000 13770		-Cl		-H	-H	-H	-H	13.4	0.5

NCL-000 13774		-Cl		-Cl	-H	-H	-H	0.04	0.01
NCL-000 13775		-Cl		-Cl	-H	-H	-H	1.30	0.01
NCL-000 14527		-Cl	-OH	-H	-H	-H	-H	>20	
NCL-000 14528		-Cl	-OH	-H	-H	-H	-H	>20	
NCL-000 14529		-Cl		-H	-H	-H	-H	0.82	0.01
NCL-000 14530		-Cl		-H	-H	-H	-H	1.7	0.4
NCL-000 14531		-Cl		-H	-H	-H	-H	14.6	1.3
NCL-000 14532		-Cl	-OH	-H	-H	-H	-H	>20	
NCL-000 14533		-Cl		-H	-H	-H	-H	>20	
NCL-000 16045		-Cl	-OH	-H	-H	-H	-H	85.4	
NCL-000 16046		-Cl	-OH	-H	-H	-H	-H	90.1	
NCL-000 16047		-Cl	-OH	-H	-H	-H	-H	> 100	
NCL-000 16106		-Cl		-H	-H	-H	-H	57.8	
NCL-000 16107		-Cl		-H	-H	-H	-H	71.2	

NCL-000 16147		-Cl		-H	-H	-H	-H	4.4	0.04
NCL-000 16148		-Cl	-CN	-H	-H	-H	-H	48.2	3.7
*NCL-00 016149		-Cl		-Cl	-H	-H	-H	0.016	0.003
NCL-000 16653		-Cl		-Cl	-H	-H	-H	0.12	0.02
NCL-000 16654		-Cl	-OH	-H	-H	-H	-Cl	4.5	
NCL-000 16655		-H	-OH	-H	-H	-H	-H	87.0	
NCL-000 16656		-H		-H	-H	-H	-H	8.3	
NCL-000 16657		-F	-OH	-H	-H	-H	-H	9.5	
NCL-000 16658		-Cl	-CH ₂ OH	-H	-H	-H	-H	6.8	
NCL-000 16659		-Cl		-Cl	-H	-H	-H	0.10	0.03
NCL-000 16865		-Cl		-H	-H	-H	-H	2.3	0.1
NCL-000 16866		-Cl		-H	-H	-H	-H	1.9	1.0
NCL-000 16867		-Cl		-H	-H	-H	-H	> 50	
NCL-000 16895		-Cl		-H	-H	-H	-H	0.6	0.1
NCL-000 16896		-F		-H	-H	-H	-H	2.3	0.5

NCL-000 16897		-Cl	-OH	-Cl	-F	-H	-H	40	6
NCL-000 16957		-Me		-H	-H	-H	-H	1.2	
NCL-000 16958		-Cl		-H	-H	-H	-H	> 20	
NCL-000 16985		-Cl	-CO ₂ H	-H	-H	-H	-H	7.7	1.9
NCL-000 16986		-Cl		-Cl	-F	-H	-H	0.2	0.05
NCL-000 17305		-Cl		-Cl	-H	-H	-H	0.12	0.02
NCL-000 17306		-Cl		-Cl	-H	-H	-H	0.12	0.03
NCL-000 17310		-Cl		-Cl	-H	-H	-H	4.1	0.2
NCL-000 17311		-Cl		-Cl	-H	-H	-H	4.3	
NCL-000 17325		-Cl	-OH	-H	-H	-H	-H	168.3	3.4
NCL-000 17326		-Cl	-OH	-H	-H	-H	-H	> 200	
NCL-000 17327		-Cl	-OH	-H	-H	-H	-H	> 200	
NCL-000 17328		-Cl	-OH	-H	-H	-H	-H	9.8	1.2
NCL-000 17365		-Cl		-H	-H	-H	-H	0.46	0.03

The IC₅₀ values for isoindolin-1-one compounds with similar structure were compared as a group within the same ELISA plate to obtain further accurate SAR information, and the results are shown in Figure 3. 2.

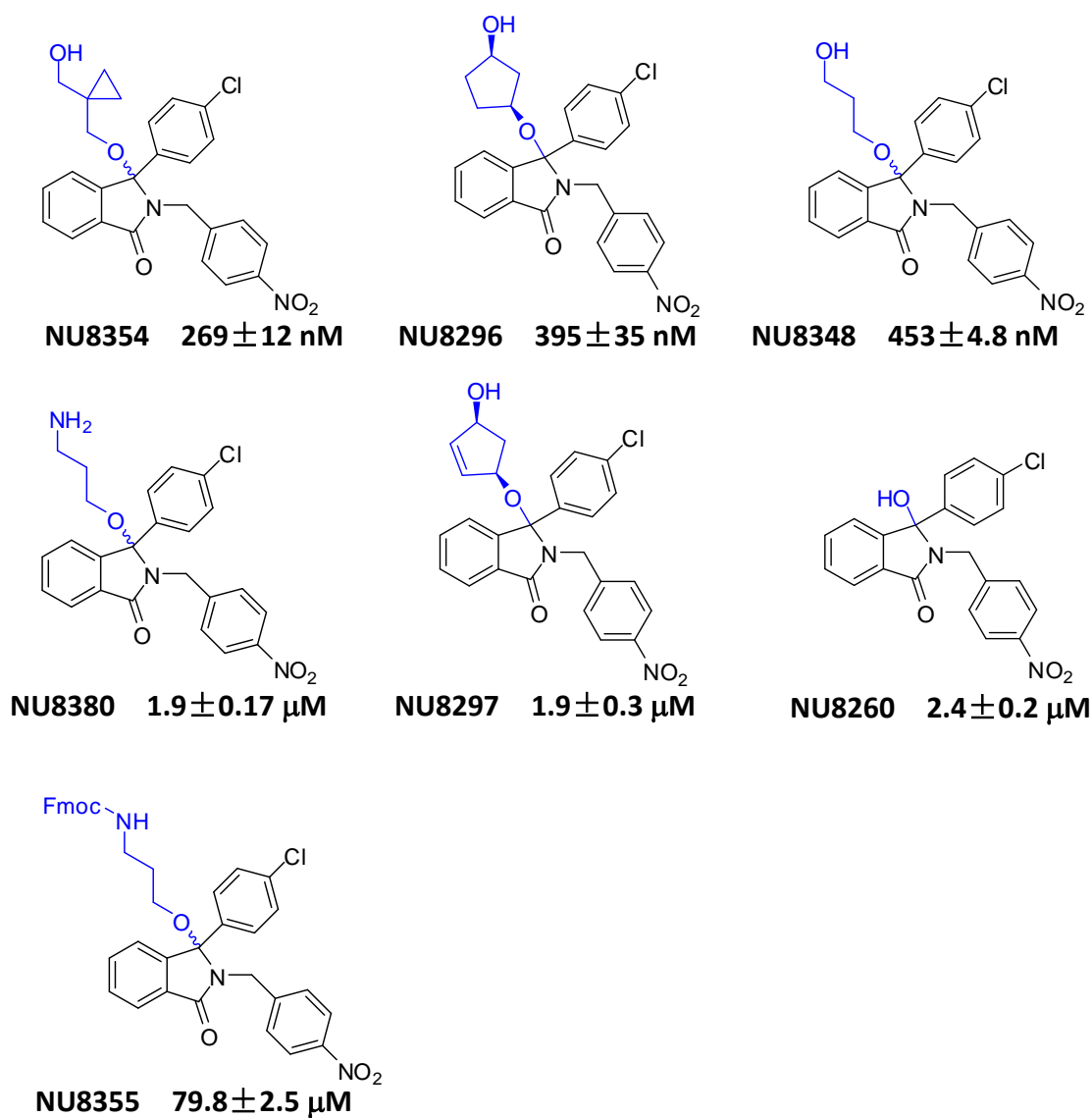


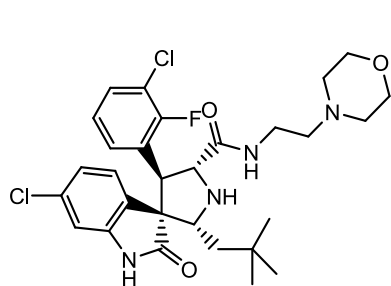
Figure 3. 2 Comparison of IC₅₀ Values for Inhibition of the MDM2-p53 Binding Interaction by Isoindolin-1-ones with Side-chain Variation in the R₂ position.

3.2.2 IC₅₀ Comparison of MI-63, Nutlin-3, (-)-Nutlin-3 and potent isoindolin-1-ones as MDM2/p53 Inhibitors

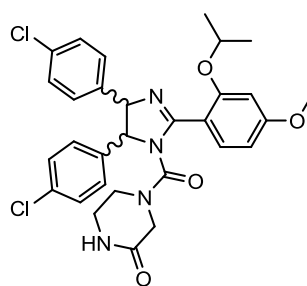
After obtained the MI-63 and potent Nutlin-3 enantiomer (-)-Nutlin-3, I evaluated and compared their IC₅₀ values together with our potent isoindolin-1-one compounds as single enantiomers NU8354A, NU8406A, NCL-00017305 and NCL-00017306; together with the compound NCL-00016149 (Figure 3. 3) which was designed as a prodrug with the adding of the oxobutanoic acid side-chain at the end of –R2 position to improve water solubility. The compound is stable under acidic condition (e.g. in stomach) and can be hydrolyzed in mild basic condition (e.g. in intestines).

Three independent ELISA assays were carried out on these compounds with specific ranges of concentrations for each individual compound. Mean and SD values of percentage inhibition for each concentration were calculated and non-linear regression curves fitted to the data to generate accurate IC₅₀ values using PRISM software embedded programme 'log (inhibitor) vs. response -- Variable slope' (Figure 3. 4).

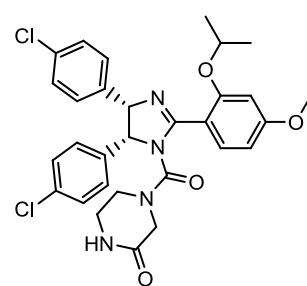
MI-63 was the most potent MDM2/p53 inhibitor in this comparison set, with a 9 nM IC₅₀ value, followed by NCL-00016149, (-)-Nutlin-3 and NU8406A; all the remaining compounds had IC₅₀ values above 100 nM.



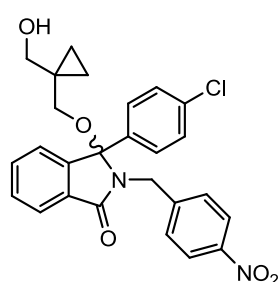
MI-63



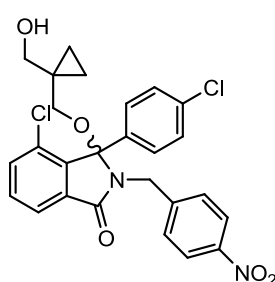
Nutlin-3



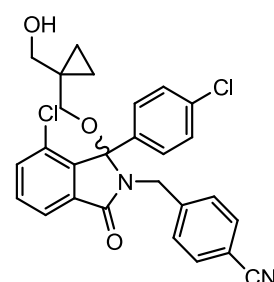
(-)-Nutlin-3



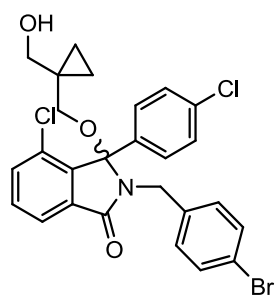
NU8354A



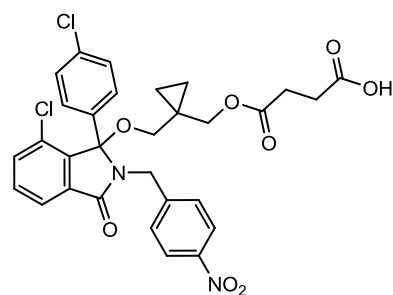
NU8406A



NCL-00017305

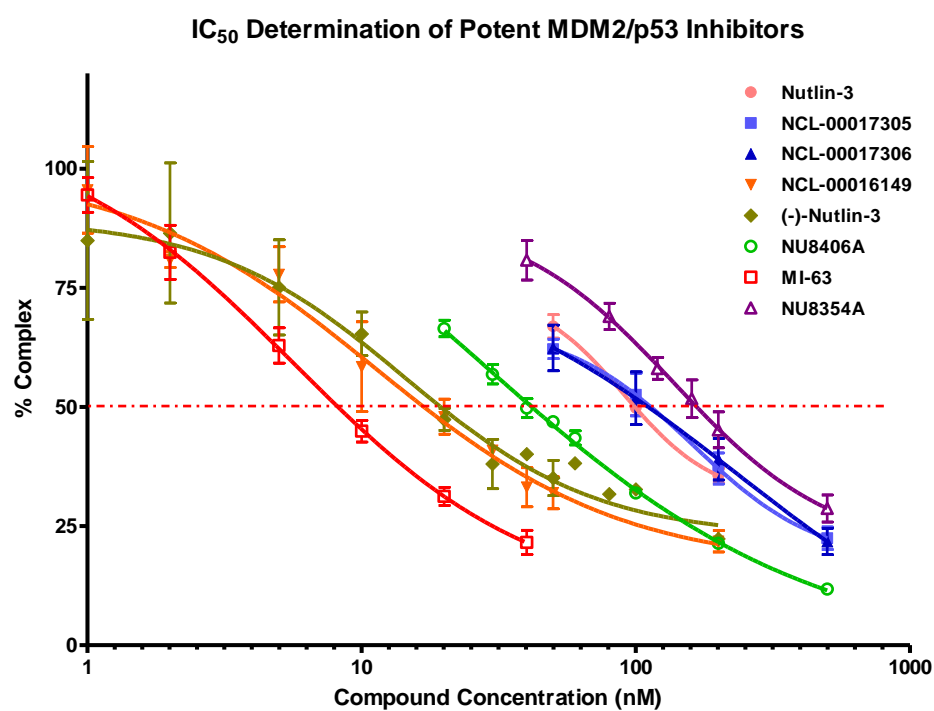


NCL-00017306



NCL-00016149

Figure 3. 3 Structures of MI-63, Nutlin-3, (-)-Nutlin-3 and potent isoindolin-1-ones NU8354A, NU8406A, NCL-00017305 and NCL-00017306 and NCL-00016149



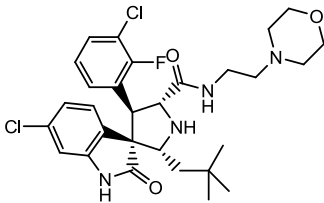
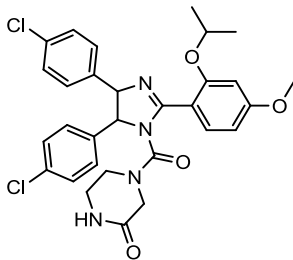
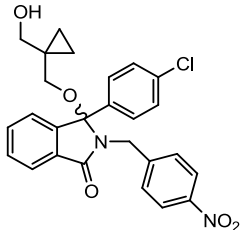
Compounds	MI-63	Nutlin-3	(-)-Nutlin-3	NU8354A	NU8406A	NCL-00017305	NCL-00017306	NCL-00016149
IC ₅₀ (nM)	9.0±1.3	103.3±10.6	22.75±5.3	173.4±20.1	42.8±2.6	107.9±15.3	109.1±25.8	18.90±4.1

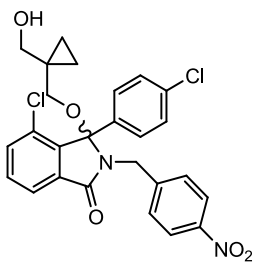
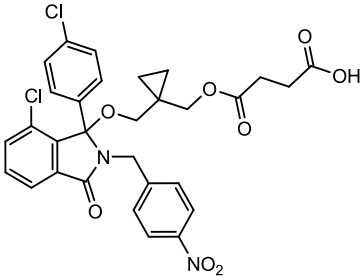
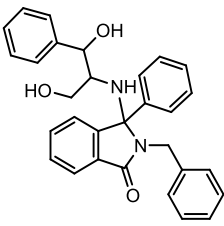
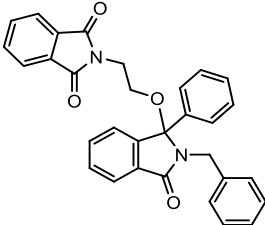
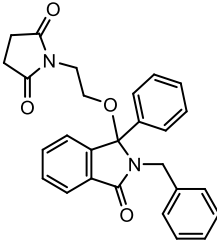
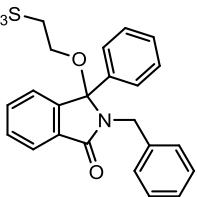
Figure 3. 4 IC₅₀ comparison of MI-63, Nutlin-3, (-)-Nutlin-3 and potent isoindolin-1-ones as MDM2/p53 inhibitors

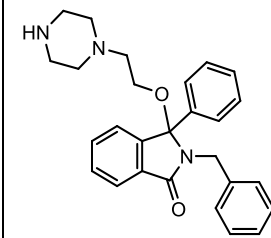
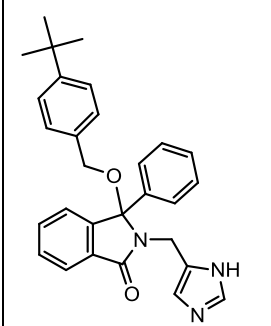
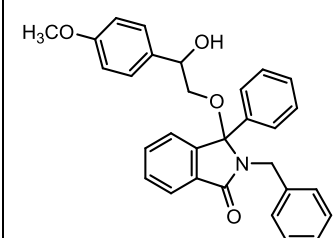
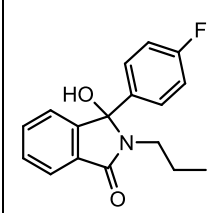
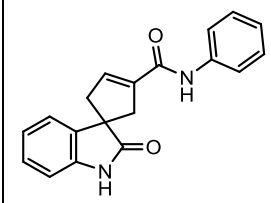
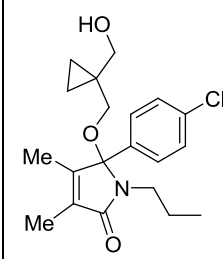
3.2.3 Screening of isoindolin-1-ones as MDMX/p53 Inhibitors

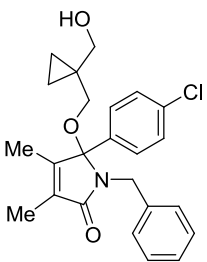
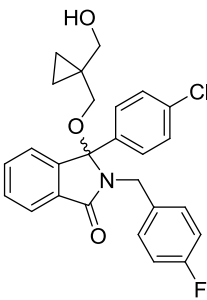
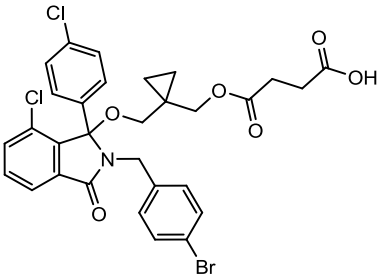
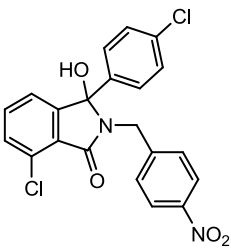
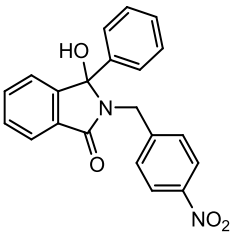
Based on the protein sequence similarity and the hydrophobic binding pocket structural similarity between MDM2/p53 and MDMX/p53 X-ray co-crystal structures, we also selected and screened some isoindolin-1-one scaffold compounds together with Nutlin-3 and MI-63 for activity as MDMX/p53 inhibitors, as listed in [Table 3. 2](#). If the compound IC₅₀ value could not be obtained, the percentage inhibition at the highest concentration was presented in the table.

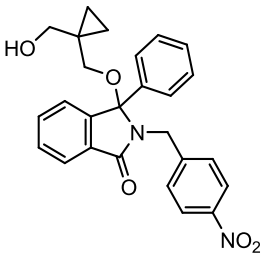
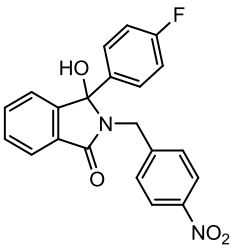
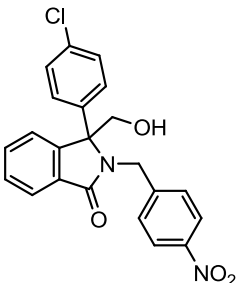
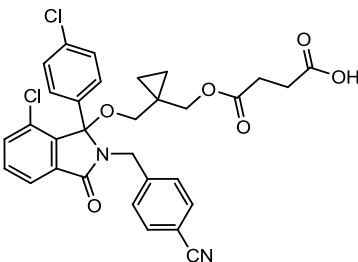
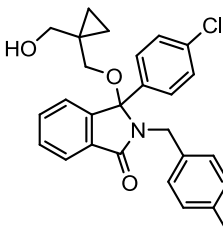
Table 3. 2 Compounds evaluated as MDMX/p53 interaction inhibitors

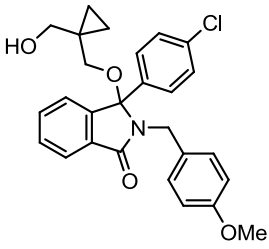
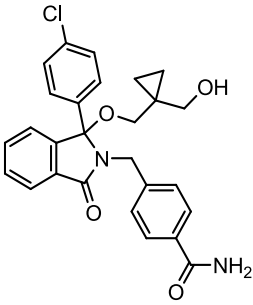
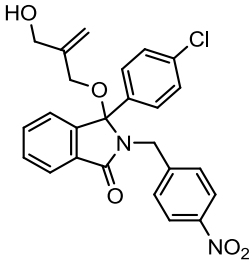
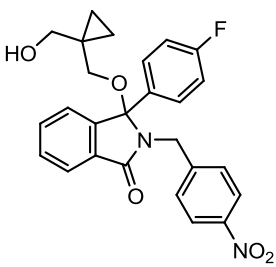
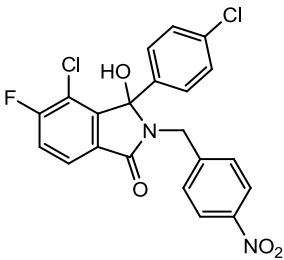
Compound Code	Structure	Highest Concentration (μ M)	% Inhibition
MI-63		25	-10.4
Nutlin-3		25	23.8
NU8354A		25	-14.1
NU8354B		25	-23.8

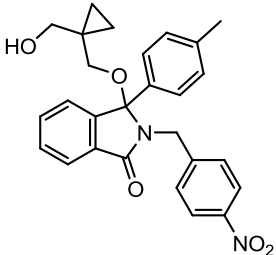
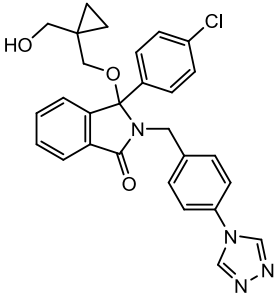
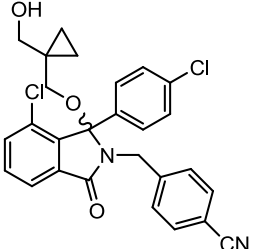
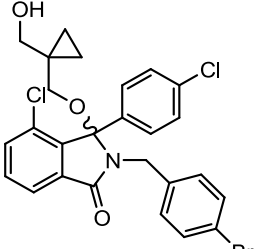
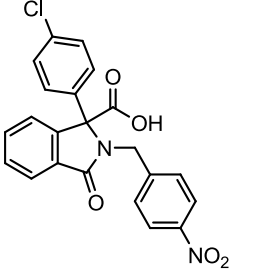
NU8406		100	20.5
NU8406A		50	34.7
NU8406B		50	-8.3
NCL-00016149		100	87.9
NU8110		100	-7.8
NU8117		100	32.5
NU8136		100	-16.5
NU8210		100	7.8

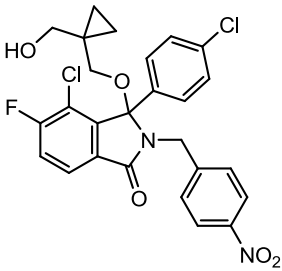
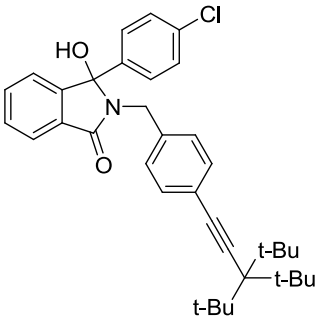
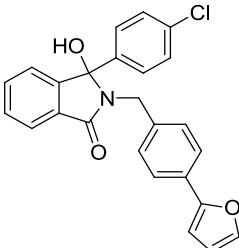
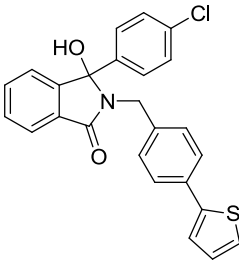
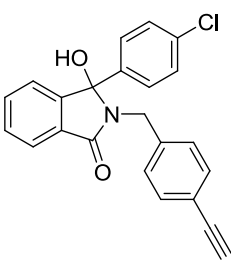
NU8211		100	-5.1
NU8214		100	-31.9
NU8219		100	-18.9
NU8275		100	-29.2
NU8285		100	11.4
NU8435		100	23.0

NU8436		100	-1.3
NCL-00014530		100	-10.7
NCL-00016653		50	52.3
NCL-00016654		100	37.3
NCL-00016655		100	-13.6

NCL-00016656		100	-4.4
NCL-00016657		100	-5.7
NCL-00016658		100	1.5
NCL-00016659		50	41.1
NCL-00016865		50	-8.8

NCL-00016866		50	-62.9
NCL-00016867		50	3.2
NCL-00016895		50	-5.9
NCL-00016896		50	37.5
NCL-00016897		50	24.1

NCL-00016957		20	7.1
NCL-00016958		20	11.3
NCL-00017305		50	28.7
NCL-00017311		50	22.3
NCL-00017306		50	34.1
NCL-00017310		50	29.1
NCL-00016985		50	6.6

NCL-00016986		50	2.0
NCL-00017325		200	70.0
NCL-00017326		200	24.8
NCL-00017327		200	31.6
NCL-00017328		200	33.2

3.3 Structure-activity Relationships for the analysis of ELISA

IC₅₀ data

3.3.1 Isoindolin-1-one compounds side-chain comparison

Selected isoindolin-1-ones were grouped based on the side-chain difference highlighted in blue in [Figure 3. 5](#) and in the following tables put alongside with compound codes and their IC₅₀ values so that the relationship between potency differences, and these side-chain variations can be compared.

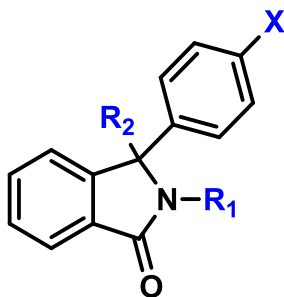


Figure 3. 5 Three side chains of isoindolin-1-one compounds with the modification to be discussed highlighted in blue

3.3.1.1 Isoindolin-1-one compounds side-chain –R1 modification

Grouped isoindolin-1-one IC₅₀ values in [Table 3. 3](#) illustrated the effect of modifying side-chain position –R1.

The ELISA results comparison showed that using –C≡CH, –Br or –CN to replace –NO₂ leads to a modest decrease of the compound potency, but using –F, –Cl, –I or –Me residues resulted in a marked loss of inhibitory activity, which may contribute to further refinement of the binding mode model and structure optimization.

Although the IC₅₀ values showed that the nitrobenzyl side-chain was still the most suitable one for its binding position, this makes the compounds likely to be unstable *in vivo* due to reductive metabolism of the nitrobenzyl group (184-185), the bromobenzyl, ethynylbenzyl or methyl-benzonitrile groups may be alternative candidates for maintaining MDM2/p53 inhibitory activity *in vivo*.

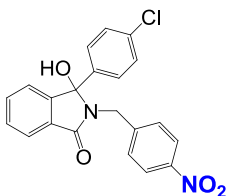
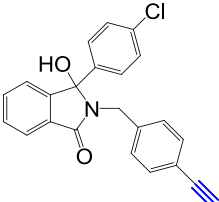
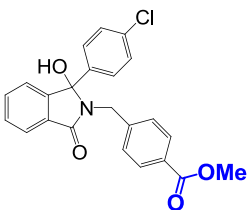
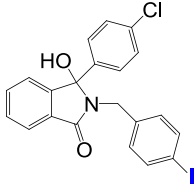
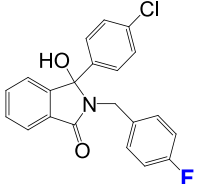
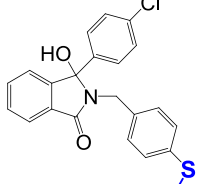
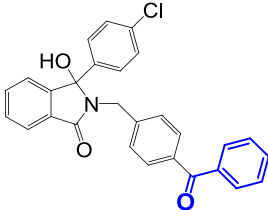
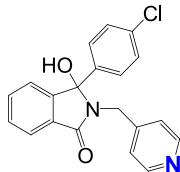
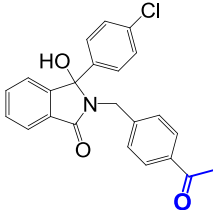
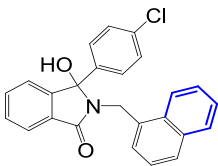
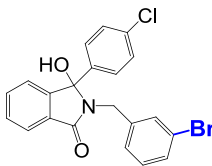
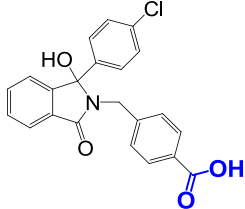
The modification results of side-chain –R1 indicated not only space occupying effects between the isoindolin-1-one compounds within the p53/MDM2 binding pocket, but also electronic effects and hydrogen bonding of the nitrobenzyl group with MDM2 residues, which might contribute to the higher binding potency of the –NO₂ group compared to all other side-chain candidates we have tested.

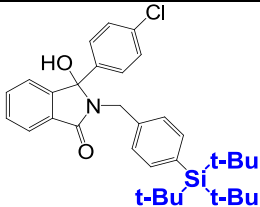
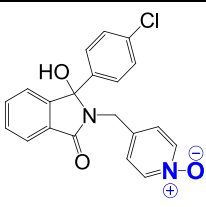
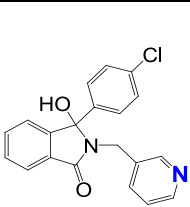
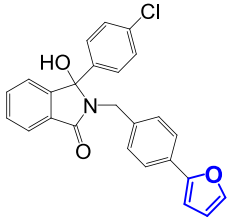
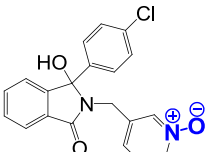
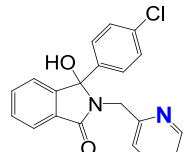
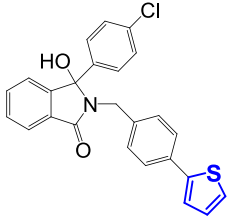
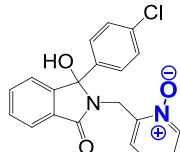
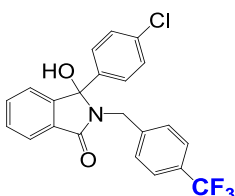
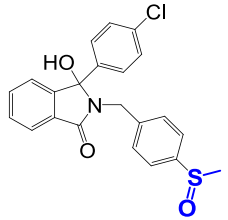
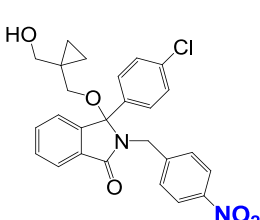
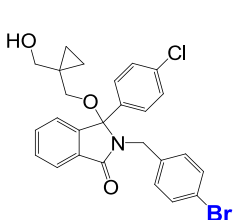
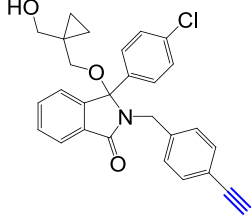
On changing the bromobenzyl group at the –R1 position into either chlorobenzyl, iodobenzyl or fluorobenzyl, the binding potency was decreased markedly, which may contribute to further refinement of the binding mode model and structure optimization, for example, considering the relationship between the size of this side-chain with the potencies of compounds.

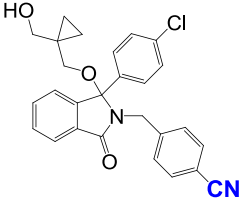
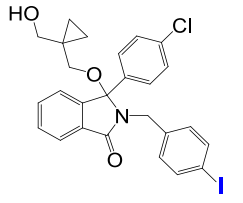
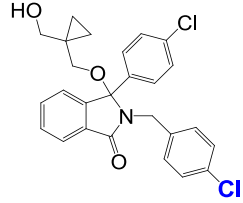
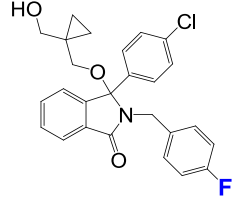
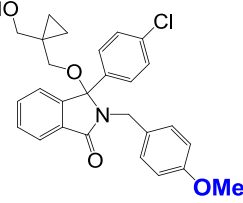
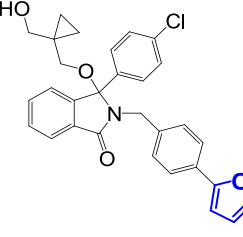
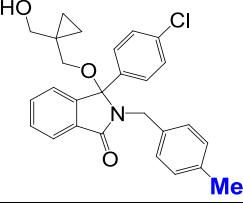
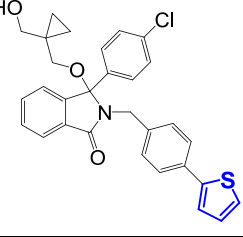
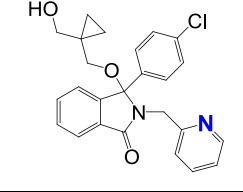
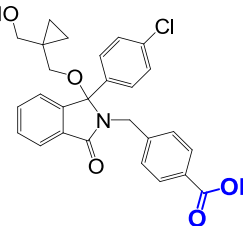
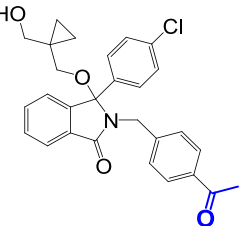
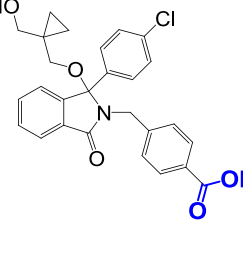
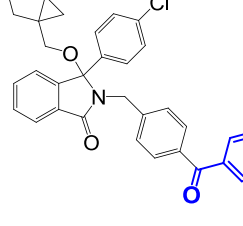
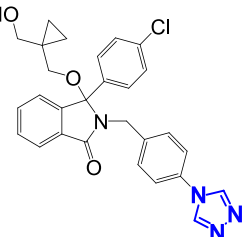
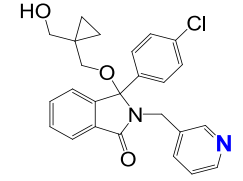
Moreover, the observation that the methoxybenzyl group was more potent than the methylbenzyl group and the (furan-2-yl) benzyl group was more potent than (thiophen-2-yl) benzyl, indicated a relationship between the hydrogen bond effects of this side-chain and the compound's potency.

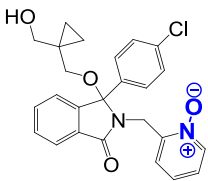
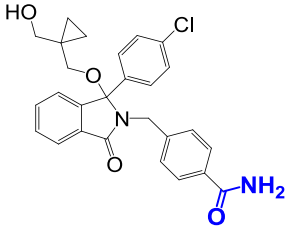
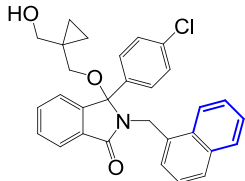
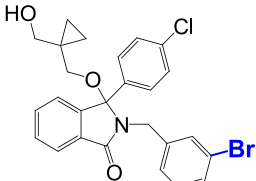
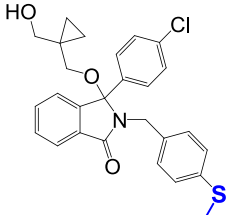
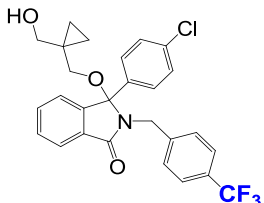
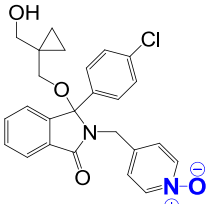
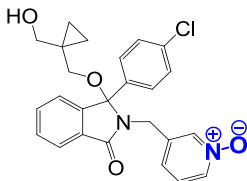
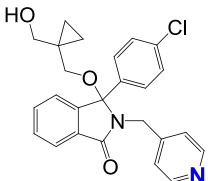
Other modifications in this side-chain position displayed in Table 3. 3 also indicated the influence of the side-chain size and H-bonding capacity effects on compound potency.

Table 3. 3 Side-chain –R₁ modification comparison

		
NU8260 IC₅₀ 2.4 ± 0.2 μM	NCL-00012328 IC₅₀ 9.8 ± 1.2 μM	NU8346 IC₅₀ 10.8 ± 3.8 μM
		
NCL-00014527 IC₅₀ > 20 μM	NCL-00014528 IC₅₀ > 20 μM	NCL-00016656 IC₅₀ > 20 μM
		
NCL-00014532 IC₅₀ > 20 μM	NU8402 IC₅₀ > 20 μM	NCL-00016045 IC₅₀ 85.4 μM
		
NCL-00016046 IC₅₀ 90.1 μM	NCL-00016047 IC₅₀ > 100 μM	NU8386 IC₅₀ > 100 μM

		
NCL-00017325 IC₅₀ 168.3 ± 3.4 μM	NU8420 IC₅₀ > 200 μM	NU8422 IC₅₀ > 200 μM
		
NCL-00017326 IC₅₀ > 200 μM	NU8426 IC₅₀ > 200 μM	NU8423 IC₅₀ > 200 μM
		
NCL-00017327 IC₅₀ > 200 μM	NU8427 IC₅₀ > 200 μM	NU8407 IC₅₀ 433 μM
		
NU8409 IC₅₀ > 500 μM		
		
NU8354 IC₅₀ 0.27 ± 0.01 μM	NU8417 IC₅₀ 0.39 ± 0.06 μM	NCL-00017365 IC₅₀ 0.46 ± 0.03 μM

		
NU8415 IC₅₀ 0.63 ± 0.02 μM	NCL-00014529 IC₅₀ 0.82 ± 0.01 μM	NU8416 IC₅₀ 0.89 ± 0.06 μM
		
NCL-00014530 IC₅₀ 1.71 ± 0.44 μM	NCL-00016866 IC₅₀ 1.88±0.96 μM	NCL-00016896 IC₅₀ 2.25±0.46 μM
		
NCL-00016865 IC₅₀ 2.29±0.05 μM	NCL-00016656 IC₅₀ 8.29 μM	NU8429 IC₅₀ 10.6±0.8 μM
		
NU8388 IC₅₀ > 10 μM	NCL-00014531 IC₅₀ 14.58 ± 1.31μM	NU8378 IC₅₀ > 20 μM
		
NCL-00014533 IC₅₀ > 20 μM	NCL-00016958 IC₅₀ > 20 μM	NU8428 IC₅₀ 28.5 ± 6 μM

		
NU8431 IC₅₀ 32.9 ± 2.9 μM	NCL-00016867 IC₅₀ > 50 μM	NCL-00016106 IC₅₀ 57.8 μM
		
NCL-00016896 IC₅₀ 71.2 μM	NU8410 IC₅₀ 175 μM	NU8408 IC₅₀ 214 μM
		
NU8421 IC₅₀ >200 μM	NU8430 IC₅₀ >200 μM	NU8411 IC₅₀ 252 μM

3.3.1.2 Isoindolin-1-one compounds side-chain –R2 modification

Grouped isoindolin-1-one scaffold compounds information in [Table 3. 4](#) illustrated the modification of position –R2.

Based on the binding mode prediction results using virtual docking software and SAR analysis, it appears that this side-chain is quite special, because the predicted binding mode can be quite different based on whether one considers the aqueous solvent environment effect or not (Appendix I), and one example is demonstrated in

Figure 3. 6, by using Molegro Virtual Docking software (Free Trial Version) from Bioinformatics Research Center, University of Aarhus (molegro bioinformatics solutions) to predict the mode of NU8354 binding with the p53 binding pockets of MDM2. The MDM2 protein surface images in Figure 3. 6 are produced based on volume electric charge density distribution. The colour 'blue' corresponds to the electropositive surface, 'white' corresponds to neutral surface and 'red' to electronegative surface. The compound NU8354 is presented as a 3D stick structure and colour coded as 'green' for carbon, 'white' for hydrogen, 'blue' for nitrogen and 'red' for oxygen. The H-bonds are shown as green dashes. In the left hand side image, it shows the binding mode taking into consideration the effect of the water molecules from the aqueous environment (presented as red dots). The -R2 position side-chain of NU8354, (1-(methoxymethyl)cyclopropyl)methanol group, interacts with a H₂O molecule, the oxygen atom on the isoindolin-1-one ring interacts with another two H₂O molecules, and one oxygen atom on the 4-nitrobenzyl side-chain interacts with a nearby H₂O molecule as well. These interactions enabled the three functional groups of NU8354 to seal the surface of the p53 binding pocket and leave the chlorophenyl side-chain of NU8354 to project into the p53 tryptophan side-chain binding pocket of MDM2. The importance of this binding mode is discussed in detail in the following section. In the right hand side image, the binding mode is quite different, although the MoleDock Score and Docking Score values are very similar to the one we have mentioned before. Without the water solvation effect, the (1-(methoxymethyl)cyclopropyl)methanol group points towards the p53

peptide Phe19 side-chain binding pocket of MDM2, the oxygen atom on the isoindolin-1-one ring interacts with an amino acid residue of MDM2 protein, and one oxygen atom on the nitrobenzyl side-chain interacts with another amino acid residue of the MDM2 protein. These interactions force the chlorophenyl side-chain of NU8354 into the remaining p53 binding pocket on MDM2, *i.e.* the Leu26 binding pocket.

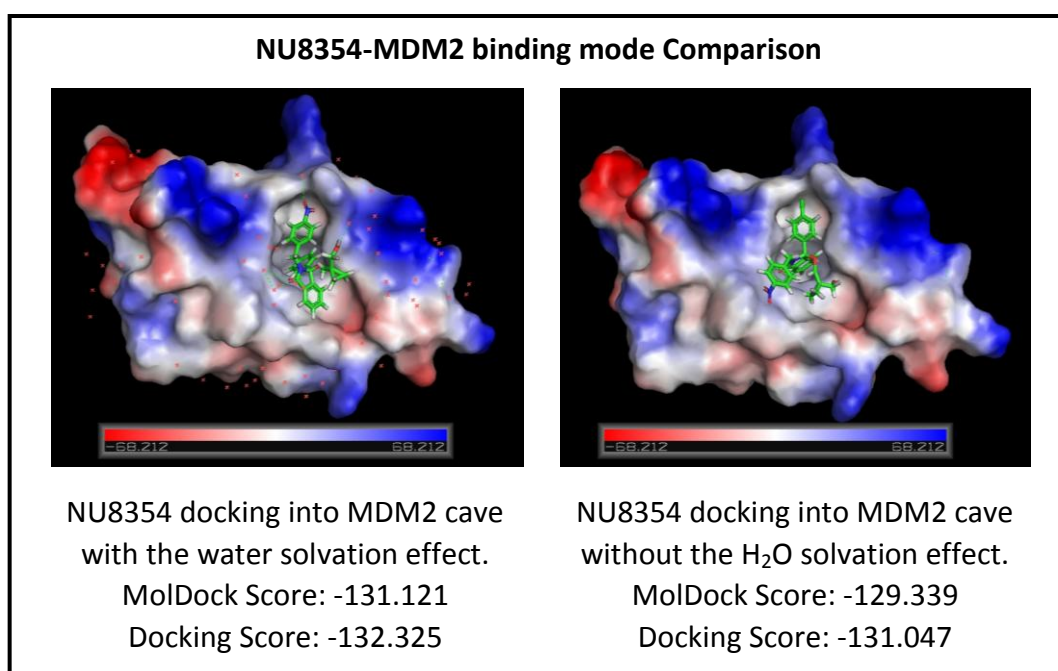


Figure 3. 6 NU8354-MDM2 Docking Results Generated by Using Molegro Virtual Docking Software Indicated Different Binding Modes with whether Considering Water Solvation Effects or Not.

The most appropriate model is one which considers the aqueous environment, since this is the condition present in both the ELISA binding method, which is carried out in PBS solution, and in the cytoplasm and nucleoplasm environment of intact mammalian cells which is predominantly aqueous.

The results in Table 3. 4 indicated that the length, shape and water solubility of the side-chain affected the compound's potency markedly.

NCL-00016149, and NU8354 were the most potent among the batch of compounds grouped in Table 3. 4, and different $-R_2$ side-chain structures lead to different potency.

Changing the terminal oxygen on the $-R_2$ side-chain into nitrogen led to a 4-fold decrease of compound potency (compare NU8348 with NU8380), and the difference between NU8348 with NU8380 was only changing the terminal $-OH$ group of the $-R_2$ side-chain into an $-NH_2$ group, which indicated the H-bond acceptor effect plus the H-bond donor effect of the $-OH$ group is perhaps bigger than the combined effects of the $-NH_2$ group.

Comparison of NU8260 with NU8348 shows the extension of the $-OH$ group with an n-propyl carbon chain increases the potency by a factor of 4 to 5 fold, which supports the hypothesis that a hydrophilic group of appropriate extension direction, shape and length of the carbon chain at the $-R_2$ position contributes to enhancing the potency of isoindolin-1-one compounds.

This hypothesis is also supported by the fact that with the influence of a large hydrophobic side-chain e.g. an $-Fmoc$ group at the end of the $-R_2$ side chain, the potency of the compound decreased markedly (NU8355).

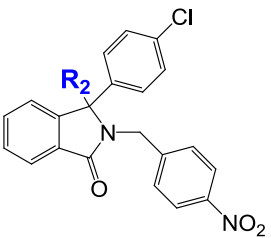
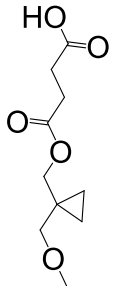
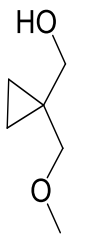
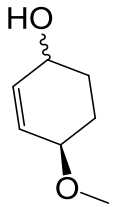
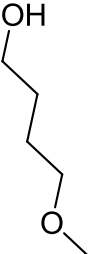
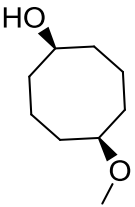
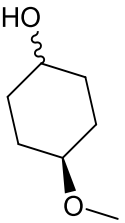
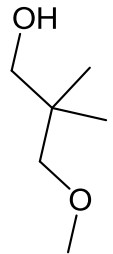
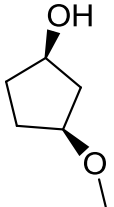

Although compound NCL-00016149 contained a chlorine atom on the isoindolin-1-one ring, which contributed to the increase of the compound's potency, another important factor was the adding of the oxobutanoic acid at the end of $-R_2$ side chain, which markedly enhanced the compound's potency by 8-fold.

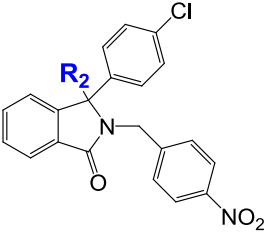
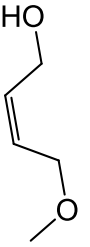
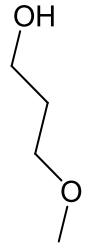
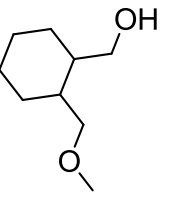
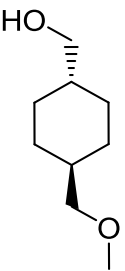
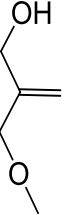

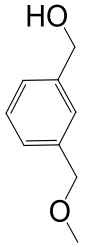
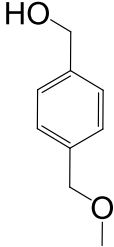
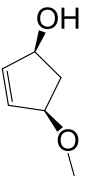
Changing the oxygen into carbon to link the isoindolin-1-one ring with the $-R_2$ side-chain should enhance the stability of the compounds (with the removal of the oxygen linkage), but their potencies were markedly sacrificed at the same time (compare NU8260 with NCL-00010497, NCL-00016147, NCL-00016658), which indicated some positive effect of this oxygen. However, comparing NCL-00016147 with NCL-00016658 and NCL-00010497 with NCL-00016985, an interesting phenomenon with the extension of the side-chain is observed, *i.e.* increasing the distance between the hydrophilic groups from the main scaffold result in slightly better potencies, which needs further side-chain variation to explore the possible reason.

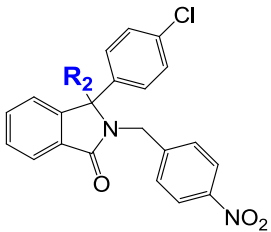

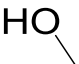
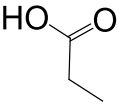
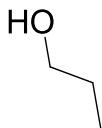
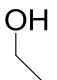
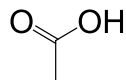
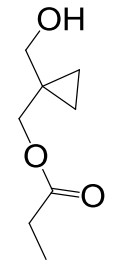
The relationship between the $-R_2$ side-chain variation and the compound potency from NU8354 to NU8297, especially the comparison of the IC_{50} results between NU8296 and NU8297, which also showed a 5 fold difference of potency, suggested another attractive hypothesis (which may need further experiments to examine). The residues on the $-R_2$ side-chain may also contribute to the binding between isoindolin-1-ones with MDM2, possibly interacting with the same MDM2 binding position as the Leu22 of the p53 peptide. Also informing this potential binding

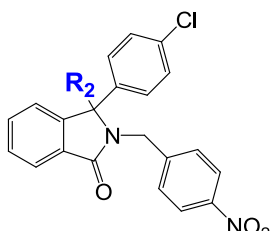
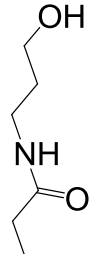
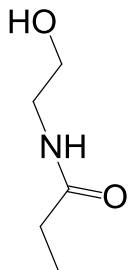

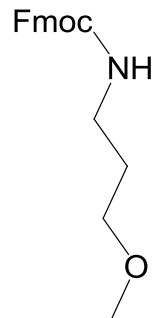
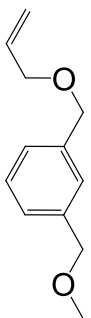
mode is the observation that the double bond in the five-carbon ring of NU8297 which would have decreased flexibility of the $-R_2$ side chain, resulting in a marked decrease of potency compared with NU8296.

Table 3. 4 Side-chain –R₂ modification comparison

Compound Code	NCL-00016149	NU8354	NU8361	NU8349	NU8352	NU8360	NU8353	NU8296	NU8350
									
IC50 (μM)	0.0158+Cl	0.269	0.306	0.357	0.375	0.388	0.395	0.395	0.402

Compound Code	NU8351	NU8348	NU8359	NU8358	NCL-00016695	NU8357	NU8367	NU8366	NU8297
									
IC50 (μM)	0.405	0.453	0.569	0.582	0.617	0.656	0.732	0.983	1.90

Compound Code	NU8380	NU8260	NCL-00010497	NCL-00016147	NCL-00016658	NCL-00016985	NCL-00013768
							
IC50 (μM)	1.90	2.40	4.16	4.41	6.83	7.67	10.46

Compound Code	NCL-00013770	NCL-00013769	NCL-00016148	NU8355	NU8371		
							
IC50 (μM)	13.36	15.99	48.16	79.8	> 100		

3.3.1.3 Isoindolin-1-one compounds side-chain –X modification

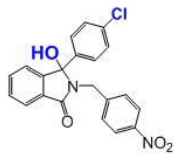

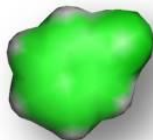


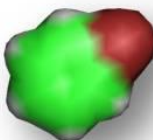
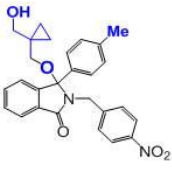
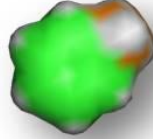


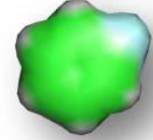
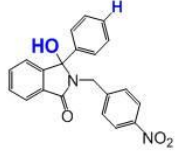

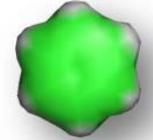
Table 3. 5 compares isoindolin-1-one scaffold compounds with variation of the –X position, including the corresponding space filling view reproduced by using PyMOL software (the side-chain –X was colour coded as: green to –Cl, brown to –Br, cyan to –F and light orange to the carbon atom of –CH₃ group, with the white coding all the hydrogen and light green to the carbon atoms on benzene ring).

When the chlorine atom was replaced by other halogen atoms, hydrogen or a methyl group the change in the IC₅₀ results indicated that it might be the size of this side-chain and the van der Waals interaction between the side-chain and the MDM2 protein side chains around the tryptophan binding pocket, rather than a halogen ‘salt-bridge effect’, that determined the binding potency.

The binding model poses with the –X group docking into the tryptophan binding pocket of MDM2 indicated that the sizes of bromo and methyl were too large for the binding pocket, and the sizes of fluoro and hydrogen were too small to occupy the binding pocket fully. Chloro was the most suitable group for this position, which is quite similar to the comparison of the peptide side-chain binding with the tryptophan binding pocket of MDM2 (125). The predicted binding mode also indicated that the chlorophenyl side-chain embedded into the p53 peptide tryptophan binding pocket of MDM2 protein had the lowest docking energy. This is also supported by the increase in binding potency produced with p53 peptide binding studies by the substitution of tryptophan by 6-chlorotryptophan.

Based on these two side-chain SAR analyses, we have generated a ‘**See-Saw Theory**’ for the binding mode (See Chapter 7).

Table 3. 5 Side-chain –X modification comparison

Compounds code & IC ₅₀	Compounds Structure	Compounds code & IC ₅₀	Compounds Structure	Side Chain –X with benzene ring Image
NU8260 2.4 ± 0.2 μM		NU8354 269 ± 12 nM		
NU8389 3.1 ± 0.2 μM		NU8391 368 ± 45 nM		
		NCL-00016957 1.24 μM		
NCL-00016657 9.46 μM		NCL-00016896 2.25 ± 0.46 μM		
NCL-00016655 87.01 μM		NCL-00016656 8.29 μM		

3.3.1.4 Isoindolin-1-one compounds modification on the main scaffold

Finally is the isoindolin-1-one ring modification as summarised in Figure 3. 7.

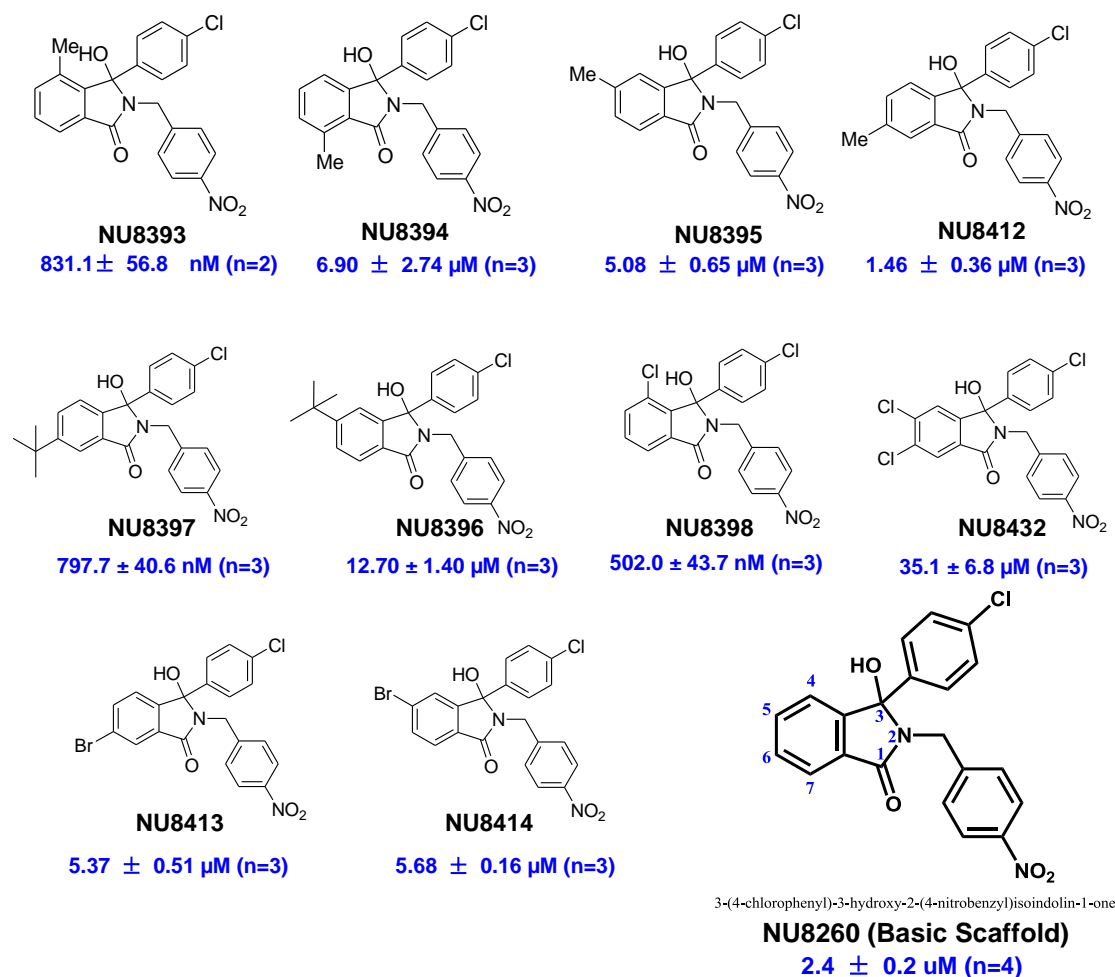


Figure 3. 7 Modification of the isoindolin-1-one ring based on the NU8260 scaffold

Comparing the four compounds NU8393, NU8394, NU8395 and NU8412, with a methyl residue at the 4-, 5-, 6- or 7- position of the isoindolin-1-one ring, the IC₅₀ results showed marked differences (Figure 3. 7). Comparing the potency of these compounds with the unsubstituted NU8260 basic scaffold compound, we can conclude that the addition of hydrophobic residues at the 4- and 6- position enhanced compound potency, but at the 5- and 7- position have lead to a marked loss of potency.

This conclusion was supported by compounds NU8396, NU8397 and NU8398, however, NU8413 and NU8414 with the –Br at the 5-/6- position do not follow the same pattern.

On the other hand, the scaffold with two Cl residues on the ring leads to a marked loss of potency, which may not only be due to the binding affinity decreasing because of a poor fit to the MDM2 binding pocket, but also because of solubility decreasing.

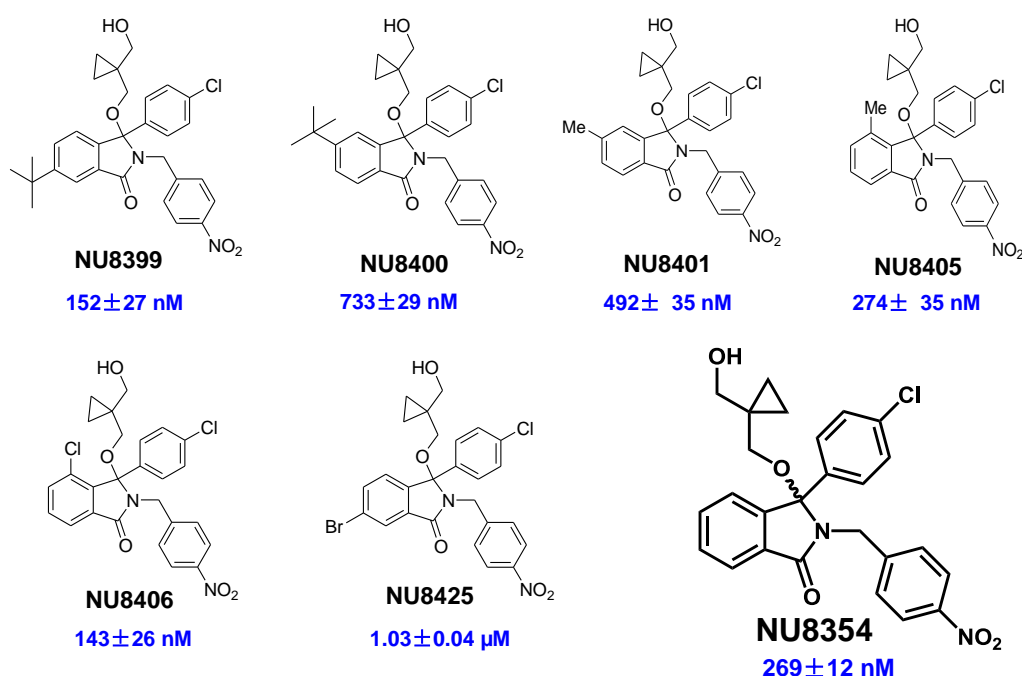


Figure 3. 8 Modification on isoindolin-1-one ring based on the NU8354 scaffold

With the addition of the '(1-(methoxymethyl)cyclopropyl)methanol' side-chain at the –R2 position, the compound potencies all increased markedly and became comparable to Nutlin-3 (Figure 3. 8).

Furthermore, the most potent isoindolin-1-one compound within the group shown in Figure 3. 8, NU8046, was a racemic mixture with an IC₅₀ of 143 nM. This encouraged us to anticipate that a pure active enantiomer might be comparable to or even more

potent than Nutlin-3. This also potentially provided a binding mode confirmation, when compared with the structure of NU8399, which, with a bulky tert-butyl substituent, had been predicted to be a negative control, but proved to be a quite potent compound (further discussion in the context of western blotting results in Section 4.2.3).

3.3.2 Isoindolin-1-one compounds as MDMX/p53 interaction inhibitors

The results of selected isoindolin-1-one compounds as MDMX/p53 binding inhibitors indicated that, almost none of them were able to disrupt the binding between MDMX and p53 effectively. However, detailed inhibition potency results gave us some more information, which might be encouraging (Figure 3. 9).

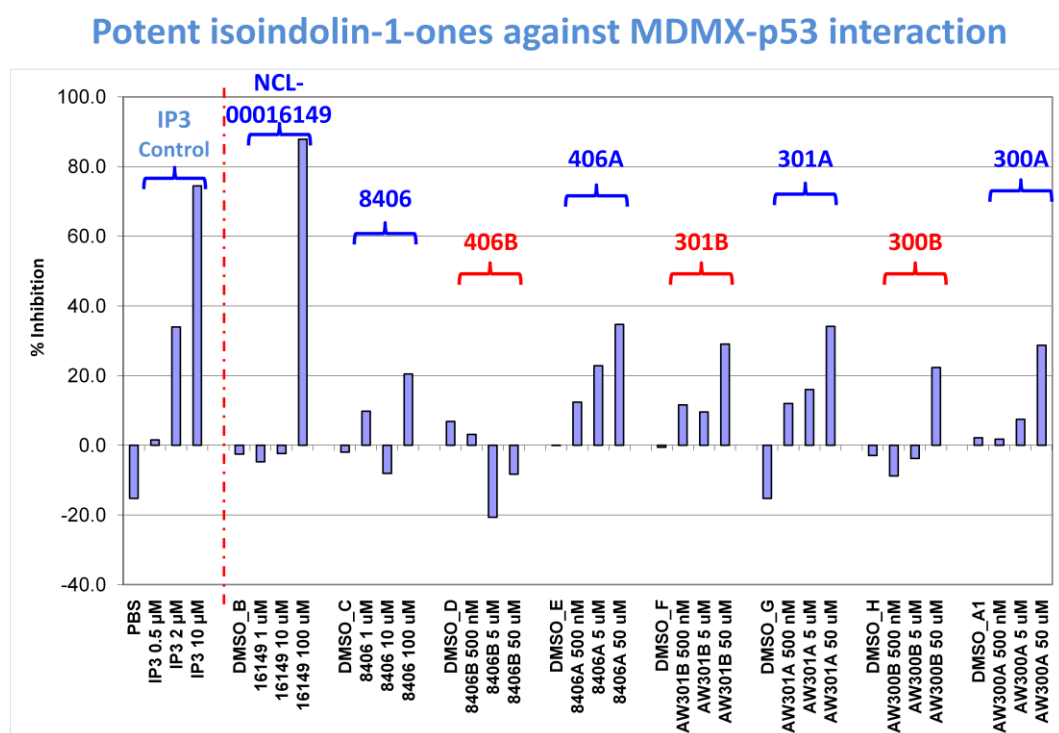


Figure 3. 9 ELISA for isoindolin-1-one compounds as MDMX inhibitors

The results displayed in [Figure 3. 9](#) indicated that potent MDM2 inhibitor isoindolin-1-one enantiomers (NU8406A, NCL-00017305_300A & NCL-00017306_301A) showed a greater, albeit weak, ability to inhibit MDMX/p53 binding than the less potent MDM2 inhibitor isoindolin-1-one enantiomers, and some of the less potent compounds showed a negative effect; i.e. appeared to promote binding.

Furthermore, the succinate ester NCL-00016149 showed greater than 50 percent inhibition potency at 100 μ M concentration. These observations indicated that the binding pocket of MDMX differs markedly from that of MDM2 so that MDM2 inhibitors are not automatically MDMX inhibitors; however, they also have some similarity, and it is still possible to develop MDMX inhibitors based on the already obtained MDM2 inhibitors as potential leads. One of the key question would be how different would they need to be and what kind of modification needs to be made to turn an MDM2 inhibitor into an MDMX inhibitor or a joint MDM2 and MDMX inhibitor.

For this reason, further research has been carried out by using different scaffold compounds and peptides, and this is discussed in detail in Chapter Five.

Chapter Four

Isoindolin-1-one Compounds: Evaluation of Cellular Activity

4.1 Introduction

The previous chapter described the use of the cell-free ELISA to identify small molecular weight compounds that can interrupt the protein-protein binding interaction between p53 and MDM2, and to compare their potency with the positive control compounds Nutlin-3 and MI-63. However, this alone does not necessarily predict their behavior in intact mammalian cells, and questions such as: Will they be able to cross the cell membrane efficiently? Will the cells resist their effect by effluxing them out directly? Are there any off-target cellular effects, *etc.* need to be explored and answered by evaluation in cellular assays.

With the progression of the research project, several isoindolin-1-one scaffold compounds with potency comparable to Nutlin-3 as MDM2/p53 inhibitors were identified by the ELISA screening method. The next step was to evaluate their cellular activity to ascertain whether they had effects on cells that were consistent with inhibition of MDM2-p53 binding.

During the lead optimisation phase of development, the structures of these compounds were designed and synthesized step by step based on the SAR analysis ([Figure 4. 1](#)). The cellular responses of the compounds at each step were evaluated by western blotting to evaluate and compare their ability to induce p53 pathway protein expression. Compounds showing cellular responses as inducers of p53 activity were

taken forward to evaluate their growth inhibitory and cytotoxic properties. The potency for growth inhibition was compared using the SRB assay to determine the concentration of compound required to inhibit growth by fifty percent (GI_{50}).

The key compound structures along the path of lead optimisation and associated IC_{50} values are listed in [Figure 4. 1](#).

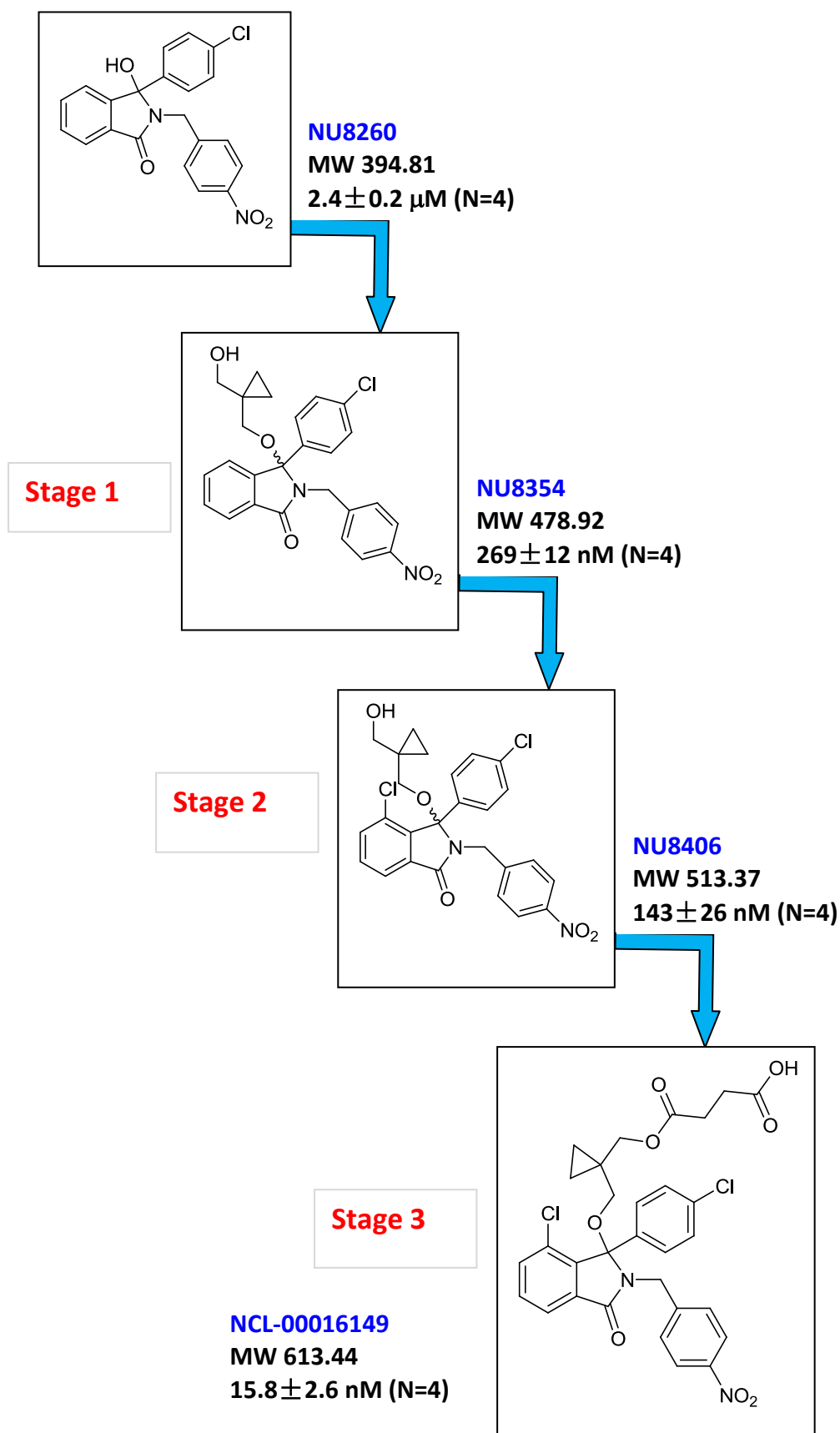


Figure 4. 1 Progression of isoindolin-1-one scaffold compounds during lead optimisation as MDM2-p53 binding interaction inhibitors

4.2 Western Blotting for Cellular Activity Evaluation and Comparison of Isoindolin-1-one Compounds

4.2.1 Western Blot Result for Stage 1 Isoindolin-1-one Compounds

All the selected stage 1 isoindolin-1-one compounds produced a dose-dependent increase in MDM2, p53 and p21, consistent with the release of p53 from MDM2 binding and its transcriptional activation (Figure 4. 2-a, -b & -c). The corresponding quantitative analysis of the western blot band optical densities are shown in Figure 4. 3 and comparison showed that the cellular activity of NU8354 and NU8361 was approximately two to three times less potent than Nutlin-3 for induction of MDM2 protein expression as a marker of p53 activation.

The most potent stage 1 isoindolin-1-one compound, NU8354, as determined by ELISA bioassay, was selected for further comparison with Nutlin-3 to ascertain whether they have similar effects on cells that were consistent with specific inhibition of MDM2-p53 binding. For this purpose, three cell lines, SJSA-1, HCT116_{p53+/+} and HCT116_{p53-/-} were selected for further cellular evaluation of the MDM2/p53 inhibitors. The cells were treated with 10 μ M and 20 μ M NU8354 for 6, 24 and 48 hours respectively, and the concentration of Nutlin-3 was 10 μ M with the same time scale of treatment as NU8354. Cells were lysed after treatment for each time point and levels of MDM2, p53 and p21^{WAF1} were investigated by western blotting (Figure 4. 4-a, b&c).

The SJSA-1 cell line western blot result (Figure 4. 4-a) showed that all the tested stage 1 isoindolin-1-one compounds were able to induce p53 accumulation with a dose-dependent downstream target MDM2 and p21 activation in SJSA-1 cells; and

their cellular activities were similar to the Nutlin-3 effect. NU8354 was the most potent one also in western blotting assay.

Both Nutlin-3 and NU8354 have the ability to inhibit the interaction between MDM2 and p53 protein and activate p53-dependent transcription and consequent protein accumulation when compared with DMSO solvent control, as evidenced by the induction of increased levels of p53, MDM2 and p21^{WAF1} protein after 6 and 24 hours treatment. For both Nutlin-3 and NU8354, at the longer treatment time of 48 hours MDM2 and p21^{WAF1} protein levels tended to decrease compared with the 24 hour levels, although interestingly the p53 protein levels continued to increase. These results indicated that NU8354 can inhibit the MDM2-p53 protein-protein interaction with a similar mechanism to Nutlin-3, although with slightly lower potency than Nutlin-3.

A comparison of the western blotting bioassay results between HCT116_{p53+/+} and HCT116_{p53-/-} cell lines ([Figure 4. 4-b and -c](#)) showed that p53, MDM2 and p21 protein in both Nutlin-3 and NU8354 treated HCT116_{p53+/+} tumour cells increased markedly compared to DMSO solvent control by 6 hours. In contrast, there were no p53 protein bands, as expected, and very faint MDM2 bands in the western blot result of HCT116_{p53-/-} tumour cells, although the p21 protein bands were still detectable, but without marked variation. At longer time points, Nutlin-3 showed continued activity against HCT116_{p53+/+} tumour cells, but the cellular effect of NU8354 tended to decrease markedly from 6 h to 24 h and then 48 h, especially at the 20 μ M concentration. Based on these observations, the stability of NU8354 has to be considered, although the exact reason has not been determined so far.

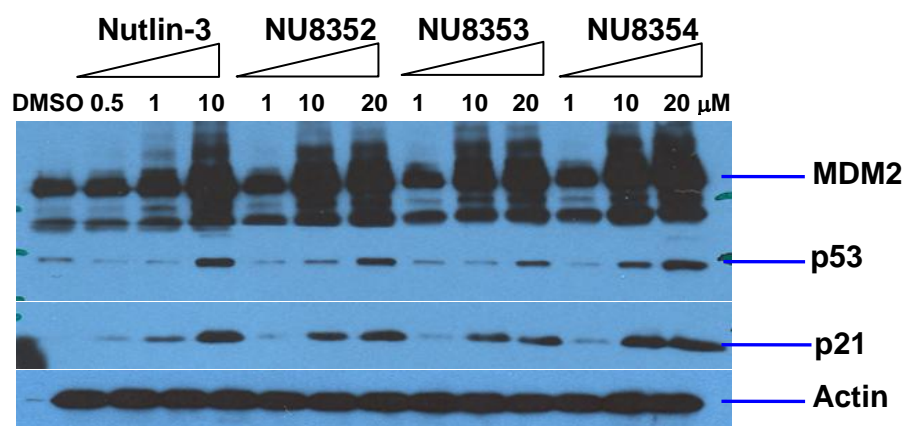


Figure 4.2-a

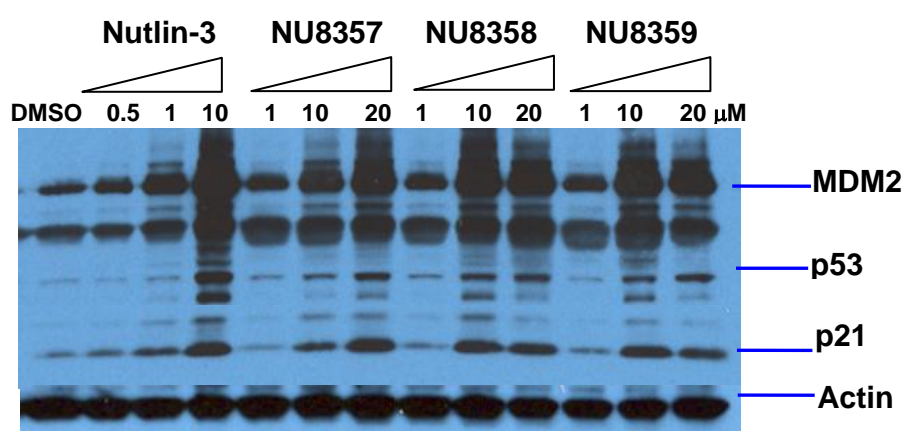


Figure 4.2-b

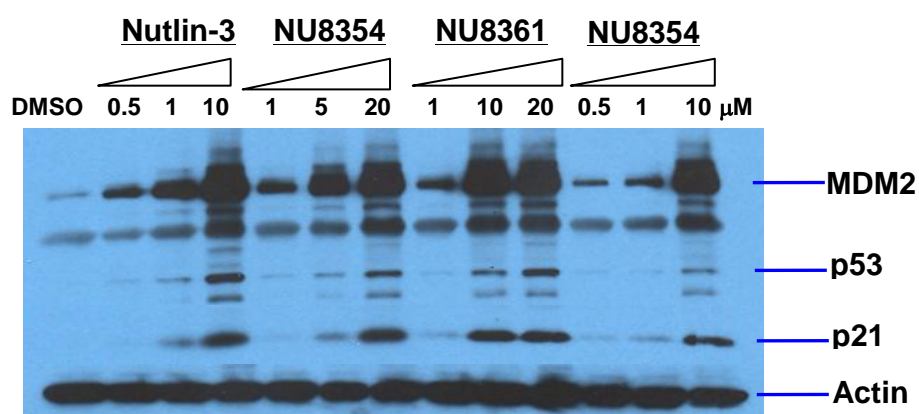


Figure 4.2-c

Figure 4. 2 Western blotting evaluations of dose-dependent cellular effects of selected stage 1 isoindolin-1-one compounds and Nutlin-3 using the SJSA-1 cell line

Cells were treated with increasing concentrations of isoindolin-1-one compounds (1 μ M, 10 μ M and 20 μ M) and positive control Nutlin-3 (0.5 μ M, 1 μ M and 10 μ M). Then cells were lysed after treatment with compounds for 4 hours. Proteins involved in p53-dependent cell regulation including MDM2, p53 and p21^{WAF1} were detected by western blot analysis and either β -actin protein was evaluated as a loading control.

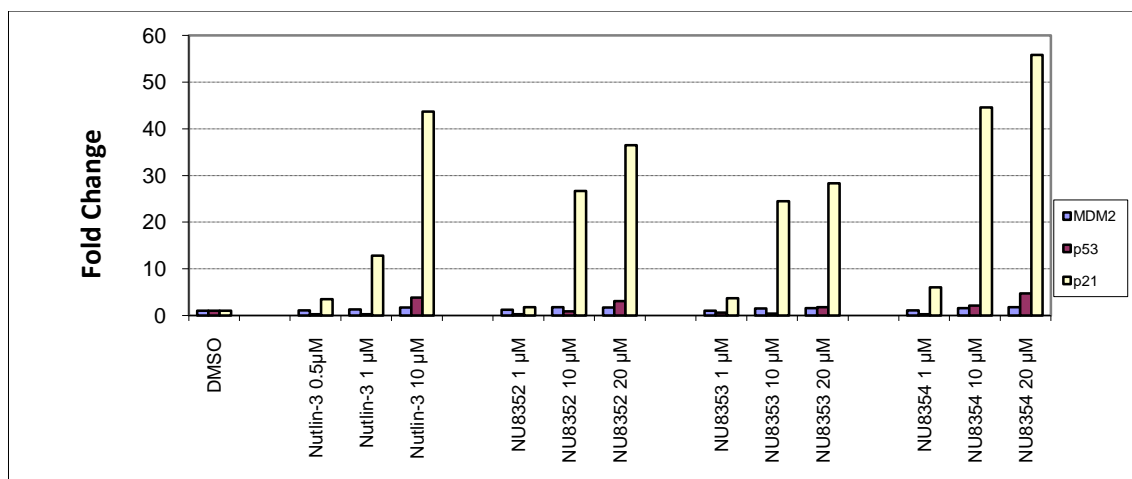


Figure 4.3-a

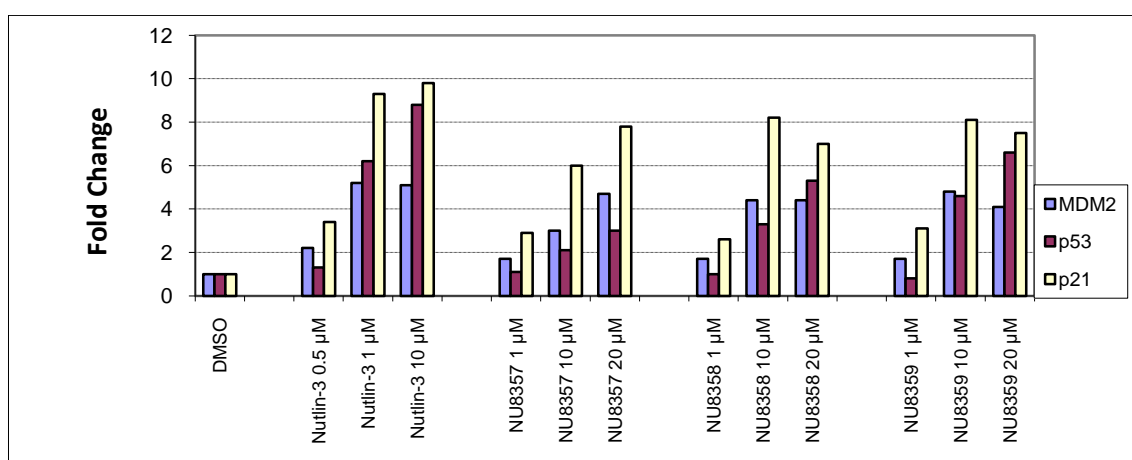


Figure 4.3-b

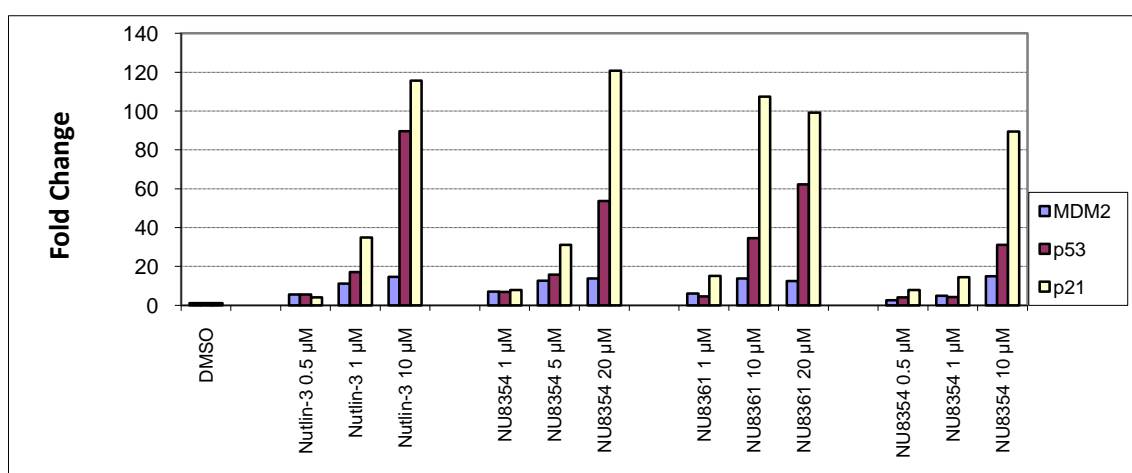


Figure 4.3-c

Figure 4. 3 Densitometry analyses of protein bands densities of MDM2, p53 and p21^{WAF1} for the western blotting results in Figure 4.2

The densitometry analyses results confirmed the observation in Figure 2 with a quantitative comparison.

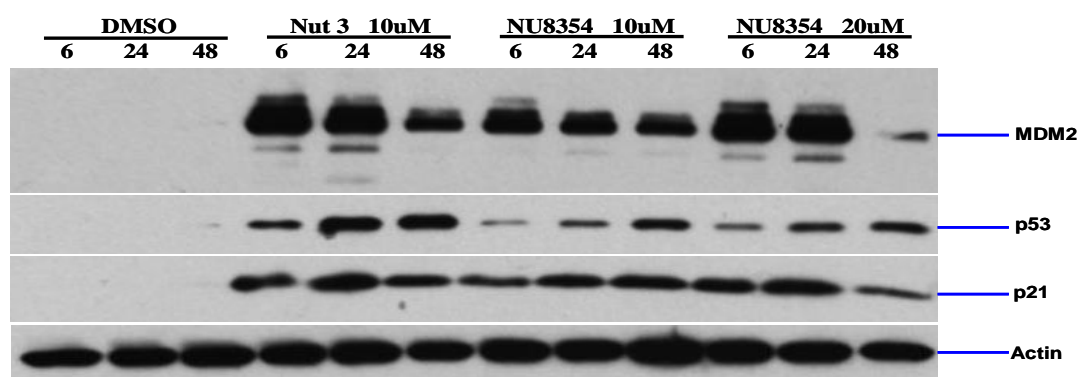


Figure 4.4-a (SJSA-1 Cell Line)

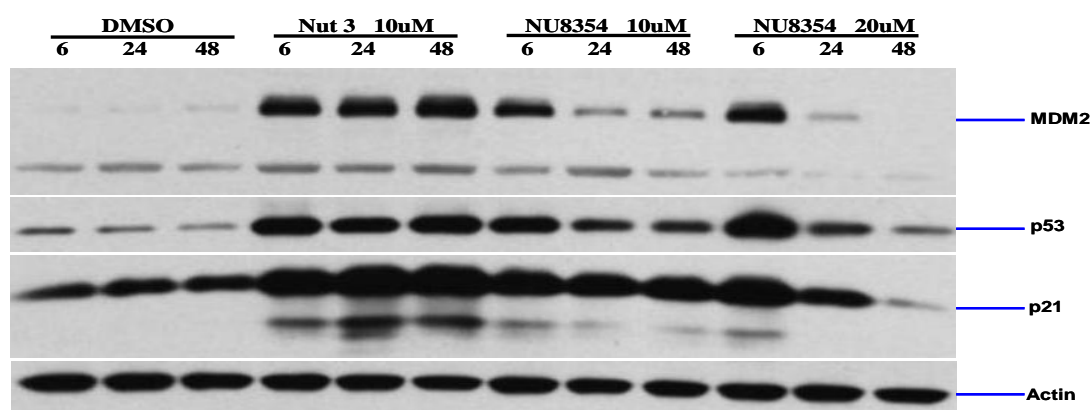


Figure 4.4-b (HCT116 p53+/+ Cell Line)

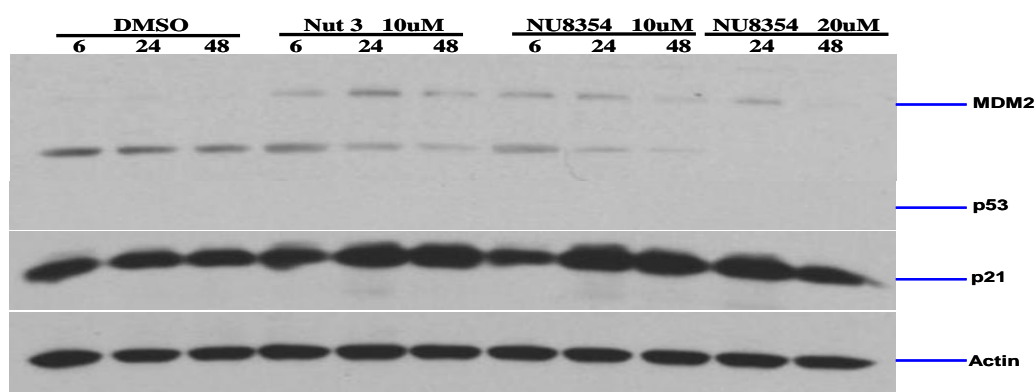


Figure 4.4-c (HCT116 p53-/- Cell Line)

Figure 4. 4 Western blot analysis of p53, MDM2 and p21^{WAF1} for three time points of treatment with NU8354 compared with Nutlin-3 in a) SJSA-1, b) HCT116_{p53+/+} & c) HCT116_{p53-/-} cell lines

Cells were treated with increasing concentrations of isoindolin-1-one compounds (1μM, 10 μM and 20 μM) and positive control Nutlin-3 (0.5 μM, 1 μM and 10 μM). Then cells were lysed after treatment with compounds for 4 hours. Proteins involved in p53-dependent cell regulation including MDM2, p53 and p21^{WAF1} were detected by western blot analysis and either β-actin protein was evaluated as a loading control.

4.2.2 Western Blot Comparison of MDM2/p53 Inhibitors and X-ray Irradiation Time Course Cellular Effects

To obtain a better understanding of the different mechanisms of activating the p53 pathway, the effect of MDM2/p53 binding antagonists was compared with DNA damage induced by X-ray irradiation using SJSA-1 and NGP tumour cell lines ([Figure 4. 5](#) & [Figure 4. 6](#)).

The images in [Figure 4. 5](#) show the response of the SJSA-1 cell line with different treatments. Changes in MDM2, p53 and p21^{WAF1} protein levels were investigated, together with ser15-p53 phosphorylation. β -actin was probed for as a loading and transfer control.

The DMSO control ([Figure 4. 5-1](#)) showed very stable expression of MDM2 protein and no marked p53 pathway protein induction in all the sample time points.

Shortly after X-ray irradiation treatment (10 minutes), the ser-15 p53 band density increased and peaked at 1-2 hours, before decreasing back to near control unirradiated levels by 4 hours ([Figure 4. 5-5](#)).

With Nutlin-3 and MI-63 treatment ([Figure 4. 5-3 & 4](#)), the ser-15 p53 signal appeared later than the increase in p53, and the increase were maintained continuously from the 2 hour treatment samples to 48 hour treatment samples.

The effect of 5 μ M NU8354A ([Figure 4. 6-2](#)) was different from both of them. The expression of p53 was detected as early as 30 minutes after compound treatment, and achieved highest band density after 2 hour treatment, then continued to be detectably elevated for 48 hours; but the ser-15 p53 phosphorylation was detected from 30 mins

after compound treatment, and then continued to increase in the 2 hour time point sample, returning to only faintly detectable levels in all the remaining time point samples.

On the other hand, the pattern of activation of the p53 pathway downstream targets, MDM2 and p21 was quite similar in SJSA-1 cell line samples with all three compound treatments (Figure 4. 5-2, 3 & 4). The MDM2 protein expression started to increase after 2 hours compound treatment, then remained over 24 hours of compound treatment, before slightly decreasing in the 48 hours time point samples. The accumulation of p21 protein started at the 4 hours time point samples and continued to increase until the 24 hours time point, and then continued to increase in the NU8354A and Nutlin-3 treated 48 hour time point samples, but decreased in the MI-63 treated 48 hours time point sample. With X-ray irradiation, both MDM2 and p21 protein expression in the SJSA-1 cell line started to increase in the 2 hours time point sample, and then remained elevated for up to 48 hours (Figure 4. 5-5).

In summary, based on the time course western blot comparison result using SJSA-1 cancer cells, the NU8354A showed similar cellular effect as the published potent MDM2-p53 interaction antagonists Nutlin-3 and MI-63 induced cellular response (mainly relies on interruption of MDM2-p53 binding interaction), which is different from the X-ray irradiation reaction (mainly relies on p53 phosphorylation). The observation of multiple protein bands above and /or below p53 and p21 may need further experiment to confirm their existence and explore the mechanism in future.

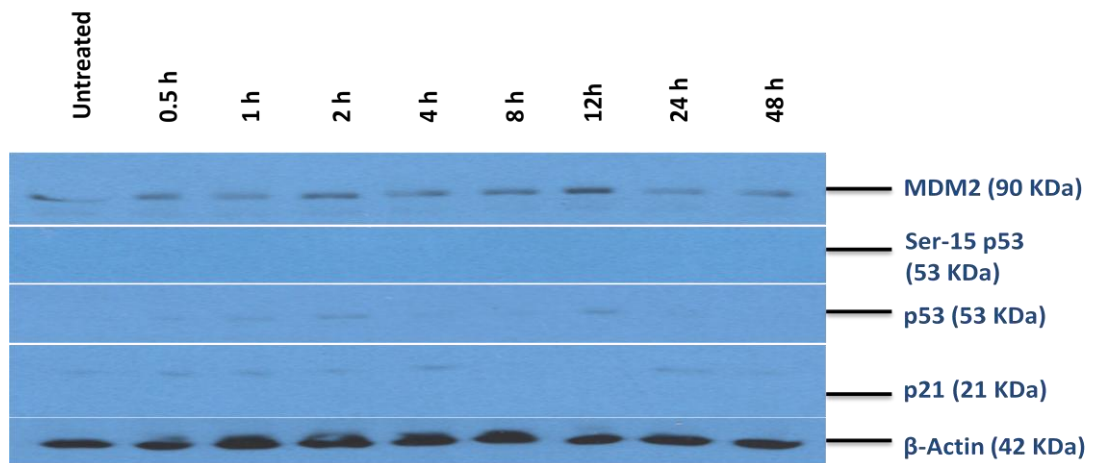


Figure 4.5-1 DMSO Control

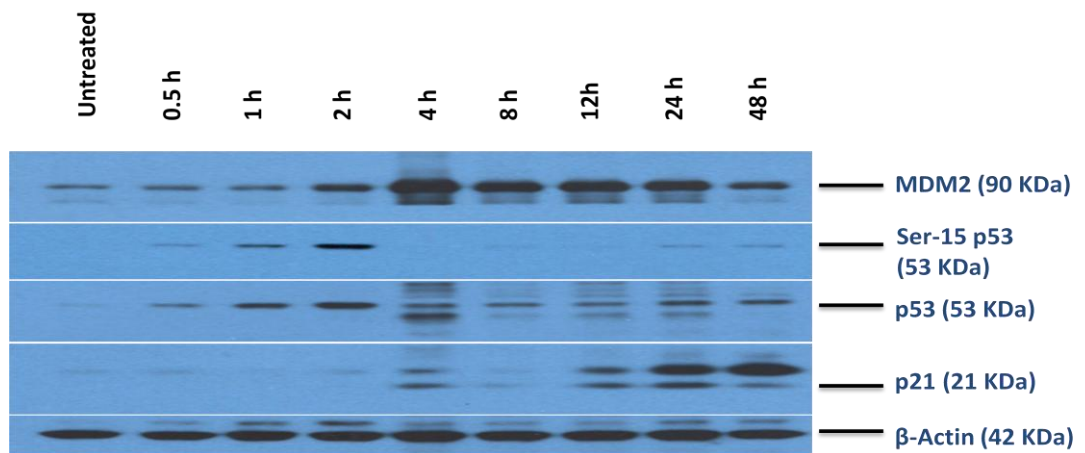


Figure 4.5-2 NU8354A 5 μ M Treatments

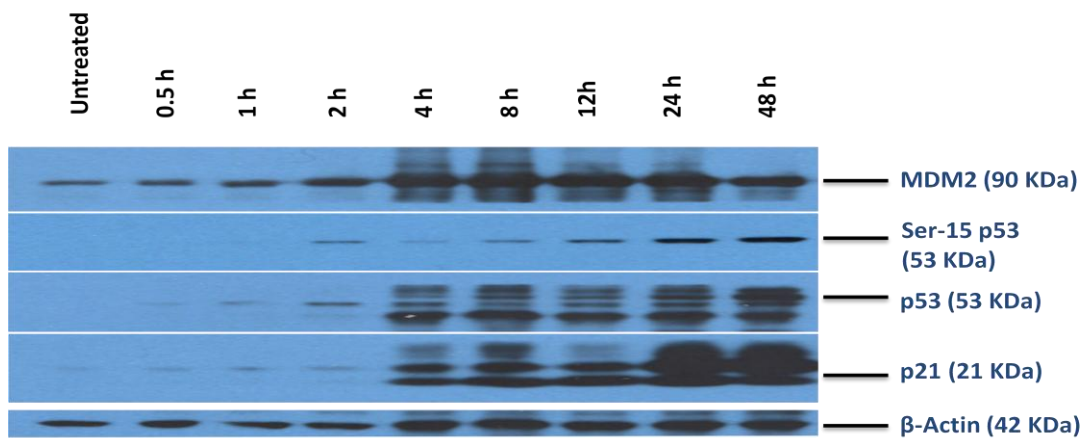


Figure 4.5-3 Nutlin-3 5 μ M Treatments

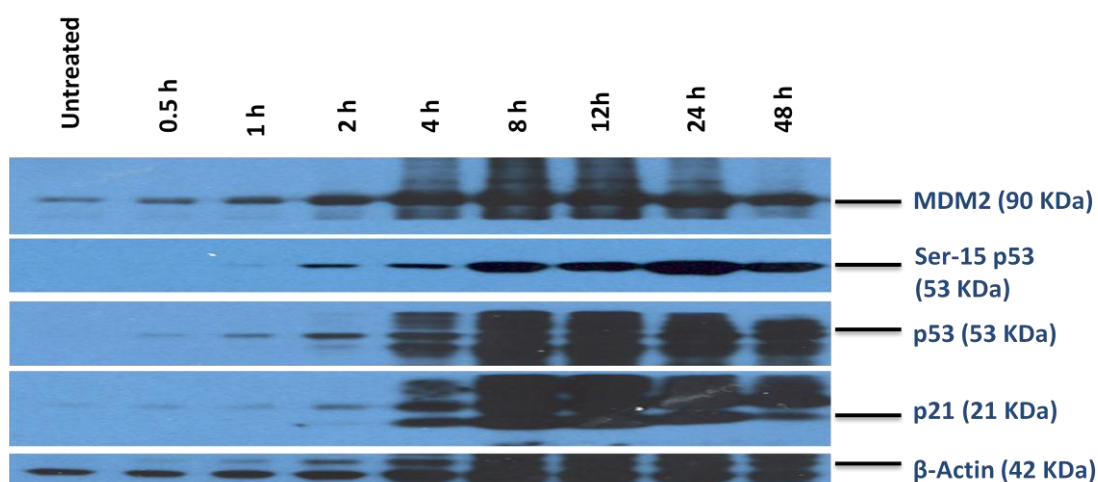


Figure 4.5-4 MI-63 5 μM Treatment

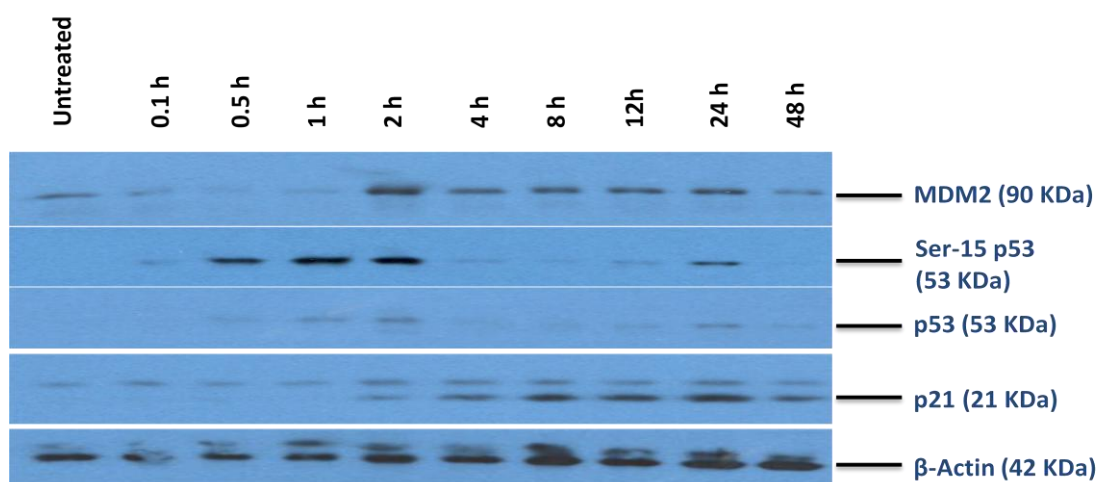


Figure 4.5-5 X-ray Irradiation Treatments

Figure 4. 5 Western blot time courses of SJS-A1 cellular effects comparing NU8354A with Nutlin-3, MI-63 and X-ray irradiation treatments.

The time course effects of MDM2/p53 inhibitors Nutlin-3, MI-63 and the isoindolin-1-one compound 'NU8354A' were compared together with DMSO control and X-ray irradiation by using SJS-A1 cell line. Plated cells were treated with either 1% DMSO, test compounds at 5 μM, or 6.3 Gy X-ray radiation; cell lysates were then collected at each time point and analyzed by western blotting. MDM2, Ser-15 phosphorylated p53, p53, p21 protein expression were considered, and actin was probed as a loading and transfer control.

The cellular responses of the NGP cell line with various treatments are displayed in [Figure 4. 6](#). Levels of proteins involved in p53-dependent cell regulation including MDM2, p53, p21WAF1, PUMA and cleaved caspase-3 were investigated by western blot analysis, and changes in MDMX, ser15-p53 and β -actin were also evaluated.

The DMSO control result ([Figure 4. 6-1](#)) illustrated very stable expression of MDMX protein and no marked p53 pathway protein expression in all time point samples. The only protein expression variation that was detected was PUMA protein accumulation from 12 hours to 48 hours.

Both Nutlin-3 and MI-63 treated NGP cell samples showed obvious p53 pathway activation ([Figure 4. 6-3, 4](#)). Noticeable accumulation of p53 started from after 2 hours compound treatment, and this increase was maintained over the 48 hours compound treatment; MDM2 accumulation started from 4 hours compound treatment and then was reduced in the 24 and 48 hour samples; p21 accumulated markedly from 8 hours drug treatment then was reduced after 48 hours drug treatment; cleaved caspase-3 activation was evident after 24 and 48 hours treatment. Following the peak accumulation of MDM2, MDMX protein expression started to decrease at the 12 hours time point with the Nutlin-3 treatment, and much later but to a greater extent with the MI-63 treatment at the 24 hours time point, and could not be detected in 48 hour time point samples. Interestingly, the expression trends of PUMA in samples treated by both of the two drugs were quite similar, and the accumulation starting time points were the same as for p53 protein accumulation.

The NGP cell responses with 5 μ M NU8354A treatment were not very marked ([Figure 4. 6-2](#)), which might because of the lower potency of the compound compare to

Nutlin-3 and MI-63. However, accumulation time points of p53, MDM2 and PUMA were the same with Nutlin-3 and MI-63 treated cell samples, although protein band densities were very low. Furthermore, decreased MDMX expression was also detected in the 48 hour time point sample.

The X-ray irradiation effects were quite different ([Figure 4. 6B-5](#)). The MDMX expression started to decrease only 30 minutes after irradiation, and then continued until the end, although there was no marked MDM2 accumulation in all time point samples. Marked Ser-15 p53 phosphorylation was detected in 2 hours post-irradiation sample, decreased by 4 hours and almost vanished at subsequent time points. PUMA accumulation started to be detected by 2 hours, continued to increase until 48 hours, although there was no detectable accumulation of p53 protein. Accumulation of p21 protein was detected at 8 and 24 hour time points, with a reduced level at the intervening 12 hour time point. No cleaved caspase-3 was detected in any of the X-ray irradiated samples.

In summary, based on the time course western blot comparison result using NGP cancer cells, the NU8354A showed similar but weaker cellular effect than the published potent MDM2-p53 interaction antagonists Nutlin-3 and MI-63 induced cellular response, which is different from the X-ray irradiation reaction (mainly relies on p53 phosphorylation). Moreover, as one of the indicators of apoptosis pathway activation, cleaved caspase-3 showed better specificity than PUMA, since PUMA expression was not only detected in MDM2 antagonists and X-ray irradiation treated samples, but also in DMSO treated samples, although the initiating time is different.

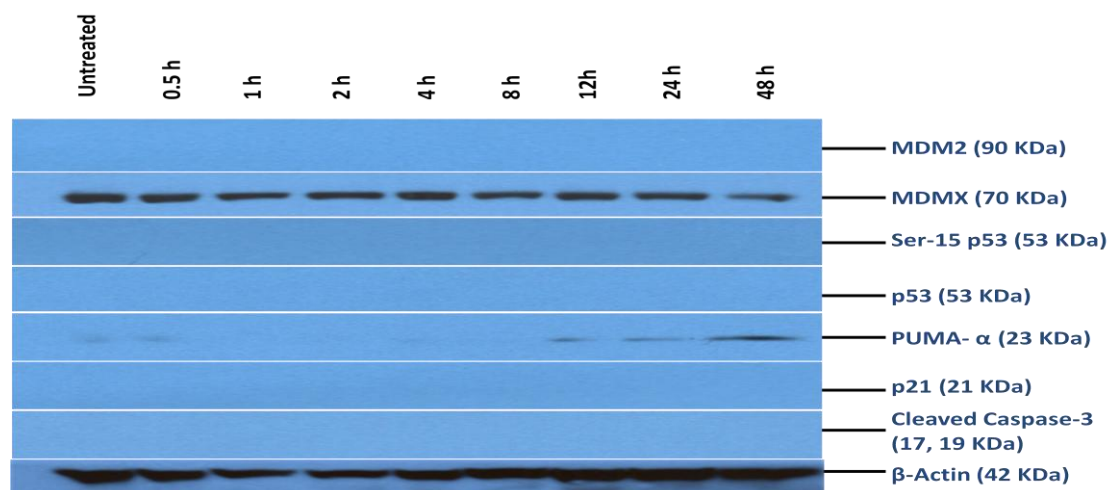


Figure 4.6-1 DMSO Control

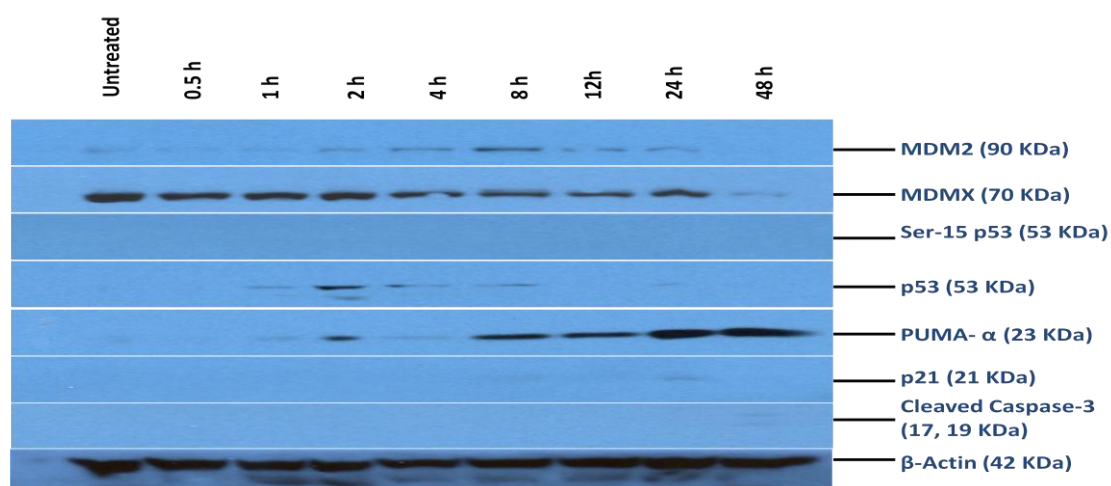


Figure 4.6-2 NU8354A 5 μ M Treatment

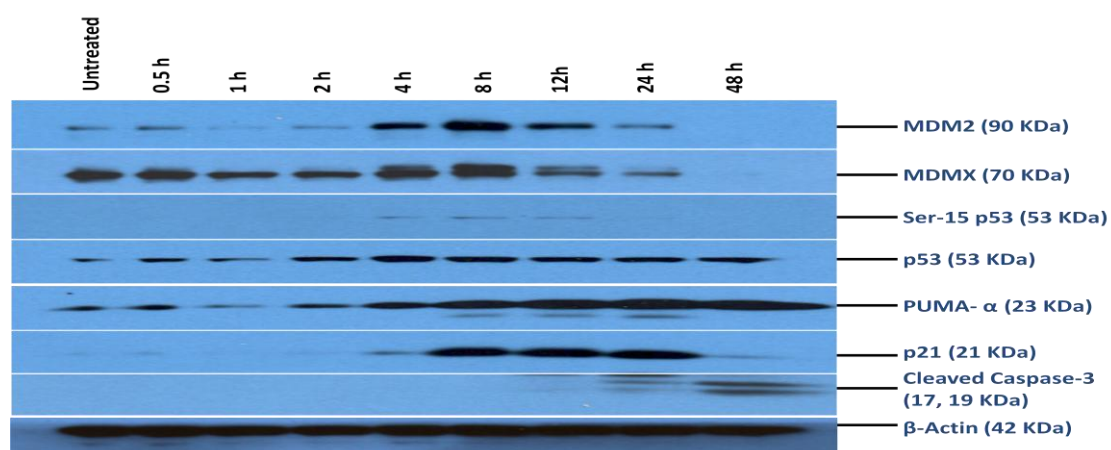


Figure 4.6-3 Nutlin-3 5 μ M Treatment

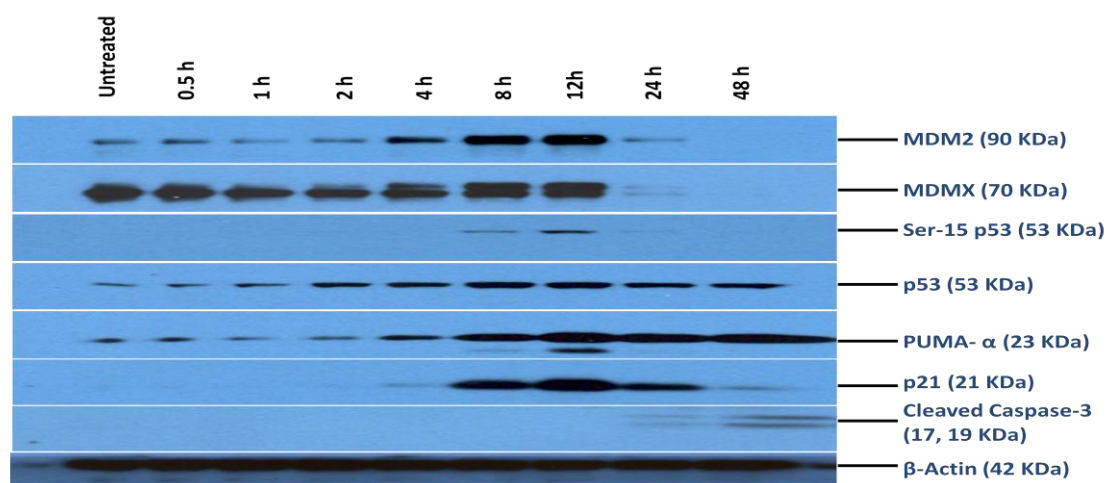


Figure 4.6-4 MI-63 5 μM Treatment

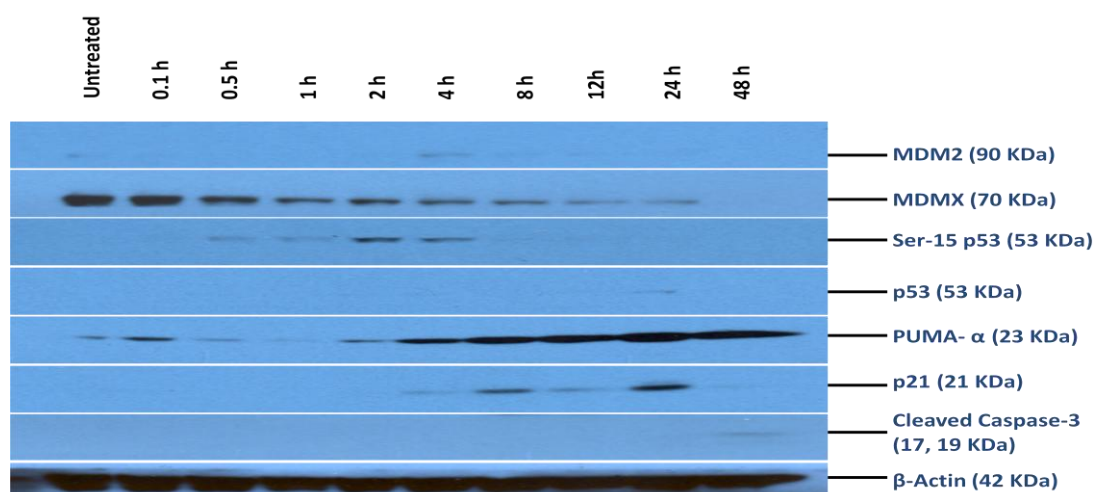


Figure 4.6-5 X-ray Irradiation Treatment

Figure 4. 6 Western blot time courses of NGP cellular effects comparing NU8354A with Nutlin-3, MI-63 and X-ray irradiation treatments.

The time course effects of MDM2/p53 inhibitors Nutlin-3, MI-63 and the isoindolin-1-one compound 'NU8354A' were compared together with DMSO control and X-ray irradiation by using NGP cell line. Plated cells were treated with either 1% DMSO, test compounds at 5 μM, or 6.3 Gy X-ray radiation; cell lysates were then collected at each time point and analyzed by western blotting. MDM2, MDMX, Ser-15 phosphorylated p53, p53, PUMA, p21 and cleaved caspase 3 expression were considered, and actin was probed as a loading and transfer control.

4.2.3 Western Blot Analysis of the Cellular Effects of Potent Stage 2 and 3 Isoindolin-1-one Compounds

The three most potent stage 2 (Figure 4. 1) isoindolin-1-ones NU8399, NU8405 and NU8406 were selected for dose-dependent cellular activity evaluation by using SJSA-1, HCT116_{+/+} and HCT116_{-/-} cell lines; with Nutlin-3 as positive control. Compound structures and western blotting results are displayed in Figure 4. 7, Figure 4. 8 & Figure 4. 9.

The western blotting results for both SJSA-1 and HCT116_{+/+} cell lines indicated that NU8399 induced less p53 accumulation and p53 downstream targets MDM2, p21 activation than expected on the basis of its relative IC₅₀ value in the cell-free ELISA. This means its cellular potency was not corresponding to the IC₅₀ value. The result of HCT116_{-/-} indicated that all these compounds have no cellular effects in p53 null cancer cells.

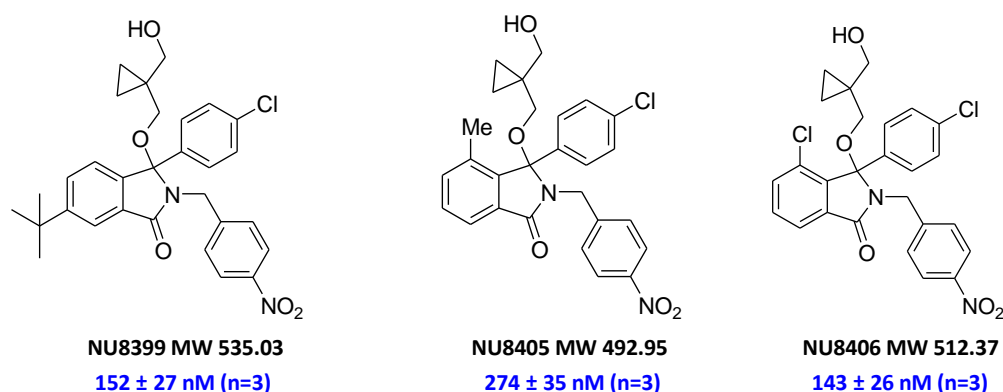


Figure 4. 7 Structures, molecular weights and IC₅₀ values of stage 2 isoindolin-1-one compounds selected for western blot analysis.

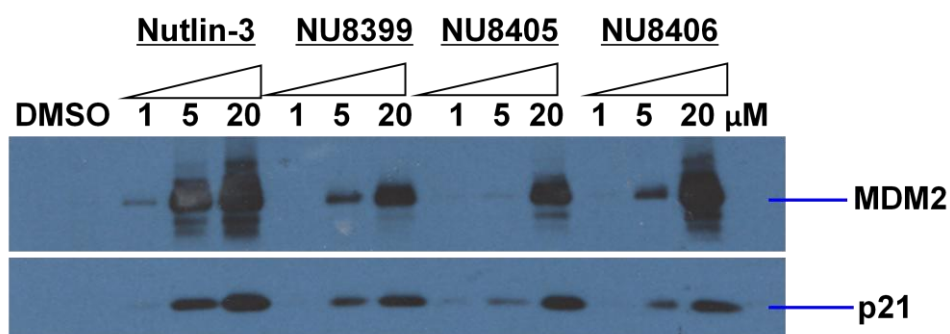
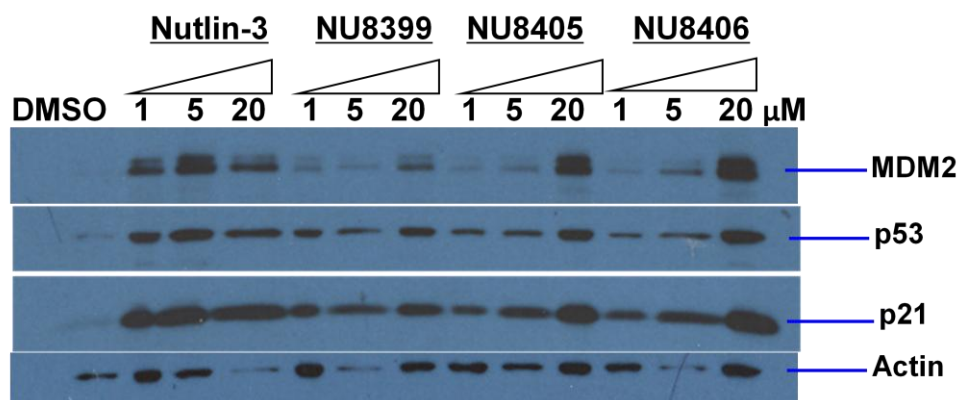
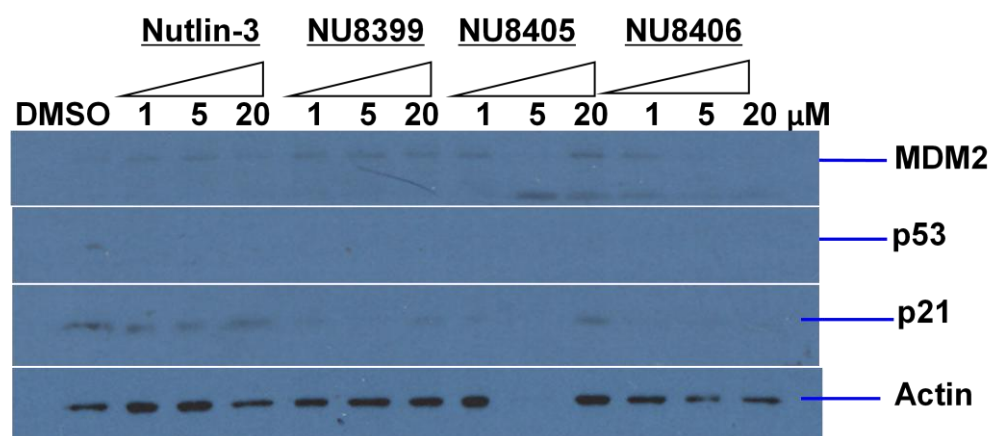


Figure 4. 8 Western blot result of selected stage 2 isoindolin-1-one compounds compared with Nutlin-3 using the SJS-A1 cell line



HCT116^{+/+}

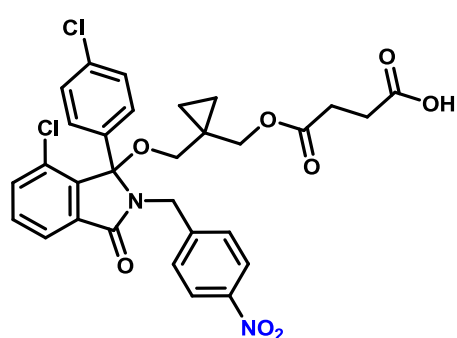


HCT116^{-/-}

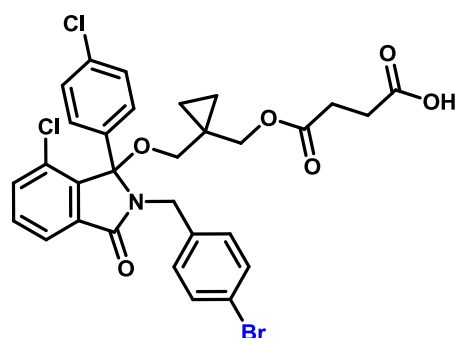
Figure 4. 9 Western blot result of selected stage 2 isoindolin-1-one compounds compared with Nutlin-3 using HCT116^{+/+} & ^{-/-} cell lines

The three most potent stage 3 isoindolin-1-one compounds were selected for dose dependent cellular activity evaluation using the SJSA-1 cell line with Nutlin-3 as a positive control. Compound structures and western blotting results are displayed in [Figure 4. 10](#) & [Figure 4. 11](#).

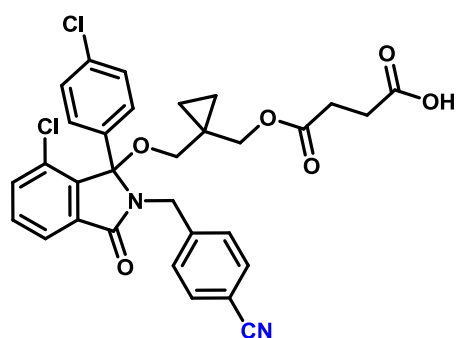
In addition to p53, MDM2 and p21, the protein expression levels of PARP and p53 ser-15 phosphorylation status were also considered. Both NCL-00016149 and NCL-00016659 showed quite similar dose-dependent cellular effects to those observed with the positive control Nutlin-3, although NCL-00016653 induced slightly less p53 and phosphorylated p53 ser-15 accumulation in the SJSA-1 cell line.



NCL-00016149 MW 613.48
15.8 ± 2.6 nM (n=3)



NCL-00016653 MW 647.37
119 ± 17 nM (n=3)



NCL-00016659 MW 593.49
97 ± 30 nM (n=3)

Figure 4. 10 Structures, molecular weights and IC₅₀ values of stage 3 isoindolin-1-one compounds selected for western blot analysis.

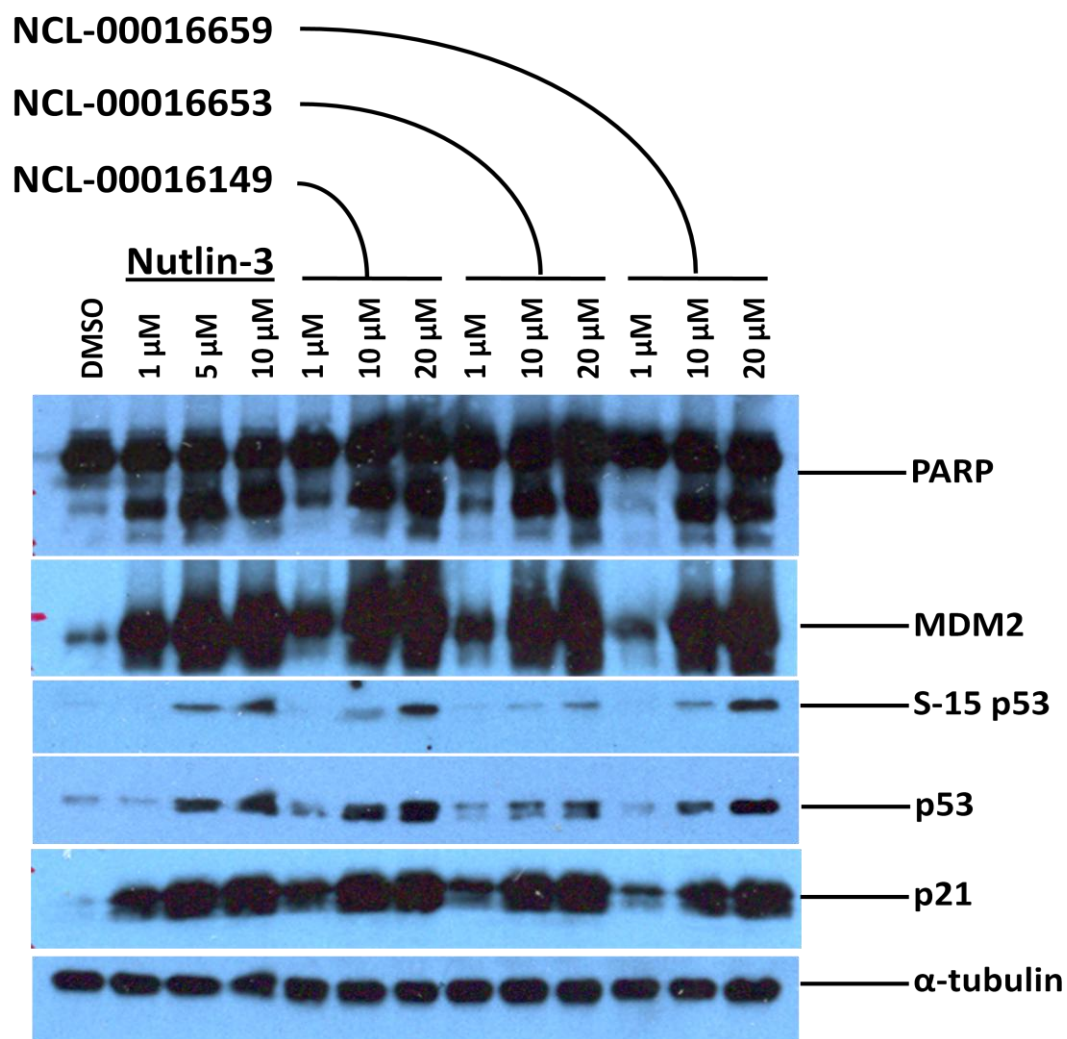


Figure 4. 11 Western blot showing the dose dependent effect of selected stage 3 isoindolin-1-one compounds compared with Nutlin-3 using SJSA-1 cell line.

4.2.4 Potency Comparison of Isoindolin-1-one Enantiomers

4.2.4.1 Background

Because of the chiral carbon present in the isoindolin-1-one core structure, all of the isoindolin-1-one compounds synthesised are racemic mixtures. Furthermore, the shape of the MDM2 binding pocket strongly suggests that inhibition of p53 binding by isoindolin-1-ones is likely to be stereoselective, *i.e.* only one enantiomer was able to interrupt the MDM2/p53 binding effectively, and the other one not or only showed weak activity. This possibility would contribute to further structure design. To address this question, the resolving of pure enantiomers was required.

NU8354 enantiomers were resolved successfully by using chiral HPLC (by Dr Karen Haggerty) (Figure 4. 12), and designated NU8354 A (the first eluting peak in chiral HPLC) and NU8354 B (the 2nd peak in chiral HPLC) for activity evaluation and comparison.

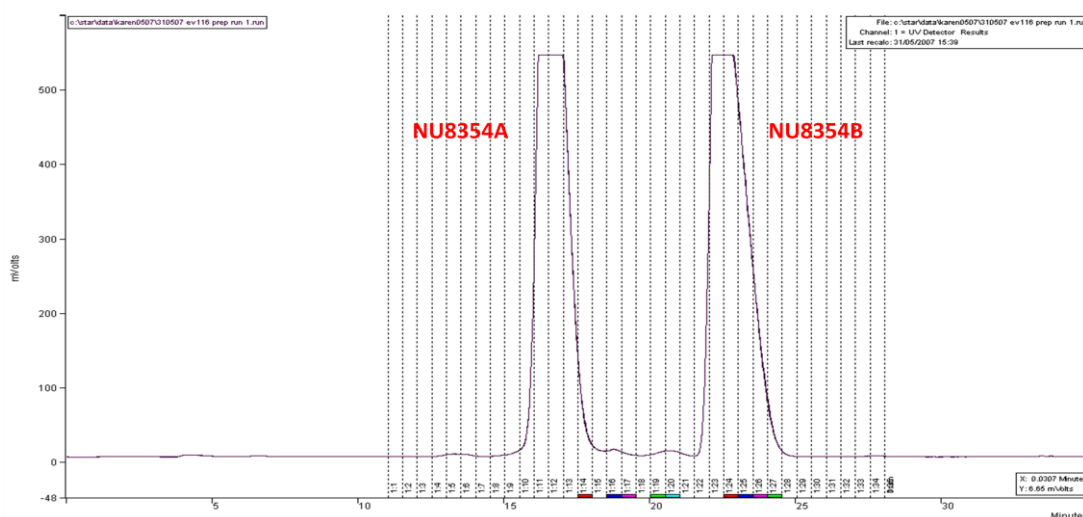


Figure 4. 12 Resolution of enantiomers of NU8354 by using HPLC and a chiral column.

Then, following the successful design and synthesis of stage 2 compounds, enantiomers of the key compound NU8406 were also successfully resolved by using chiral HPLC (by Dr Karen Haggerty) (Figure 4. 13), and designated NU8406 A (the first peak in chiral HPLC) and NU8406 B (the 2nd peak in chiral HPLC) for activity evaluation and comparison using the same methods used for NU8354.

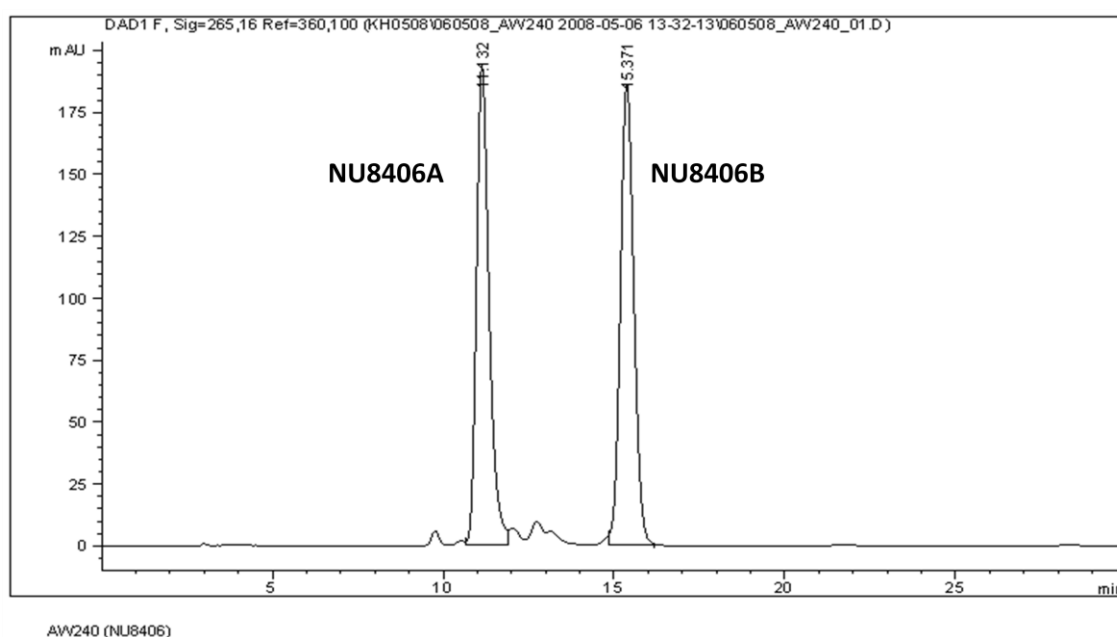


Figure 4. 13 Resolution of enantiomers of NU8406 by using HPLC and a Prep-chiral column.

Nutlin-3, NU8354, NU8354A, NU8354B, NU8406, NU8406A and NU8406B were evaluated for their relative activity as MDM2-p53 binding antagonists. The ELISA method was used for cell-free IC₅₀ evaluation, and comparison and western blotting for intact cell activity as indicated by altered levels of proteins involved in p53-dependent cell regulation including MDM2, p53 and p21^{WAF1}; α -tubulin expression was also investigated for loading and transfer control, and the SRB method was employed to determine cell culture growth inhibition (GI₅₀) in response to antagonist treatment. The SJSA-1 osteosarcoma cell line was used for evaluation of cellular

response. Data analysis was carried out using PRISM software for IC₅₀ determination, generating growth inhibition curves and enabling GI₅₀ determination.

4.2.4.2 NU8354 racemic mixture and NU8354 A & B enantiomers comparison

The structures of racemic NU8354 and NU8354A & B are displayed below. The A and B nomenclature was initially designated (Figure 4. 14) without a knowledge of which of the two enantiomers they corresponded to.

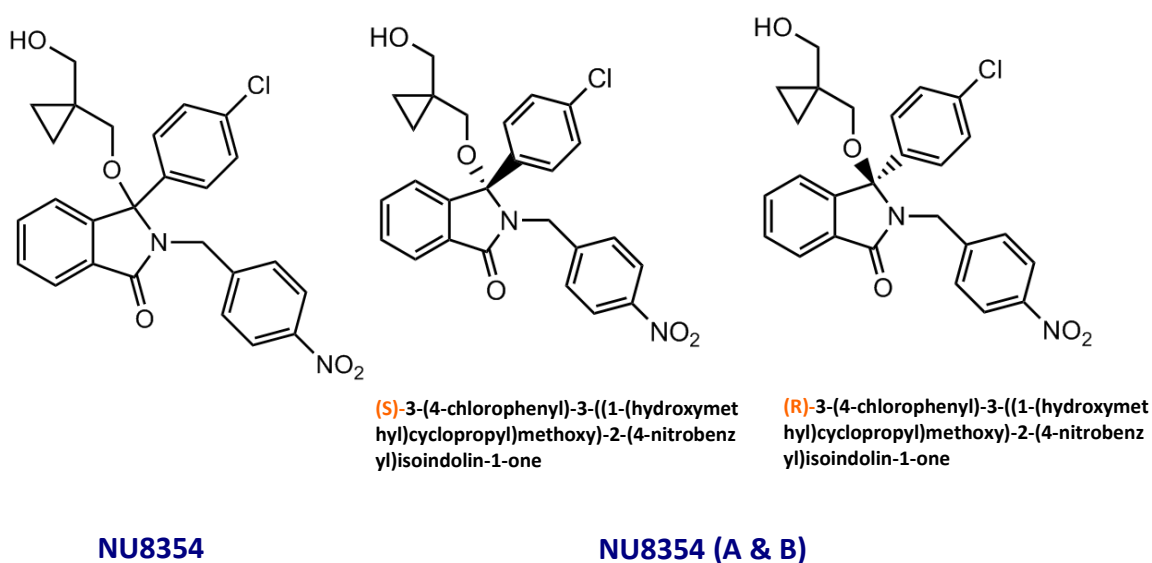


Figure 4. 14 NU8354 and Related Enantiomer Structures

4.2.4.2.1 IC₅₀ determination and comparison.

As displayed in Figure 4. 15, with the successful separation of the two enantiomers, we obtained a more potent homochiral compound NU8354A with an IC₅₀ = 164 nM compared to the racemic mixture NU8354 (IC₅₀ = 269 nM). The other enantiomer NU8354B was much less active with the IC₅₀ > 1 μM.

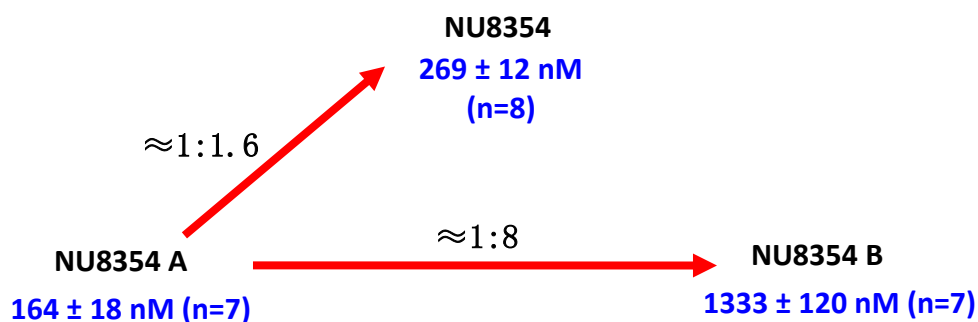


Figure 4. 15 IC_{50} Comparison of NU8354 Enantiomers.

4.2.4.2.2 Western blot comparison of the cellular response to NU8354 enantiomers.

As can be seen in **Error! Reference source not found.**, both NU8354 and NU8354A treated SJSA-1 cells showed a marked dose-dependent accumulation of p53, MDM2 and p21 proteins as observed with Nutlin-3 treated SJSA-1 cells; however, even 20 μM NU8354B did not induce an obvious increase in p53 and its downstream targets MDM2 and p21, which reflected the cell-free (ELISA) potency difference between the two enantiomers.

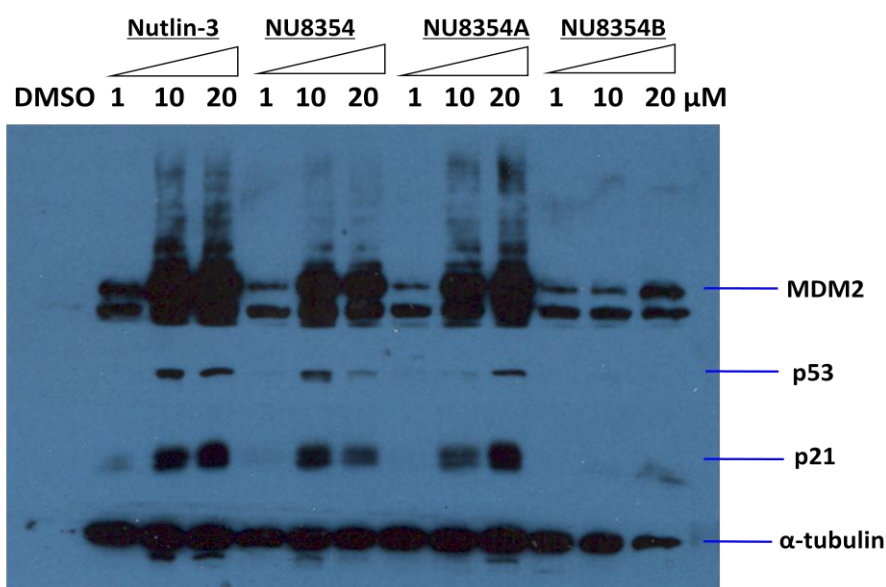


Figure 4. 16 Western Blot Analysis of the Cellular Response to NU8354 enantiomers.

(SJSA-1 Cell Line)

4.2.4.2.3 SRB assay for cellular GI₅₀ evaluation and comparison.

In order to confirm the cellular response difference between the two NU8354 enantiomers, their growth inhibitory effects on SJSA-1 cells were evaluated using the SRB method. The SJSA-1 cell line growth inhibition curves and GI₅₀ values in response to NU8354A & B are presented in Figure 4. 17, which shows the marked difference in growth inhibition and 4-fold difference of GI₅₀ values in response to the two enantiomers, with NU8354A being the more active form, consistent with the difference in IC₅₀ observed in cell-free assays and p53 activation in intact cells.

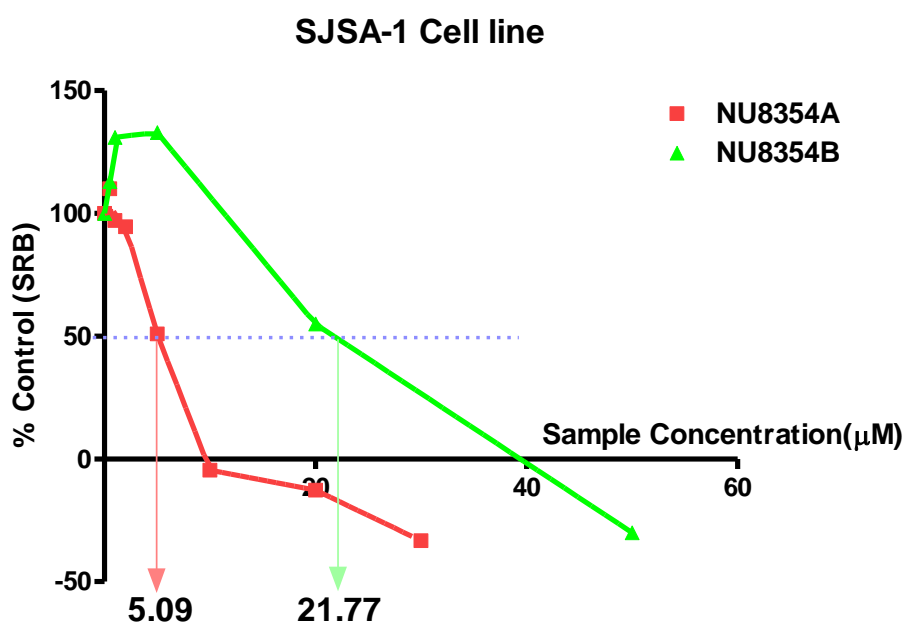


Figure 4. 17 Comparison of the Growth Inhibitory Effect of NU8354 Enantiomers.

4.2.4.3 Comparison of NU8406 racemic mixture with NU8406 A & B

The structures of NU8406 racemic mixture and NU8406A & B are displayed below. The A and B nomenclature was initially designated (Figure 4. 18) without determining which of the two enantiomers they corresponded to in absolute term.

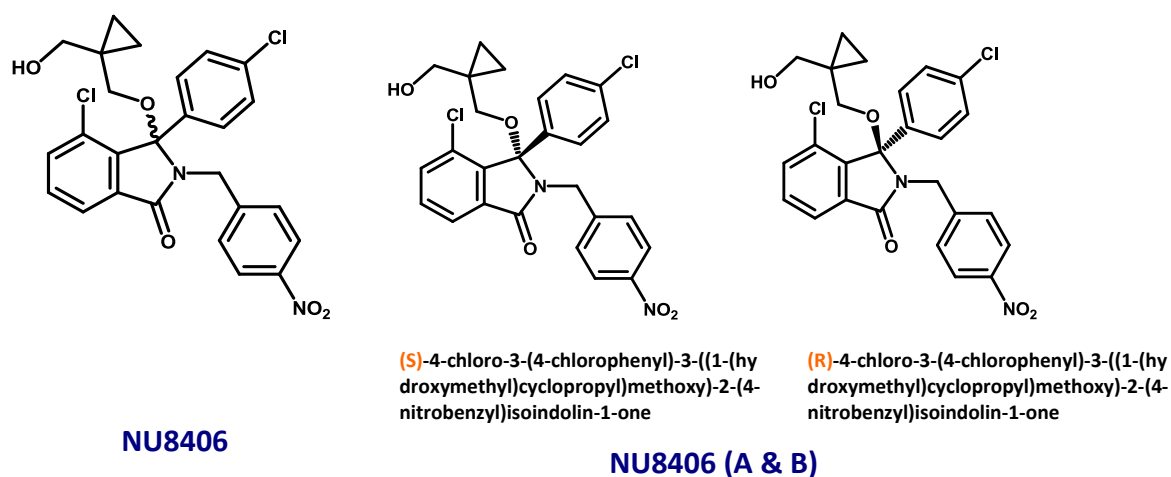


Figure 4. 18 NU8406 enantiomers structures

4.2.4.3.1 IC₅₀ determination and comparison.

With the successful separation of the two enantiomers, a markedly more potent enantiomer, NU8406A (IC₅₀ = 40 nM), was obtained, with almost a 4-fold higher potency compared with the racemic NU8406 (IC₅₀ = 143 nM). The less potent enantiomer, NU8406B, was also obtained, which was 32-fold less active than NU8406A, with an IC₅₀ value above 1 μ M (Figure 4. 19).

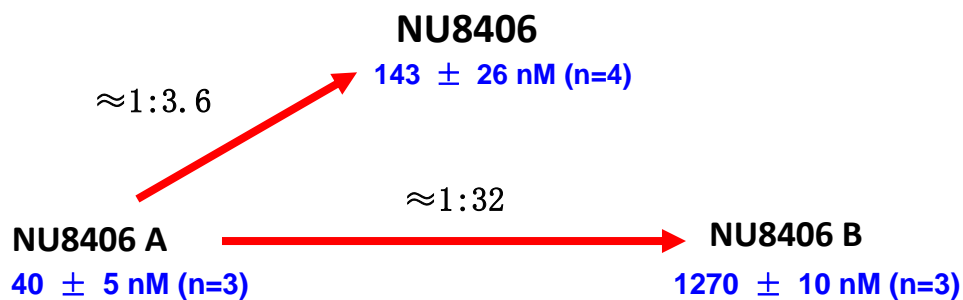


Figure 4. 19 IC₅₀ Comparison of NU8406 Enantiomers.

4.2.4.3.2 Western blot comparison of the cellular response to NU8406 resolved enantiomers.

The cellular effect of the NU8406 series of compounds can be seen in [Figure 4. 20](#). Both NU8406 and NU8406A treated SJSA-1 cells showed a marked dose-dependent accumulation of p53, MDM2 and p21 proteins comparable to Nutlin-3 treated SJSA-1 cells; however, even a 20 μ M concentration of NU8406B did not induce an obvious increase of p53, although there was some dose-dependent accumulation of its downstream targets, MDM2 and p21, which to some extent reflected the potency difference between the two enantiomers, but also indicated that the less potent enantiomer can also show some activation of p53 at higher doses, possibly by a weaker interruption of the MDM2/p53 binding interaction or off-target effects.

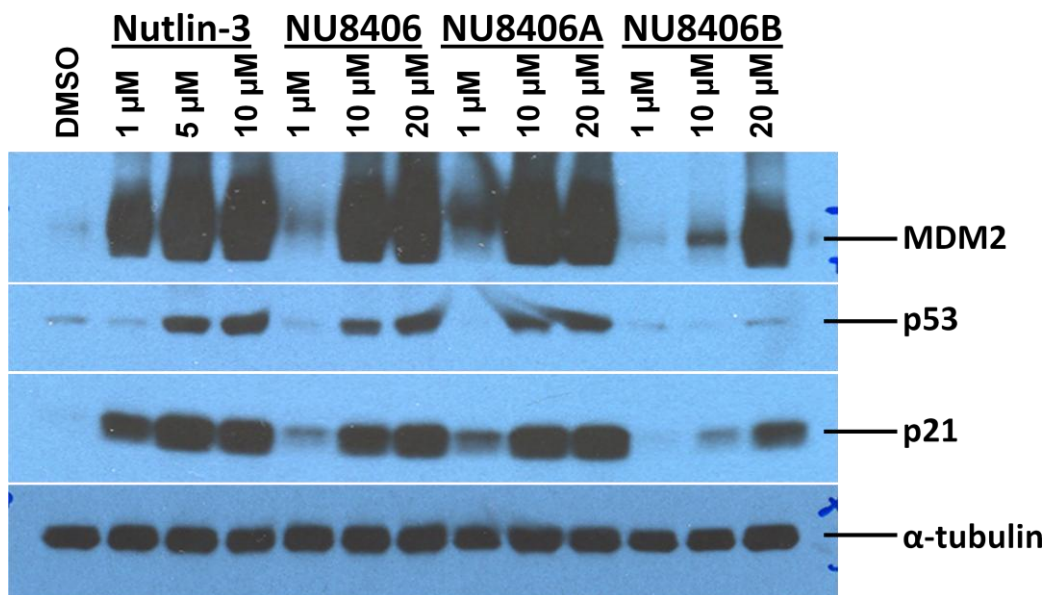


Figure 4. 20 Western Blot Analysis of the Cellular Response to NU8406 enantiomers.
(SJSA-1 Cell Line)

4.2.4.3.3 SRB assay for cellular GI_{50} evaluation and comparison.

In order to confirm whether the difference in p53 pathway response translates into a growth inhibitory difference between the two NU8406 enantiomers, and also to compare them with the NU8406 racemic mixture, SRB assays were carried out. The SJSA-1 cell line growth inhibition curves and GI_{50} values in response to the three compounds are presented in [Figure 4. 21](#), which shows an 8-fold difference of GI_{50} values in response to treatment with the two enantiomers. Moreover, the GI_{50} values of the three compounds correlated closely with the differences in their IC_{50} values.

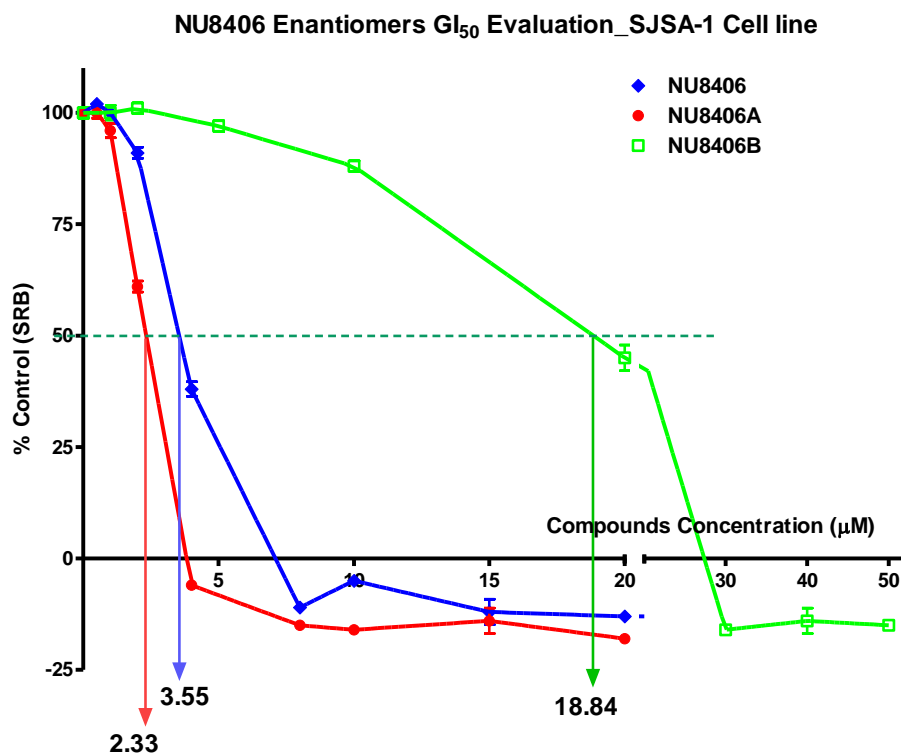


Figure 4. 21 Comparison of the Growth Inhibitory Effect of NU8406 Enantiomers.

4.3 The Growth Inhibitory Activity (GI₅₀) of Isoindolin-1-one Compounds compared with Nutlin-3 and MI-63

4.3.1 Background

With the improved activity of isoindolin-1-ones as the MDM2/p53 inhibitor drug development project progressed, we obtained the compounds NCL-00016149 and NU8406A with comparable IC₅₀ values to those published for Nutlin-3 and MI-63. For accurate comparison, SRB assays were performed to compare MI-63 and Nutlin-3 side by side with our high potency isoindolin-1-one compounds.

4.3.2 Materials and Methods

Cell line: Osteosarcoma cancer cell SJSA-1, Neuroblastoma cancer cell NGP;
Compounds: MI-63, Nutlin-3, NCL-00016149, NU8406, NU8406A and NU8406B; Drug concentration range: 0.5, 1, 2, 4, 8, 10, 15, 20 μ M for MI-63, Nutlin-3, NU8406, NU8406A; 0.5, 1, 2, 4, 6, 8, 10, 20 μ M for NCL-00016149; 1, 2, 5, 10, 20, 30, 40, 50 μ M for NU8406B. The SRB assay with a re-designed plate arrangement was used to evaluate growth inhibitory effects and PRISM software was used to generate growth inhibition curves and determine GI₅₀ values.

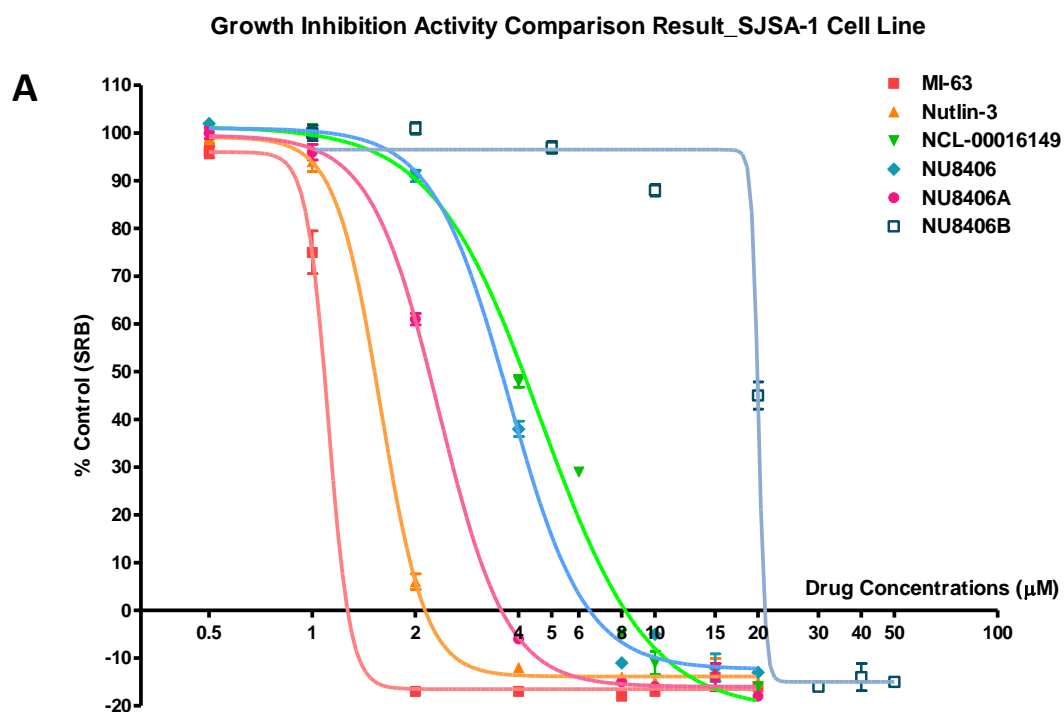
4.3.3 Results

The growth Inhibition Curves of the six compounds against SJSA-1 and NGP cancer cell lines are displayed in [Figure 4. 22](#); the IC₅₀ values of the six compounds and the absolute GI₅₀ values with the SJSA-1 and NGP cancer cell lines are listed in [Table 4. 1](#).

By using MI-63 values as standard values and dividing each value with their corresponding standard value, we have generated [Table 4. 2](#) such that the relative differences in IC₅₀ and GI₅₀ values can be more easily compared.

Based on the growth inhibition curves in [Figure 4. 22](#) and GI₅₀ values in [Table 4. 1](#), NCL-00016149 showed comparable growth inhibitory effects to those published for the potent MDM2/p53 inhibitors, MI-63 and Nutlin-3.

Although NCL-00016149 showed higher potency than NU8406 and NU8406A in the ELISA results, its cellular activity was lower than NU8406A in both of the two cell lines. Also, the two cell lines showed slightly different cellular response to NU8406 enantiomers.



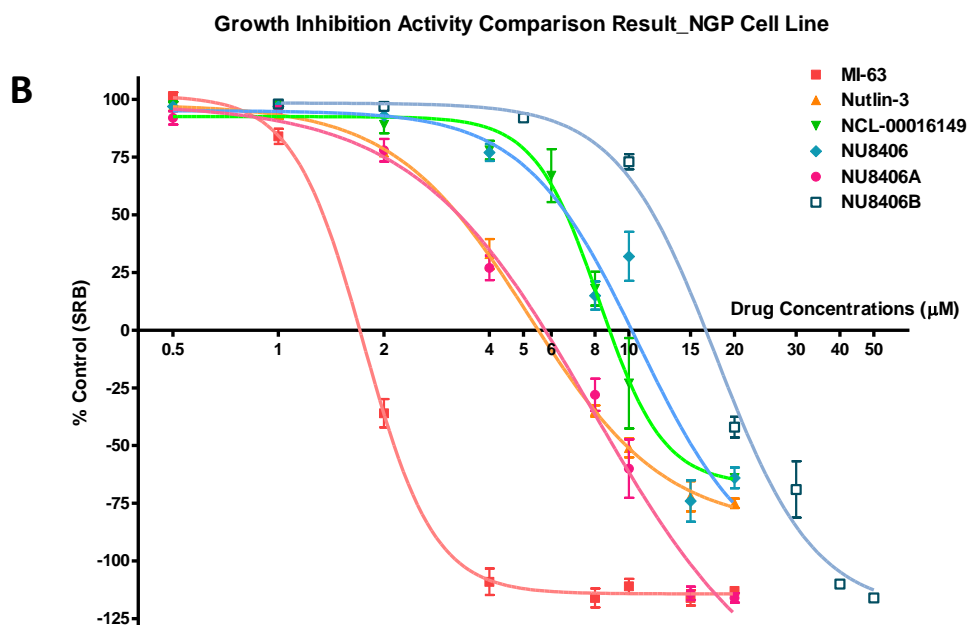


Figure 4. 22 SRB Assay Comparison of the Growth Inhibitory Effects of MDM2/p53 Inhibitors against (A) SJSA-1 and (B) NGP Cell Lines.

Table 4. 1 IC_{50} and SJSA-1 and NGP Cell Line GI_{50} value Comparison of Potent MDM2/p53 Interaction Inhibitors

Compounds	MI-63	Nutlin-3	NCL-00016149	NU8406	NU8406A	NU8406B
ELISA IC_{50} (nM)	9.0 ± 1.3	103.3 ± 10.6	18.9 ± 4.1	143.0 ± 26.0	42.8 ± 2.6	1270.0 ± 10.0
SJSA-1 GI_{50} (μM)	1.3 ± 0.2	1.6 ± 0.1	4.6 ± 0.4	3.8 ± 0.1	2.3 ± 0.1	20.1 ± 1.9
NGP GI_{50} (μM)	1.8 ± 0.1	5.2 ± 0.5	8.2 ± 0.7	10.7 ± 3.8	7.9 ± 1.9	17.7 ± 1.5

Table 4. 2 MDM2/p53 Inhibitors IC_{50} value and SJSA-1 and NGP Cell Line GI_{50} Standardised Value Comparison

Compounds	MI-63	Nutlin-3	NCL-00016149	NU8406	NU8406A	NU8406B
ELISA IC_{50} std.	1	11.5	2.1	15.9	4.8	141.1
SJSA-1 GI_{50} std.	1	1.2	3.5	2.9	1.8	15.5
NGP GI_{50} std.	1	2.9	4.6	5.9	4.4	9.8

4.4 Apoptotic Effect of Isoindolin-1-one Compounds in SJSA-1 Cells

4.4.1 Background

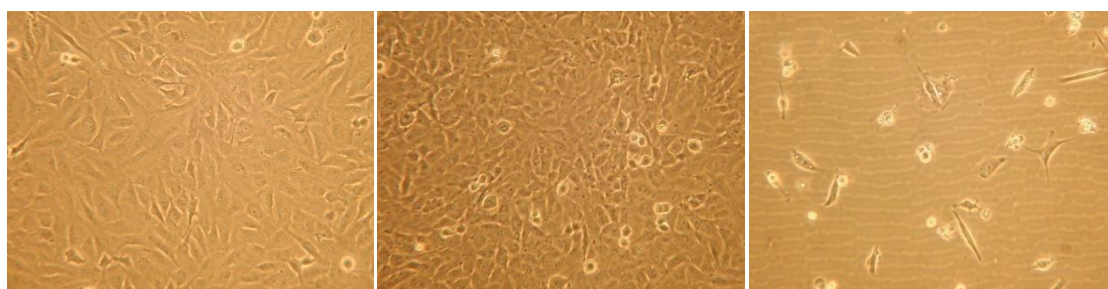
In the last section, the growth inhibition effects and p53 pathway activation induced after 4 hours by NU8354 and NU8406 isoindolin-1-one enantiomers was presented, and demonstrated the difference between the cellular effect of the racemic mixture and that of the potent and less active separated enantiomers. This section describes experiments to measure the potential apoptotic effects consequent on p53 pathway activation, using western blot analysis of poly (ADP-ribose) polymerase (PARP) and caspase 3 protein cleavage, and a caspase 3 & 7 luminometer-based enzyme activity assay.

The time course of apoptotic response to 5 μ M NU8354A, Nutlin-3 and MI-63 treatment was determined, and compared with the response to X-ray irradiation as a positive control. The response to the inactive enantiomer, NU8406B, was also included as a non-potent, but structurally closely related control.

4.4.2 Results

Microscope images of SJSA-1 cells treated with a range of compound concentrations for 48 hours were taken before collecting the cell lysates ([Figure 4. 23](#)). The images showed very marked cell density differences compare with the DMSO control when treated with high concentrations (Nutlin-3 10 μ M, NU8354A 20 μ M, NU8406A 10 and 20 μ M) of the compounds.

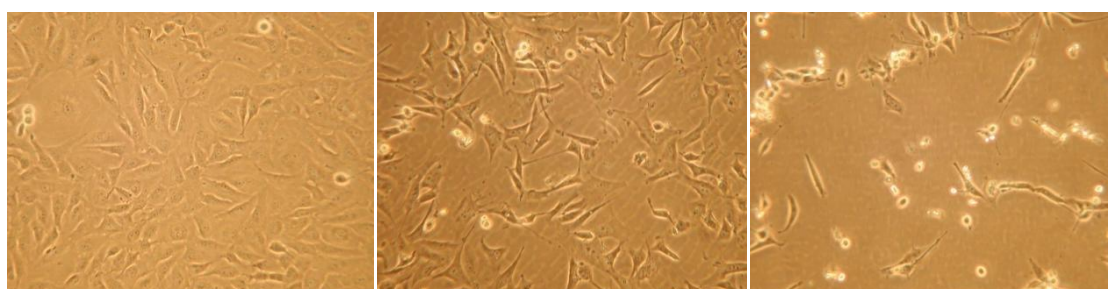
With increasing compound concentration, there were fewer cells still attached to the bottom of sample wells and more cells floating in the medium.



DMSO

Nutlin-3 1 μ M

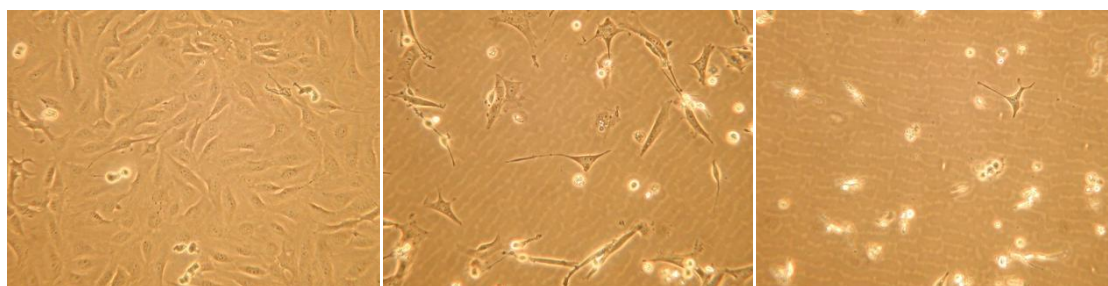
Nutlin-3 10 μ M



NU8354A 1 μ M

NU8354A 10 μ M

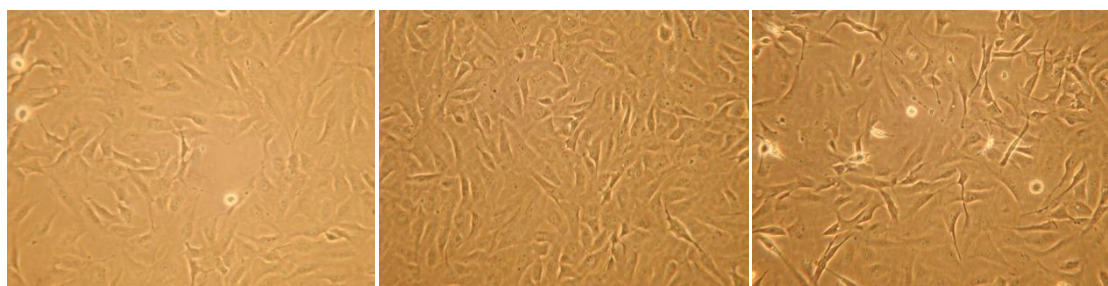
NU8354A 20 μ M



NU8406A 1 μ M

NU8406A 10 μ M

NU8406A 20 μ M



NU8406B 1 μ M

NU8406B 10 μ M

NU8406B 20 μ M

Figure 4. 23 SJSA-1 Cell Images with 48 hours Antagonist Treatment

Based on this observation, it would be interesting to check the whole protein concentration in the cell lysate samples that were collected by using the same amount of lysate buffer to confirm the cellular effects of the MDM2 antagonists quantitatively, which is like a simple version of SRB assay. The protein concentrations of all cell lysate samples were evaluated by using the BCA assay (see Section 2.3.4) and the results were generated using GraphPad Prism software and displayed in [Figure 4. 24](#).

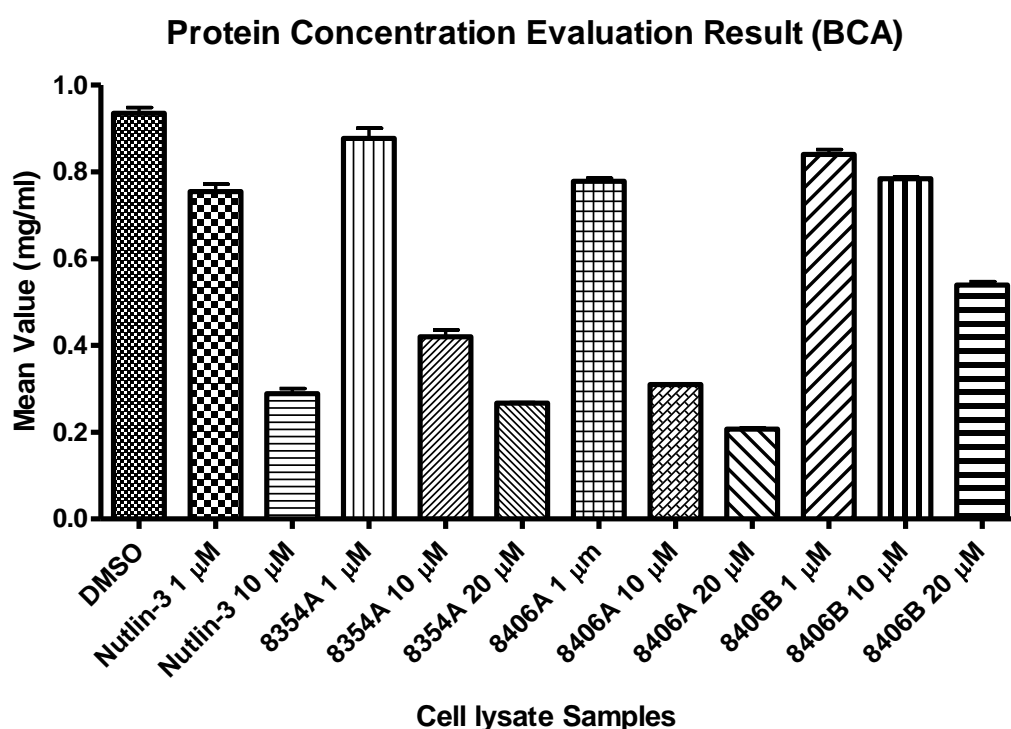


Figure 4. 24 BCA Assay Showed Marked Protein Concentration Variation of the Cell Lysate Samples in a Dose- and Potency-Dependent Manner

The result showed that the protein concentration of cell lysate samples after 48 hours compounds treatment were markedly different, which reflected the dose and potency dependent cellular effects and correlated with the images displayed in [Figure 4. 23](#) . As can be seen from [Figure 4. 24](#) , both 20 μ M NU8354A and NU8406A treated samples showed a lower protein concentration than 10 μ M Nutlin-3 treated sample, which is very close to the 10 μ M NU8406A treated sample. On the other hand, the inactive

enantiomer NU8406B has also shown a dose-dependent reduction in protein content, although the effect was much less than for other compounds.

After equalising the protein concentration of each sample, a western blot analysis was carried out with the 48 hours drug treated SJSA-1 cell lysate samples, loading an equal amount of protein (Figure 4. 25).

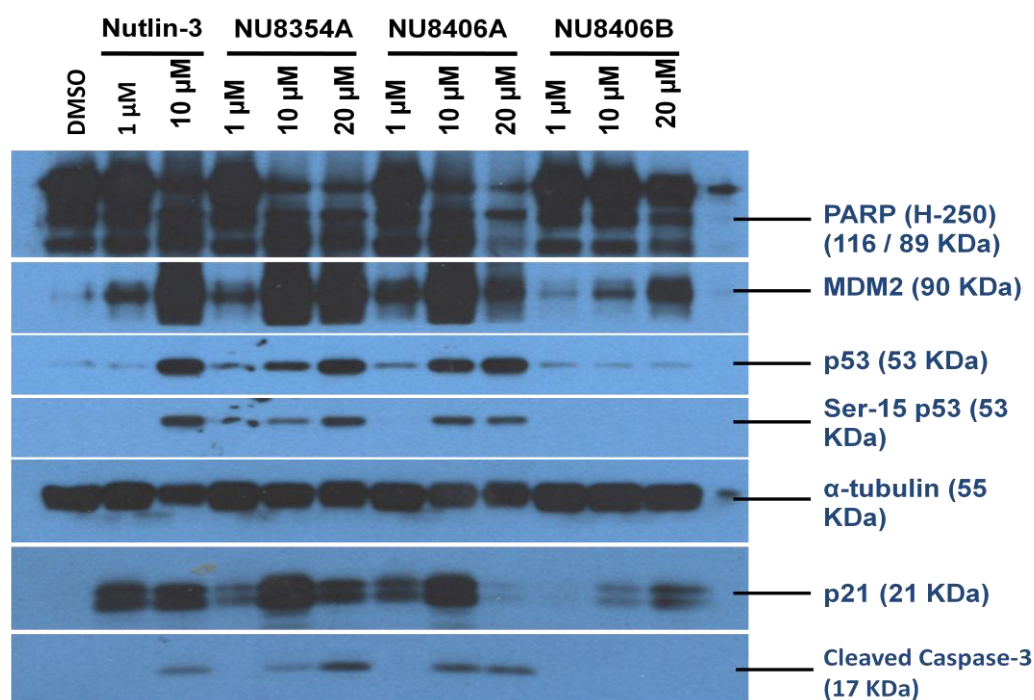


Figure 4. 25 Western blot result of SJSA-1 cells treated with MDM2 antagonists for 48 hours

The results indicated that MDM2 antagonist treatment caused p53 stabilization and accumulation, p53 ser-15 phosphorylation and then p53 downstream pathway activation indicated by an increase of MDM2 and p21 protein level. In addition, the induction of apoptosis markers was observed, with cleaved caspase-3 protein and the cleavage of PARP protein with the high concentration Nutlin-3 (10 μM), NU8354A (10 & 20 μM) and NU8406A (10 & 20 μM) treatment. The western blot result also showed that high concentration NU8406B (20 μM) can also induce some p53 downstream target MDM2 and p21 accumulation, but with no evidence of apoptosis markers.

Interestingly, markedly decreased MDM2, p21 and PARP protein expression was observed in the 20 μ M NU8406A treated sample, which correlated with the limited cell number after 48 hours drug treatment as displayed in [Figure 4. 24](#); however, as the cell images in [Figure 4. 23](#) displayed, with 10 μ M Nutlin-3 and 20 μ M NU8354A treatment, the attached cell numbers were also very low, but in their corresponding western blot result, the expression of MDM2 and p21 has no marked decrease, so the reduction in cell number is not by itself responsible for the reduced expression.

To provide additional confirmatory evidence of an apoptotic effect, the Caspase-Glo 3/7 enzymatic assay (see Section 2.5) was used, which can numerically evaluate the relative caspase-3/7 activity in cells treated by cytotoxic compounds as an indicator of apoptosis effect ([Figure 4. 26](#)).

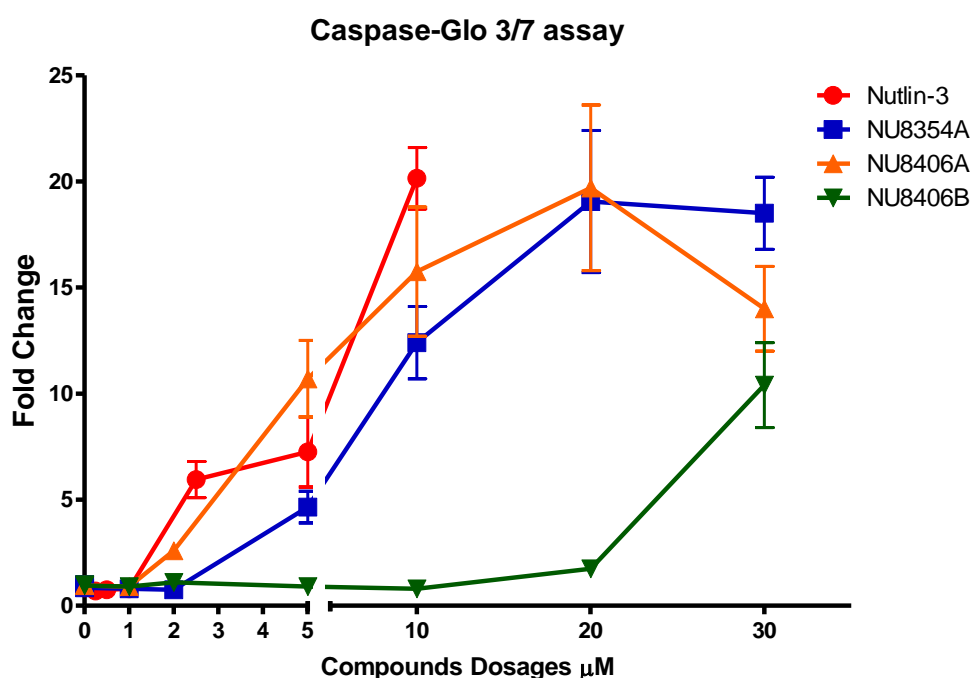


Figure 4. 26 Caspase-Glo 3/7 assay for SJSA-1 cells treated with MDM2 antagonists for 48 hours indicated the dose-dependent cellular effect of apoptosis induction.

As displayed in [Figure 4. 26](#) , NU8354A started to induce caspase 3/7 activity from 5 μ M and showed a dose-dependent effect up to 20 μ M concentration, then plateaued at 30 μ M. As a more potent isoindolin-1-one compound based on IC_{50} , NU8406A started to induce caspase 3/7 activation at 2 μ M concentration, continued to show dose-dependent effect higher than the NU8354A induced caspase 3/7 activity with each concentration and plateaued at 20 μ M concentration to approximately 22 fold higher than untreated cells, then dropped down to about 16 fold, which was even lower than the 30 μ M NU8354A induced caspase 3/7 activity. As a positive control, Nutlin-3 has also shown the ability to induce dose-dependent caspase 3/7 activation. Interestingly, 20 μ M NU8406B has also slightly induced caspase 3/7 activation, which indicated that the sensitivity of this assay for Caspase 3 activity detection is higher than the western blot assay; above 11 fold increase of caspase 3/7 activity was obtained by enhancing the NU8406B concentration to 30 μ M, which together with the western blot result, confirmed that NU8406B can still induce caspase 3/7 activation by interrupting p53-MDM2 binding (or maybe due to some off-target effect at such high dose), although the caspase 3/7 activation effect is much weaker than for NU8406A.

4.5 Conclusion and Discussion

4.5.1 The Cellular Effects of the Lead Isoindolin-1-ones are Comparable to Nutlin-3 Treatment

As a result of progressive lead optimisation, a series of isoindolin-1-one compounds was developed that had activity as inhibitors of MDM2-p53 binding with cell free ELISA IC_{50} values in the range from 15.8 nM (NCL-00016149) to 269 nM (NU8354), comparable to the IC_{50} measured for Nutlin-3 in the same assay. Once in this range, compounds (NU8354, NU8361 and NU8406, *etc.*) were chosen to test for activity as

disrupters of the MDM2-p53 binding interaction and activators of the p53 pathway in intact cells. The selected isoindolin-1-one compounds produced a dose-dependent increase of MDM2, p53 and p21 protein band densities, consistent with the release of p53 from MDM2 binding and p53-dependent transcriptional transactivation (Figure 4. 2, Figure 4. 8 and Figure 4. 11). The semi-quantitative analysis of the band densities indicated that the cellular activity of NU8354 and NU8361 was approximately two- to three- times less potent than Nutlin-3.

Most of the isoindolin-1-one compounds' cellular activities were related to their potencies (IC_{50}) evaluated by the cell-free ELISA. However, NU8399 showed an impaired cellular response that did not correlate with its IC_{50} value (Section 4.2.4). This observation indicated the possibility that compound physical characteristics, such as hydrophilicity, H-bonds, *etc.*, may influence solubility, cellular uptake and stability in cell culture environment.

Stage 3 compounds NCL-00016149, NCL-00016653 and NCL-00016659 also showed similar marked dose-dependent cellular effects, as seen with Nutlin-3, but were not as potent as Nutlin-3 in the cellular assays as might have been expected from their ELISA IC_{50} values. However, they were previously designed as prodrugs that contain ionizable side chains and these charged side chains may prevent them from readily passing through cell membranes. As a result, further research would have to be carried out to examine if they were hydrolyzed before entering the cells or not.

4.5.2 The Mechanism of p53 Pathway Activation by MDM2-p53 Binding Antagonists differs from that of X-ray irradiation

The time course of cellular responses to NU8354, together with Nutlin-3 and MI-63 treatment when compared with the effect of X-ray irradiation ([Figure 4. 5](#) & [Figure 4. 6](#)) indicated differing mechanisms of p53 pathway activation.

With X-ray irradiation, the p53 protein levels increased half an hour after the detection of p53 ser-15 phosphorylation, which is caused by activation of the ATM pathway ([186](#)). In contrast, with the MDM2/p53 inhibitor treatments, the p53 protein accumulated about half an hour earlier than the increase of p53 ser-15 phosphorylation. Also from [Figure 4. 5](#) & [Figure 4. 6](#), it can be seen that p53 downstream target MDM2 expression was enhanced after 2 hours incubation with MDM2/p53 inhibitors or X-ray irradiation treatment, which indicated the p53/MDM2 feedback loop effect was about 1-2 hours later than any activation of the p53 pathway by DNA damage dependent phosphorylation.

These observations indicated that both MDM2/p53 inhibitor treatment and X-ray irradiation can activate the p53 downstream pathways when the cancer cells contain wild type p53; however, the detailed mechanisms of the two processes are different.

By using MDM2/p53 inhibitors, we can block the hydrophobic binding pocket of the MDM2 protein to prevent binding of the transcriptional activation domain of wt-p53 to MDM2 and so break the auto-regulatory feedback loop, allowing the freed wt-p53 to activate its downstream pathway. This in turn can cause cell cycle arrest and/or apoptosis, and these cellular stresses cause the activation of other pathways and lead to p53 phosphorylation as a later event, rather than the initiating event associated

with response to DNA damage. It remains to be established whether the later onset p53 phosphorylation seen with MDM2-p53 antagonists is necessary to further drive activation of the p53 pathway and contribute to growth inhibition and apoptosis.

4.5.3 Comparison of Isoindolin-1-one Enantiomers

The ELISA IC₅₀ values showed that enantiomer NU8354A was approximately 8-fold more potent than NU8354B and about 2-fold more potent than the racemic mixture, which means that enantiomer NU8354A has a better binding affinity with MDM2 protein than NU8354B.

Western blotting results using the SJSA-1 cell line confirmed that the potency difference between NU8354A and B extended to activity in intact cells. Furthermore, NU8354A showed very similar cellular effects to Nutlin-3.

By applying the SRB assay using the SJSA-1 cell line, growth inhibition GI₅₀ results for NU8354A and B were obtained, which showed a 4-fold difference between the NU8354A and B enantiomers.

Noticeably, the difference of potencies between NU8354A and B was not as marked as between Nutlin-3a and b (77), which may not be because of the potency difference between NU8354 and Nutlin-3 racemic mixtures, but because the binding energies of the two enantiomers of NU8354 with the MDM2 protein were closer to each other than for Nutlin-3a compared with Nutlin-3b. By analyzing the synthetic route of Nutlin(187) series compounds, I observed that single enantiomer starting materials were used to limit the number of different enantiomers in the final products, which may also have caused the bigger difference between Nutlin-3 enantiomers than

between NU8354 enantiomers. Also for this reason, the resolution of Nutlin-3a and b was likely to have been much easier than NU8354A and B separation.

The separation of NU8406A and B enabled us to confirm the relationship between isoindolin-1-one compound enantiomer structures and their IC₅₀ values, cellular p53 activation activities and GI₅₀ values for growth inhibition.

Since the NU8406 racemic mixture was more potent than the NU8354 racemic mixture, as expected the potent enantiomer NU8406A (IC₅₀=40 ± 5 nM) also showed a markedly higher potency than NU8354A (IC₅₀=164 ± 18 nM). Moreover, NU8406A was 3.6 times more potent than the racemic NU8406 and 32 times more potent than NU8406B purified enantiomer. The possible reason could be because the introduction of a chloro group, not only enhanced the binding affinity of NU8406A with the MDM2 protein, but also strengthened the stereo specific binding difference between NU8406A and B compared with the NU8354 enantiomers.

Comparison of the SRB assay results of NU8354 enantiomers with NU8406 enantiomers, demonstrates a clear relationship between compound potency (ELISA IC₅₀ value) and their cellular activity. Since these data were obtained by using compounds with the same core structure and very similar final structures, they are more reliable for illustrating the relationship between the ELISA IC₅₀ values with SRB assay GI₅₀ values.

4.5.4 The Cellular Activity Comparison of MDM2 Antagonists

By using the SRB assay, the cellular growth inhibitory activity of potent isoindolin-1-one compounds NCL-00016149, NU8406A and NU8406 were evaluated

together with the published potent MDM2/p53 inhibitors Nutlin-3 and MI-63; NU406B was used as a low potency compound control.

The comparisons of these compounds and their IC₅₀ and GI₅₀ values showed that MI-63 was still the most potent inhibitor of the MDM2-p53 binding interaction, having the lowest IC₅₀ (Table 4. 1) and gave the highest cellular potency of the compounds tested. Although the isoindolin-1-one compound NCL-00016149 was 5-fold more potent than Nutlin-3 in the ELISA evaluation, its GI₅₀ values in both SJSA-1 and NGP cell lines were not only higher than MI-63 generated GI₅₀ values, but also higher than Nutlin-3 generated GI₅₀ values. On the other hand, the pure enantiomer NU8406A generated GI₅₀ values very similar to Nutlin-3 generated values, and even NU8406 had higher cellular potencies in the SJSA-1 cell line than NCL-00016149. This observation indicate that although derivatizing the (1-(hydroxymethyl)cyclopropane)methoxy side-chain with a 4-oxobutanoic acid group has enhanced the binding affinity between the isoindolin-1-one compound and the MDM2 protein, either the molecular weight or other properties of the compound may have counteracted its activity in the cellular assays.

The western blot assay result for 48 hours treatment of SJSA-1 cell samples with the MDM2 antagonists and Caspase-Glo 3/7 assay results confirmed the ability of isoindolin-1-one compounds to induce apoptosis. Moreover, NU8406A showed comparable cellular effects in SJSA-1 cells to those observed with Nutlin-3.

Chapter Five

Alternative Scaffold Compounds as MDM2/p53 and MDMX/p53 Interactions Inhibitors

5.1 Introduction

With the development of MDM2/p53 interaction antagonists by our research group, we were invited to join a European consortium that successfully won a European FP6 Grant, with the title DePPICT (**D**esigning **T**herapeutic **P**rotein-**P**rotein **I**nhibitors for **B**rain **C**ancer **T**reatment). This project was focused on α -helix binding groove interactions, using the MDM2/p53 interaction as a test-bed for developing design tools and thus novel templates. Since its target was brain cancer, blood-brain-barrier penetration was taken into consideration together with the drug-like parameters to guide design approaches. Since the focus of the project was on α -helix binding groove interactions and for the possibility to interrogate in more depth the role of p53 interactions with MDM2/MDMX proteins via selective (MDM2 or MDMX) or pan-active (MDM2 and MDMX) inhibitors, parallel studies on MDMX and its inhibitors were also planned.

One of our responsibilities within this project was the *in vitro* screening of *in silico* selected small molecular compounds from commercially available compound libraries and fragments using MDM2/p53 & MDMX/p53 interactions as test-beds, for 1) better understanding of the binding groove of MDM2/MDMX for the purpose of small molecular inhibitor design; 2) optimization of computer screening methods, especially

for MDM2/p53 and MDMX/p53 interaction antagonists; 3) Confirmation of hits and identification of core scaffolds for the purpose of further drug development.

All together, more than 3800 compounds (4 batches) were screened by me and hit compounds were re-evaluated against both MDM2 and MDMX targets by using dose-dependent ELISA to generate IC_{50} values. Optimized binding modes were then predicted for hit compounds using automatic docking software combined with manual docking. For one hit compound with an $IC_{50} \leq 10 \mu M$, cellular activity was tested for both MDM2 and MDMX inhibitory using the NGP cell line, which is a neuroblastoma cell line with *MDM2* amplification, wild type p53 and relatively high MDMX expression. In addition, some in-house pyrrole scaffold compounds were evaluated using the ELISA method to test for activity against both MDM2 and MDMX targets.

Furthermore, for the purpose of better understanding the difference between MDM2/p53 and MDMX/p53 binding, some specially designed peptide analogues of p53 were also evaluated and compared using the ELISA, for both MDM2 and MDMX inhibition activity.

5.2 Materials and methods of ELISA for *in vitro* activity evaluation

All the compounds selected by *in silico* screening by our colleagues in Siena Biotech and Crystax Ltd were available from commercial sources.

Four batches of compound samples were received as 20 μL 10 mM concentration DMSO solutions in 96-well plates, with 63 samples per plate. Hit compounds were re-evaluated using the dose-dependent ELISA method and compounds with confirmed

activity were resupplied as 100 μ L 10 mM DMSO solutions in small tubes after passing quality control analysis.

IV-MDM2 and IV-MDMX protein samples were prepared with the detailed methods described in Chapter 2. Nutlin-3 was used as positive control for MDM2 inhibitor screening; IP3 peptide and NU8325 (an in-house pyrrole scaffold compound, IC_{50} = 4.52 ± 0.28 μ M as an MDMX inhibitor, [Figure 5. 7](#)) were the positive controls for MDMX inhibitor screening.

For MDM2/MDMX inhibitors screening, the ELISA method was carried out with the plate arrangement shown in [Figure 5. 1](#), 63 compounds of the same concentration could be screened within one plate. The first three vertical lines of wells were solvent controls and three different concentrations of positive controls (Nutlin-3 50, 100, 200 nM for MDM2 inhibitor screening, IP3 peptide or NU8325 0.1, 1, 10 μ M for MDMX inhibitor screening) were placed in the top row 9 wells with 3 wells for each concentration.

For dose-dependent IC_{50} evaluation, the ELISA assay were carried out with the plate arrangement shown in [Figure 5. 2](#), 7 compounds could be tested within one plate. The first three vertical lines of wells were solvent controls and three different concentrations of positive controls (Nutlin-3 50, 100, 200 nM for MDM2 inhibitor screening, IP3 peptide or NU8325 0.1, 1, 10 μ M for MDMX inhibitor screening) were placed in the top row 9 wells. Each concentration of every compound was plated out in triplicate at three different concentrations.

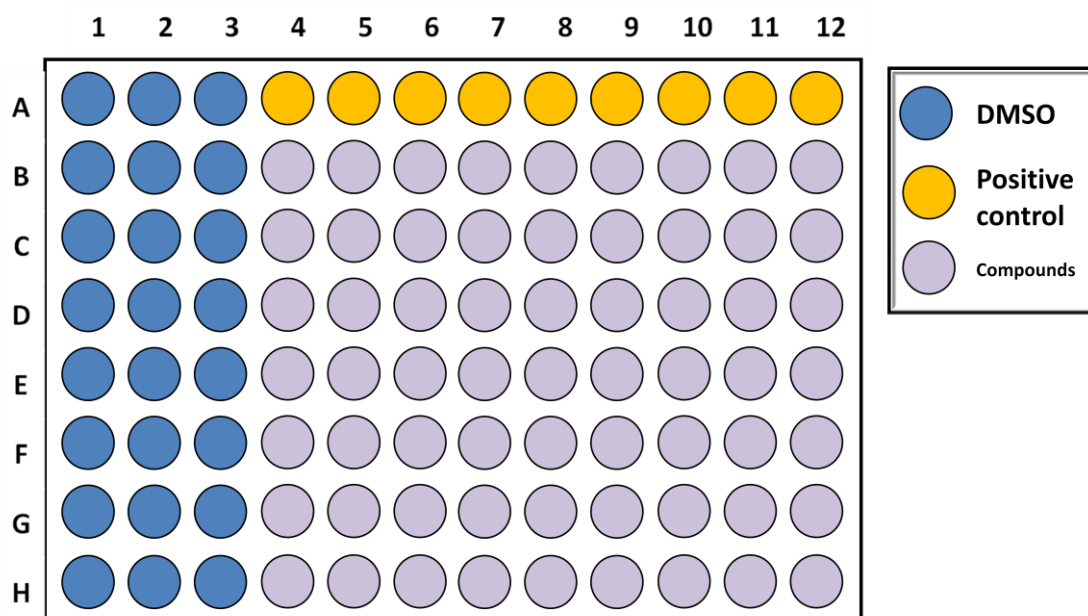


Figure 5. 1 Plate arrangements for MDM2/MDMX inhibitors screening purpose

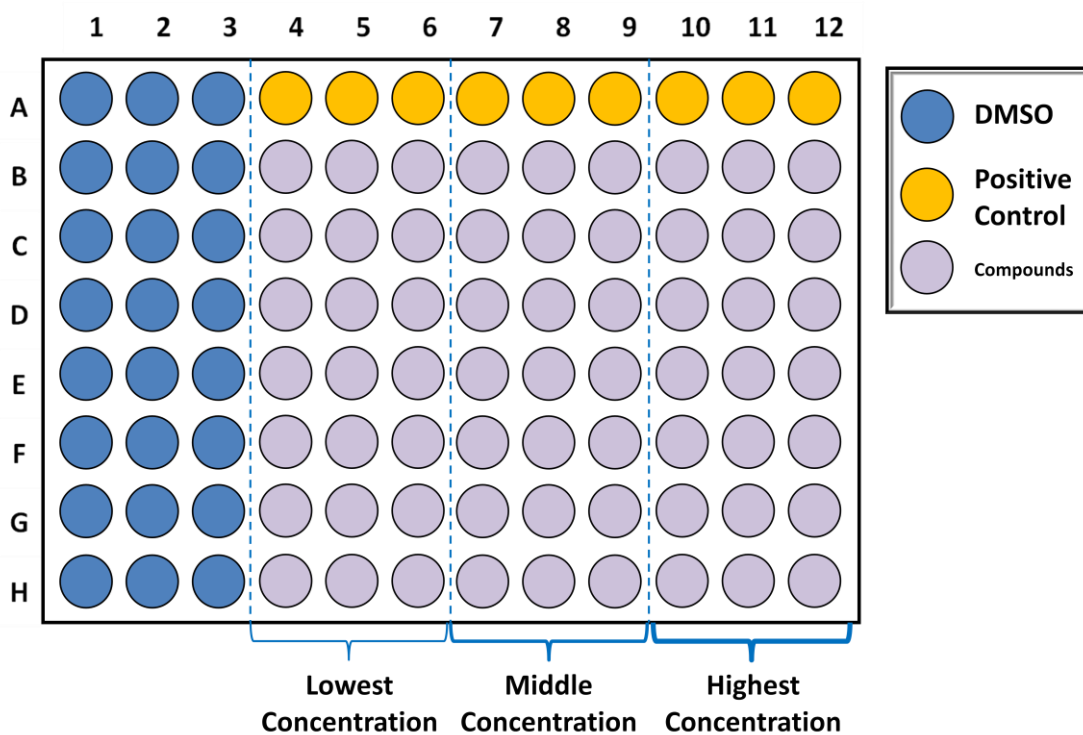


Figure 5. 2 Plate for MDM2/MDMX inhibitor dose-dependent activity evaluation

5.3 Results

5.3.1 DePPICT compound screening

An initial batch of 334 compounds were received from Siena Biotech for MDM2 and MDMX inhibitor screening. After screening using the ELISA method, hit compounds that showed high percentage inhibition values (> 50 %) were re-tested using the dose-dependent ELISA method, and then the cellular activity of the most potent compound was evaluated using the NGP cell line.

5.3.1.1 MDM2 and MDMX Inhibitor Screening via ELISA Assay of the batch 1 DePPICT compounds

The screening results against the MDM2 target are displayed in [Figure 5. 3](#).

Compounds in different plates are grouped by different colour codes and every dot represents the percentage inhibition value for one compound. The medium value bars of compounds' inhibition percentage values of each plate were short red lines. A dashed red line at the 50% inhibition value position was used to indicate the inhibition values above 50%.

The result in [Figure 5. 3a](#) illustrates that with 10 μ M final concentration, most of the compounds showed less than 50% inhibitory activities against MDM2/p53 interaction (between $\pm 40\%$), and from all of the 334 compounds, only one compound in plate 0029234 showed inhibitory activity above 50%.

When the final concentration was increased to 50 μ M ([Figure 5. 3b](#)), 6 compounds showed inhibitory activity above 50% and one of them in plate 0029234 exhibited the highest inhibition percentage, and was confirmed as the same one highlighted in [Figure 5. 3a](#).

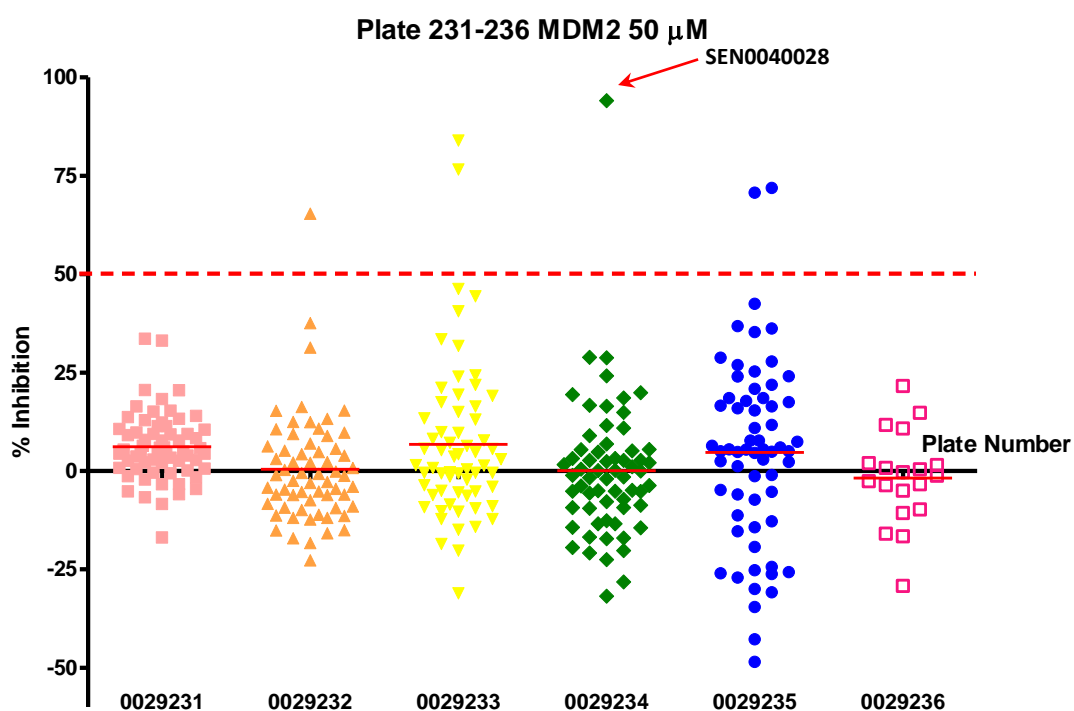
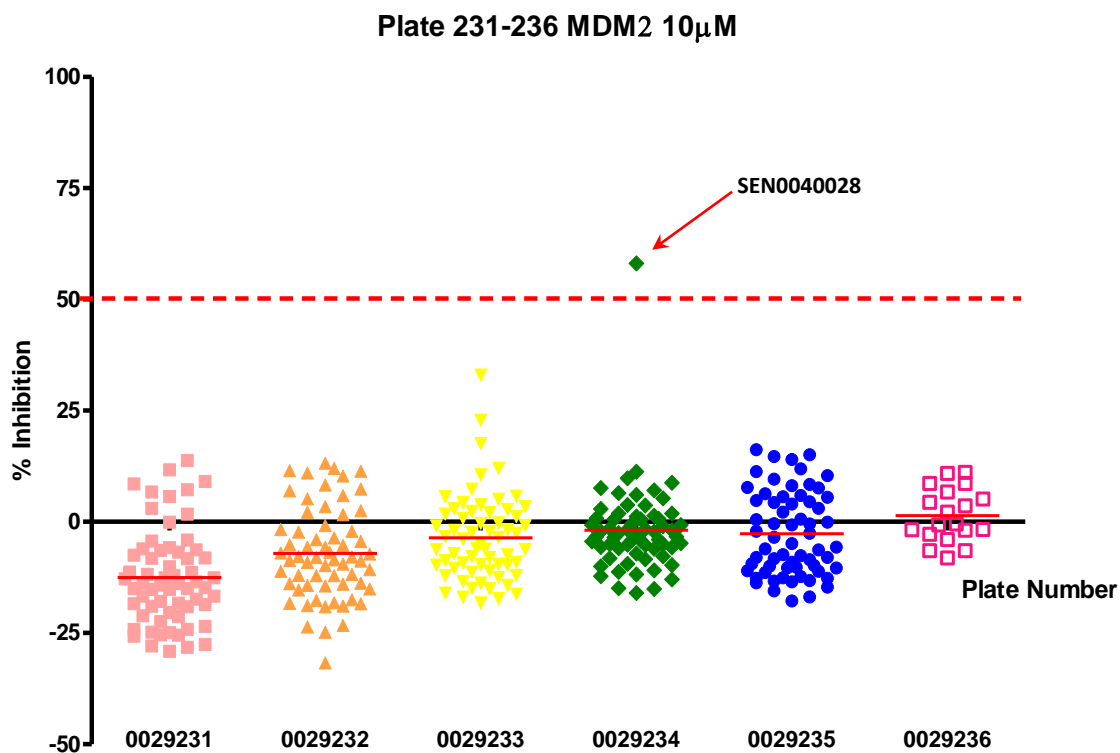


Figure 5. 3 a. Inhibitory activity against the MDM2/p53 interaction for the batch 1 compounds screened at 10 μ M final concentration (the most potent one is indicated by a red arrow together with its compound ID); b. Batch 1 compounds screened for inhibitory activity against the MDM2/p53 interaction with 50 μ M final concentration (the most potent one is indicated by a red arrow together with its compound ID).

Interestingly, though most of the compounds showed increased inhibitory activity with an increase of concentration, there were nevertheless some compounds that showed even lower percentage inhibition when using 50 μ M final concentrations compared with 10 μ M final concentrations, especially in plate 0029235 and 0029236.

The batch 1 compounds with above 30% inhibition values against the MDM2/p53 interaction at 50 μ M final concentrations are listed in [Table 5. 1](#), with their plate location, compound ID and 10 μ M final concentration inhibition percentage values against the MDM2/p53 interaction.

Table 5. 1 Potent compounds in the batch 1 compounds screening results for inhibitory activity against MDM2/p53 interaction.

Location	Compound ID	% inhibition (10 μ M)	% inhibition (50 μ M)
P1B4	SEN0000739	-11.4	33.6
P1G12	SEN0031371	-0.1	33.1
P2B7	SEN0031443	-11.8	31.4
P2D7	SEN0031445	11.0	65.4
P2F6	SEN0031436	2.5	37.6
P3C6	SEN0031520	-4.5	84.0
P3D10	SEN0031562	33.0	44.4
P3G4	SEN0031505	22.9	76.6
P3H4	SEN0031506	5.8	40.6
P3H6	SEN0031526	10.6	33.5
P3H7	SEN0031536	3.9	31.8
P3H9	SEN0031558	17.6	46.3
P4B8	SEN0040028	58.1	94.1
P4C6	SEN0037768	-1.6	28.9
P4E7	SEN0040024	-1.0	28.8
P5D11	SEN0045653	6.3	33.7
P5E11	SEN0045654	8.1	27.6
P5F8	SEN0041719	-4.9	43.3
P5F11	SEN0045655	16.2	72.3
P5G10	SEN0045649	-8.5	38.0
P5G11	SEN0045656	-3.5	37.4
P5H10	SEN0045650	11.9	59.3

Compounds with inhibition percentage values higher than 50% at 50 μ M are highlighted in yellow background, and the compound with the highest percentage inhibition value is highlighted by a orange background. The reason of negative percentage inhibition data will be discussed in section 5.4.4.

Structures of the highlighted compounds in Table 5. 1 are shown in Figure 5. 4 and the most potent one (SEN0040028) is highlighted in blue.

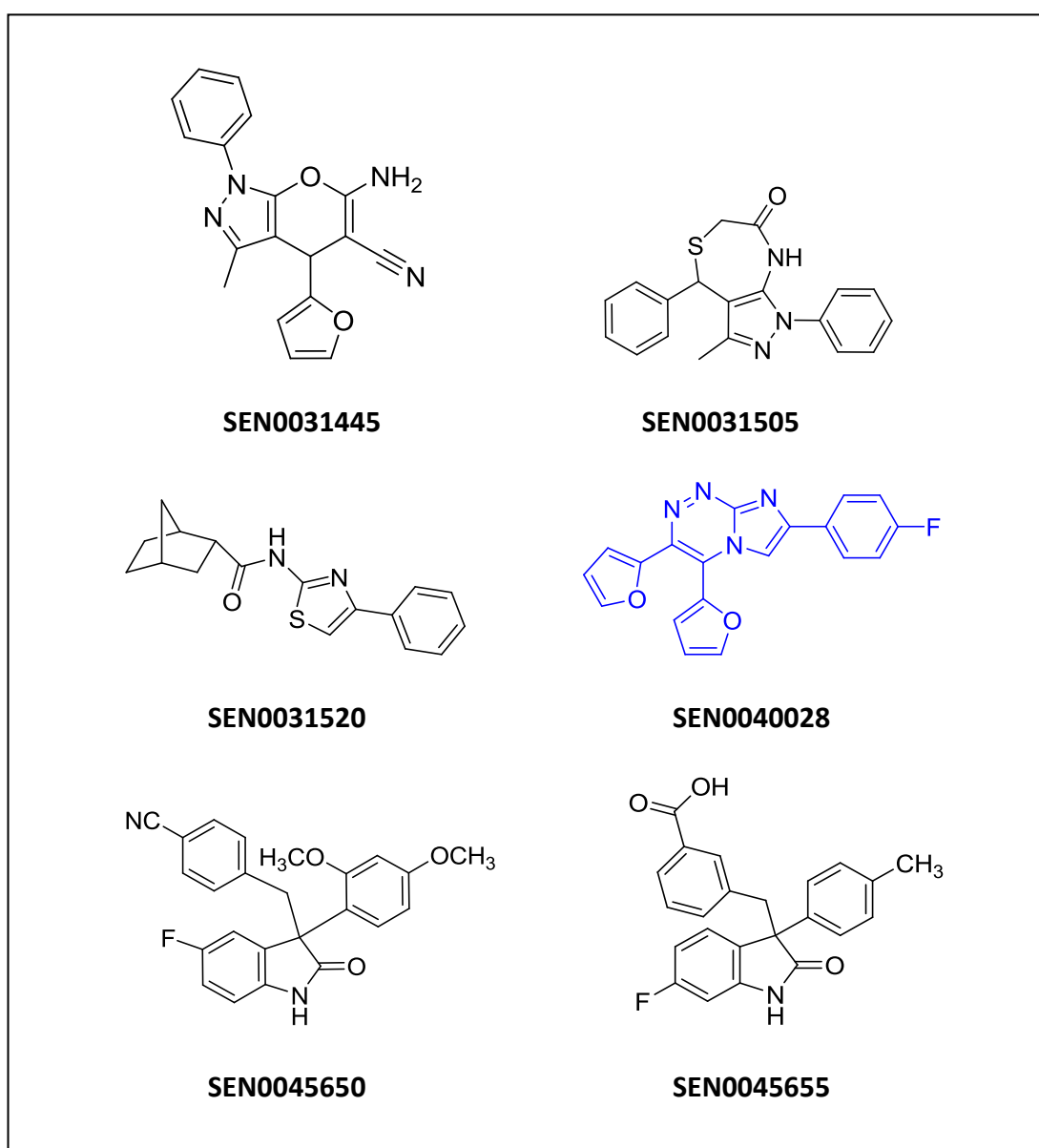


Figure 5. 4 Structures of the batch 1 hit compounds with inhibitory activity against the MDM2/p53 interaction.

The result for the first batch of compounds from Siena Biotech screened against the MDMX/p53 interaction are displayed in [Figure 5. 5](#).

[Figure 5. 5a](#) shows that at a 10 μ M final concentration, most of the compounds showed less than 50% inhibition against the MDMX/p53 interaction (between 40% and -60%), and only one compound in plate 0029234 showed inhibitory activity above 50% in all the screened 334 compounds. Importantly, this compound was confirmed to be the one highlighted in [Figure 5. 3](#), which was also the most active against MDM2/p53 interaction. Further discussion and binding mode prediction see section 5.4.2.

When the final concentration was increased to 50 μ M ([Figure 5. 5b](#)), 4 compounds showed inhibitory activity above 50% and one of them in plate 0029234 had the highest percentage inhibition, and was confirmed to be the same one highlighted in [Figure 5. 5a](#).

Interestingly, it seemed that the increase in compound concentration could only enhance the percentage inhibition values of some compounds, and there were still some compounds that showed even lower percentage inhibition values, especially in plate 0029234.

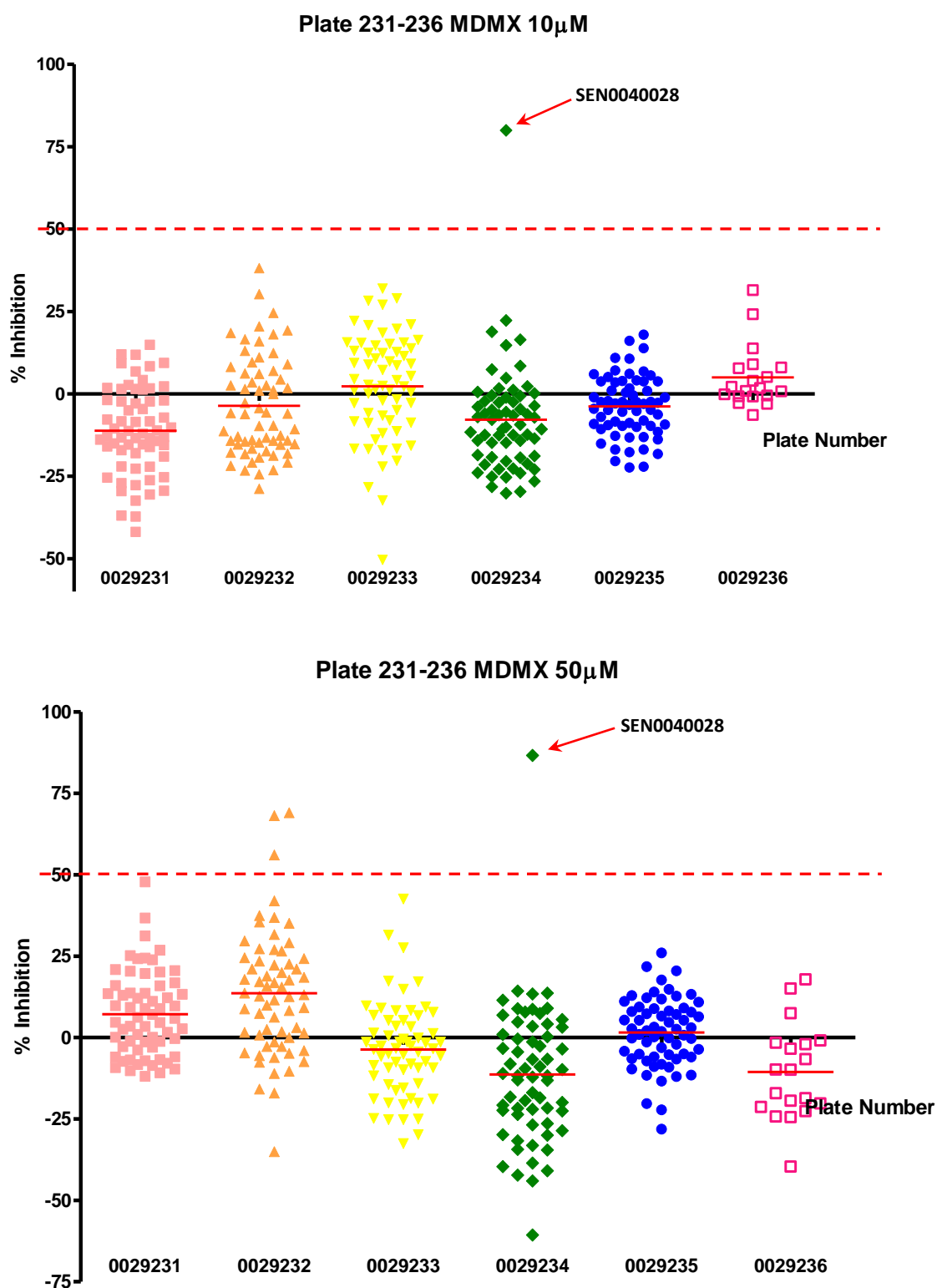


Figure 5. 5 Inhibitory activity against the MDMX/p53 interaction for the batch 1 compounds screened at 10 μ M final concentration (the most potent one is indicated by a red arrow together with its compound ID); b. Batch 1 compounds screened for inhibitory activity against the MDMX/p53 interaction with 50 μ M final concentration (the most potent one is indicated by a red arrow together with its compound ID).

The batch 1 compounds with inhibition percentage values against MDMX/p53 interaction above 30% at 50 μ M final concentrations are listed in [Table 5. 2](#), with their plate location, compound ID and 10 μ M final concentration percentage inhibition values against the MDMX/p53 interaction.

Compounds with percentage inhibition values higher than 50% at 50 μ M are highlighted in orange background and the compound with the highest percentage inhibition value is highlighted in red background.

Table 5. 2 Potent compounds in the batch 1 compounds screening results for inhibitory activity against MDMX/p53 interaction.

Location	Compound ID	% inhibition (10 μ M)	% inhibition (50 μ M)
P1B4	SEN0000739	-3.5	36.7
P1D6	SEN0024849J	-2.8	47.8
P1D11	SEN0031364	-15.3	31.2
P2B7	SEN0031443	19.0	31.7
P2B8	SEN0031452	-10.7	37.5
P2B10	SEN0031471	21.7	35.1
P2B11	SEN0031479	26.8	36.9
P2B12	SEN0031487	40.0	68.2
P2C12	SEN0031488	22.5	56.1
P2D7	SEN0031445	32.9	69.1
P2D11	SEN0031481	9.6	42.0
P2E11	SEN0031482	8.4	35.5
P3F5	SEN0031513	31.9	35.6
P3G4	SEN0031505	-0.7	40.1
P4B8	SEN0040028	83.7	89.8
P4B12	SEN0040432	32.0	33.8

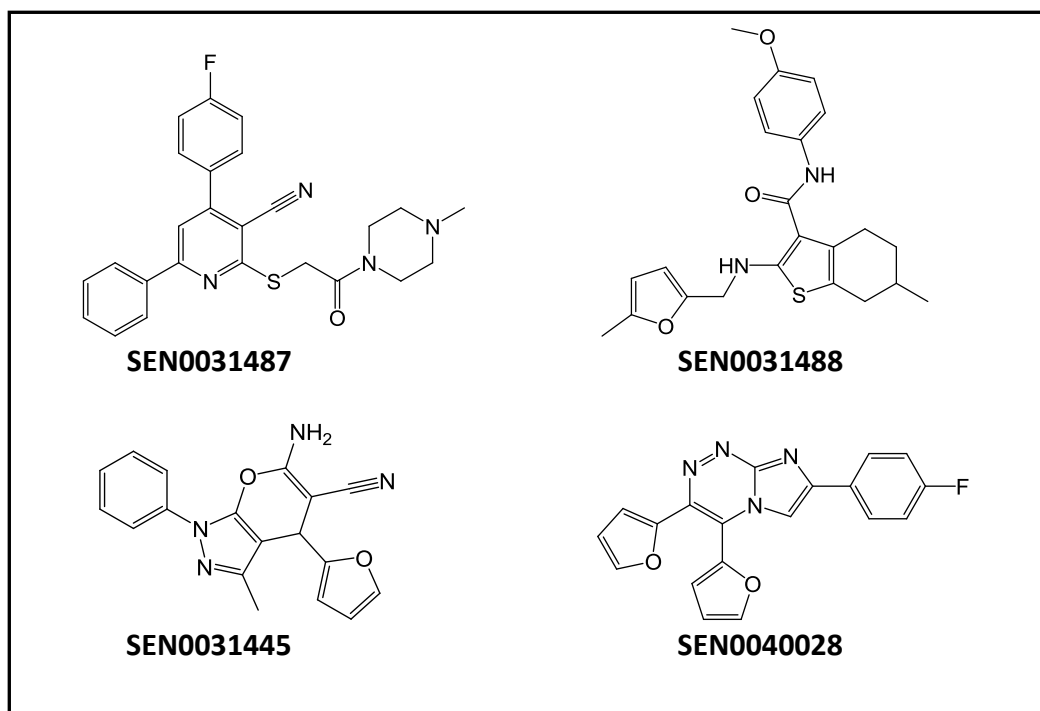
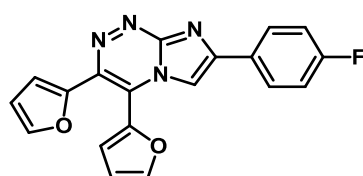


Figure 5. 6 Hit compounds against MDMX/p53 interaction at 50 μ M final concentration

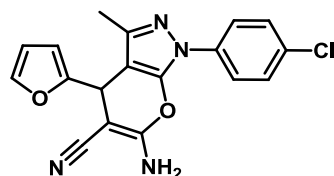
5.3.1.2 Dose-dependent-activity (DDA) evaluation for potent 1st batch DePPICT compounds

One of the important purposes of screening the batch 1 compounds was to evaluate the reliability of the ELISA assay method, using the dose-dependent-activity ELISA to check the reproducibility of screening results was adopted as a standard validation procedure.

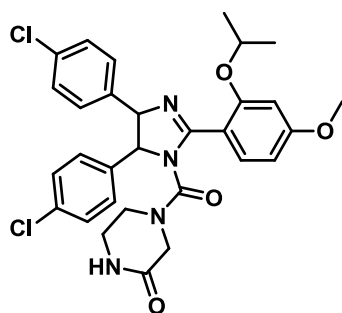
The two compounds SEN0040028 and SEN0031562, which showed a dose-dependent percentage inhibition increase after the concentration increased from 10 to 50 μ M, were selected for MDM2 target hit compound dose-dependent-activity evaluation via ELISA assay, using Nutlin-3 as a positive control. SEN0040028 was also tested as an MDMX target hit compound by using NU8325 as a positive control. The four compounds' structures are displayed in Figure 5. 7.



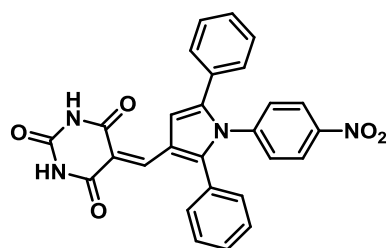
SEN0040028



SEN0031562



Nutlin-3



NU8325

Figure 5. 7 Structures of compounds tested for dose dependent activity against MDM2/p53 and/or MDMX/p53 binding interaction.

Both SEN0031562 and SEN0040028 were evaluated for their dose-dependent-activity as MDM2/p53 interaction inhibitors. For each compound, three concentrations, 0.1, 1 and 10 μM were tested. IC_{50} results of all compounds were calculated using Prism GraphpadTM software by point-to point and non-linear regression.

As displayed in [Figure 5. 8a](#), the 10 μM concentration percentage inhibition values for the two compounds were very close to the screening results. The IC_{50} value of SEN0040028 after calculation using Prism software, was 7.3 μM .

The result in [Figure 5. 8b](#) shows that SEN0040028 inhibitory activity against MDMX/p53 interaction is also dose-dependent, with an $\text{IC}_{50} = 8.6 \mu\text{M}$.

However, it was noticeable that the percentage inhibition value against MDMX/p53 interaction at 10 μM was much lower than the original value obtained on screening. This might relate to its limited solubility. The compound may not be able to dissolve and distribute evenly in the DMSO with high concentration, as a result, the concentrations

of diluted samples may variable from time to time, and these variable concentration may lead to inaccurate IC_{50} value.

Because of this observation, it was decided to check the solubility of received compounds before ELISA evaluation in subsequent experiments.

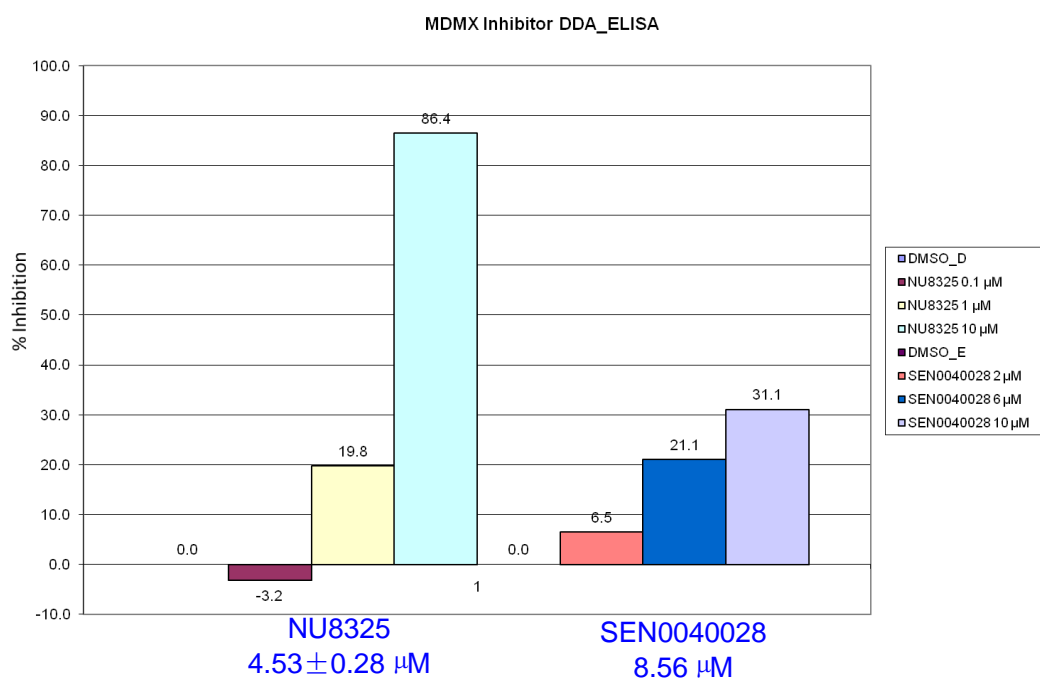
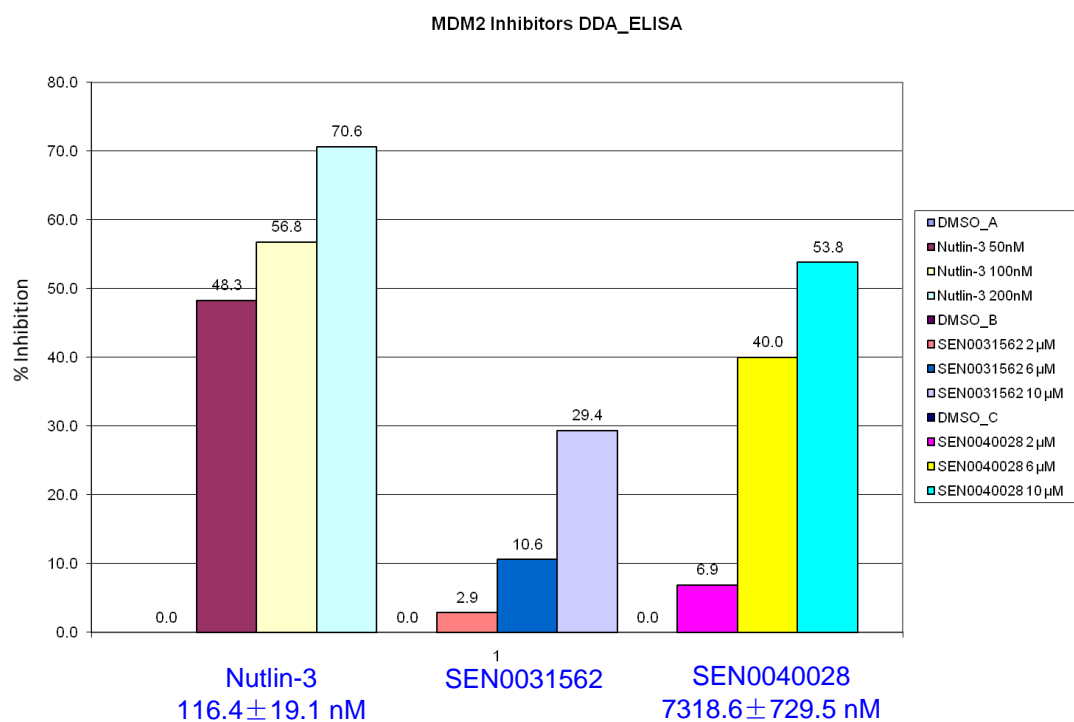


Figure 5. 8 a) Dose-dependent-activity (DDA) of SEN0040028 and SEN0031562 as the MDM2/p53 interaction inhibitors (ELISA); b) dose-dependent-activity of NU8325 and SEN0040028 as the MDMX/p53 interaction inhibitors (ELISA).

5.3.1.3 Cellular Activity Evaluation for DePPICT Hit SEN0040028

Nutlin-3 was selected as the positive control and the Michigan University compound MI-63 supplied by Siena Biotech was also included for comparison.

Images of untreated NGP cells and cells treated using 1% DMSO, 1 μ M or 10 μ M Nutlin-3 or MI-63 and 5, 20 and 50 μ M SEN0040028 for 24 hours are displayed in [Figure 5. 9](#).

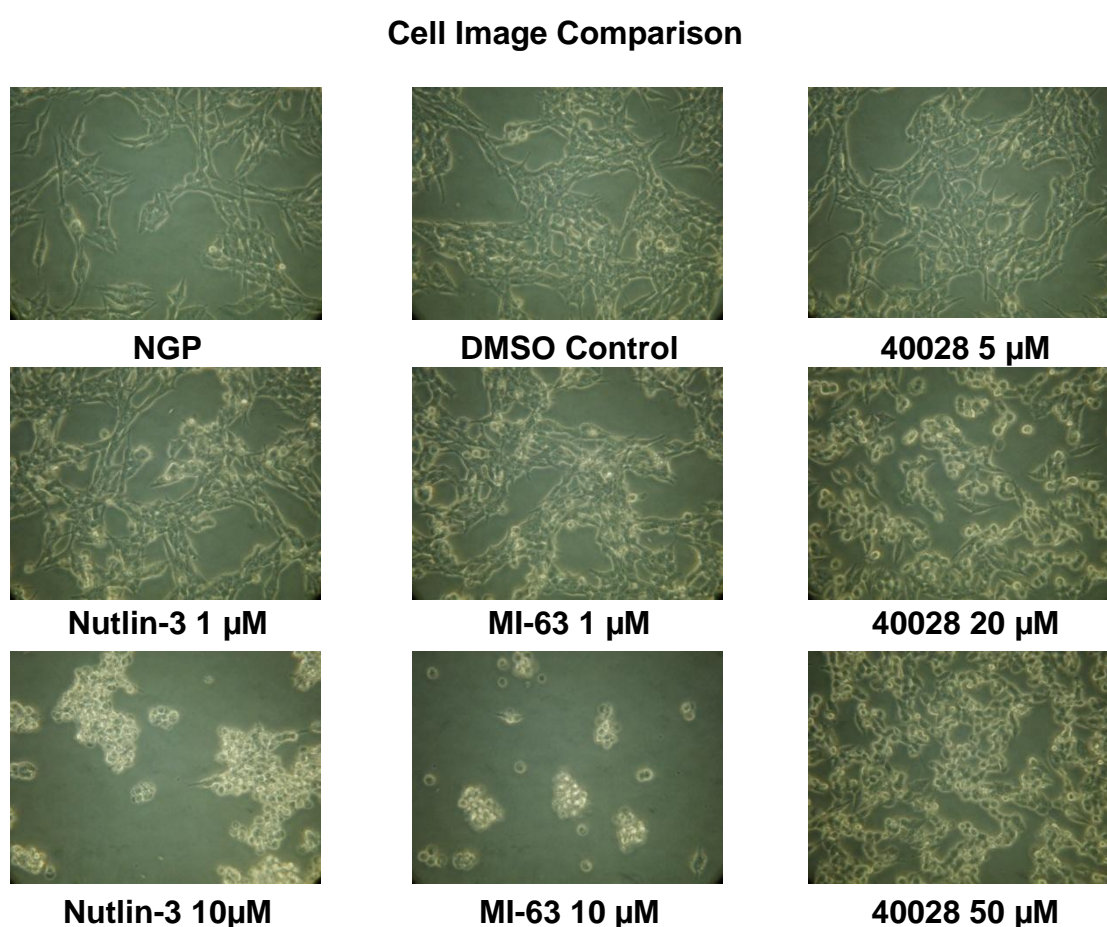


Figure 5. 9 Images of NGP cells treated with various concentrations of Nutlin-3, MI-63 and SEN0040028 for 24 hours

As can be seen from the result, after 24 hours, NGP cell cultures treated with 10 μ M Nutlin-3 or MI-63 showed marked decrease in number and change in morphology; but NGP cell cultures treated with 20 or 50 μ M SEN0040028 compound showed only slight loss of adherence ability and change in morphology that was very similar to 1 μ M

Nutlin-3 or MI-63 treated cells. In addition, some yellowish undissolved crystal-like compound clusters were observed under the microscope in 50 μ M SEN0040028 treated NGP cell culture media (Figure 5. 10), which indicated the limited solubility of this compound in an aqueous environment.

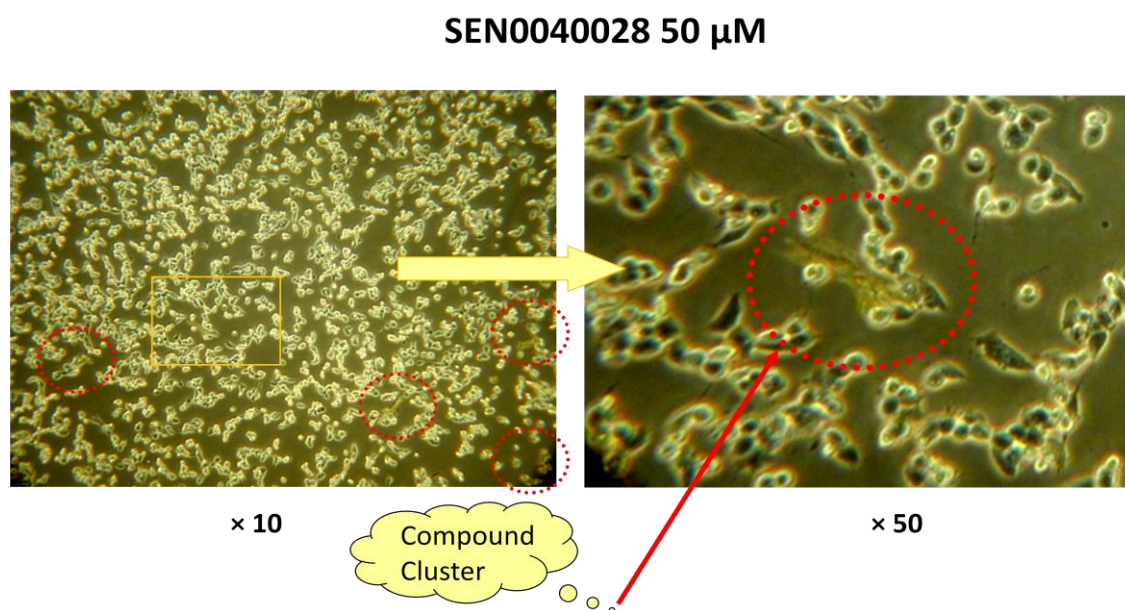


Figure 5. 10 Undissolved compound clusters (surrounded with red circles) observed in 50 μ M SEN0040028 treated NGP cell culture media.

5.3.2 DePPICT compound screening as MDM2/MDMX inhibitors

After initial confirmation of activity, the compounds were resupplied for full IC_{50} evaluation. In addition, further batches of compounds and so called fragments were sent for 1st stage screening at a single 10 μ M final concentration for standard compounds (from Siena Biotech) and 250 μ M final concentration for fragment compounds (identified at Crystax Ltd by NMR based screening). After screening using the ELISA, hit compounds that showed percentage inhibition values close to and higher

than 50% were selected and initially confirmed by testing for dose-dependent activity with the ELISA.

The further compound screening results against MDM2 and MDMX targets are displayed in [Figure 5. 11 to Figure 5. 19](#). As can be seen from the whole screening results, we found that most of the compounds have shown inhibition percentage values below 50% inhibition potency. Altogether, there were only 7 compounds with percentage inhibition values above 50% out of more than 2500 compounds screened as MDM2 inhibitor candidates, and only 2 compounds from more than 1000 compounds screened as MDMX inhibitor candidates at 10 μ M final concentration; with the fragment compounds sent by Crystax Ltd. ([Figure 5. 13](#)), only 6 compounds showed greater than 50% inhibitory activity at 250 μ M final concentration.

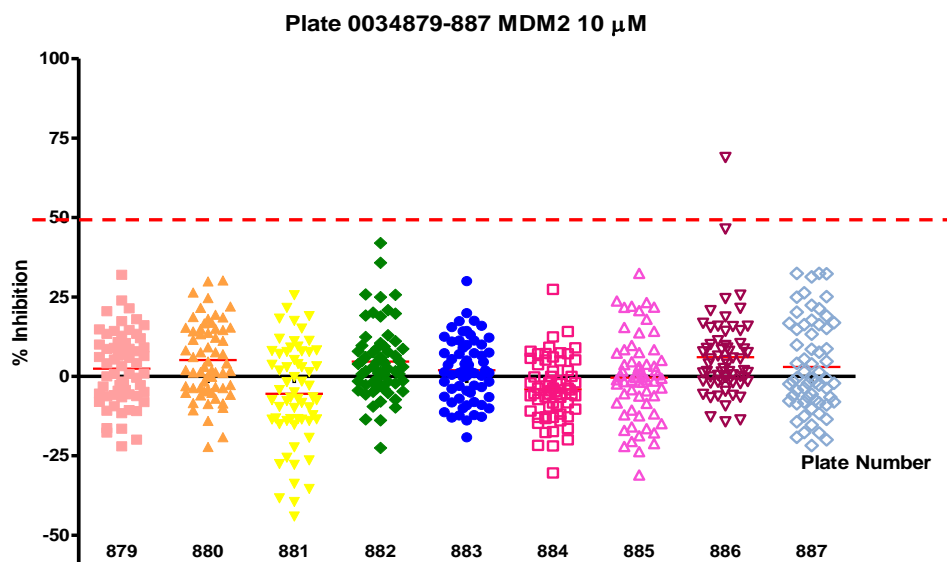


Figure 5. 11 Screening of plates 0034879-34887 for compounds with inhibitory activity against the MDM2/p53 interaction at 10 μ M final concentration.

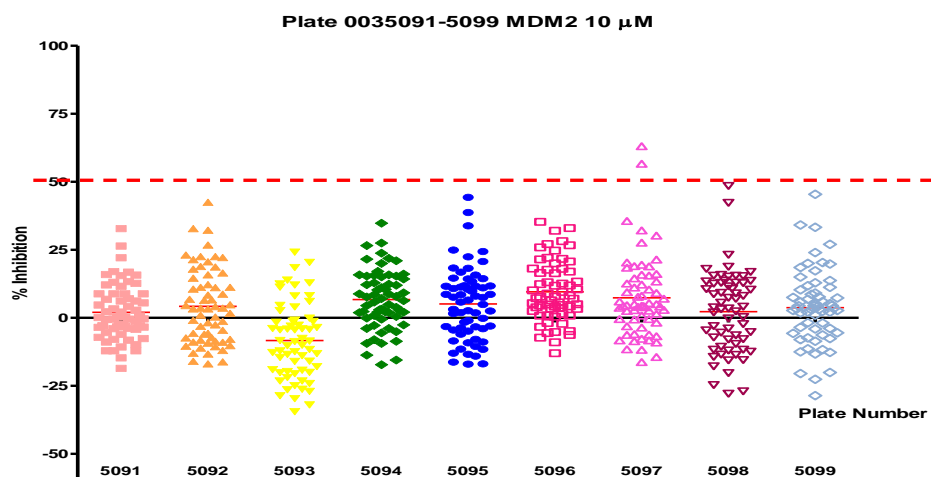


Figure 5. 12 Screening of plates 0035091-35099 for compounds with inhibitory activity against the MDM2/p53 interaction at 10 μ M final concentration.

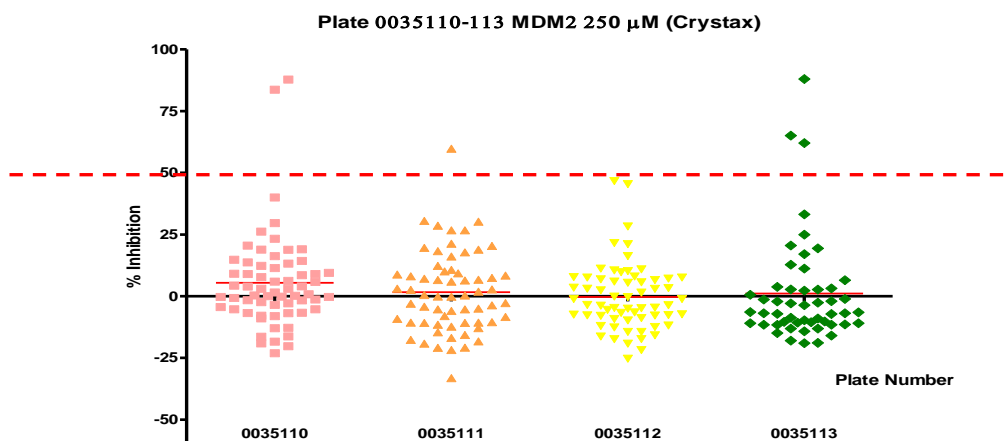


Figure 5. 13 Screening of plates 0035110-35113 for Crystax fragment compounds with inhibitory activity against the MDM2/p53 interaction at 250 μ M final concentration.

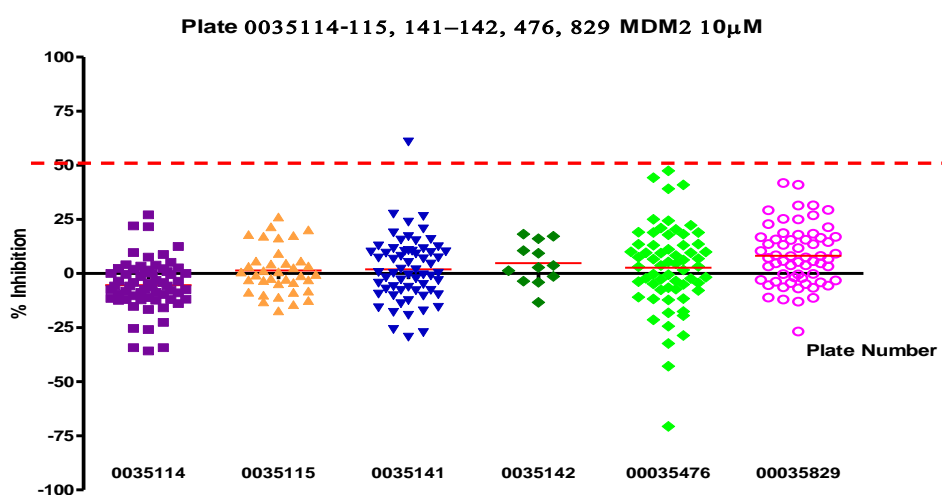


Figure 5. 14 Screening of plates 0035114-35115, 35141-35142, 35476 and 35829 for compounds with inhibitory activity against the MDM2/p53 interaction at 10 μ M final concentration.

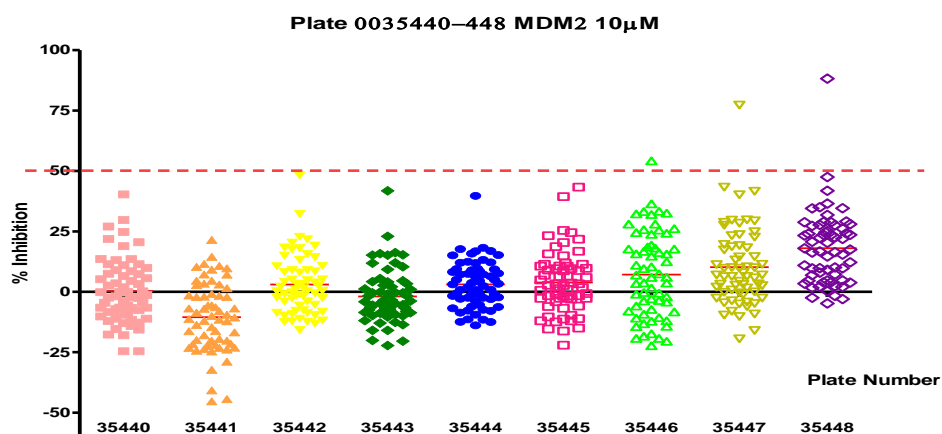


Figure 5. 15 Screening of plates 0035440-35448 for compounds with inhibitory activity against the MDM2/p53 interaction at 10 μ M final concentration.

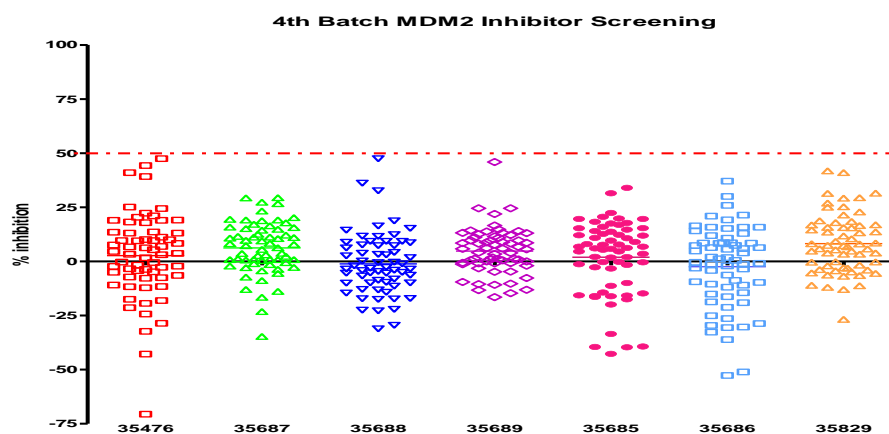


Figure 5. 16 Screening of batch 4 plates for compounds with inhibitory activity against the MDM2/p53 interaction at 10 μ M final concentration.

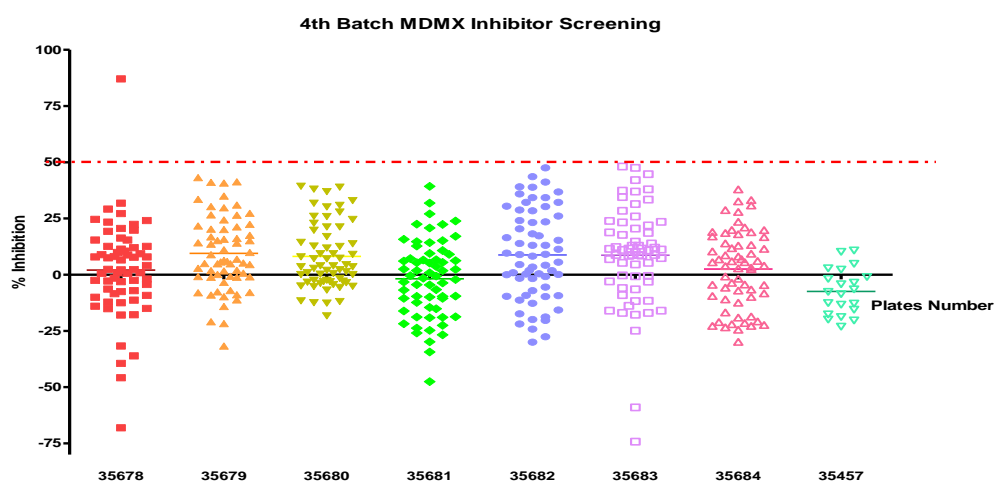


Figure 5. 17 Screening of batch 4 plates for compounds with inhibitory activity against the MDMX/p53 interaction at 10 μ M final concentration.

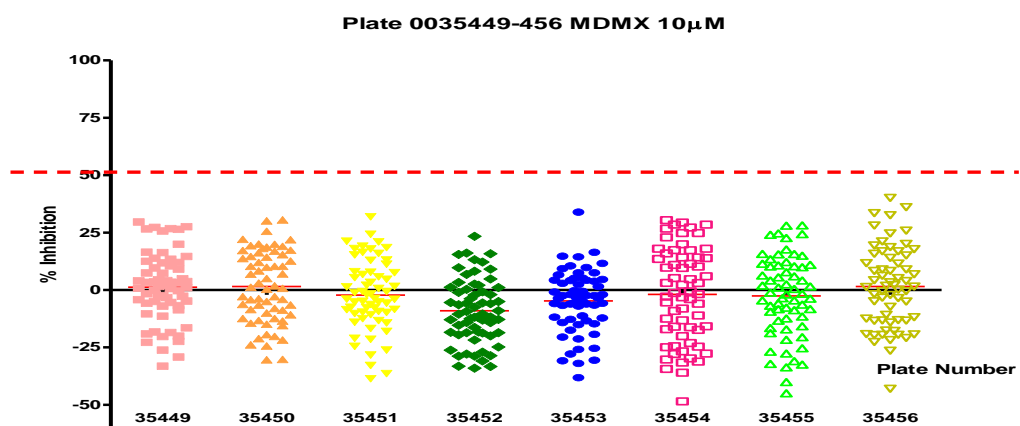


Figure 5. 18 Screening of plates 0035449-35456 for compounds with inhibitory activity against the MDMX/p53 interaction at 10 μ M final concentration.

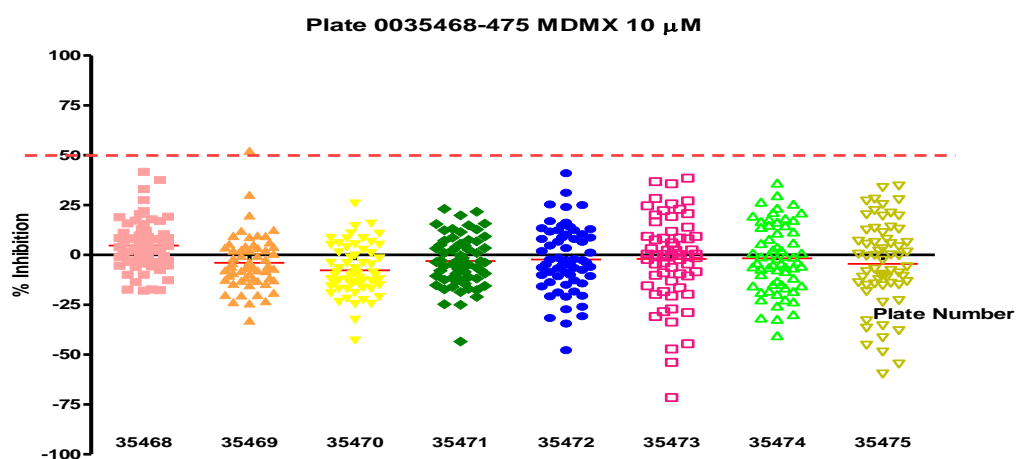


Figure 5. 19 Screening of plates 0035468-35475 for compounds with inhibitory activity against the MDMX/p53 interaction at 10 μ M final concentration.

5.3.3 Threshold value determination of DePPICT compounds

Previously, we had set the threshold value for the definition of a hit to be above 50% inhibitory activity at 10 μ M final concentration, such and hit compounds were then taken forward for confirmation and further evaluation using a dose-dependent ELISA. After the whole screening procedure, we combined inhibitory activity results of all 10 μ M samples as MDM2 inhibitors together and obtained the curve shown in [Figure 5. 20](#), which supported the choice of threshold value that had been selected.

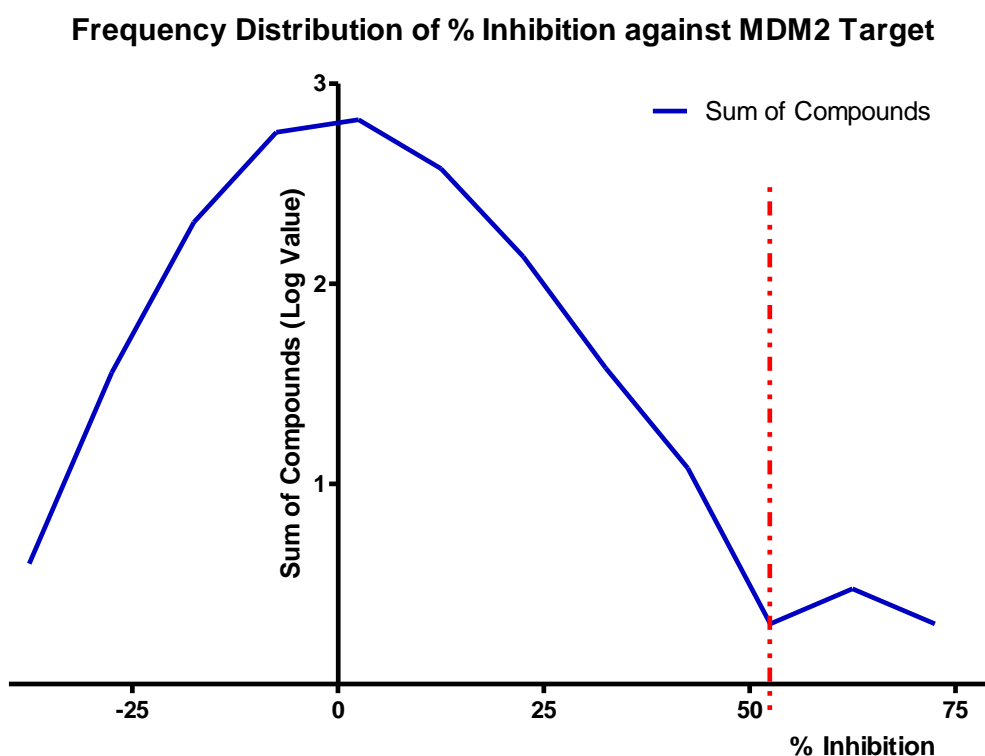


Figure 5. 20 Frequency distribution of percentage inhibition values for DePPICT compounds screened for activity as MDM2/p53 interaction inhibitors.

The blue curve represents the number of compounds distributing based on percentage inhibition values. The valley between two peak values, which is highlighted by using a red-dashed line, indicate the threshold value location that is close to 50% value position.

5.3.4 Pyrrole Compounds as MDM2/p53 and/or MDMX/p53 Inhibitors

The Pyrrole scaffold compounds tested as MDM2/p53 and/or MDMX/p53 interaction inhibitors by the ELISA are listed in [Table 5. 3](#).

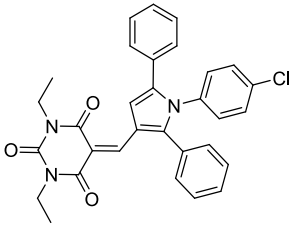
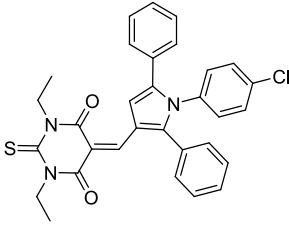
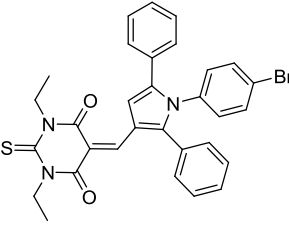
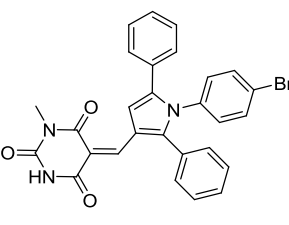
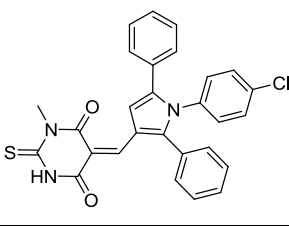
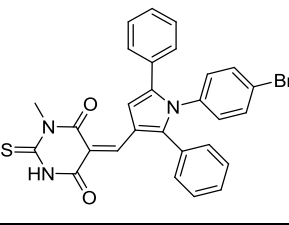
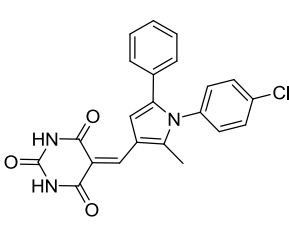
Each concentration of every compound was plated out in triplicate at three different concentrations and the experiments were repeated at least three times for confirmation.

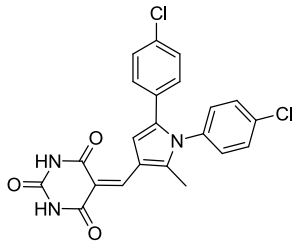
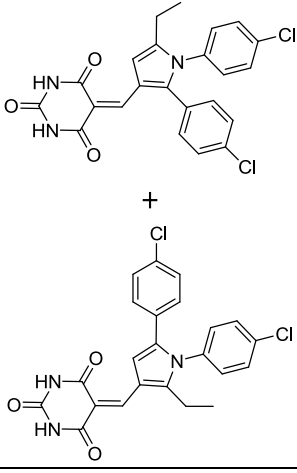
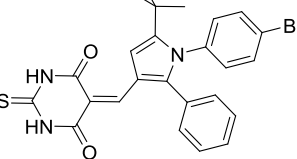
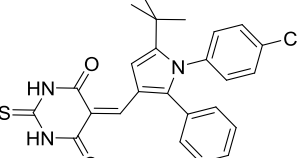
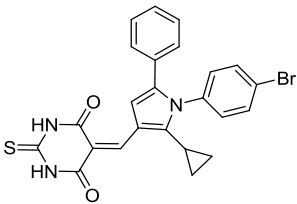
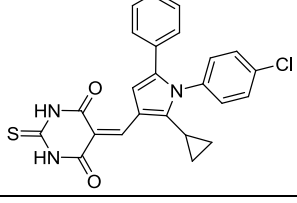
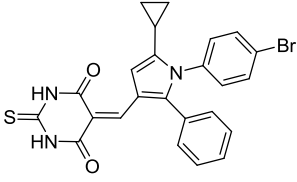
IC₅₀ results of all compounds were calculated using Prism Graphpad™ software by build-in point to point calculation programme.

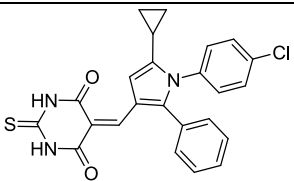
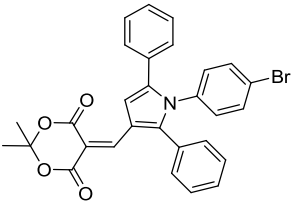
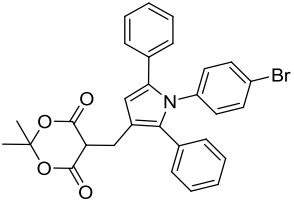
As the solubility of some pyrrole compounds was poor even in dimethyl sulphoxide (DMSO), we have used tetrahydrofuran (THF) as an alternative solvent, diluting to the required concentration with 2% THF in final DMSO solution, resulting in 0.01% THF in ELISA. However, an even higher concentration of THF was used for less soluble pyrrole compounds ([Table 5. 3](#)), with the solvent-only control also changed to give the same percentage of concentration THF in DMSO.

Table 5. 3 Inhibition Potency of Pyrrole Compounds as MDM2/p53 and MDMX/p53 Interaction Antagonists

Compounds Code	Structure	IC ₅₀ nM	SE (nM)
NU8291		105 [*]	20
NU8323		195	50
		994.9	21.1 MDMX
NU8324		168	62
		855.3	40.1 MDMX
NU8325		153	59
		4530	280 MDMX
NU8327		255 [*]	44
NU8356		888 ^{**}	44

NU8372		613 ^{***}	
NU8373		300 [*]	55
NU8374		255 [*]	48
NU8375		341 [*]	80
NU8376		113 [*]	12
* NU8377		72.6 ^{**}	2.2
NU8379		1290	

NU8381		736	61
NU8382		663	44
NCL-00016067		524.4	96.2
		963.2	n=1 MDMX
NCL-00016068		494.1	76.4
		1684.6	n=1 MDMX
NCL-00016393		740.2	105.1
		3428.3	n=1 MDMX
NCL-00016394		641.4	280.3
		3486.8	n=1 MDMX
NCL-00016395		642.8	151.9
		5322.4	n=1 MDMX

NCL-00016396		583.9	228.9
		4916.0	n=1 MDMX
NCL-00016746		19930	626
		38.9%, 50 μM	n=1 MDMX
NCL-00016747		1670	
		10100	n=1 MDMX

NB:

IC₅₀ values as MDM2 inhibitors are displayed using plain texts, and IC₅₀ values as MDMX inhibitors are displayed using bold texts.

*Normally the compounds were tested using DMSO as the solvent, however some pyrrole compounds could not be dissolved in DMSO, as a result THF was used to dissolve them and * was used to indicate these compounds.*

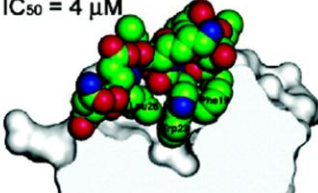
** Means the final concentration is 0.2% THF in DMSO solvent, ** means 0.4% THF in DMSO and *** means 0.8-1% THF in DMSO.*

5.3.5 Comparison of Peptide Inhibitors against both MDM2 and MDMX Targets

The research breakthrough of potent peptide inhibitors ([Figure 5. 21](#)) for MDM2/p53 interaction started almost at the same time as the report of discovering and developing potent MDM2/p53 small molecular inhibitors, and quite a lot of these peptides have been reported together with the publication of the MDM2/inhibitor co-crystal structures ([12, 125](#)).

entry	sequence	IC ₅₀ (nM) ^b
1	Ac-Gln ¹⁶ -Glu-Thr-Phe-Ser-Asp ²¹ -Leu-Trp-Lys-Leu-Leu-Pro ²⁷ -NH ₂	8673 ± 164
2	Ac-Met-Pro-Arg-Phe ¹⁹ -Met-Asp-Tyr-Trp-Glu-Gly-Leu ²⁶ -Asn-NH ₂	313 ± 10
3	Ac-Phe ¹⁹ -Met-Asp-Tyr-Trp-Glu-Gly-Leu ²⁶ -NH ₂	8949 ± 588
4	Ac-Phe ¹⁹ -Met-Aib-Tyr-Trp-Glu-Ac ₃ c-Leu ²⁶ -NH ₂	2210 ± 346
5	Ac-Phe ¹⁹ -Met-Aib-Pmp-Trp-Glu-Ac ₃ c-Leu ²⁶ -NH ₂	314 ± 88
6	Ac-Phe ¹⁹ -Met-Aib-Pmp-6-F-Trp-Glu-Ac ₃ c-Leu ²⁶ -NH ₂	14 ± 1
7	Ac-Phe ¹⁹ -Met-Aib-Pmp-6-Me-Trp-Glu-Ac ₃ c-Leu ²⁶ -NH ₂	10 ± 1
8	Ac-Phe ¹⁹ -Met-Aib-Pmp-6-Cl-Trp-Glu-Ac ₃ c-Leu ²⁶ -NH ₂	5 ± 1

15-mer wt-p53 peptide
IC₅₀ = 4 μM



8-mer p53 peptide analogue
IC₅₀ = 5 nM

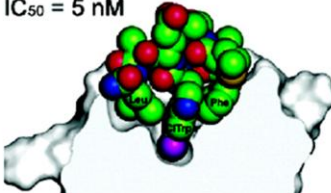


Figure 5. 21 Potent peptide inhibitors for MDM2-p53 interaction and crystal structure analysis of p53 related peptide bound to the MDM2 protein([12, 125](#))

A recently published co-crystal structure of MDMX binding with p53 peptide ([168](#)) allowed the comparison of the MDM2 and MDMX binding pockets side by side.

As an initial approach, the MDM2 (1YCR) ([116](#)) and MDMX (3DAB) ([168](#)) crystal structures were superimposed using PyMOL software, to compare the difference between their p53 binding grooves. The most marked differences was highlighted ([Figure 5. 22](#)). Firstly, the red arrow shows that the MDMX side chains make the Leu26 binding pocket of MDMX to be smaller than that of MDM2; Secondly, in the red circle surrounded area, MDMX side chains make the Trp23 binding pocket of MDMX

shallower than that of MDM2; Finally, the red twin-arrow points out that the Phe19 binding pocket of MDMX is wider than that of MDM2, which may be because of the whole p53 transactivation domain being pushed backward, when binding with MDMX because of the smaller Leu26 binding pocket, then the Phe19 side-chain of p53 makes this pocket open wider. This observation suggests that the p53 peptide binding groove of MDM2/MDMX might be flexible and the shape may adapt according to the nature of the ligand which binds to the pocket, although the flexibility may be very limited.

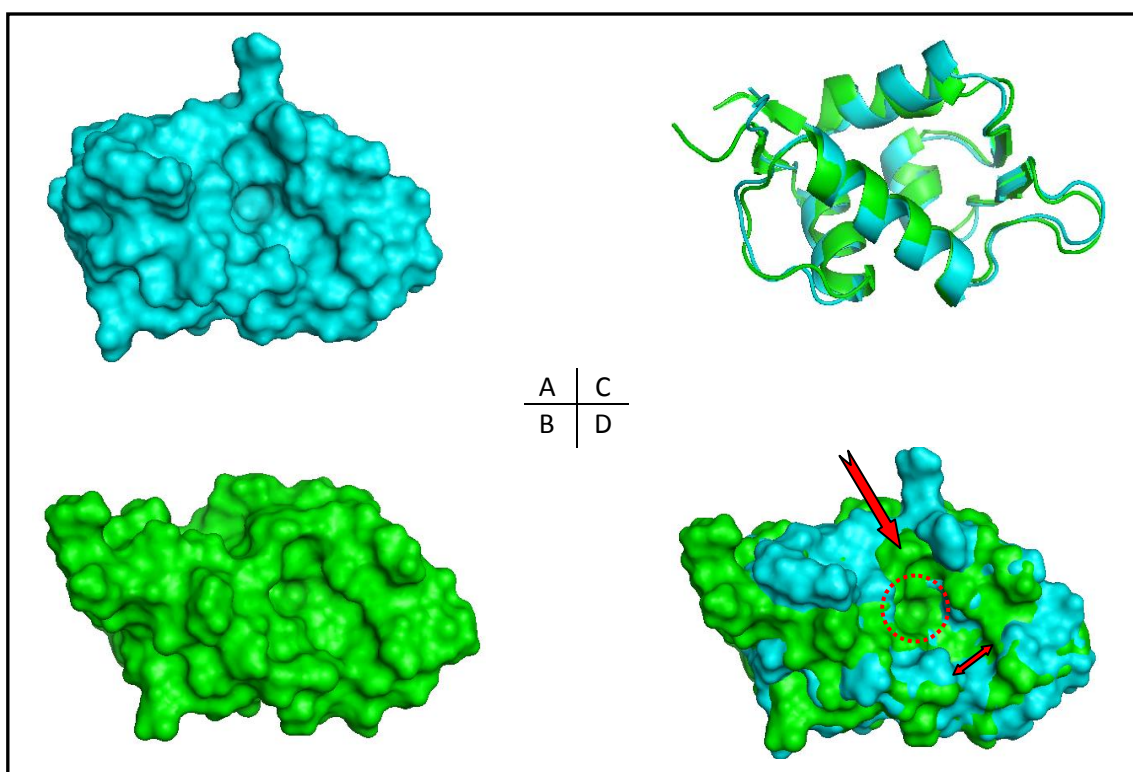


Figure 5. 22 Binding groove comparison of MDM2 1YCR and MDMX 3DAB structure

The cartoons above showed the comparison of MDM2 and MDMX protein 3D structure. A. Surface image of MDM2 protein colour coded as cyanine; B. Surface image of MDMX protein colour coded as green; C. Superimposed MDM2 and MDMX cartoon as 3D ribbon structures; D. Superimposed MDM2 and MDMX surface image with key differences highlighted by red circle and arrows. The figures were generated using PyMOL ([DeLano, 2002](#)).

Then to compare the MDM2/p53 and MDMX/p53 binding grooves in detail and with some quantitative results, the surface representations of human MDMX (3DAB &

3DAC) and two human MDM2 (1YCR & 1T4F) protein structures are displayed in [Figure 5. 23](#).

Marked differences in the shape of the p53 binding pocket are clearly visible in the light green colour filled area in the first row of images. Amino acid side chains of MDM2/MDMX proteins that are responsible for forming the binding groove are displayed in the second row of images; amino acid side chains of MDM2/MDMX proteins that surrounding the highlighted binding grooves are also listed in the third row.

In the list, the same side chains at the same location are coded in bold black, the different side chains at the same location are coded in bold red, the amino acid only present in the MDM2 protein crystal structures is coded in bold green (Phe86), and one amino acid side-chain (Ile103) present only in the MDM2 (1YCR) crystal structure is indicated in normal Font.

Moreover, the volume, surface area and depth of each pocket were calculated by using Molegro Virtual Docker software, as displayed in [Figure 5. 23](#).

Clearly from this comparison, the binding pocket of MDMX is smaller and shallower than the MDM2 binding pocket when they bind to the p53 peptide. This result indicates that a smaller compound candidate may be more suitable for MDMX inhibitor screen and/or design. Their differences between the surrounding side chains may lead themselves to be exploited to design selective inhibitors of MDMX.

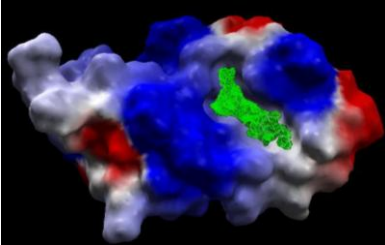
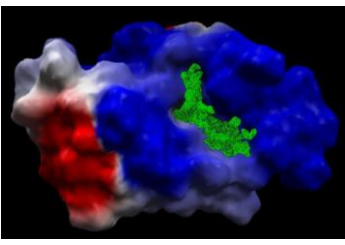
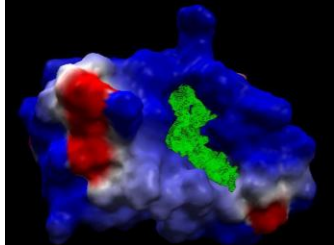
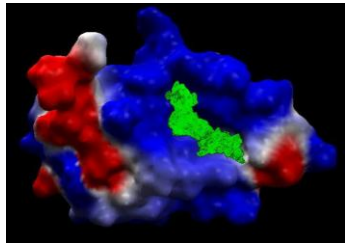
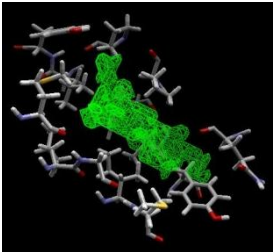
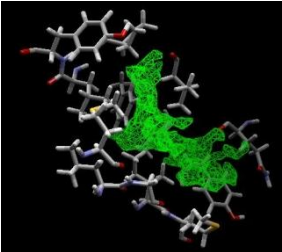
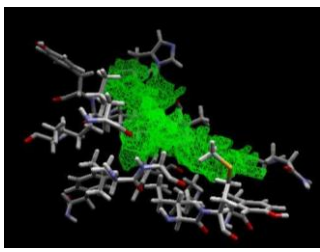
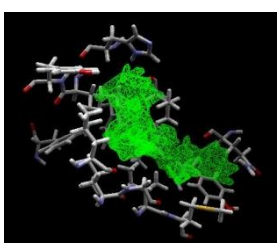
PDB Code	3DAB (MDMX)	3DAC (MDMX)	1YCR (MDM2)	1T4F (MDM2)
Cavity highlighted with Protein Surface Image				
Protein Side Chains Surrounding the Highlighted Cavity				
List of protein Side Chains Surrounding the Highlighted Cavity	Met53, Leu56, Gly57, Ile60, Met61, Tyr66, Gln71, Val74, Phe90, Val192, Pro95, Leu98, Tyr99.	Met50, Leu53, Gly54, Ile57, Met58, Tyr63, Gln68, Val71, Phe87, Pro92, Leu95, Tyr96.	Leu54, Leu57, Gly58, Gln59, Ile61, Met62, Tyr67, Gln72, Val175, Phe86, Phe91, Val193, His96, Ile99, Tyr100, Ile103.	Leu54, Leu57, Gly58, Ile61, Met62, Tyr67, Gln72, Val75, Phe86, Phe91, Val93, His96, Ile99, Tyr100.
Cavity Volume (Å ³)	68.904	71.064	126.576	115.128
Cavity Surface (Å ²)	295.92	343.44	516.96	453.60
Cavity Depth (Å)	0.233	0.207	0.244	0.254

Figure 5. 23 MDM2 and MDMX binding pockets comparison by using 3DAB, 3DAC, 1YCR and 1T4F protein database structures.

Based on this comparison, it was hypothesised that suitable modification of the structure of MDM2 peptide inhibitors might make them more potent against MDMX, which could inform the development of small molecule inhibitors of MDMX/p53 interaction and provide a better understanding of the hydrophobic binding pocket differences between MDM2 and MDMX protein when they bind with the p53 transactivation domain. Based on the research reports shown in [Figure 5. 21](#), three p53 peptide analogues were synthesised (by Dr Nicola O'Reilly, ICRF Peptide Synthesis Laboratory), as listed in [Table 5. 4](#), with the differences between them highlighted by using different colours. In particular, the APv2 peptide was made without the chlorine modification of the tryptophan residue in the β -AP peptide on the hypothesis that the former would better fit the more shallow MDMX tryptophan binding pocket.

Table 5. 4 Modified peptides made for binding affinity evaluation with MDM2/MDMX

Name	Sequence
IP3 peptide	Ac-Phe ¹⁹ -Met- Asp-Tyr-Trp ²³ -Glu- Gly -Leu ²⁶ -NH ₂
β -AP peptide	Ac-Phe ¹⁹ -Met- Aib-Pmp-6-Cl-Trp ²³ -Glu- Ac₃c -Leu ²⁶ -NH ₂
APv2 peptide	Ac-Phe ¹⁹ -Met- Aib-Pmp-Trp ²³ -Glu- Ac₃c -Leu ²⁶ -NH ₂

By using the ELISA, binding inhibition curves and IC₅₀ values were obtained for all the three peptides as MDM2 and MDMX inhibitors ([Figure 5. 24](#)).

Interestingly, as can be seen from [Figure 5. 24](#), the IP3 peptide showed the weakest binding affinity with both MDM2 and MDMX proteins among all the three p53 peptide analogues; β -AP peptide showed the strongest binding affinity with MDM2, which was about 8-fold stronger than APv2 and 1000-fold stronger than the IP3

peptide; however, its binding affinity with MDMX protein was 2.5 folds weaker than the APv2 peptide, though still 9 times stronger than the IP3 peptide. It is also worth pointing out that by modifying the p53 peptide analogue side chains, although we can still enhance their binding affinity with the MDMX protein, but the enhancement ratios are much lower than the modification confers on their binding affinity with the MDM2 protein.

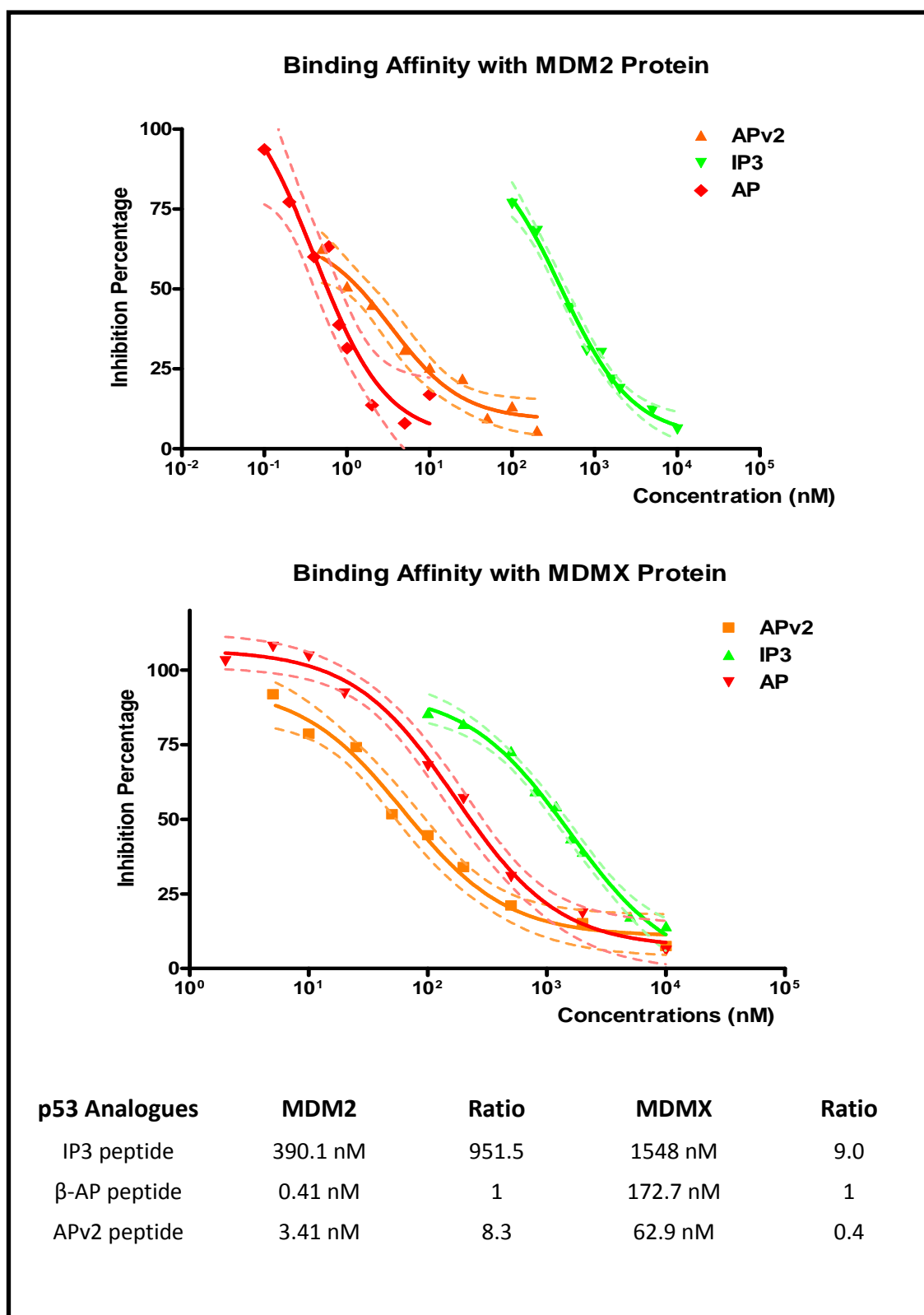


Figure 5. 24 Comparisons of the binding affinity of three p53 peptide analogues with MDM2 and MDMX by using ELISA method.

Manual docking of the two p53 peptide analogues β -AP peptide and APv2 peptide with both MDM2 (from 1YCR) and MDMX (from 3DAC) proteins crystal structure binding pockets are represented in [Figure 5. 25](#).

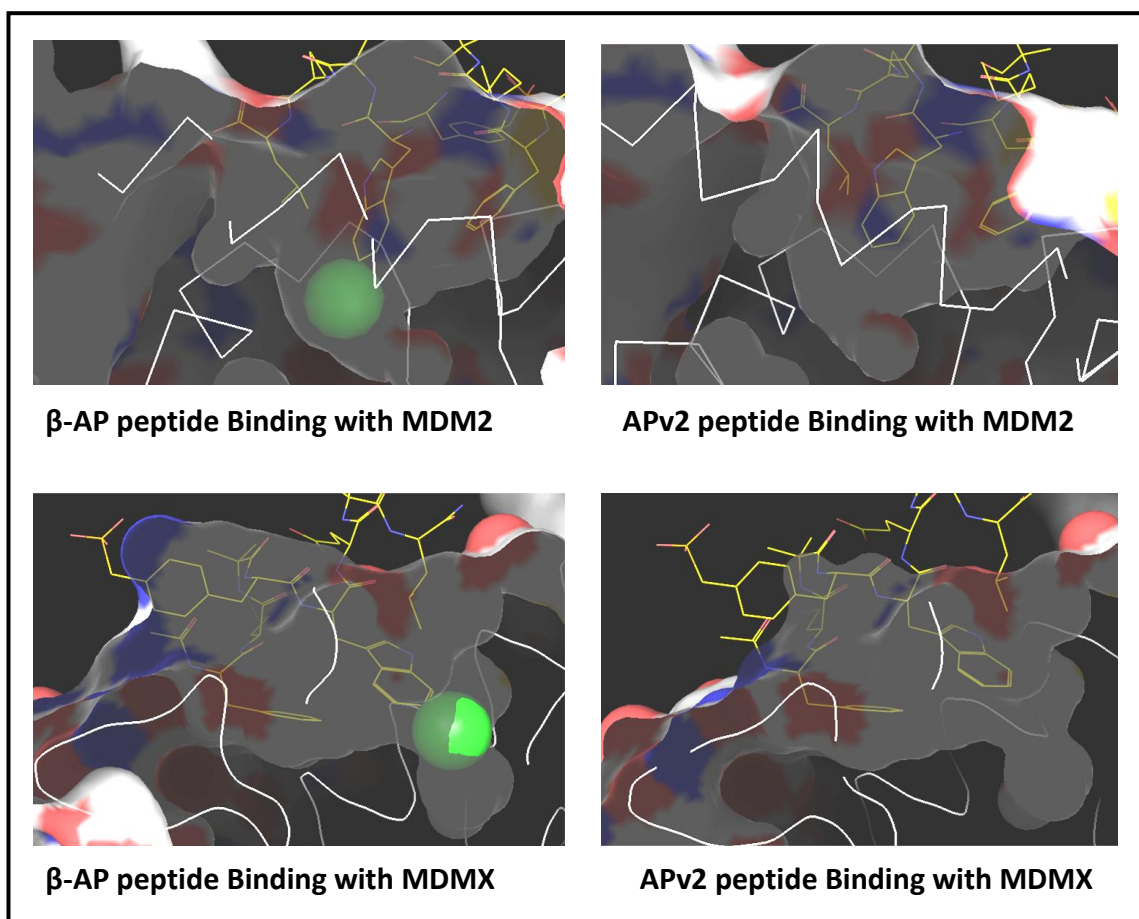


Figure 5. 25 Comparisons of peptides binding with MDM2 and MDMX by manual docking.

The chloro group at the 6-position of the tryptophan side-chain of β -AP peptide, which was colour coded as light green and displayed in a space occupying mode, could fill the remaining space in the tryptophan binding pocket of MDM2 and enhance their binding affinity; however, since the MDMX protein binding groove was smaller and shallower as illustrated in [Figure 5. 23](#), the chlorine atom would either stick out of the tryptophan binding pocket of the MDMX protein; or force the

tryptophan binding pocket to change shape to accommodate it, which would consume more energy; or force the whole peptide move away from the binding groove, which would decrease the binding affinity between the peptide with MDMX protein.

Both of the two mechanisms will cause the binding affinity of β -AP peptide with MDMX to be lower than APv2 peptide binding with MDMX.

Together with the observation made in Chapter 3 about the isoindolin-1-one scaffold compound side chains modification, I have referred to this phenomenon in terms of a '**See-Saw Theory**' that we will be discussed in detail in Chapter 7.

5.4 Conclusion and Discussion

5.4.1 The DePPICT project as a successful attempt to use virtual screening technology

Our colleagues in Siena Biotech and Crystax Ltd. have analyzed millions of commercially available compounds by using Glide or GOLD virtual docking software and narrowed the total number down to no more than 4,000 compounds for us to screen by the ELISA method.

This has generated a number of hit compound leads that showed dose-dependent activity as MDM2/p53 and/or MDMX/p53 binding interaction inhibitors. Moreover, seven scaffold series were selected, within which there was evidence of structure-activity relationships and further SAR exploration was started to be carried out by using synthetic chemistry technology.

As a result, I believe with the continued progress of this project, which has identified novel core structures of some potent candidate compound series and started to develop a systematic SAR analysis, we may be able to obtain new series of potent MDM2 and/or MDMX inhibitors in the near future.

The aim of this project was not only to obtain potent MDM2/MDMX inhibitors, but also to learn from the combination of technologies such as *in silico* screen and binding mode prediction, biochemistry, cellular biology, synthetic chemistry, crystallography, animal model design, which have been carried out within the DePPICT project. Everyone who had the opportunity to be involved will have gained enormous knowledge from the international collaboration.

5.4.2 DePPICT compound SEN0040028 binding mode prediction

One interesting hit compound SEN0040028 was identified from the screened batch one compounds with above 50% inhibition activity for both MDM2/p53 and MDMX/p53 interaction at the concentration lower than 10 μ M. As a result, the computer-predicted binding mode of this compound with MDM2 and MDMX was investigated to gain insight into the binding groove difference between these two proteins and to obtain some ideas about the potential further development of this class of MDMX/p53 antagonist.

The energy-minimized 3D structure of SEN0040028 was produced by using Chemdraw 3D and by using PyMOL software ([DeLano, 2002](#)). A 3D docking structure was built,

and a potential binding mode of the compound with both MDM2 (1YCR) and MDMX (3DAB) via manual docking was generated (Figure 5. 26).

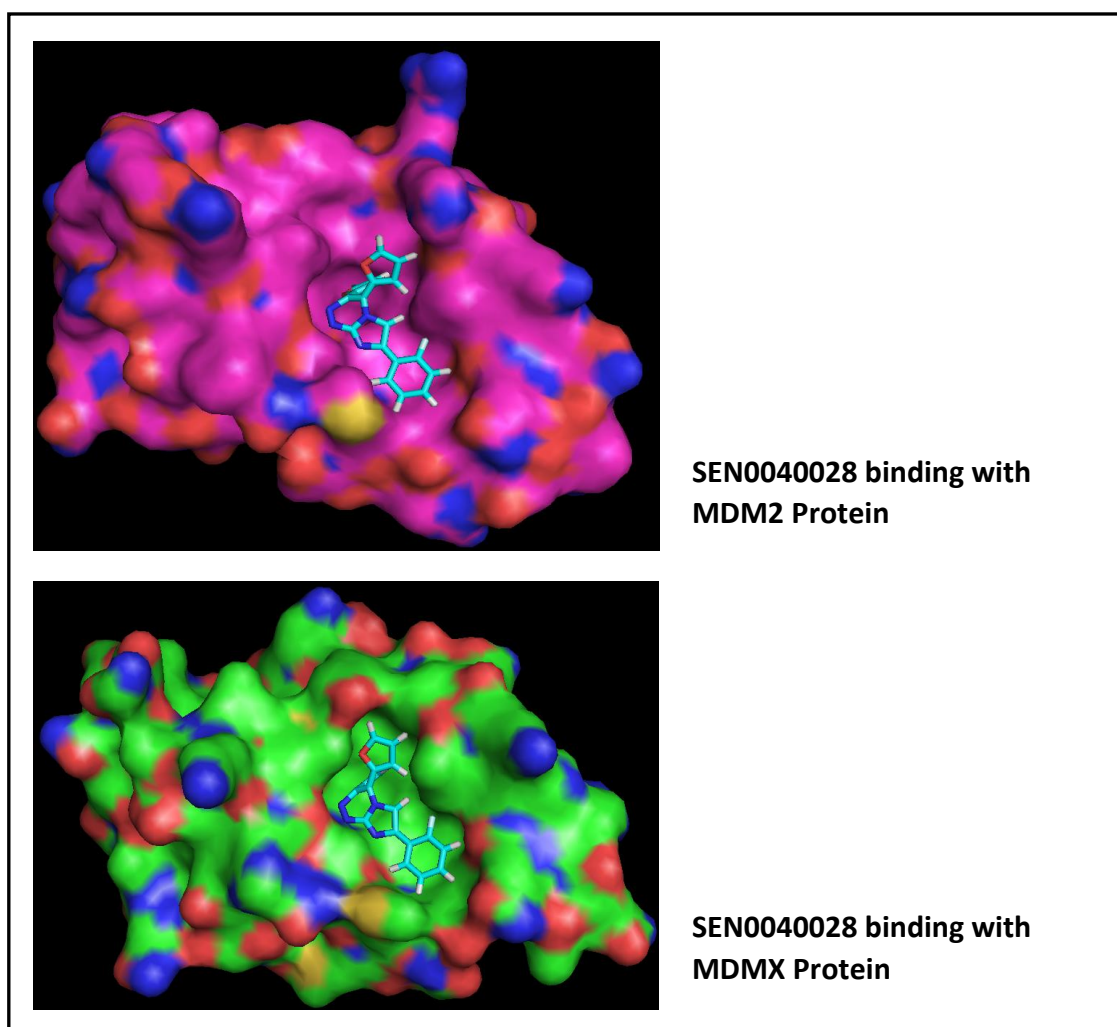


Figure 5. 26 Comparisons of predicted binding mode of SEN0040028 binding with MDM2 and MDMX by manual docking.

As can be seen in Figure 5. 26, SEN0040028 can fit into both the MDM2 and MDMX grooves. In the predicted binding mode, one of its furan rings can occupy the Leu26 binding pocket and the other stretches into the Trp23 binding pocket, with the 4-fluorophenyl side-chain covering the Phe19 binding pocket; furthermore, the

imidazo[2,1-c][1,2,4]triazine scaffold in the middle may also contribute to the binding with some H-bond donor effects.

As a compound with a molecular weight of only 346.31, the 7.3 μM IC_{50} values against MDM2 and 8.6 μM against MDMX is very encouraging.

5.4.3 Cellular evaluation of SEN0040028 and potential drug design direction

After passing the quality control analysis, the cellular activity of SEN0040028 was tested. However, no cellular activity in NGP cells was detected by using this compound at quite high concentrations (up to 50 μM), although both Nutlin-3 and MI-63 positive controls have shown marked cellular effects. Moreover, yellowish crystal-like compound clusters were observed in tissue culture medium contain 50 μM SEN0040028, which indicated that the compound was precipitating in culture medium due to poor aqueous solubility.

However, a possible way to overcome this limitation is to connect a hydrophilic side-chain on the imidazo[2,1-c][1,2,4]triazine scaffold, which may result in some higher potency MDM2/MDMX antagonists with better solubility in tissue culture medium, as has been shown in the development of the isoindolin-1-one scaffold MDM2/p53 antagonists (Chapter 3 and 4).

5.4.4 The possible reason for marked negative percentage inhibition values in the binding assay

Within the screening results, we have observed frequent marked negative percentage inhibition values, and some of them became even more negative when the compound concentration was increased.

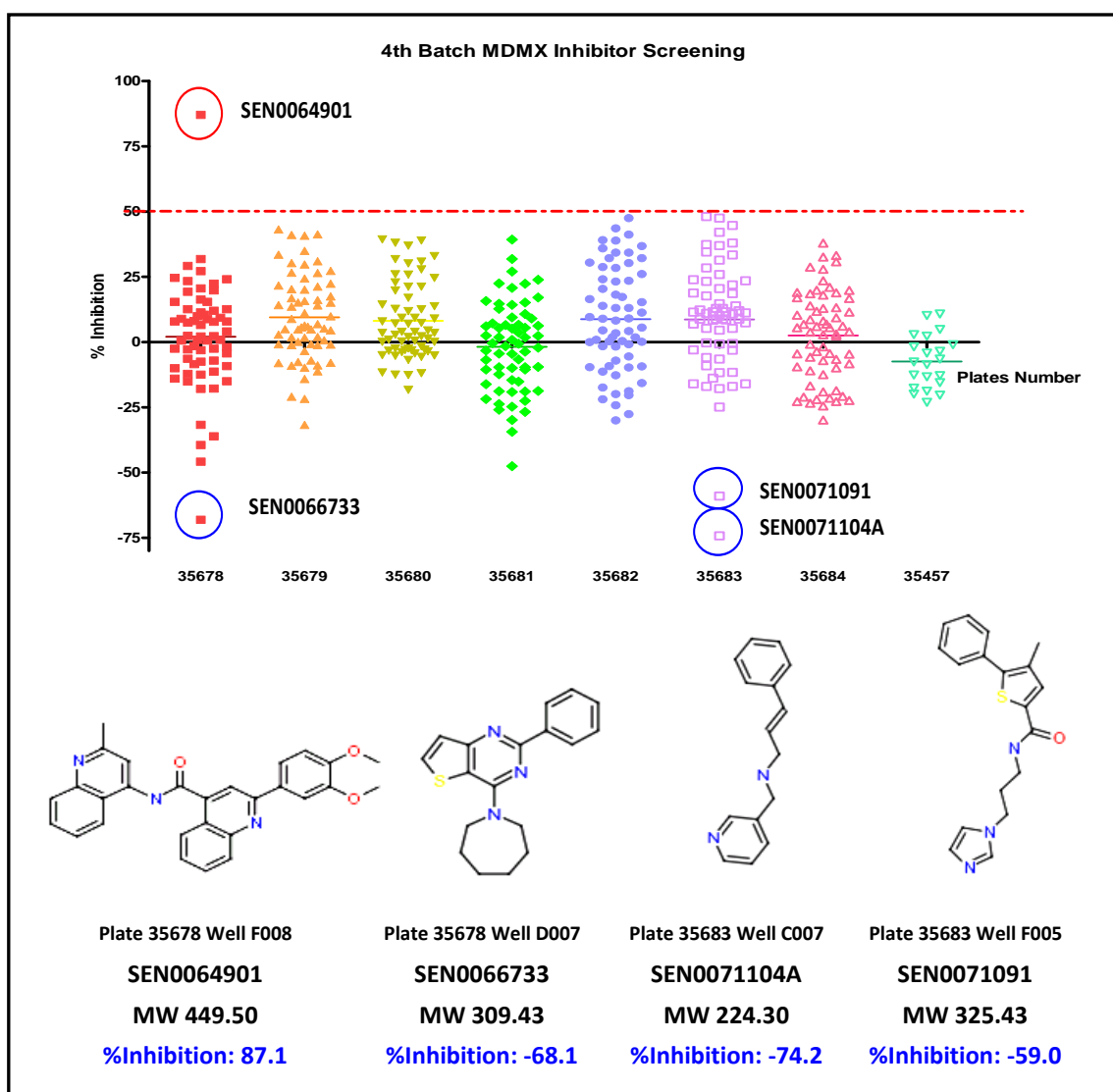


Figure 5. 27 Example of DePPICT compounds screening results showing lower than -50% MDMX inhibition values and their related compounds structures.

For example, in [Figure 5. 27](#), one compound SEN0064901 showed above 85% inhibition potency, however, another compound (SEN0066733) within the same plate showed -68% inhibition value, and there were another two compounds (SEN0071091 and SEN0071104A) which also showed <-50% inhibition values. These three compounds shared the properties when compared to the potent one (SEN0064901): much lower molecular weight (~300), smaller scaffold and more lipophilic.

Nevertheless, they might not be mischosen compounds through the virtual screening procedure, but may represent compounds that have a high binding affinity with MDMX proteins. As we have seen from their structure, the only problem with these compounds is that they are all very small lipophilic molecules, as a result, they may be able to form a 'bridge' between the MDMX/MDM2 binding groove and p53 peptide, which could contribute to their binding.

This hypothesis may open up a potential drug design direction to turn these negative potency compounds into high potency antagonists, i.e. based on their computer generated binding mode, one could add a hydrophilic side-chain opposite to their binding side. Such a side chain, would solve the water solubility problem and potentially be able to break the 'bridge' effect. In addition, this side-chain might act as Leu22 does in the p53 peptide and contribute to an enhancement of the binding affinity.

5.4.5 Pyrrole scaffold compounds as a potent MDM2 and MDMX inhibitor lead compounds

As has been shown in section 5.2.4, the pyrrole scaffold compounds were interesting due to their high potency as MDM2 inhibitors and acceptable activity against MDMX.

However, the solubility of this series of compounds was very poor, which is a hindrance for them to become a drug candidate. As a result, further development should be focused on solving the solubility problem and also building up a reliable structure-activity relationship map. On the other hand, an attempt to generate a co-crystal structure of pyrrole scaffold compounds with either MDM2 or MDMX protein, or predict their binding mode by using virtual docking might be worth trying. All information obtained by these approaches together with the research based on an optimized peptide, will contribute to not only the further development of these compounds, but also a better understanding of the MDM2/MDMX binding groove 'appetite'.

Chapter Six

Generation and Characterization of MDM2/p53 Inhibitor Resistant Cell Lines

6.1 Introduction

So far, several potent and selective small-molecular MDM2 antagonists have been identified, e.g. Nutlin-3 (77) and MI-63 (13, 133). Studies with these compounds have strengthened the concept that selective, non-genotoxic p53 activation might represent an alternative to current cytotoxic chemotherapy (68, 188-189).

The entry of these agents into clinical trials (189) raises the question of drug resistance effects that may lead to relapse.

This chapter describes our research into the potential for drug resistance against p53-MDM2 binding antagonists in order to understand any underlying mechanisms that would inform potential therapeutic strategies to circumvent this. We have established a series of clonal variants resistant to Nutlin-3 and MI-63 from NGP neuroblastoma and SJSA-1 osteosarcoma parental cell lines, which contain wild type p53 with the transcriptional activity suppressed by amplified and over-expressed MDM2. The drug resistance phenotypes of these clones were evaluated by SRB growth inhibition assay, western blotting for activation of p53 and downstream mediators of p53 dependent growth inhibition and cytotoxicity, as well as cell cycle and caspase-3/7 activation analysis. DNA sequence analysis was used for p53

mutation detection and a FISH assay was also conducted to explore possible resistance mechanisms involving allelic loss of the *p53* gene.

6.2 Overview of resistant cell line selection and characterization

The NGP human neuroblastoma and SJSA-1 osteosarcoma cell lines were used for selection of cell clones resistant to MDM2-p53 antagonists. They both contain wild type *p53* genes with the p53 transcriptional transactivation activity suppressed by over-expressed MDM2 as a result of gene amplification. In addition, the NGP cells also express MDMX, which contributes to the negative regulation of p53.

Based on the potencies of Nutlin-3 and MI-63 evaluated in the ELISA and their GI_{50} value for growth inhibition of NGP and SJSA-1 parental cell lines, various drug concentrations were applied to select for resistant cell clones. NGP and SJSA-1 cell lines were exposed to increasing concentrations of Nutlin-3 (3- 40 μ M) and MI-63 (1-6 μ M), respectively. Single cell clones were isolated with cloning cylinders and the colonies expanded by growth in fresh culture medium containing the original selective concentrations of MDM2 antagonists, which was refreshed weekly. Stage one resistant cell clones were obtained after 60 days drug treatment by using relatively low concentrations (for SJSA-1, 1 μ M MI-63 or 3 μ M Nutlin-3; for NGP, 3 μ M MI-63 or 5 μ M Nutlin-3) ([Figure 6. 1](#)).

The derived resistant clones were named by starting with the parental cell line's initial, followed by the initial of the antagonist used for generating the cell clone and

then the drug concentration, then the 'R' designation to indicate a 'Resistant clone', and ending with the clone number. For example, S_M1R1, means resistant clone 1, generated from the SJSA-1 cell line by using 1 μ M MI-63; N_N5R1, means resistant clone 1 generated from the NGP cell line by using 5 μ M Nutlin-3. Altogether, there were 3 SJSA-1 resistant cell clones obtained from MI-63 treatment, 5 SJSA-1 resistant cell clones obtained from Nutlin-3 treatment; for NGP Resistant clones, there were 4 clones obtained from MI-63 treatment and only one clone from Nutlin-3 treatment.

The images in [Figure 6. 1](#) show that some cells survived and were growing in the continued presence of Nutlin-3 or MI-63. After analysing the first set of selected clones by SRB assay, western blotting and DNA sequencing, treatment was increased by using higher drug concentrations based on the GI₅₀ evaluation results. Based on DNA sequencing results, which in SJSA-1 resistant cell clones showed heterozygous point mutation in the two MI-63 induced resistant cell clones and the Nutlin-3 induced resistant cell clone S_N3R2, and homozygous point mutation in S_N3R1, and all NGP resistant cell clones showed heterozygous point mutation; S_M1R1 and S_N3R1 were chosen for further selection of SJSA-1 resistant clones, and N_M3R2, N_M3R4 and N_N5R1 were chosen for further selection of NGP resistant clones. After another 30 days drug treatment, two SJSA-1 resistant cell clones were obtained from MI-63 treatment and four from Nutlin-3 treatment; two NGP resistant cell clones obtained from MI-63 treatment and two from Nutlin-3 treatment.

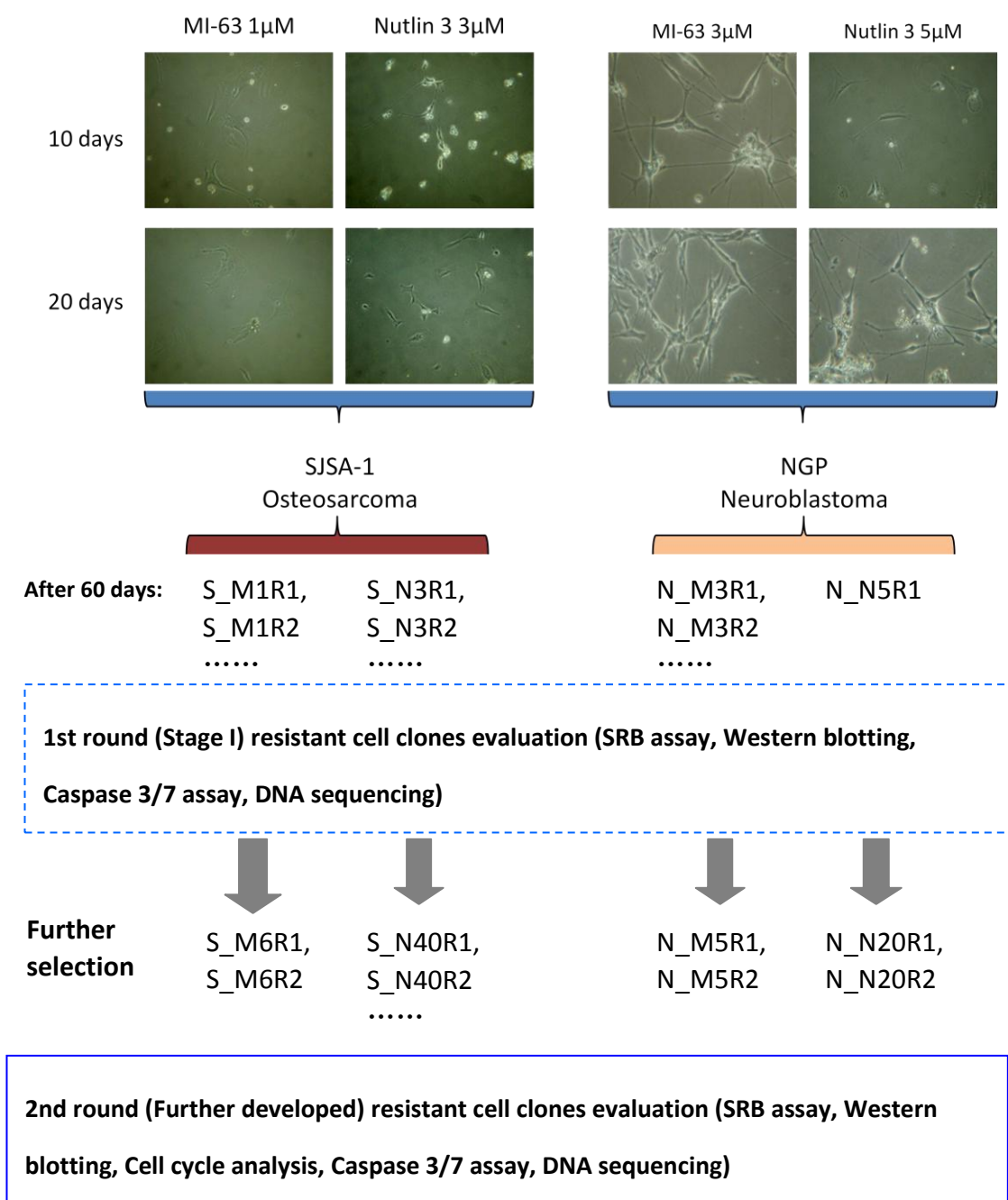


Figure 6. 1 Selection of SJSA-1 and NGP resistant cell clones.

6.3 Characterization Stage I selected resistant cell lines

6.3.1 Resistant potency evaluation

To compare the sensitivity of the selected resistant clones to the parental cell lines and investigate cross resistance between Nutlin-3 and MI-63 selection, the GI_{50} values for Nutlin-3 and MI-63 induced cell growth inhibition were determined by Sulphorhodamine B (SRB) assay, as described previously (Section 2.4). Briefly, adherent exponentially growing cells were seeded into 96-well plates at 2×10^3 cells/well for SJSA-1 parental and resistant cell clones and 5×10^3 cells/well for NGP parental and resistant cell clones. After 24 hours incubation at 37°C, the medium was replaced with fresh medium containing MDM2 antagonists at appropriate ranges of drug concentrations in 1% DMSO. After a drug exposure period of 72 hours (equivalent to three cell population doubling times), the cells were fixed by adding trichloroacetic acid (TCA) to a final concentration of 10% into each well, left in 4°C for 24 hours, washed with water, air dried, and then stained with SRB solution. The absorbance per well was measured, the percentage cell density curves were generated for comparison and fifty percent cell growth inhibition values (GI_{50}) determination after calculation. By using parental cell line GI_{50} s, we have also calculated the GI_{50} ratios of resistant cell clones to that of their parental lines as a measure of fold-resistance.

[Figure 6. 2](#) and [Figure 6. 3](#) show the differences in the cellular growth inhibition response between the parental and resistant cell clones, and the stage I resistant cell

clones established by using either MI-63 or Nutlin-3 for both the SJSA-1 (tested by Dr Xiaohong Lu) and NGP cell lines. The cross-resistance effects are also shown.

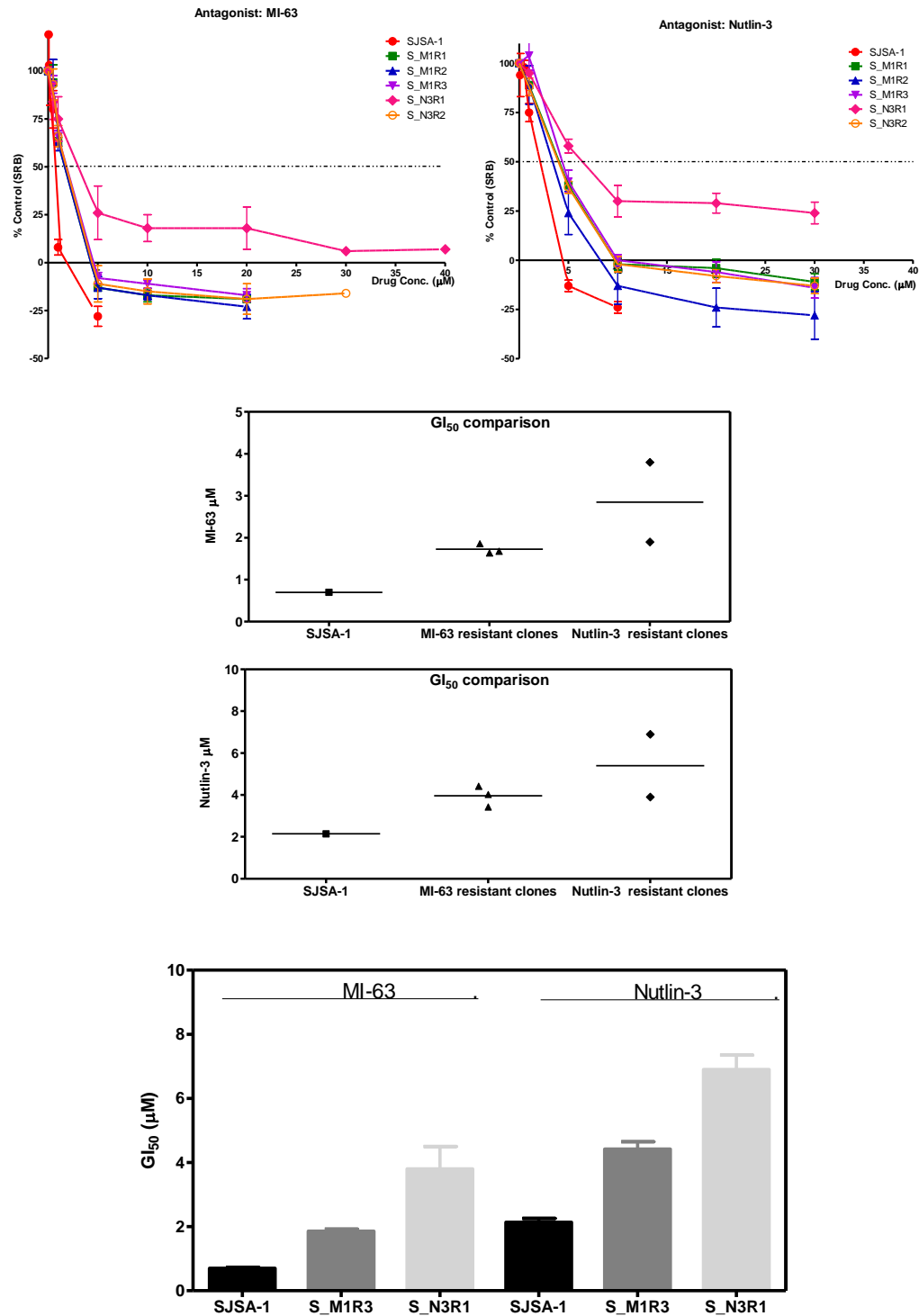


Figure 6. 2 SJSA-1 parental and stage I resistant cell clone GI₅₀ Comparison.

(Tested by Dr Xiaohong Lu)

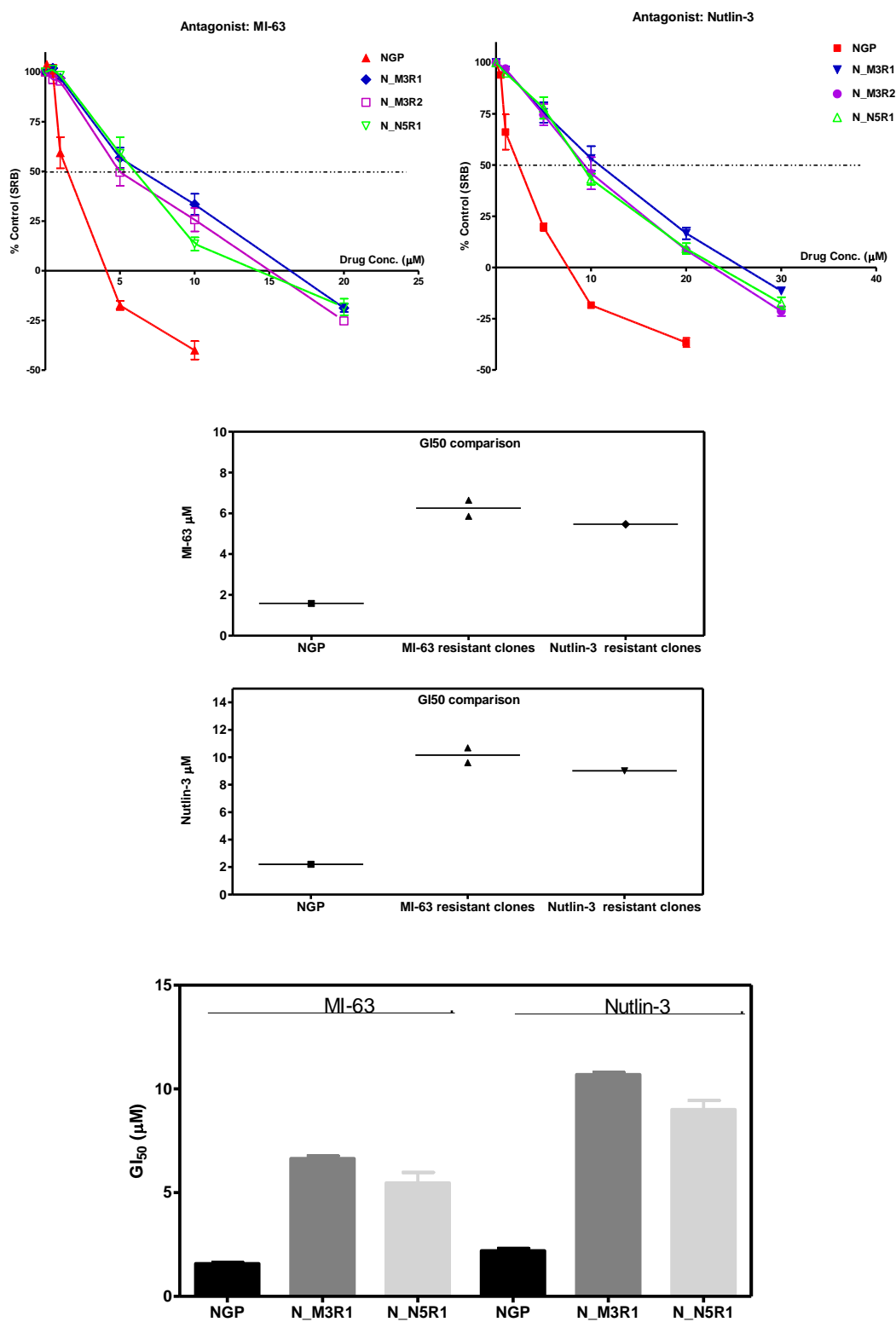


Figure 6.3 NGP parental and stage I resistant cell clone GI_{50} Comparison.

The potency differences between the two antagonists was reflected not only by the SJSA-1 and NGP parental cell lines, but also by their resistant cell clones.

The GI₅₀ results and the fold-changes in them between parental and resistant cell clones for both of the two cell lines are shown in [Table 6. 1](#). In all cases, the selected clones showed increase in GI₅₀. Interestingly, the Nutlin-3 generated SJSA-1 resistant cell clone S_N3R1 showed a greater level of resistance to MI-63 and Nutlin-3 than all the MI-63 generated SJSA-1 resistant cell clones. However, the Nutlin-3 generated NGP resistant cell clone N_N5R1 showed slightly weaker resistance than the two MI-63 generated NGP resistant cell clones.

Table 6. 1 GI₅₀ comparison of stage I resistant clones with their parental cell lines

Cell Clones	MI-63_GI50	Folds change	Nutlin-3_GI50	Folds change
SJSA-1	0.70 ± 0.05 µM (n=3)	1	2.1 ± 0.2 µM (n=3)	1
S_M1R1	1.68 ± 0.09 µM (n=3)	2.4	4.0 ± 0.1 µM (n=3)	1.9
S_M1R2	1.64 ± 0.15 µM (n=3)	2.34	3.4 ± 0.4 µM (n=3)	1.6
S_M1R3	1.86 ± 0.11 µM (n=3)	2.66	4.4 ± 0.4 µM (n=3)	2.1
S_N3R1	3.8 ± 1.4 µM (n=4)	5.43	6.9 ± 0.9 µM (n=4)	3.3
S_N3R2	1.9 ± 0.3 µM (n=4)	2.71	3.9 ± 0.3 µM (n=4)	1.9
NGP	1.58 ± 0.21 µM (n=3)	1	2.20 ± 0.39 µM (n=3)	1
N_M3R1	6.65 ± 1.01 µM (n=3)	4.21	10.69 ± 1.29 µM (n=3)	4.86
N_M3R4	5.86 ± 0.98 µM (n=3)	3.71	9.62 ± 1.23 µM (n=3)	4.37
N_N5R1	5.47 ± 0.51 µM (n=3)	3.46	9.01 ± 0.44 µM (n=3)	4.09

6.3.2 Measurement of p53, MDM2 and p21^{WAF1} expression.

To investigate whether the resistance of selected SJSA-1 clones was reflected in the induction of p53 and its downstream targets MDM2 and p21^{WAF1} protein, SJSA-1 resistant cell clones S_M1R1 and S_N3R1 were selected to compare with the SJSA-1 parental cell line. After MDM2 antagonist treatment, the expression of these proteins was determined using total cell extracts prepared from untreated control or cells treated with DMSO, 5 μ M MI-63 or Nutlin-3 for 6 hours and α -tubulin in each sample was also evaluated as a loading and transfer control (Figure 6. 4).

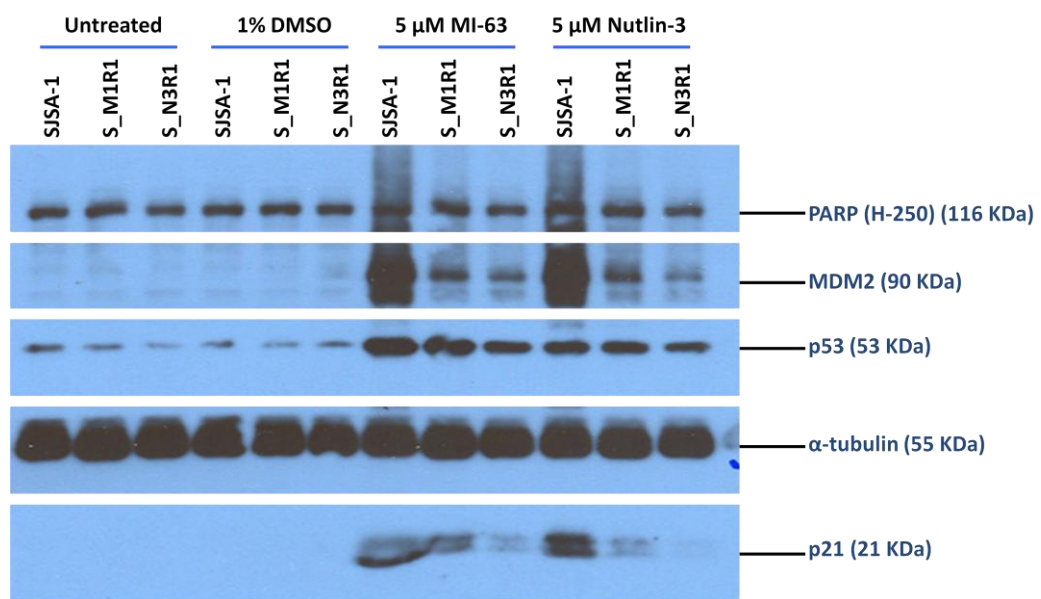


Figure 6. 4 Western blot showing p53 pathway activation by Nutlin-3 and MI-63 for the SJSA-1 parental cell line and reduced activation in stage I resistant cell clones.

The western blotting results for the SJSA-1 parental cell line and stage I resistant clones ([Figure 6. 4](#)) indicated that both MI-63 and Nutlin-3 can disrupt the interaction between MDM2 and p53 protein and release the p53 transactivation domain from MDM2 binding in both the SJSA-1 parental cell line and its resistant cell clones, resulting in p53 accumulation and transcriptional transactivation of MDM2 and p21, when compared to untreated or DMSO only treated cell samples. However, the band densities of MDM2 and p21 proteins in resistant clones were lower than parental clones indicating an attenuated p53 activation, especially in the Nutlin-3 generated resistant cell clone S_N3R1, which reflected the SRB result in [Figure 6. 2](#) and [Table 6.](#)

1. The cross resistance effect is also evident in the western blot result.

To investigate whether the resistance effect in NGP resistant clones was also reflected in the induction of p53 and its downstream target MDM2 and p21^{WAF1} protein, NGP resistant cell clones N_M3R1, N_M3R4 and S_N5R1 were chosen to compare with the NGP parental cell line. After MDM2 antagonist treatment, the expression of these proteins together with MDMX protein were determined using total cell extracts prepared from untreated control or cells treated with DMSO, 5 μ M MI-63 or Nutlin-3 for 4 hours β -actin in each sample was also evaluated as loading control ([Figure 6. 5](#)).

The western blotting results for the NGP series cell clones ([Figure 6. 5](#)) also indicated that both MI-63 and Nutlin-3 can disrupt the interaction between MDM2 and p53 protein and release p53 transactivation domain from MDM2 binding in both NGP parental cell line and its resistant cell clones, and there were no marked difference in p53 levels between parental and resistant clones after two antagonists treatment.

However, attenuated MDM2 and especially p21 expression were observed in resistant clones after treatment with the two antagonists.

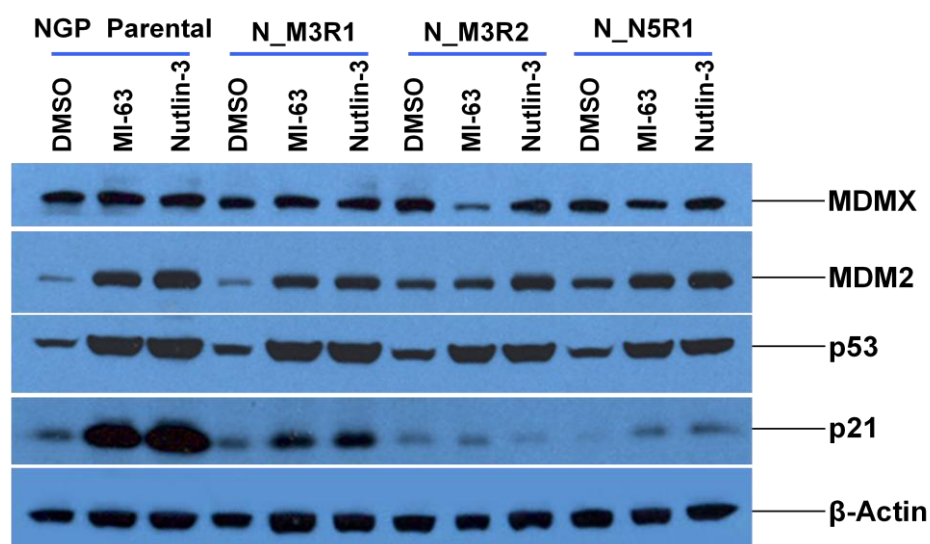


Figure 6. 5 Western blot comparing p53 activation by Nutlin-3 and MI-63 in the NGP parental cell and stage I resistant cell clones.

On the other hand, interestingly, the MDMX expression was quite stable in both parental and resistant NGP cell clones, with or without the treatment of the MDM2 antagonists.

Furthermore, cross resistant effects were evident in all three cell clones established by using different antagonists, which was consistent with the SRB assay results.

6.3.3 DNA Sequencing of p53 in Stage I Resistant Cell Clones

Since both the growth inhibition and western blotting analysis experiments showed marked resistance effects and attenuation of p53 pathway activation in the cell clones developed from both SISA-1 and NGP cell lines, the functional inactivation of p53 by mutation was investigated.

To determine the p53 status of the resistant cell clones, total DNA was extracted from each cell clone for the analysis. PCR products of Exons 4 to 9 that encode the DNA binding domain of p53 were sequenced. We analyzed the sequencing results of all PCR products produced by using primers (gifts from Dr Claire Hutton and Dr Jennifer Jackson) for the coding strand first and compared them with both p53 full sequence and relative to PCR products of the parental cell line DNA samples, when sequence differences were detected, they were confirmed by analyzing sequences from the opposite strand using the antisense primers.

In all SJSA-1 resistant cell clones only one missense point mutation was detected, which was present within all SJSA-1 resistant cell clones established by using both of the two antagonists. The mutation was at codon 285, changing GAG to AAG, which corresponds to an amino acid change from Glutamic acid to Lysine ([Figure 6. 6](#), [Figure 6. 7](#) & [Figure 6. 8](#)). This amino acid lies within the codon 280-286 region which forms an alpha-helix that docks with the major groove of DNA ([Figure 1. 3](#) in Section 1.1.1.2). Interestingly, the sequencing trace images showed that in resistant cell clones S_M1R1, S_M1R2 and S_N3R2, the point mutation peaks were the same height as the non-mutant peaks; however, both the SN and ASN primer PCR products of S_N3R1 showed almost pure mutation peaks, suggesting a homozygous mutation. This observation showed an interesting relationship to the GI₅₀ evaluation results shown in [Table 6. 1](#), in which the S_N3R1 resistant cell clone showed higher resistance compared with all the other SJSA-1 resistant cell clones.

In all three tested NGP resistant cell clones (N_M3R1, N_M3R4 and N_N5R1) one missense point mutation was detected ([Figure 6. 9](#) & [Figure 6. 10](#)). This point mutation was detected at codon 152 in Exon 5, changing CCG to ACG, which corresponds to an amino acid change from proline to threonine. The sequencing trace images showed that in all analyzed NGP resistant cell clones, the point mutation peaks were nearly the same height as the non-mutant peaks. This observation was also consistent with the GI₅₀ evaluation results showed in [Table 6. 1](#), in which all selected cell clones showed similar levels of resistance.

Cell Clones		Sequencing results of PCR Products produced from sense primers						
SJSA-1	S_JSA-1	v14500	v14510	v14520	v14530	v14540	v14550	v14560
		TGTCCTGGGAGAGACCGGCGCACAGAGGAAGAGAATCTCCGCAAGAAAGGGGAGCCTCACCACGAGCTG	TGTCCTGGGAGAGACCGGCGCACAGAGGAAGAGAATCTCCGCAAGAAAGGGGAGCCTCACCACGAGCTG	TGTCCTGGGAGAGACCGGCGCACAGAGGAAGAGAATCTCCGCAAGAAAGGGGAGCCTCACCACGAGCTG	TGTCCTGGGAGAGACCGGCGCACAGAGGAAGAGAATCTCCGCAAGAAAGGGGAGCCTCACCACGAGCTG	TGTCCTGGGAGAGACCGGCGCACAGAGGAAGAGAATCTCCGCAAGAAAGGGGAGCCTCACCACGAGCTG	TGTCCTGGGAGAGACCGGCGCACAGAGGAAGAGAATCTCCGCAAGAAAGGGGAGCCTCACCACGAGCTG	TGTCCTGGGAGAGACCGGCGCACAGAGGAAGAGAATCTCCGCAAGAAAGGGGAGCCTCACCACGAGCTG
S_M1R1	S_M1R1	v14500	v14510	v14520	v14530	v14540	v14550	v14560
		TGTCCTGGGAGAGACCGGCGCACAGAGGAAGAGAATCTCCGCAAGAAAGGGGAGCCTCACCACGAGCTG	TGTCCTGGGAGAGACCGGCGCACAGAGGAAGAGAATCTCCGCAAGAAAGGGGAGCCTCACCACGAGCTG	TGTCCTGGGAGAGACCGGCGCACAGAGGAAGAGAATCTCCGCAAGAAAGGGGAGCCTCACCACGAGCTG	TGTCCTGGGAGAGACCGGCGCACAGAGGAAGAGAATCTCCGCAAGAAAGGGGAGCCTCACCACGAGCTG	TGTCCTGGGAGAGACCGGCGCACAGAGGAAGAGAATCTCCGCAAGAAAGGGGAGCCTCACCACGAGCTG	TGTCCTGGGAGAGACCGGCGCACAGAGGAAGAGAATCTCCGCAAGAAAGGGGAGCCTCACCACGAGCTG	TGTCCTGGGAGAGACCGGCGCACAGAGGAAGAGAATCTCCGCAAGAAAGGGGAGCCTCACCACGAGCTG
S_M1R2	S_M1R2	v14500	v14510	v14520	v14530	v14540	v14550	v14560
		TGTCCTGGGAGAGACCGGCGCACAGAGGAAGAGAATCTCCGCAAGAAAGGGGAGCCTCACCACGAGCTG	TGTCCTGGGAGAGACCGGCGCACAGAGGAAGAGAATCTCCGCAAGAAAGGGGAGCCTCACCACGAGCTG	TGTCCTGGGAGAGACCGGCGCACAGAGGAAGAGAATCTCCGCAAGAAAGGGGAGCCTCACCACGAGCTG	TGTCCTGGGAGAGACCGGCGCACAGAGGAAGAGAATCTCCGCAAGAAAGGGGAGCCTCACCACGAGCTG	TGTCCTGGGAGAGACCGGCGCACAGAGGAAGAGAATCTCCGCAAGAAAGGGGAGCCTCACCACGAGCTG	TGTCCTGGGAGAGACCGGCGCACAGAGGAAGAGAATCTCCGCAAGAAAGGGGAGCCTCACCACGAGCTG	TGTCCTGGGAGAGACCGGCGCACAGAGGAAGAGAATCTCCGCAAGAAAGGGGAGCCTCACCACGAGCTG
S_N3R1	S_N3R1	v14500	v14510	v14520	v14530	v14540	v14550	v14560
		TGTCCTGGGAGAGACCGGCGCACAGAGGAAGAGAATCTCCGCAAGAAAGGGGAGCCTCACCACGAGCTG	TGTCCTGGGAGAGACCGGCGCACAGAGGAAGAGAATCTCCGCAAGAAAGGGGAGCCTCACCACGAGCTG	TGTCCTGGGAGAGACCGGCGCACAGAGGAAGAGAATCTCCGCAAGAAAGGGGAGCCTCACCACGAGCTG	TGTCCTGGGAGAGACCGGCGCACAGAGGAAGAGAATCTCCGCAAGAAAGGGGAGCCTCACCACGAGCTG	TGTCCTGGGAGAGACCGGCGCACAGAGGAAGAGAATCTCCGCAAGAAAGGGGAGCCTCACCACGAGCTG	TGTCCTGGGAGAGACCGGCGCACAGAGGAAGAGAATCTCCGCAAGAAAGGGGAGCCTCACCACGAGCTG	TGTCCTGGGAGAGACCGGCGCACAGAGGAAGAGAATCTCCGCAAGAAAGGGGAGCCTCACCACGAGCTG
S_N3R2	S_N3R2	v14500	v14510	v14520	v14530	v14540	v14550	v14560
		TGTCCTGGGAGAGACCGGCGCACAGAGGAAGAGAATCTCCGCAAGAAAGGGGAGCCTCACCACGAGCTG	TGTCCTGGGAGAGACCGGCGCACAGAGGAAGAGAATCTCCGCAAGAAAGGGGAGCCTCACCACGAGCTG	TGTCCTGGGAGAGACCGGCGCACAGAGGAAGAGAATCTCCGCAAGAAAGGGGAGCCTCACCACGAGCTG	TGTCCTGGGAGAGACCGGCGCACAGAGGAAGAGAATCTCCGCAAGAAAGGGGAGCCTCACCACGAGCTG	TGTCCTGGGAGAGACCGGCGCACAGAGGAAGAGAATCTCCGCAAGAAAGGGGAGCCTCACCACGAGCTG	TGTCCTGGGAGAGACCGGCGCACAGAGGAAGAGAATCTCCGCAAGAAAGGGGAGCCTCACCACGAGCTG	TGTCCTGGGAGAGACCGGCGCACAGAGGAAGAGAATCTCCGCAAGAAAGGGGAGCCTCACCACGAGCTG

Figure 6. 6 SJSA-1 parental and resistant cell clones DNA sequencing alignment results of Exon 8 SN primers PCR products showed similar 14522 genomic DNA position point mutation.

Cell Clones		Sequencing results of PCR Products produced from anti-sense primers						
SJSA-1	S_JSA-1	v14560	v14550	v14540	v14530	v14520	v14510	v14500
		TCGTGGTGAGGCTCCCCTTTCTTGCGGAGATTCTCTTCCTCTGTGCGCCGGTCTCTCCCAGGACAGGCAC	TCGTGGTGAGGCTCCCCTTTCTTGCGGAGATTCTCTTCCTCTGTGCGCCGGTCTCTCCCAGGACAGGCAC	TCGTGGTGAGGCTCCCCTTTCTTGCGGAGATTCTCTTCCTCTGTGCGCCGGTCTCTCCCAGGACAGGCAC	TCGTGGTGAGGCTCCCCTTTCTTGCGGAGATTCTCTTCCTCTGTGCGCCGGTCTCTCCCAGGACAGGCAC	TCGTGGTGAGGCTCCCCTTTCTTGCGGAGATTCTCTTCCTCTGTGCGCCGGTCTCTCCCAGGACAGGCAC	TCGTGGTGAGGCTCCCCTTTCTTGCGGAGATTCTCTTCCTCTGTGCGCCGGTCTCTCCCAGGACAGGCAC	TCGTGGTGAGGCTCCCCTTTCTTGCGGAGATTCTCTTCCTCTGTGCGCCGGTCTCTCCCAGGACAGGCAC
		^260	^270	^280	^290	^300	^310	^320
S_M1R1	S_M1R1	v14560	v14550	v14540	v14530	v14520	v14510	v14500
		TCGTGGTGAGGCTCCCCTTTCTTGCGGAGATTCTCTTCCTCTGTGCGCCGGTCTCTCCCAGGACAGGCAC	TCGTGGTGAGGCTCCCCTTTCTTGCGGAGATTCTCTTCCTCTGTGCGCCGGTCTCTCCCAGGACAGGCAC	TCGTGGTGAGGCTCCCCTTTCTTGCGGAGATTCTCTTCCTCTGTGCGCCGGTCTCTCCCAGGACAGGCAC	TCGTGGTGAGGCTCCCCTTTCTTGCGGAGATTCTCTTCCTCTGTGCGCCGGTCTCTCCCAGGACAGGCAC	TCGTGGTGAGGCTCCCCTTTCTTGCGGAGATTCTCTTCCTCTGTGCGCCGGTCTCTCCCAGGACAGGCAC	TCGTGGTGAGGCTCCCCTTTCTTGCGGAGATTCTCTTCCTCTGTGCGCCGGTCTCTCCCAGGACAGGCAC	TCGTGGTGAGGCTCCCCTTTCTTGCGGAGATTCTCTTCCTCTGTGCGCCGGTCTCTCCCAGGACAGGCAC
		^260	^270	^280	^290	^300	^310	^320
S_M1R2	S_M1R2	v14560	v14550	v14540	v14530	v14520	v14510	v14500
		TCGTGGTGAGGCTCCCCTTTCTTGCGGAGATTCTCTTCCTCTGTGCGCCGGTCTCTCCCAGGACAGGCAC	TCGTGGTGAGGCTCCCCTTTCTTGCGGAGATTCTCTTCCTCTGTGCGCCGGTCTCTCCCAGGACAGGCAC	TCGTGGTGAGGCTCCCCTTTCTTGCGGAGATTCTCTTCCTCTGTGCGCCGGTCTCTCCCAGGACAGGCAC	TCGTGGTGAGGCTCCCCTTTCTTGCGGAGATTCTCTTCCTCTGTGCGCCGGTCTCTCCCAGGACAGGCAC	TCGTGGTGAGGCTCCCCTTTCTTGCGGAGATTCTCTTCCTCTGTGCGCCGGTCTCTCCCAGGACAGGCAC	TCGTGGTGAGGCTCCCCTTTCTTGCGGAGATTCTCTTCCTCTGTGCGCCGGTCTCTCCCAGGACAGGCAC	TCGTGGTGAGGCTCCCCTTTCTTGCGGAGATTCTCTTCCTCTGTGCGCCGGTCTCTCCCAGGACAGGCAC
		^260	^270	^280	^290	^300	^310	^320
S_N3R1	S_N3R1	v14560	v14550	v14540	v14530	v14520	v14510	v14500
		TCGTGGTGAGGCTCCCCTTTCTTGCGGAGATTCTCTTCCTCTGTGCGCCGGTCTCTCCCAGGACAGGCAC	TCGTGGTGAGGCTCCCCTTTCTTGCGGAGATTCTCTTCCTCTGTGCGCCGGTCTCTCCCAGGACAGGCAC	TCGTGGTGAGGCTCCCCTTTCTTGCGGAGATTCTCTTCCTCTGTGCGCCGGTCTCTCCCAGGACAGGCAC	TCGTGGTGAGGCTCCCCTTTCTTGCGGAGATTCTCTTCCTCTGTGCGCCGGTCTCTCCCAGGACAGGCAC	TCGTGGTGAGGCTCCCCTTTCTTGCGGAGATTCTCTTCCTCTGTGCGCCGGTCTCTCCCAGGACAGGCAC	TCGTGGTGAGGCTCCCCTTTCTTGCGGAGATTCTCTTCCTCTGTGCGCCGGTCTCTCCCAGGACAGGCAC	TCGTGGTGAGGCTCCCCTTTCTTGCGGAGATTCTCTTCCTCTGTGCGCCGGTCTCTCCCAGGACAGGCAC
		^260	^270	^280	^290	^300	^310	^320
S_N3R2	S_N3R2	v14560	v14550	v14540	v14530	v14520	v14510	v14500
		TCGTGGTGAGGCTCCCCTTTCTTGCGGAGATTCTCTTCCTCTGTGCGCCGGTCTCTCCCAGGACAGGCAC	TCGTGGTGAGGCTCCCCTTTCTTGCGGAGATTCTCTTCCTCTGTGCGCCGGTCTCTCCCAGGACAGGCAC	TCGTGGTGAGGCTCCCCTTTCTTGCGGAGATTCTCTTCCTCTGTGCGCCGGTCTCTCCCAGGACAGGCAC	TCGTGGTGAGGCTCCCCTTTCTTGCGGAGATTCTCTTCCTCTGTGCGCCGGTCTCTCCCAGGACAGGCAC	TCGTGGTGAGGCTCCCCTTTCTTGCGGAGATTCTCTTCCTCTGTGCGCCGGTCTCTCCCAGGACAGGCAC	TCGTGGTGAGGCTCCCCTTTCTTGCGGAGATTCTCTTCCTCTGTGCGCCGGTCTCTCCCAGGACAGGCAC	TCGTGGTGAGGCTCCCCTTTCTTGCGGAGATTCTCTTCCTCTGTGCGCCGGTCTCTCCCAGGACAGGCAC
		^260	^270	^280	^290	^300	^310	^320

Figure 6. 7 SJSA-1 parental and resistant cell clones DNA sequencing alignment results of Exon 8 ASN primers PCR products confirming the 14522 p53 genomic DNA point mutation.

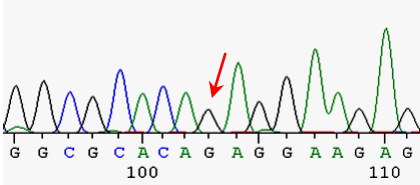
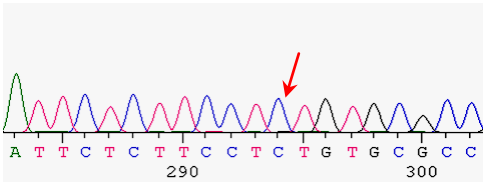
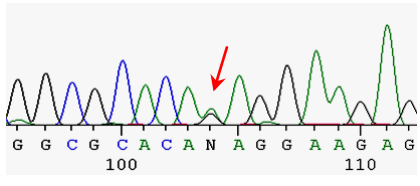
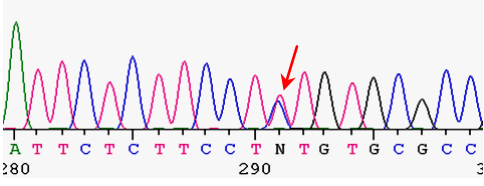
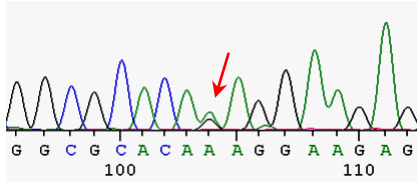
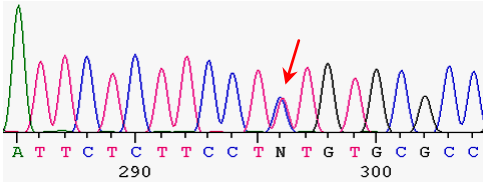
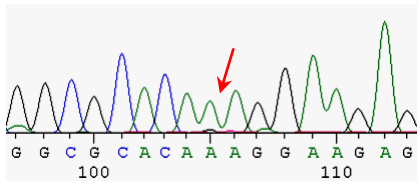
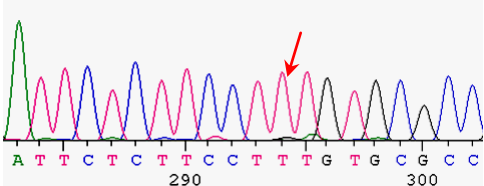
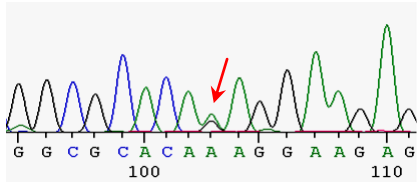
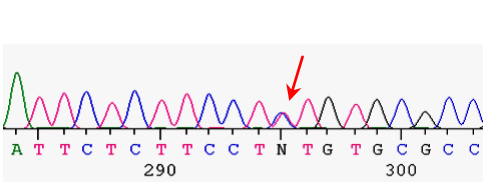
Cell Clones	Sequencing traces of PCR Products of both SN and ASN primers	
	SN Primers products	ASN Primers products
SJSA-1		
S_M1R1		
S_M1R2		
S_N3R1		
S_N3R2		

Figure 6. 8 SJSA-1 parental and resistant cell clones DNA sequencing traces of Exon 8 PCR products confirming the 14522 point mutation corresponding to codon 285, changing GAG to AAG.

Cell Clones

Sequencing results of PCR Products produced from sense primers

	v13110	v13120	v13130	v13140	v13150	v13160	v13170
	GCAGCTGTGGGTTGATTCCACACCCCGCCCGGCACCCGCGTCCGCGCCATGGCCATCTACAAGCAGTC						
NGP	GCAGCTGTGGGTTGATTCCACACCCCGCCCGGCACCCGCGTCCGCGCCATGGCCATCTACAAGCAGTC						
	^80	^90	^100	^110	^120	^130	^140
	v13110	v13120	v13130	v13140	v13150	v13160	v13170
	GCAGCTGTGGGTTGATTCCACACCCCGCCCGGCACCCGCGTCCGCGCCATGGCCATCTACAAGCAGTC						
N_M3R1	GCAGCTGTGGGTTGATTCCACACCCCGCCCGGCACCCGCGTCCGCGCCATGGCCATCTACAAGCAGTC						
	^80	^90	^100	^110	^120	^130	^140
	v13110	v13120	v13130	v13140	v13150	v13160	v13170
	GCAGCTGTGGGTTGATTCCACACCCCGCCCGGCACCCGCGTCCGCGCCATGGCCATCTACAAGCAGTC						
N_M3R4	GCAGCTGTGGGTTGATTCCACACCCCGCCCGGCACCCGCGTCCGCGCCATGGCCATCTACAAGCAGTC						
	^70	^80	^90	^100	^110	^120	^130
	v13110	v13120	v13130	v13140	v13150	v13160	v13170
	GCAGCTGTGGGTTGATTCCACACCCCGCCCGGCACCCGCGTCCGCGCCATGGCCATCTACAAGCAGTC						
N_N5R1	GCAGCTGTGGGTTGATTCCACACCCCGCCCGGCACCCGCGTCCGCGCCATGGCCATCTACAAGCAGTC						
	^80	^90	^100	^110	^120	^130	^140

A
B

Cell Clones

Sequencing of PCR Products produced from anti-sense primers

	v13160	v13150	v13140	v13130	v13120	v13110	v1310
	TGGCCATGGCGCGGACGCGGGTGCCGGGCGGGGGTGTGGAATCAACCCACAGCTGCACAGGGCAGGTC						
NGP	TGGCCATGGCGCGGACGCGGGTGCCGGGCGGGGGTGTGGAATCAACCCACAGCTGCACAGGGCAGGTC						
	^90	^100	^110	^120	^130	^140	^
	v13160	v13150	v13140	v13130	v13120	v13110	v1310
	TGGCCATGGCGCGGACGCGGGTGCCGGGCGGGGGTGTGGAATCAACCCACAGCTGCACAGGGCAGGTC						
N_M3R1	TGGCCATGGCGCGGACGCGGGTGCCGGGCGGGGGTGTGGAATCAACCCACAGCTGCACAGGGCAGGTC						
	^90	^100	^110	^120	^130	^140	^150
	v13160	v13150	v13140	v13130	v13120	v13110	v1310
	TGGCCATGGCGCGGACGCGGGTGCCGGGCGGGGGTGTGGAATCAACCCACAGCTGCACAGGGCAGGTC						
N_M3R4	TGGCCATGGCGCGGACGCGGGTGCCGGGCGGGGGTGTGGAATCAACCCACAGCTGCACAGGGCAGGTC						
	^80	^90	^100	^110	^120	^130	^140
	v13160	v13150	v13140	v13130	v13120	v13110	v1310
	TGGCCATGGCGCGGACGCGGGTGCCGGGCGGGGGTGTGGAATCAACCCACAGCTGCACAGGGCAGGTC						
N_N5R1	TGGCCATGGCGCGGACGCGGGTGCCGGGCGGGGGTGTGGAATCAACCCACAGCTGCACAGGGCAGGTC						
	0	^140	^150	^160	^170	^180	^190

Figure 6. 9 NGP parental and resistant cell clones DNA sequencing results

- (A) DNA sequencing results for Exon 5 SN primers indicated the p53 genomic DNA position 13133 point mutation,
 (B) DNA sequencing for Exon 5 ASN primers confirmed the p53 genomic DNA position 13133 point mutation.

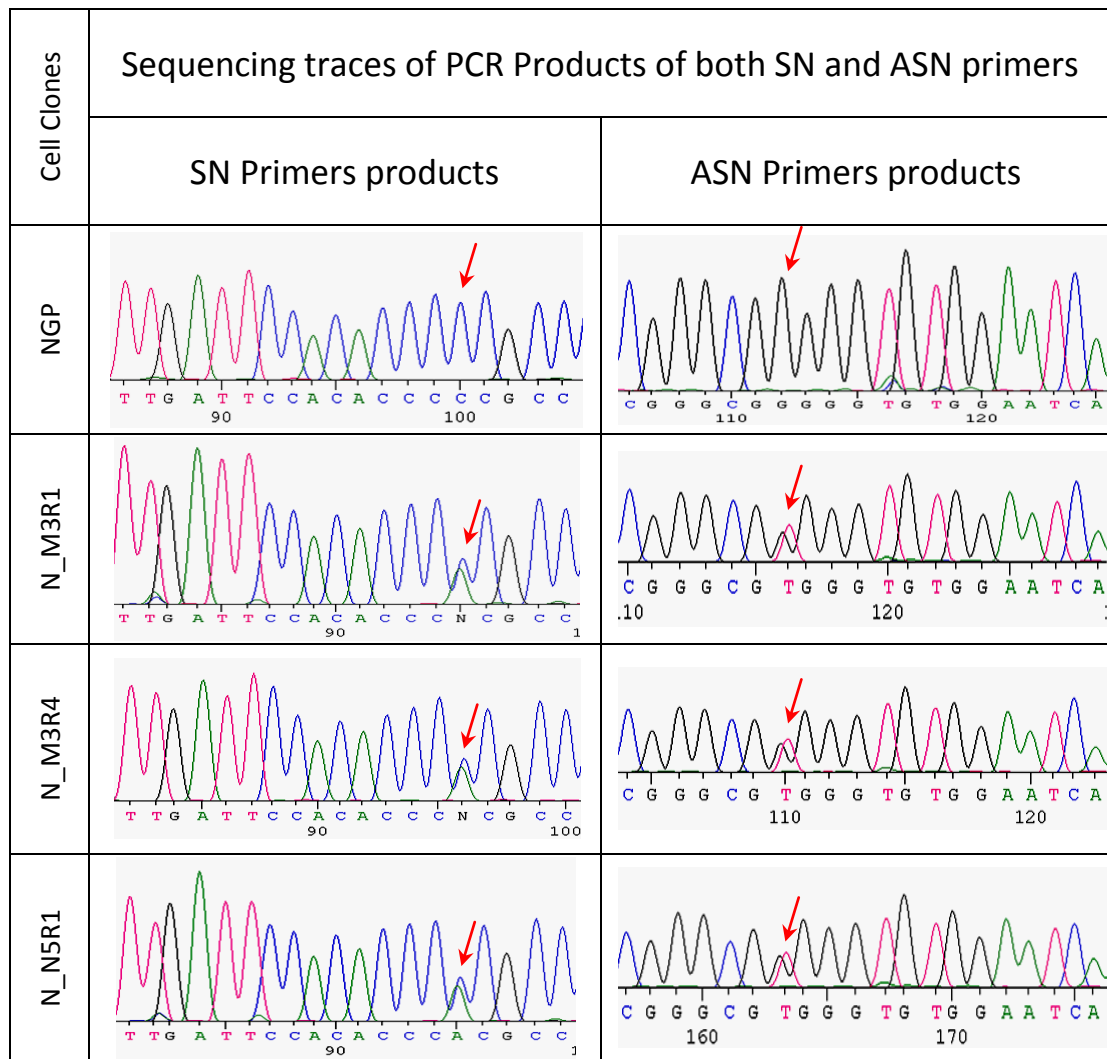


Figure 6. 10 NGP parental and resistant cell clones DNA sequencing traces of Exon 5 PCR products confirmed the 13133 point mutation corresponding to codon 152, changing CCG to ACG.

6.4 Further developed resistant cell clones: characterization and analysis of potential mechanism

After analyzing the DNA sequencing results of stage I resistance clones, further selection under higher concentrations of inhibitors was carried out to test whether resistance levels could be increased. Based on DNA sequencing results, S_M1R1 and S_N3R1 were chosen for further selection of SJSA-1 resistant clones, and N_M3R1, N_M3R4 and N_N5R1 were chosen for further selection of NGP resistant clones. After a further 30 days of drug treatment at the higher concentration, two SJSA-1 resistant cell clones were obtained from MI-63 treatment and four from Nutlin-3 treatment; two NGP resistant cell clones were obtained from MI-63 treatment and two from Nutlin-3 treatment. I have mainly focused on investigating the SJSA-1 series of cell clones ([Figure 6. 1](#)).

6.4.1 Growth curve comparison

After the further development of the resistance clones, the cell population doubling times were evaluated. After 5 passages of the resistant clones in fresh medium without drugs, the growth curves of SJSA-1 parental and resistant clones were determined using the SRB assay.

Briefly, adherent exponentially growing cells were seeded into 96-well plates at a range of initial cell densities from 24,000 to 12 cells/well (with half cell density than the previous row for 12 rows) for SJSA-1 parental and resistant cell clones (S_M6R1 and N_N40R1). After every 24 hours within a period of 9 days, the cells were fixed by

adding trichloroacetic acid (TCA) to a final concentration of 10 % into each well, left in 4°C for above 24 hours, washed with water, air dried, and then stained with SRB solution. The absorbance per well was measured, the cell density curves were generated (Figure 6. 11) for comparison.

The doubling times (dT) were calculated from the seeding densities at 6000, 3000 and 1500 cells/well, over the time period when the cells were growing exponentially (approximately 70 % confluent) using the equation:

$$dT_{\text{Cell line}_X} = \ln 2 / k_{\text{Cell line}_X},$$

where k is the growth rate constant, and the mean values and standard errors for the doubling time of each cell line were calculated based on the three selected seeding densities.

The results indicated that both SJSA-1 parental and resistant cell population doubling times were quite similar ($dT_{\text{SJSA-1}} = 32.5 \pm 1.6$ h, $dT_{\text{S_M6R1}} = 35.7 \pm 2.0$ h and $dT_{\text{S_N40R1}} = 33.5 \pm 2.5$ h) within appropriate cell densities.

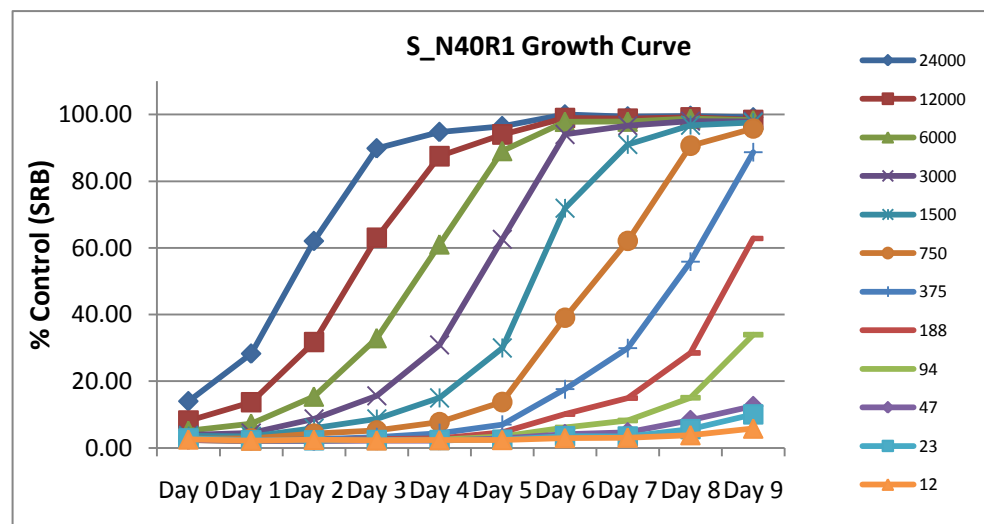
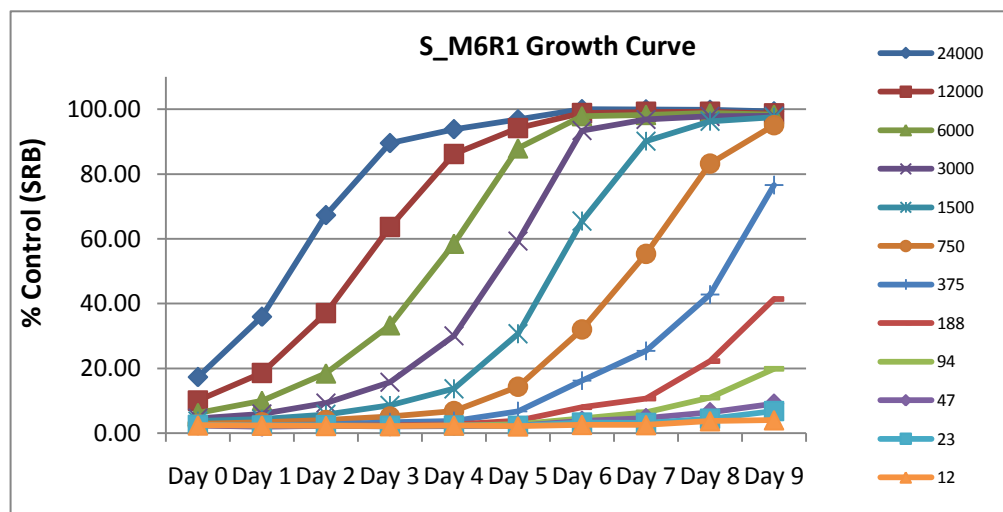
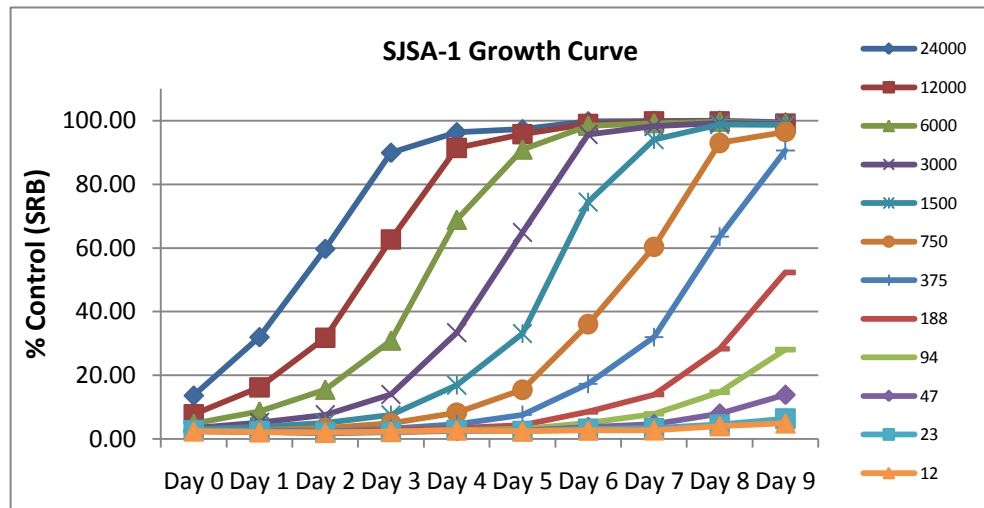


Figure 6. 11 Growth curves of SJSA-1 parental cell line and resistant cell clones

6.4.2 Resistance evaluation for stage II resistant cell clones

Because of the observation that the gaps of drug concentrations for parental cell lines treatment might be too big ([Figure 6. 2](#) & [Figure 6. 3](#)), when I was designing the SRB assay for the further developed resistant clones, I included a narrower range of concentrations around their GI_{50} values to obtain more accurate GI_{50} values for parental cell lines.

The GI_{50} results and the ratios between parental and resistant cell clones for both of the two cell lines in [Table 6. 2](#) showed marked increase in resistance for the SJSA-1 stage II resistant clones, and higher resistance levels for the NGP resistant clones, which will be discussed in detail later.

[Figure 6. 12](#) and [Figure 6. 13](#) show the marked differences of the cellular response between the parental and the stage II resistant cell clones established by using either MI-63 or Nutlin-3. Both of the SJSA-1 and NGP resistant cell lines showed cross resistance effects to Nutlin-3 and the other MDM2 inhibitor MI-63. Moreover, the potency differences between the two antagonists reflected not only by the SJSA-1 and NGP parental cell lines, but also reflected in the responses of their resistant cell clones.

Table 6. 2 Comparison of stage II resistant cell clones with their parental cell lines showing marked increases in GI₅₀

Cell Clones	MI-63_GI50	Folds change	Nutlin-3_GI50	Folds change
SJSA-1	0.70 ± 0.05 µM (n=3)	1	2.1 ± 0.2 µM (n=3)	1
SJSA-1*	0.36 µM		1.14 µM	
S_M6R1	16.04 µM	22.9	43.23 µM	20.1
S_N40R1	16.74 µM	23.9	49.62 µM	23.6
NGP	1.58 ± 0.21 µM (n=3)	1	2.20 ± 0.39 µM (n=3)	1
NGP*	0.75 µM		0.74 µM	
N_M5R1	12.07 µM	7.6	31.07 µM	14.1
N_M5R2	10.54 µM	6.7	22.33 µM	10.2
N_N20R1	9.75 µM	6.2	25.85 µM	11.8

The '*' labelled rows were shown the GI₅₀ of the parental cell lines tested by using a narrower concentration range. For the consistent results comparison, the original GI₅₀ values were used to calculate the fold increase in resistance.

GI₅₀ Determination of SJSA-1 Series Cell Clones

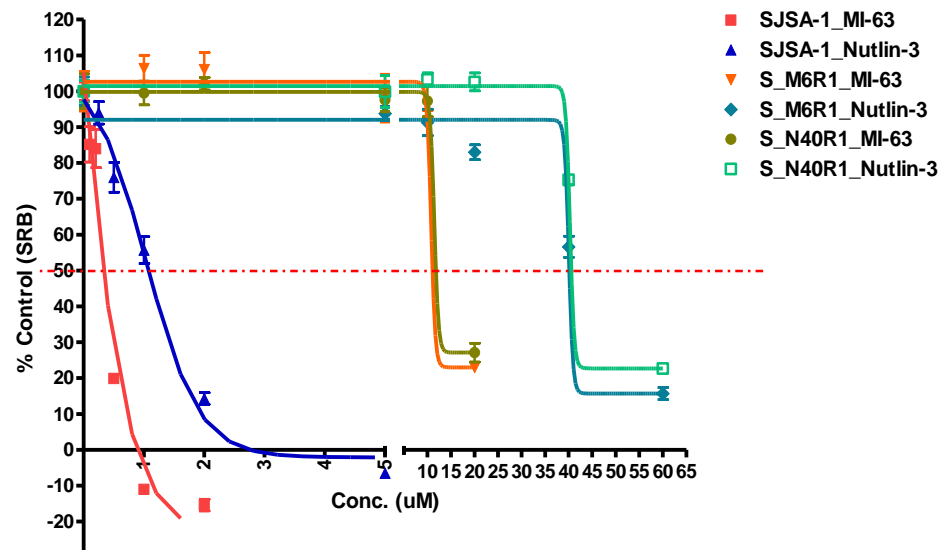


Figure 6. 12 SJSA-1 parental and resistant cell clone GI₅₀ Comparison.

GI₅₀ Determination of NGP Series Cell Clones

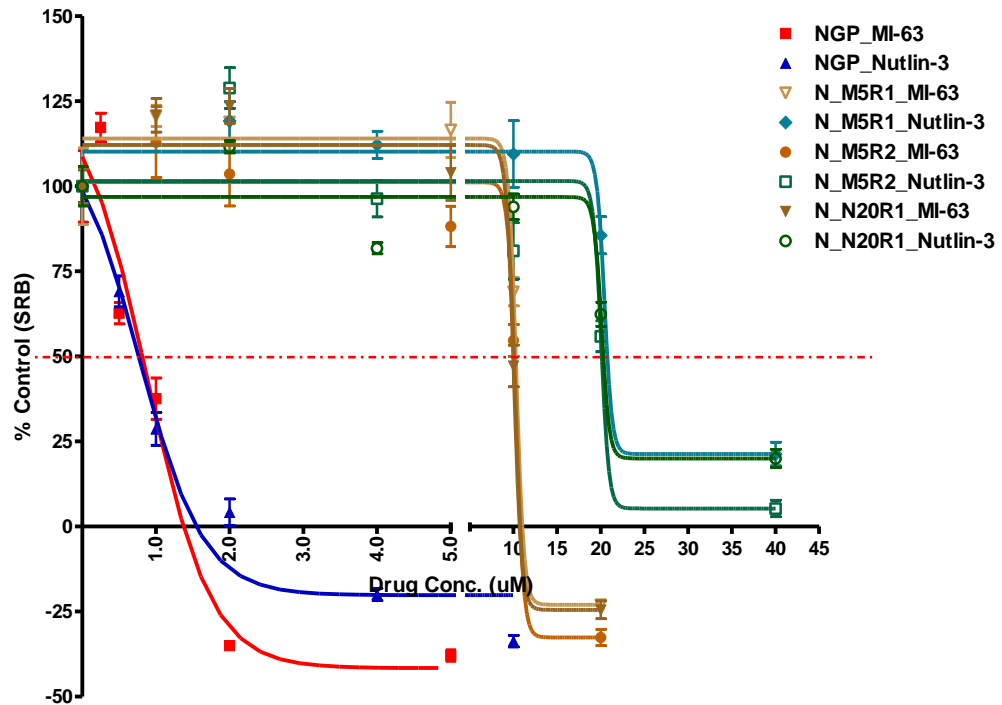


Figure 6. 13 NGP parental and resistant cell clone GI₅₀ Comparison.

6.4.3 Western blotting assay for protein expression determination

To investigate whether the increased cell resistance was related to changes of p53 and its downstream target MDM2 and p21^{WAF1} protein after MDM2 antagonist treatment, the expression of these proteins was determined using total cell extracts prepared from control or cells treated with DMSO, 5 μ M MI-63 or 20 μ M Nutlin-3 for 6 hours and α -tubulin in each sample was also evaluated as a loading and transfer control. The appearance of cleaved PARP and phosphorylated ser15 p53 were also evaluated ([Figure 6. 14](#)).

The western blotting results of the SJSA-1 parental cell line and further developed stage II resistant clones ([Figure 6. 14](#)) confirmed that both MI-63 and Nutlin-3 can disrupt the interaction between MDM2 and p53 protein and release the p53 transactivation domain from MDM2 binding in both SJSA-1 parental cell line and its resistant cell clones, causing p53 accumulation compared to untreated or DMSO only treated cell samples. However, in contrast to the response of the SJSA-1 parental cell line in which the release of p53 was seen to activate its downstream targets, the MDM2 and p21 protein bands of the two stage II resistant clones showed no marked change or increase after treatment with Nutlin-3 or MI-63.

The western blotting results also showed that after 6 hours drug treatment, the detection of cleaved PARP and phosphorylated ser-15 p53 were marked only in the SJSA-1 parental cell line, but not in the resistant clones treated by either Nutlin-3 or MI-63.

As an alternative measure of the functional integrity of p53 in the resistant clones, the time course effect of DNA damage induced by X-ray irradiation was then investigated. Adherent exponentially growing SJSA-1 parental cells and resistant cell clone S_M6R1 were seeded into 6-well plates at a density 4×10^4 cells/well. After 24 hours incubation at 37 °C, the cell samples were exposed to 6.3 Gy of X-rays from a 310 kV source (D3300 X-ray system, Gilmay Medical Ltd, Chertsey UK). Then following a period of incubation at 37 °C, cell lysate samples were collected at 0.5, 1, 2, 4 and 24 hours post-irradiation and analysed by western blotting ([Figure 6. 15](#)). The Ser-15 phosphorylated p53 and p21 protein levels were evaluated. As can be seen from the western blotting result, the Ser-15 phosphorylated p53 accumulated in parental cell lysate samples collected at 0.5, 1 and 2 hours time points after x-ray treatment and then decreased in 4 and 24 hours time points samples; also in these samples, the p21 protein expression increase was detectable from the 2 hour samples and then continued to increase with time and showed the highest levels of increase in the 4 and 24 hours samples. In the resistant cell clone S_M6R1 samples, the Ser-15 phosphorylated p53 accumulation was also detectable from the 0.5 hour time-point although the bands intensities were lower than in parental cell samples; and were seen to decrease only after 24 hours. Interestingly, although we have not observed p21 expression in SJSA-1 resistant cell clones treated by using high concentration MI-63 and Nutlin-3, we have nevertheless detected it in S_M6R1 4 and 24 hours after X-ray irradiation.

Expression of multidrug resistance proteins, P-glycoprotein (P-gp) and MDR1, were also examined as potential mechanisms of resistance to the MDM2-p53 antagonists, Nutlin-3 and MI-63. In these experiments, the cell lysates of the Madin-Darby canine kidney strain II cell line transfected with a human *MDR1* gene (MDCK II-MDR1) was used as a positive control for the P-gp expression, and the the lysates of the human lung adenocarcinoma cell line A549-cDDP, that not only expresses the *MDR1* gene but also has high level expression of the multidrug-resistance associated protein (MRP) gene was used as multidrug-resistance protein 1 (MRP1) expression positive control.

The western blotting results in [Figure 6. 16](#) demonstrated that both SJSA-1 parental cell clone and the two resistant cell clones S_M6R1 and S_N40R1 have undetectable expression of P-gp and MRP1 multidrug resistant proteins in either parental cell lysate samples or MDM2-p53 antagonists resistant cell line sample lysates, whether untreated or treated with Nutlin-3 or MI-63.

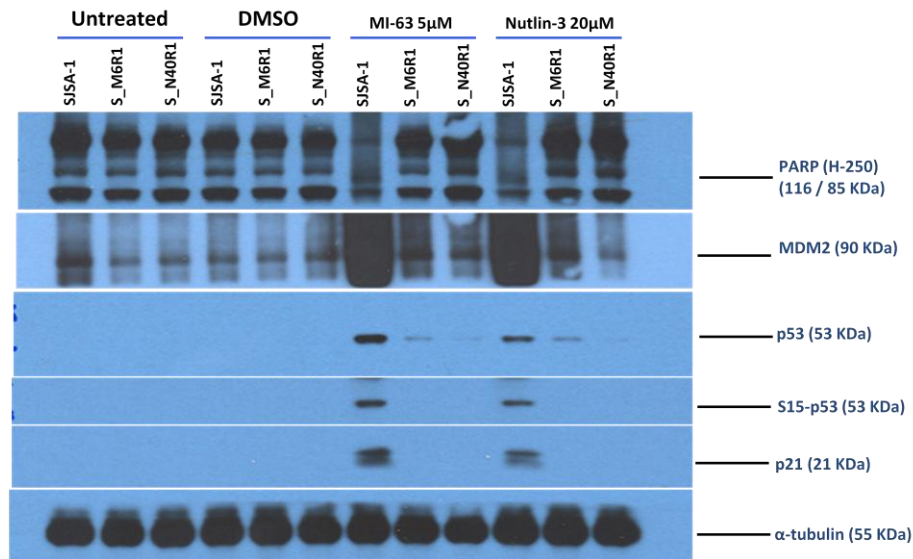


Figure 6. 14 Western blot results showing p53 pathway activation in the SJSA-1 parental cell line by Nutlin-3 and MI-63, but not in the stage II resistant cell lines, with cross resistance effects.

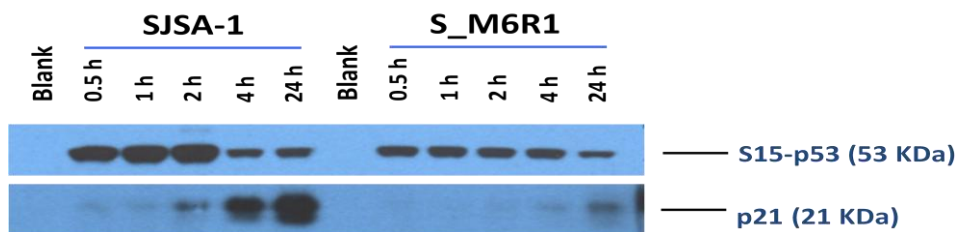


Figure 6. 15 Western blot results of the time course response of the SJSA-1 parental cell line and resistant clone S_M6R1 induced by 6.3 Gy X-ray irradiation.

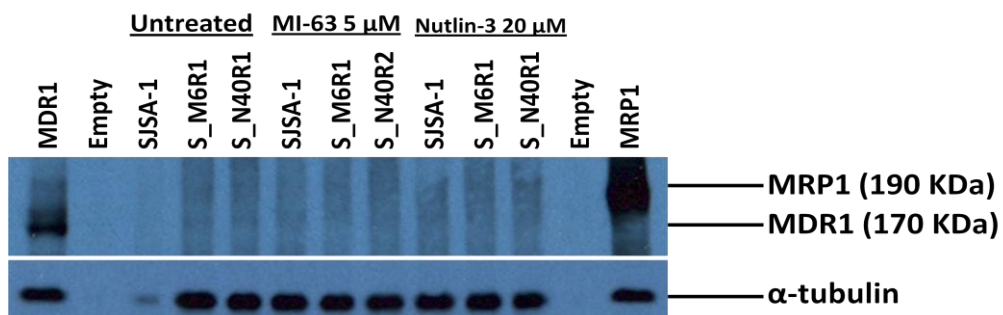


Figure 6. 16 Western blot results showing lack of increased p-glycoprotein and/or MRP1 overexpression in the SJSA-1 resistant cell clones tolerant to p53-MDM2 antagonists, compared to the parental SJSA-1 cells.

6.4.4 Cell cycle studies

The lack of p21 induction in the SJSA-1 resistant cell clones with 6 hours MDM2-p53 antagonists treatment, suggest there might be an associated resistance to G1 cell cycle arrest. To confirm this, cell cycle analysis by fluorescence activated cell sorting (FACS) was carried out, both in response to MDM2-p53 antagonists and to X-ray irradiation. The parental SJSA-1 cells showed S phase shrinkage that indicated G1 and G2/M phase arrest in response to both Nutlin-3 and MI-63, as well as in response to X-ray irradiation, which is mainly G2 phase arrest. In the contrary, for both of the two resistant cell clones, there was no obvious cell cycle change observed after MDM2-p53 antagonists treatment compared with the untreated samples; however, similar cell cycle arrest at the G1 and G2/M phase was observed with both the parental cell line and the two resistant cell clones after x-ray irradiation ([Figure 6. 17](#) and [Figure 6. 18](#)). Another interesting observation was that even without drug treatment, both of the two resistant cell clones showed a much lower percentage of S phase cells, and different G1 and G2/M phases percentages compared with the parental cell line, even though there was no noticeable difference in the overall population growth rates in the experiment described in section 6.4.1.

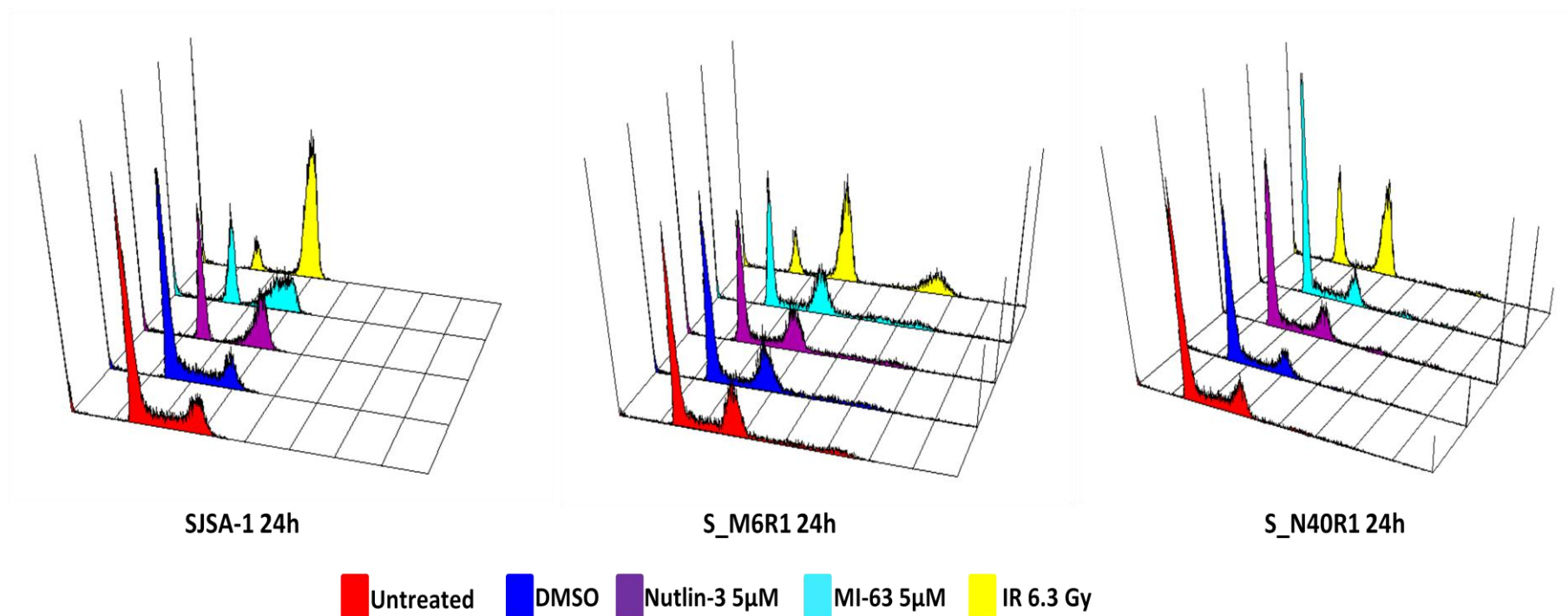


Figure 6. 17 Histogram of cell cycle distribution for the SJSA-1 parental cell line and the two resistant cell clones S_M6R1 and S_N40R1 after 24 hours treatment with Nutlin-3 or MI-63 and 24 hours post-treatment with 6.3 Gy of X-rays, compared with untreated controls.

Sub confluent cells were treated with 1% DMSO, 5 μM Nutlin-3 or MI-63 for 24 h, or with 6.3 Gy of X-ray irradiation then incubated at 37°C for 24 h, harvested, then rinsed with PBS and fixed with freezing cold (-20°C) ethanol : PBS (7:3,v/v)for >2h. The fixed cells were rehydrated and stained in PI/RNase staining buffer at 37°C for 30 minutes and analysed for DNA content on a FACScan flow cytometer (BD, San Jose, CA). 10,000 cells in total were counted for each sample analysis. Cell cycle distribution and histograms were generated with WinMDI 2.8 software.

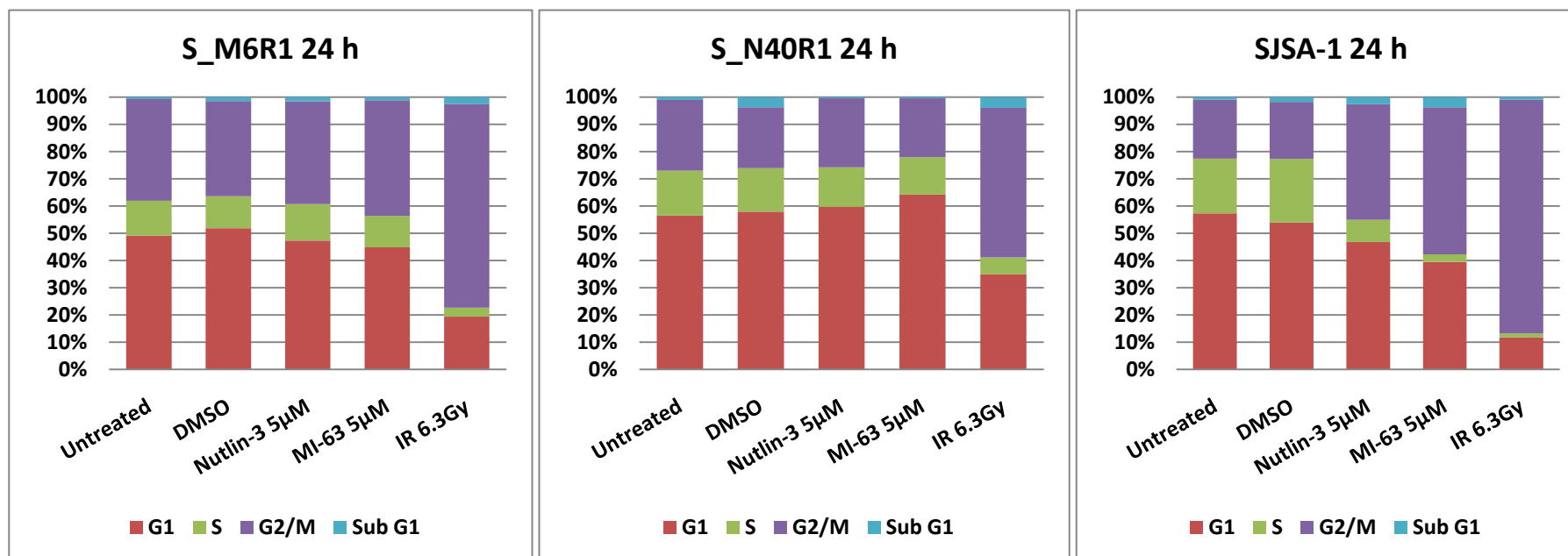


Figure 6. 18 Bar chart of cell cycle distribution for the SJSA-1 parental cell line and the two resistant cell clones S_M6R1 and S_N40R1 after 24 hours treatment with Nutlin-3 or MI-63 and 24 hours post-treatment with 6.3 Gy of X-rays, compared with untreated controls.

Bar chart of cell cycle phase population ratios were generated with Excel software.

6.4.5 Caspase-Glo® 3/7 Assay for apoptosis analysis

To assess the consequence of the p53 mutations on any apoptotic response to the MDM@-p53 antagonists, caspase 3 and 7 activities were analysed using a Caspase-Glo® 3/7 Assay Kit. Briefly, adherent exponentially growing cells were seeded into 96-well plates at 2×10^3 cells/well for SJSA-1 parental and resistant cell clones and 5×10^3 cells/well for NGP parental and resistant cell clones. After 24 hours incubation at 37°C, the medium was replaced with fresh medium containing 1 % DMSO or MDM2 antagonists Nutlin-3 or MI-63 at appropriate ranges of drug concentrations in 1 % DMSO so that the plate was containing blank, negative control and treated cells in culture medium. After a drug exposure period of 48 hours, the plate was taken out from the incubator and equilibrated to room temperature, then an equal volume of Caspase-Glo® 3/7 reagents was added into each well. The plate was covered with a lid and gently shaken at 300 rpm for 30 seconds to mix the content. The plate was incubated at room temperature for 1.5 hours, then the contents of wells were transferred into a white-walled 96-well plate and the luminescence of each sample measured in a micro plate Luminometer (Berthold Technologies, Hertfordshire, UK). Then luminescence data obtained were analyzed and line charts were generated (Figure 6. 19 A & B) with Graphpad Prism 5 software.

The SJSA-1 parental cells respond with a dose dependent increase of caspase-3/7 activity, which showed saturation at the higher dose levels (Figure 6. 19).

In contrast, no noticeable caspase-3 and 7 activities were observed in either of the two SJSA-1 resistant cell clones when treated with the concentrations ranges for MI-63 from 0.5 to 5 μ M or for Nutlin-3 from 1 to 10 μ M. The strong induction of caspase-3/7 activity in the parental cells treated with only 0.5 μ M MI-63, which showed a similar effect to that caused by 2 μ M Nutlin-3, reflected the GI₅₀ evaluation and western blotting results.

Another interesting phenomenon worth pointing out is that the untreated SJSA-1 parental cells also expressed a higher baseline caspase 3/7 activity than the two resistant clones, even though the seeding densities were the same, which indicated the expression of caspase 3/7 induced by active p53 pathway in SJSA-1 parental cell clone, even without any treatment, in which was reduced in the resistant cell clones.

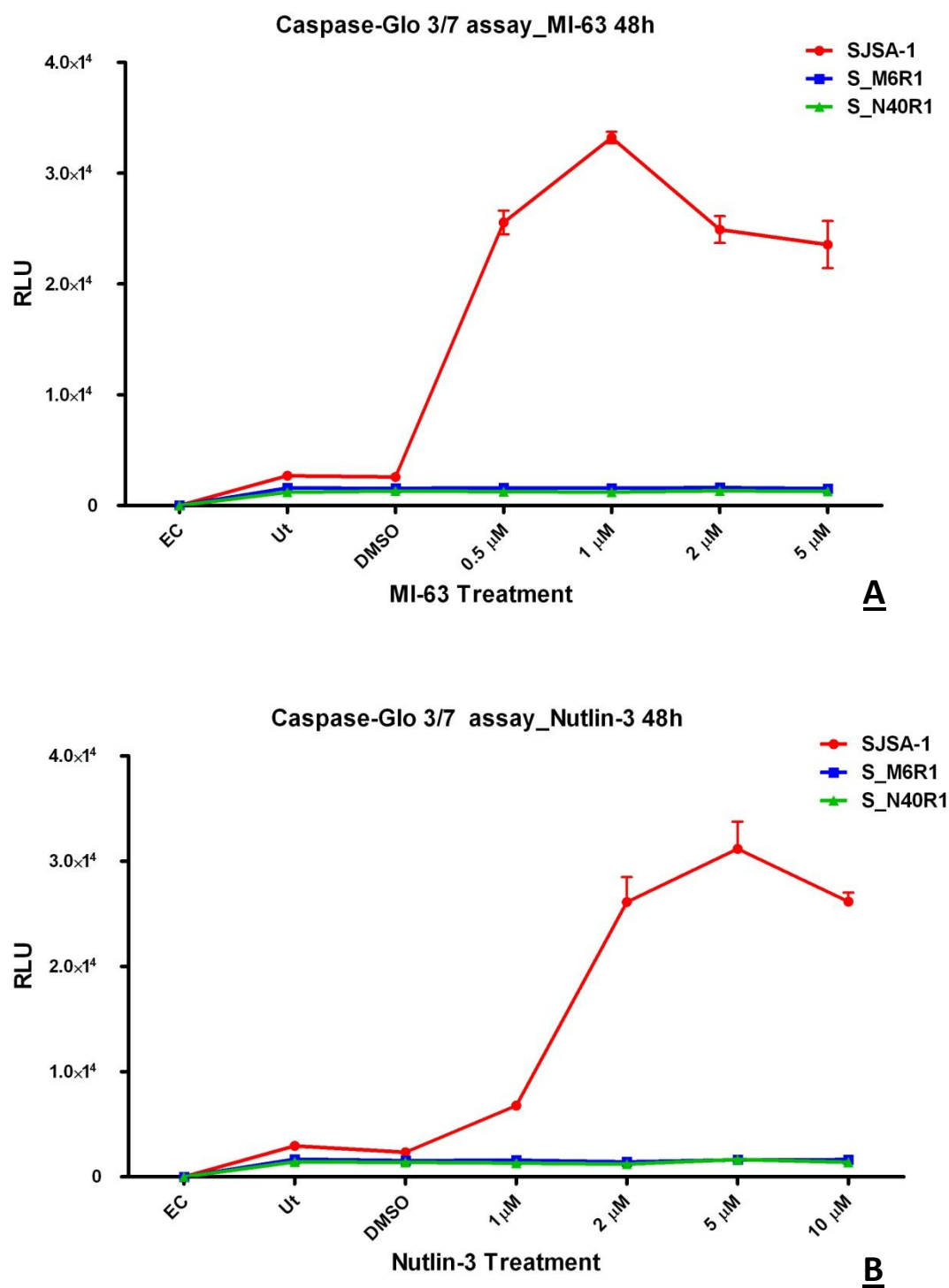


Figure 6. 19 Caspase 3/7 enzymatic activity in resistant cell clones treated by various concentrations of MI-63 (A) or Nutlin-3 (B) for 48 hours showed little induction compared to the response in SJSA-1 parental cell lines, which increased markedly.

6.4.6 DNA Sequencing of p53

To determine the p53 status of the further developed stage II resistant cell clones, total DNA was extracted from each cell clone for the analysis. PCR products of Exon 4 to 9 that represent p53 DNA binding domain were sequenced for mutation detection. As previously, the sequencing results of all PCR products produced were analysed by using SN primers first, and then the mutations were confirmed by analyzing the ASN primers generated PCR products.

In all the SJSA-1 stage II resistant cell clones there was still only one missense point mutation at codon 285 detected within all SJSA-1 (Figure 6. 20). The chromatogram shows a homozygous codon 285 mutation confirmed with both SN and ASN sequencing primers.

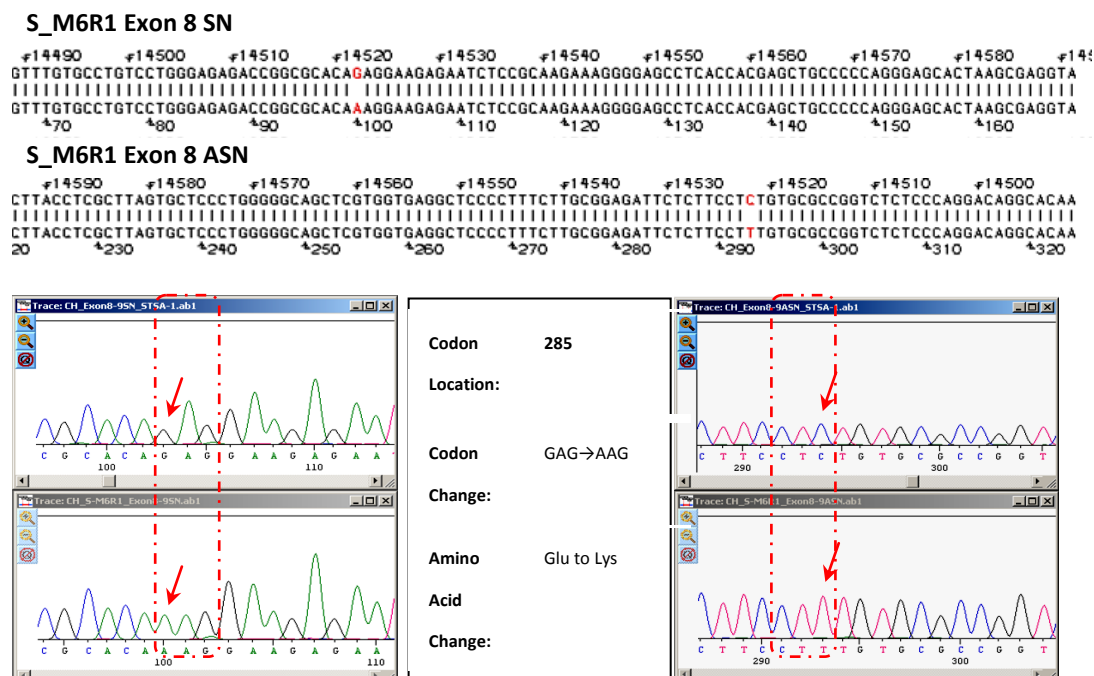


Figure 6. 20 Resistant SJSA-1 cell clone S_M6R1 DNA sequencing result showing the point missense mutation in the p53 DNA binding domain. The same point mutation was found in SJSA-1 resistant clones obtained from Nutlin-3 treatment.

6.4.7 Comparison of p53 Specific PCR Amplification of DNA from Resistant Cell Clones and parental SJSA-1 Cell line

Since the same mutation was detected in resistant clones independently derived from the same parental cell line, this suggested that the mutation was already present in a small subpopulation of the parental SJSA-1 cell line, below the level of detection by direct sequencing of the whole population. To confirm the detected mutation and test for its presence in the parental SJSA-1 cell population, a mutation specific PCR was designed. Using specifically designed primers 5'-GGA GAG ACC GGC GCA CAA-3' and 5'-TCC ACT TGA TAA GAG GTC CC-3' and PCR procedure TD63 (see Appendix II) and the method mentioned previously (Section 2.7.3). Then 30 µL of each reaction product SJSA-1 parental and resistant cell clones was compared with PCR products using normal primers on a 1.8 % agarose gel contain ethidium bromide and images were taken under UV light transillumination, using a Bio-Rad imaging system (Figure 6. 21).

The result confirmed the existence of the detected point mutation in all the SJSA-1 resistant cell clones; the low level of detectable normal sequence PCR product from the resistant cell clones indicated the predominance of mutated p53 in the resistant cell clone populations.

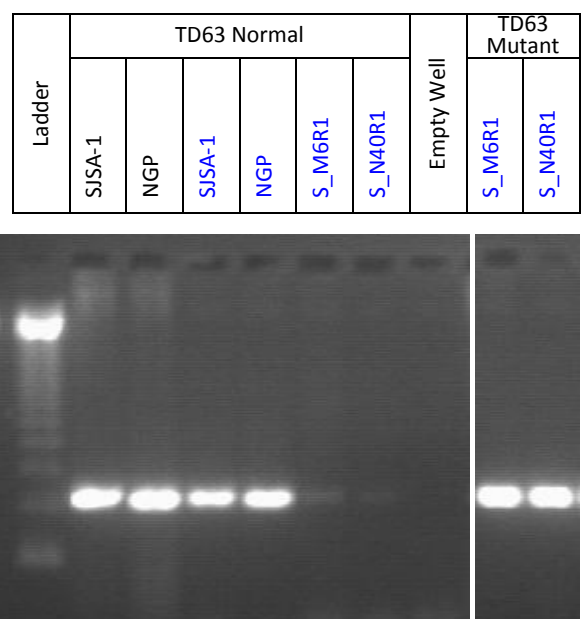


Figure 6. 21 PCR products comparison using wild-type and mutation specific p53 sequence primers to amplify DNA from SJSA-1 resistant clones and the parental cell line. NGP parental cell line DNA is included as a additional wild-type p53 positive control.

6.4.8 Low level p53 Mutation Detection in SJSA-1 parental cell line DNA extracts

To investigate the possibility of the codon 285 (GAG to AAG) p53 point mutant detected in the resistant clones was already present in the parental cell line at a low level undetectable by direct sequencing, further mutation specific PCR amplification was carried out on the SJSA-1 and NGP parental cell lines DNAs and the reaction products compared with PCR products using normal primers on 1.8% agarose gel contain ethidium bromide (Figure 6. 22).

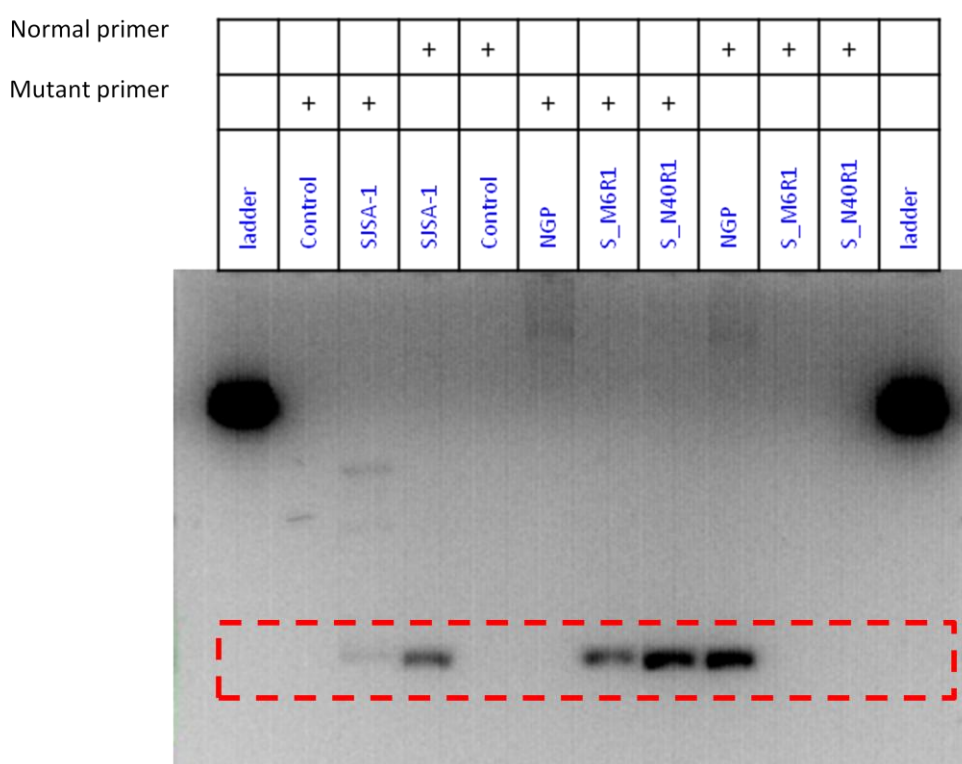


Figure 6. 22 p53 mutation specific and normal PCR products compared for SJSA-1 resistant clones and SJSA-1 and NGP parental cell line DNAs.

The PCR products produced by using p53 specific primers or normal primers are labelled with '+' on top of each cell clone name with the primer label at the left of each row. 1 Kb DNA ladder are added at both side of the gel, and controls of PCR reagents contain either normal primers or mutant specific primers and without adding any DNA sample are loaded onto the gel to inspect contamination. The red box highlighted all target PCR product bands location area.

The faint band seen in track 3 that shows the PCR product from SJSA-1 parental cell line DNA amplified with mutation specific PCR primers, confirmed the existence of the point mutation in the SJSA-1 parental cell line, although the mutant sub-population was at too low a level to be detectable by direct sequencing of the whole population DNA. The absence of detectable mutation specific PCR products within the control without any DNA sample and NGP parental cell line track DNA strengthened the reliability of the mutation specific PCR technique for point mutation confirmation.

To seek further evidence of resistant cells pre-existing in the parental cell line population, high concentrations of MDM2-p53 binding antagonists (MI-63 5 μ M, Nutlin-3 5 and 20 μ M) were used to treat the SJSA-1 parental cells directly. After 15 days treatment, low numbers of individual-morphologically intact cells were observed in the 5 μ M Nutlin-3 treated cell samples, but not in 5 μ M MI-63 or 20 μ M Nutlin-3 treated cell samples ([Figure 6. 23](#)), which might be because of either the selection of resistant cells or cells experiencing senescence, therefore, further experiment maybe required for the confirmation of the status of these cells in future.

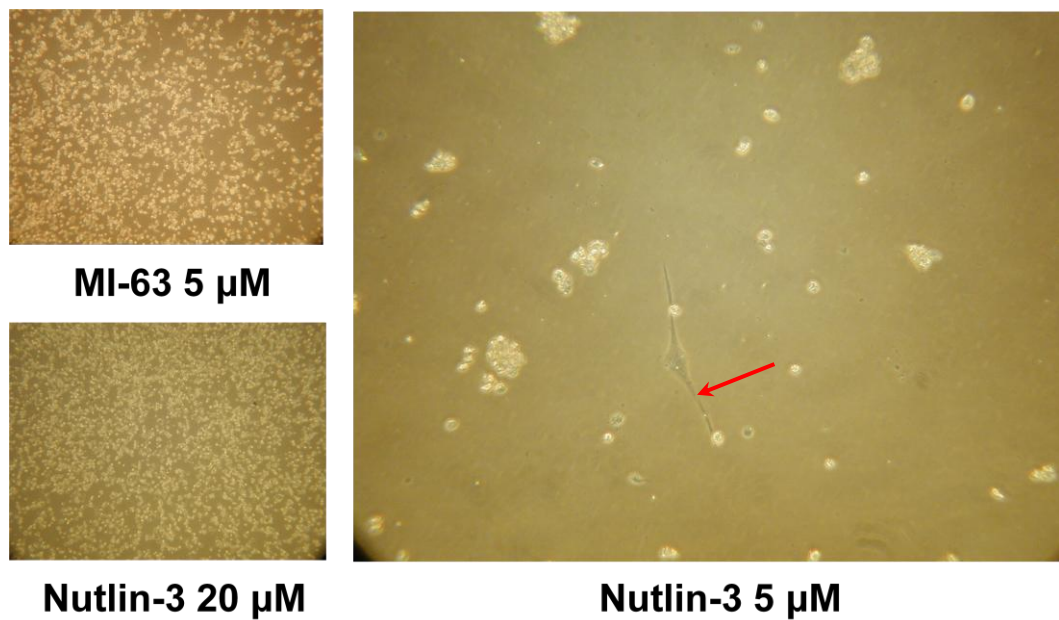


Figure 6. 23 Direct evidence of resistant cells in the parental SJSA-1 population undergoing single step selection with 5 μ M Nutlin-3

SJSA-1 parental cells treated with different concentrations of MDM2-p53 antagonists for 15 days showing the marked effects of these compounds_and also the presence of sparse numbers of surviving cells in the 5 μ M Nutlin-3 treated cell samples (red arrow), but not in the 5 μ M MI-63 or 20 μ M Nutlin-3 treated cell samples.

6.4.9 SJSA-1 parental and resistant cell clones comparison using fluorescence *in situ* hybridization (FISH) to test for allelic loss of the p53 gene

All the above described DNA sequencing and mutation specific experiments based on the stage II further developed resistant cell clones, indicated that they are relatively pure cell clones showing the same homozygous mutation, and PCR results illustrated that both of the S-M6R1 and the S_N40R1 cell clones have the same point mutation. However, at the intermediate, stage I selection ([Figure 6. 6](#), [Figure 6. 7](#) & [Figure 6. 8](#)) the DNA sequencing indicated an apparent heterozygous population. Two alternative explanations are possible for the progression of stage I apparent heterozygous mutations to the stage II detection of apparent homozygous mutations. The first possibility is that the whole stage I population contains a heterozygous mutation, with one normal allele and one mutant allele, with subsequent loss of the second allele when progressing to the stage II selected clones. The alternative possibility is that the stage I selected population is actually an approximately equal mixture of cells with two normal p53 alleles and cells with a homozygous mutation, with only a mutant allele present in them. To distinguish between these possibilities, FISH studies were performed (at Sir James Spence Institute, Royal Victoria Infirmary, Newcastle upon Tyne) to detect the p53 gene locus copy number in the stage I and stage II selected populations, as well as parental cells.

By comparing the experiments results listed above, we have observed some small differences between the S_M6R1 with S_N40R1 cell clones. Firstly, the GI₅₀ values for

them against either Nutlin-3 or MI-63 were slightly different, with S_N40R1 ($GI_{50_Nutlin-3}=16.74\ \mu M$, $GI_{50_MI-63}=49.62\ \mu M$) showing slightly higher resistance than S_M6R1 ($GI_{50_Nutlin-3}=16.04\ \mu M$, $GI_{50_MI-63}=43.23\ \mu M$). Secondly, in western blotting results, S_N40R1 showed less p53 and MDM2 protein expression than S_M6R1 with either 20 μM Nutlin-3 or 5 μM MI-63 treatment. Thirdly, in cell cycle analysis, S_M6R1 showed noticeable differences when compared with S_N40R1 when treated with either MDM2/p53 antagonists or X-ray irradiation; also with the S_M6R1 cell clone cell cycle analysis results, a marked tetraploid cell population was observed (Figure 6. 17), which may be consistent with 17p allelic loss (190) in this cell clone.

The images in Figure 6. 24 show examples of the detection of the p53 alleles on chromosome 17 in the SJSA-1 parental cell line and resistant cell clones S_M6R1 and S_N40R1. The number of p53 allele chromosome 17 centromeric probe signals per cell were recorded for a total of above 100 (Table 6. 3).

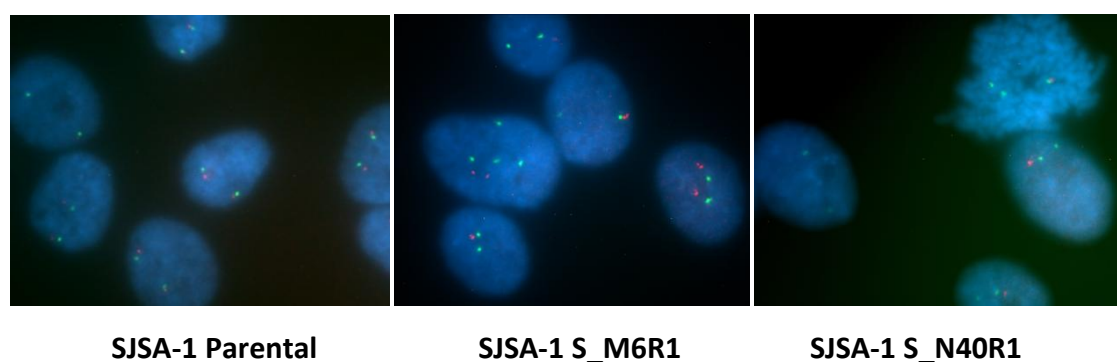


Figure 6. 24 FISH images illustrating the different p53 status (red) and chromosome 17 copy number (green) alteration in resistant cell clones S_M6R1 and S_N40R1 compared to SJSA-1 parental cell line.

Table 6. 3 FISH assay colour coded signal counting results showing marked differences between the three SJSA-1 cell clones

Cell Line Signals	SJSA-1 parental		SJSA-1 S_M6R1		SJSA-1 S_N40R1	
	Number	Percentage	Number	Percentage	Number	Percentage
2G2R	99	94.29	102	76.69	6	6.0
2G1R	5	4.76	17	12.78	68	68.00
1G1R	1	0.95	2	1.50	3	3.00
4G1R			2	1.50	1	1.00
3G3R			9	6.77		
4G2R			1	0.75		
3G1R					6	6.00
2G0R					14	14.00
1G0R					1	1.00
3G0R					1	1.00
Total	105	100.00	133	100.00	100	100.00

NB: In the first column of this table, the codes contain 'G' and 'R'. 'G' is corresponding to green signal in FISH image that indicate the copy number of chromosome 17, and 'R' is corresponding to red signal in FISH image that indicate p53 status.

The SJSA-1 parental cell line FISH results showed less than 5% p53 deletion and 1% chromosome 17 numerical variation; however, above 16% of S_M6R1 and 94% S_N40R1 cells have lost at least one p53 allele; Moreover, about 7% S_M6R1 cells contain 3 copies of chromosome 17 with 3 p53 alleles, and about 2% S_M6R1 and 8% S_N40R1 cells contain 3 or 4 chromosome 17 copies but only 1 or no p53 allele.

6.5 Conclusion and Discussion

As with other therapeutic agents, treatment with MDM2-p53 binding antagonists is likely to be subject to the development of drug resistance mechanisms.

A panel of clones selected for resistance to Nutlin-3 and MI-63 showed impaired activation of growth inhibitory and apoptotic pathways downstream of p53 in response to treatment with these agents compared to parental cells.

DNA sequencing and p53 pathway analysis were consistent with a p53 mutation resistance mechanism.

The western blotting result for multidrug resistance proteins P-gp and MRP1 expression examination indicated that the resistance effect of the two SJSA-1 selected clones was not related to the increased expression of multidrug resistant proteins. This result may correlated to the report from Michaelis *et al.* that Nutlin-3 can reverse the P-glycoprotein/MRP1-mediated multidrug resistance by including inhibition of P-gp and MRP-1 mediated efflux (191).

The western blotting and cell cycle analysis results of the comparison of SJSA-1 parental and resistant cell clones treated with X-ray irradiation pointed out a possible alternative therapeutic strategy. In western blotting results (Figure 6. 15), p21 protein was detected in the 4 and 24 hours post-X-irradiation treated S_M6R1 cell lysate samples, which suggesting the X-ray irradiation causes p53-independent induction of p21. In the cell cycle analysis results (Figure 6. 17), X-ray irradiation-induced cell cycle arrest at the G2/M phase was observed not only with the SJSA-1 parental cell line but

also the two resistant cell clones, which suggesting the X-ray irradiation causes p53-independent induction of cell cycle arrest. Interestingly, several research groups have reported that the combination of Nutlin-3 and radiotherapy (RT) showed higher efficacy than using RT alone in several cancer cell lines, e.g. lung cancer (192), prostate cancer (193) and laryngeal squamous cell carcinoma (LSCC) (194), etc. As a result, the alternative therapeutic strategy could be the treatment that not rely on p53 pathway activation.

By comparing the results of stage I and stage II SJSA-1 resistant clones, a relationship between the ratio of mutated peak and normal peak in the DNA sequencing chromatograms and the resistance of those clones was apparent. A FISH assay indicated that this resistance might be related not only to the presence of a p53 mutation but also to the progression of further resistance by subsequent selection for loss of the normal p53 allele. The intermediate level of resistance shown by the stage I selected population with predominately heterozygous mutations was further increased in the stage II population, in association with predominant loss of the wild-type p53 allele, consistent with the appearance as a homozygous mutation in the sequencing chromatograms. This suggests that mutation of one allele produces an intermediate level of resistance and loss of the second allele results in a higher level of resistance.

Chapter Seven

Further Discussion and Future Work

7.1 Further Discussion

7.1.1 Summary of Achievements

The IC₅₀ evaluation of the isoindolin-1-one scaffold compounds using the ELISA method enabled the construction of a quantitative structure-activity relationship (QSAR) map that has contributed to the step by step compound side-chain modification that has improved potency. Furthermore, based on the QSAR analysis together with the NMR data generated by our collaborators in Oxford University (Professor Martin Noble, Dr Jane Endicott and Dr Jan Gruber) I was able to propose the possible binding mode of some key isoindolin-1-one compounds, which has contributed to a better understanding of the interaction of the small molecule compounds with the MDM2 protein, and will facilitate further lead compound structure design and development.

After three years of memorable team work, the isoindolin-1-one scaffold MDM2-p53 binding interaction antagonists project has entered a very encouraging phase, in which the lead compound potency (racemic mixture) has come to below 20 nM, with cellular activity comparable to Nutlin-3 and pre-clinical *in vivo* studies will soon commence. Moreover, with the successful resolution of several potent isoindolin-1-one racemic mixtures, pure enantiomers have been obtained, which have

shown marked *in vitro* potency differences and a corresponding variation in cellular activity. These observations have helped to provide a better understanding of the binding between isoindolin-1-one enantiomers with the p53 binding groove of MDM2 and enabled us to compare them with Nutlin-3 and MI-63, which in turn has led to a refinement of the binding mode model and further structure optimization.

The testing of isoindolin-1-one scaffold compounds as MDMX-p53 binding interaction antagonists was carried out to examine the possibility of finding lead isoindolin-1-one scaffold compounds to develop as MDMX-p53 antagonists. This would be attractive because of the already large accumulation of experience on this compound series, with detailed SAR analysis and compound synthesis routes.

My involvement and contributions to the DePPICT project has enabled me to get a better understanding of the lead compound mining procedure, leading to the selection of active compound series. This experience, together with the research on pyrrole scaffold compounds and potent peptide inhibitors of the MDM2/MDMX-p53 binding interaction, will be helpful for further structure optimization of the various core scaffold lead compound series. This includes the use of *in silico* molecular modelling to inform 'scaffold hopping' in order to take active compounds forward into new series with a potentially more favourable pharmacophore.

With the anticipated possibility for drug resistance against MDM2-p53 binding antagonists, Nutlin-3 and MI-63 resistant cell clones were selected from parental SJSA-1 osteosarcoma and NGP neuroblastoma cell lines. Dysfunctional p53 point

mutation was confirmed to be the major resistance mechanism. A FISH assay indicated a sequential mechanism of resistance involving mutation of one p53 allele and loss of the normal p53 allele. These observation may benefit patients that will treated with MDM2-p53 binding interaction antagonists, indicating that the monitoring of p53 status at both presentation and relapse should be used to guide treatment.

7.1.2 “See-saw Theory” generation based on the development of MDM2/p53 and MDMX/p53 antagonists

First of all, it is important to define the ‘**See-saw Theory**’. In this theory, we assume the shape of the target protein’s binding groove is not very flexible, since the flexibility of every amino acid side-chain corresponds to breaking the balance of the interaction between amino acid residues and energy consumption and even protein function. As illustrated by the cartoon in [Figure 7. 1](#), the shape and character of the binding site of the compound candidate should be able to fit the binding groove of the target protein. As a result, we can design or develop compounds to fit this binding groove, or carry out *in silico* screening by using some virtual docking software as we have already done within the DePPICT project.

For interrupting the MDM2/p53 or MDMX/p53 binding, the principle is to design or find compound scaffolds to mimic the three key amino acid side chains, Leu26, Trp23 and Phe19, on the p53 transactivation domain that fits into the MDM2(X) binding

groove and to do so with a higher binding affinity than p53, so that they can competitively bind with MDM2(X) and release active p53 (Figure 7. 1).

With the SAR analysis of isoindolin-1-one compounds as antagonists of the MDM2/p53 binding interaction, we have observed that when we replaced the chlorine atom on side-chain -X with other halogen atoms, methyl group or hydrogen, the compound potency decreased markedly (Table 3. 5 in Chapter Three). A similar observation was made in our research, and research published on p53 peptide analogues as MDM2 (MDMX)/p53 binding interaction inhibitors. These observations indicated that a ‘**See-saw Theory**’ may be important in this kind of drug design and development.

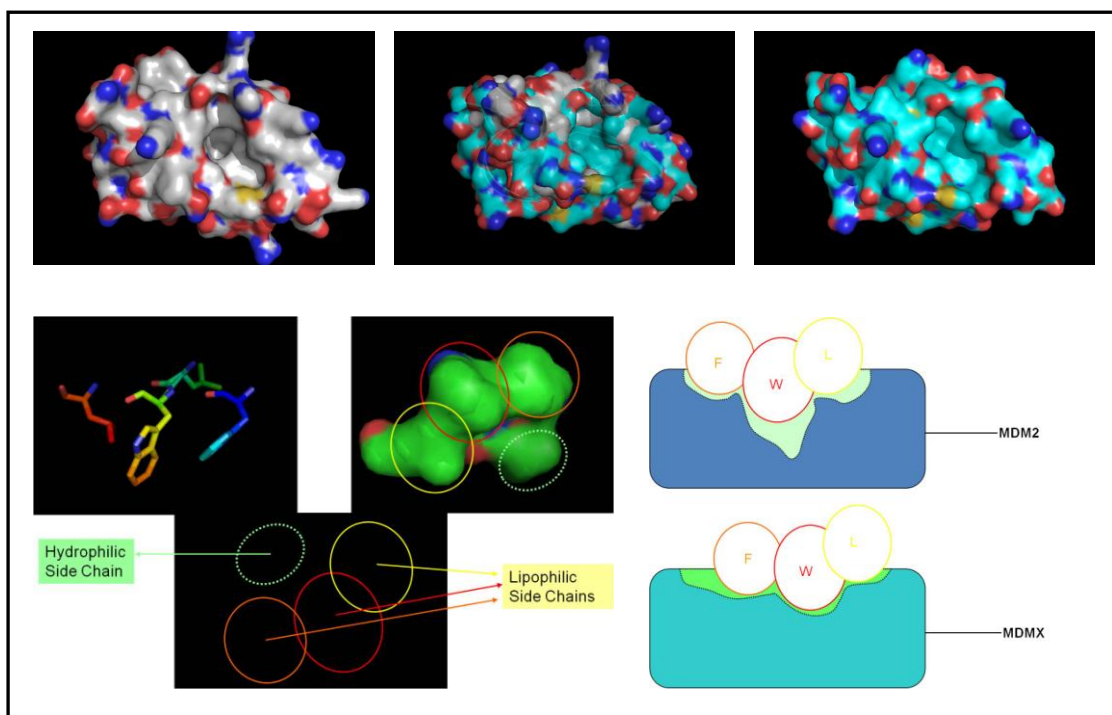


Figure 7. 1 ‘See-Saw Theory’ based on MDM2/p53 and MDMX/p53 antagonist design

Based on this theory, if the compound contains more binding points then interaction with the binding groove will induce a higher binding affinity with the target protein; on the other hand, if a target protein has a binding groove that contains more binding pockets or deeper binding clefts, then it will be more suitable to be a drug development target, i.e. the more points of interaction there are, the greater is the likelihood of designing a specific inhibitor. That is the reason why we have to mimic three key side chains of p53 peptide and see Trp23 as the most important one, rather than focus on only Leu26 and Phe19 and design compounds to just cover the binding site of MDM2, like a lid. This has lead me to conclude that MDM2 is more like a drug target than MDMX, since it has a deeper binding groove than MDMX, although both of them can bind with the p53 transactivation domain to inhibit its transcriptional function.

7.1.3 “Parachute Analogy” generation based on MDM2/p53 antagonists development

Based on the observation of the binding mode generated by using virtual docking software and SAR analysis results we obtained from isoindolin-1-one compounds development, together with the published MDM2/p53 binding interactions with small molecular inhibitors and p53 peptide analogues, we have generated a ‘**Parachute Analogy**’ to illustrate the effect of the R2 side-chain on isoindolin-1-one scaffold inhibitors.

As displayed in [Figure 7. 2](#), the hydrophilic R2 side-chain on isoindolin-1-one compound acts like a parachute.

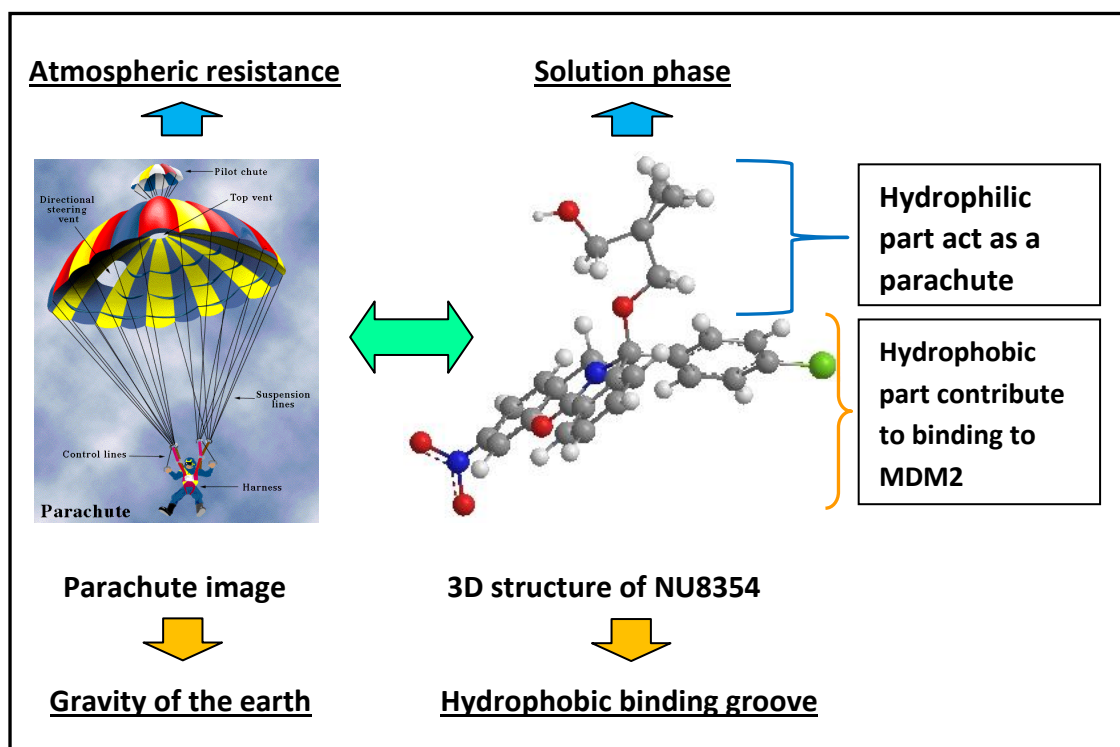


Figure 7. 2 Side-chain –R₂ of isoindolin-1-one compound NU8354 act as a parachute

Because of its hydrophilicity, it would always be forced towards solution phase and help to force the lipophilic side chains towards the hydrophobic binding groove of MDM2, which could enhance the possibility of the right isoindolin-1-one side chains to land into the most favorite binding pocket that the three key amino acid residues of p53 normally occupy. On the other hand, also because of its hydrophilicity, it could prevent p53 key amino acid residues from binding onto it. For this reason, the compound gained higher potency after the addition of hydrophilic side chains.

Based on this '**Parachute Analogy**', it will be a balance between the hydrophilicity of the side-chain with the lipophilicity of the whole compound. As a result, when we try

to modify compound structure to gain potency, we have to consider this balance, which may correspond to logP value.

As I have mentioned in Chapter 3, the –R2 side-chain may also contribute to the binding with MDM2 protein just like the Leu22 side-chain of p53 peptide does.

Therefore, the side-chain length and shape variation can also influence the whole binding affinity of the isoindolin-1-one compound with MDM2 protein (As displayed in the SAR figure in Section 3.3.2).

As a result, according to ‘**Parachute Analogy**’, the key factors such as size, shape and the balance of hydrophilicity and lipophilicity of the –R2 side-chain have to be considered for the development of isoindolin-1-one scaffold MDM2/p53 interaction inhibitors, even when the modification is introduced on other side chains.

7.1.4 “Bridge Effect Theory” based on screening data analysis of the DePPICT compounds and suggestions for future *in silico* screens

In the DePPICT project, we have observed that several compounds produced noticeable negative inhibitory percentage values, which raised the question: why did they produce such negative results even though they passed virtual screening with acceptable binding energy values?

Further detailed analysis revealed that they were all low molecular weight (~ 300) compounds with relatively high lipophilicity, and their post-binding modes may turn them into a bridge between MDM2 and p53 peptide analogues (b-IP3 peptide). This may be able to enhance the binding affinity of MDM2 with b-IP3 peptide, just like

produced another 'MDMX' like binding groove, which lead to marked negative result, as I have discussed in Chapter 5 and named the '**Bridge Effect Theory**'.

This hypothesis raised another question: how can we prevent the bridge effect?

Actually, if we can successfully prevent this effect, we may be able to develop some quite potent MDM2/p53 inhibitors at the same time based on DePPICT screening results. And the answer is, add a hydrophilic side-chain at the back of the binding side of the compound in the post-binding docking mode generated via virtual docking software.

However, it seems to be not that simple, and maybe quite inefficient, since it will take time to work out the synthetic route to add the side chain, if the compounds are not available commercially. Then, is there any way to increase the efficiency? The answer is 'Yes'. Based on the binding mode, we can do another 'screen', by synthetic chemists, to identify the candidates that can be easily produced, synthesise them and evaluate their potency by ELISA assay together with the original commercially available compounds.

7.1.5 "Predictable vs. unpredictable", the lesson learnt from MDM2/p53 antagonists resistant mechanism research

In most people's mind, cancer is a monster. Although most solid tumours may be very aggressive and can cause big problem, but we can generally find first-line treatment strategy; the unpredictable relapse tend to be another big problem.

So what can we learn from the resistant cell clones research?

First of all, we have to bear in mind that relapse is often associated with resistance to treatment and poor outcome. As a result, we have to maintain vigilance with those patients that experience a successful treatment response rather than getting excited too early. What we have done here is to make the possible mechanism and consequence more predictable, which may benefit patients in future. In this particular context, the potential for p53 mutation as the most likely resistance mechanism in cases of relapse from treatment with MDM2-p53 antagonists should be anticipated and guide appropriate strategies for further treatment.

Secondly, combinational treatment strategy may be applied from the beginning of cancer patient treatment, or if the resistant effect starts to be detected, some other pathways may have to be considered as early as possible rather than increase the dosage of the original drug to gain some more effects.

Finally, cancer patient therapeutic strategy has to become a personalized treatment plan, so that we can obtain more accurate information to optimize the treatment and also accumulate more information for future therapeutic strategy design.

7.2 Future Work

7.2.1 Possible plan for MDM2/p53 antagonists design and development

For the isoindolin-1-one scaffold MDM2/p53 antagonist development, the modification and SAR analysis of side-chain –R2 may need to be considered, especially with the fact that the ‘pro-drug’ NCL-00016149 induced much higher potency than parental compound NU8406 in ELISA evaluation. Some better

hydrophilic 'parachute' side-chains in the –R2 position may be designed with the collaboration between chemists and biologists.

On the other hand, cellular evaluation results we have obtained so far have told us a relatively more complicated story.

The western blotting and SRB assay results of stage 1 series compounds and NU8354, NU8406 enantiomers comparison have given us an idea that in cancer cells which contain wild type p53 the cellular response to drug treatment correlated with compound potency; however, the cellular behavior of stage 2 compound NU8399 told us that we should not assume this will always be the case and make this conclusion too early. There may be more factors that need to be considered, such as the balance between lipophilicity with hydrophilicity; then the cellular behaviour of stage 3 series compounds suggest that molecular weight might be another key factor we have to consider. As a result, more cellular assays, especially quantitative techniques such as SRB assay, Caspase Glo-3/7 assay, Clonogenic assay, etc. may need to be carried out in future, which may contribute to the overall SAR analysis together with the cell-free ELISA results.

7.2.2 Possible plan for MDMX/p53 antagonists design and development

For the MDMX/p53 antagonists design and development, different research strategies may need to be carried out. The first route is based on the already obtained MDM2/p53 antagonists, with the modification and SAR analysis together with detailed comparison of MDM2/MDMX binding groove. The other route is like the

research we have done in the DePPICT project, to screen or design new scaffolds based on the structure of the MDMX binding groove, and use the experience we have obtained from MDM2/p53 antagonist development. The key thing will be the design of persuasive cellular experiments to evaluate the cellular effects of compounds and confirm it is caused by the inhibition of the MDMX/p53 interaction.

7.2.3 Further research on MDM2/p53 antagonists resistant cell clones

One noticeable observation in the GI_{50} evaluation results is that the potency differences between MI-63 and Nutlin-3 were reflected not only in both SJSA-1 and NGP parental cell lines, but also in their resistant clones established by using these two drugs. Furthermore, the further developed resistant clones of both of the two cell lines established by using the two antagonists showed similar cross resistance effects. This observation may point out the existence of some other resistant mechanisms as cofactors of the p53 mutation, which may need some further experiments to reveal.

Since the GI_{50} values of the further developed resistant clones were much higher than their parental cell lines, and the variations were even bigger than that between HCT₁₁₆ p53^{+/+} and -/- cell lines, some further experiment may also need to be carried out to check if other mechanisms contribute to the overall resistance or not, although the observation that Nutlin-3 treated HCT₁₁₆ p53^{+/+} cells only experience cell cycle arrest but not apoptosis (143), could be an explanation for this phenomenon. One of the possible experiments for that purpose will be to introduce wild type p53 back into

the resistant cell clones and see if they can regain their sensitivity against MI-63 and Nutlin-3.

On the other hand, finding efficient strategies to kill resistant cell clones can be another research direction, which will obviously benefit patients experiencing clinical trials using MDM2/p53 antagonists and prevent unnecessary sacrifice of life.

Finally, I want to use a famous quote from an ancient Chinese poet Qu Yuan's poem 'Li Shao' to finish my thesis:

Though the journey towards the truth is very long, but I have urged on to seek after my dream!

路漫漫其修远兮，吾将上下而求索。

——屈原《离骚》

References

1. Soussi, T., Dehouche, K., and Beroud, C. (2000) p53 website and analysis of p53 gene mutations in human cancer: forging a link between epidemiology and carcinogenesis, *Human mutation* 15, 105-113.
2. Momand, J., Jung, D., Wilczynski, S., and Niland, J. (1998) The MDM2 gene amplification database, *Nucleic acids research* 26, 3453-3459.
3. Oliner, J. D., Kinzler, K. W., Meltzer, P. S., George, D. L., and Vogelstein, B. (1992) Amplification of a gene encoding a p53-associated protein in human sarcomas, *Nature* 358, 80-83.
4. Reifemberger, G., Liu, L., Ichimura, K., Schmidt, E. E., and Collins, V. P. (1993) Amplification and overexpression of the MDM2 gene in a subset of human malignant gliomas without p53 mutations, *Cancer research* 53, 2736-2739.
5. Takami, K., Inui, H., Nagayama, K., Watatani, M., Yasutomi, M., Kurahashi, H., Mori, T., Takai, S. I., and Nishisho, I. I. (1994) Low Grade Amplification of MDM2 Gene in a Subset of Human Breast Cancers without p53 Alterations, *Breast Cancer* 1, 95-102.
6. Hung, J., and Anderson, R. (1997) p53: functions, mutations and sarcomas, *Acta orthopaedica Scandinavica* 273, 68-73.
7. Lonardo, F., Ueda, T., Huvos, A. G., Healey, J., and Ladanyi, M. (1997) p53 and MDM2 alterations in osteosarcomas: correlation with clinicopathologic features and proliferative rate, *Cancer* 79, 1541-1547.
8. Picksley, S. M., and Lane, D. P. (1993) The p53-mdm2 autoregulatory feedback loop: a paradigm for the regulation of growth control by p53?, *Bioessays* 15, 689-690.
9. Wu, X., Bayle, J. H., Olson, D., and Levine, A. J. (1993) The p53-mdm-2 autoregulatory feedback loop, *Genes & development* 7, 1126-1132.
10. Momand, J., Zambetti, G. P., Olson, D. C., George, D., and Levine, A. J. (1992) The mdm-2 oncogene product forms a complex with the p53 protein and inhibits p53-mediated transactivation, *Cell* 69, 1237-1245.
11. Grasberger, B. L., Lu, T., Schubert, C., Parks, D. J., Carver, T. E., Koblisch, H. K., Cummings, M. D., LaFrance, L. V., Milkiewicz, K. L., Calvo, R. R., Maguire, D., Lattanze, J., Franks, C. F., Zhao, S., Ramachandren, K., Bylebyl, G. R., Zhang, M., Manthey, C. L., Petrella, E. C., Pantoliano, M. W., Deckman, I. C., Spurlino, J. C., Maroney, A. C., Tomczuk, B. E., Molloy, C. J., and Bone, R. F. (2005) Discovery and cocrystal structure of benzodiazepinedione HDM2 antagonists that activate p53 in cells, *Journal of medicinal chemistry* 48, 909-912.
12. Sakurai, K., Schubert, C., and Kahne, D. (2006) Crystallographic analysis of an 8-mer p53 peptide analogue complexed with MDM2, *Journal of the American Chemical Society* 128, 11000-11001.
13. Ding, K., Lu, Y., Nikolovska-Coleska, Z., Qiu, S., Ding, Y., Gao, W., Stuckey, J., Krajewski, K., Roller, P. P., Tomita, Y., Parrish, D. A., Deschamps, J. R., and

- Wang, S. (2005) Structure-based design of potent non-peptide MDM2 inhibitors, *Journal of the American Chemical Society* 127, 10130-10131.
14. Lu, F., Chi, S. W., Kim, D. H., Han, K. H., Kuntz, I. D., and Guy, R. K. (2006) Proteomimetic libraries: design, synthesis, and evaluation of p53-MDM2 interaction inhibitors, *Journal of combinatorial chemistry* 8, 315-325.
 15. Hardcastle, I. R., Ahmed, S. U., Atkins, H., Farnie, G., Golding, B. T., Griffin, R. J., Guyenne, S., Hutton, C., Kallblad, P., Kemp, S. J., Kitching, M. S., Newell, D. R., Norbedo, S., Northen, J. S., Reid, R. J., Saravanan, K., Willems, H. M., and Lunec, J. (2006) Small-molecule inhibitors of the MDM2-p53 protein-protein interaction based on an isoindolinone scaffold, *Journal of medicinal chemistry* 49, 6209-6221.
 16. Hardcastle, I. R., Ahmed, S. U., Atkins, H., Calvert, A. H., Curtin, N. J., Farnie, G., Golding, B. T., Griffin, R. J., Guyenne, S., Hutton, C., Kallblad, P., Kemp, S. J., Kitching, M. S., Newell, D. R., Norbedo, S., Northen, J. S., Reid, R. J., Saravanan, K., Willems, H. M., and Lunec, J. (2005) Isoindolinone-based inhibitors of the MDM2-p53 protein-protein interaction, *Bioorganic & medicinal chemistry letters* 15, 1515-1520.
 17. DeLeo, A. B., Jay, G., Appella, E., Dubois, G. C., Law, L. W., and Old, L. J. (1979) Detection of a transformation-related antigen in chemically induced sarcomas and other transformed cells of the mouse, *Proceedings of the National Academy of Sciences of the United States of America* 76, 2420-2424.
 18. Lane, D. P., and Crawford, L. V. (1979) T antigen is bound to a host protein in SV40-transformed cells, *Nature* 278, 261-263.
 19. Eliyahu, D., Raz, A., Gruss, P., Givol, D., and Oren, M. (1984) Participation of p53 cellular tumour antigen in transformation of normal embryonic cells, *Nature* 312, 646-649.
 20. Jenkins, J. R., Rudge, K., and Currie, G. A. (1984) Cellular immortalization by a cDNA clone encoding the transformation-associated phosphoprotein p53, *Nature* 312, 651-654.
 21. Jenkins, J. R., Rudge, K., Chumakov, P., and Currie, G. A. (1985) The cellular oncogene p53 can be activated by mutagenesis, *Nature* 317, 816-818.
 22. Eliyahu, D., Michalovitz, D., Eliyahu, S., Pinhasi-Kimhi, O., and Oren, M. (1989) Wild-type p53 can inhibit oncogene-mediated focus formation, *Proceedings of the National Academy of Sciences of the United States of America* 86, 8763-8767.
 23. Finlay, C. A., Hinds, P. W., and Levine, A. J. (1989) The p53 proto-oncogene can act as a suppressor of transformation, *Cell* 57, 1083-1093.
 24. Shaulsky, G., Goldfinger, N., Peled, A., and Rotter, V. (1991) Involvement of wild-type p53 protein in the cell cycle requires nuclear localization, *Cell Growth Differ* 2, 661-667.
 25. Lane, D. P. (1992) Cancer. p53, guardian of the genome, *Nature* 358, 15-16.
 26. Vogelstein, B., Lane, D., and Levine, A. J. (2000) Surfing the p53 network, *Nature* 408, 307-310.

27. Isobe, M., Emanuel, B. S., Givol, D., Oren, M., and Croce, C. M. (1986) Localization of gene for human p53 tumour antigen to band 17p13, *Nature* 320, 84-85.
28. Soussi, T., Caron de Fromental, C., Mechali, M., May, P., and Kress, M. (1987) Cloning and characterization of a cDNA from *Xenopus laevis* coding for a protein homologous to human and murine p53, *Oncogene* 1, 71-78.
29. Momand, J., Wu, H. H., and Dasgupta, G. (2000) MDM2--master regulator of the p53 tumour suppressor protein, *Gene* 242, 15-29.
30. Francoz, S., Froment, P., Bogaerts, S., De Clercq, S., Maetens, M., Doumont, G., Bellefroid, E., and Marine, J. C. (2006) Mdm4 and Mdm2 cooperate to inhibit p53 activity in proliferating and quiescent cells in vivo, *Proceedings of the National Academy of Sciences of the United States of America* 103, 3232-3237.
31. Marine, J. C., Francoz, S., Maetens, M., Wahl, G., Toledo, F., and Lozano, G. (2006) Keeping p53 in check: essential and synergistic functions of Mdm2 and Mdm4, *Cell death and differentiation* 13, 927-934.
32. Lu, H., and Levine, A. J. (1995) Human TAFII31 protein is a transcriptional coactivator of the p53 protein, *Proceedings of the National Academy of Sciences of the United States of America* 92, 5154-5158.
33. Thut, C. J., Chen, J. L., Klemm, R., and Tjian, R. (1995) p53 transcriptional activation mediated by coactivators TAFII40 and TAFII60, *Science (New York, N.Y)* 267, 100-104.
34. Gu, W., Shi, X. L., and Roeder, R. G. (1997) Synergistic activation of transcription by CBP and p53, *Nature* 387, 819-823.
35. Gu, W., and Roeder, R. G. (1997) Activation of p53 sequence-specific DNA binding by acetylation of the p53 C-terminal domain, *Cell* 90, 595-606.
36. Grossman, S. R. (2001) p300/CBP/p53 interaction and regulation of the p53 response, *Eur J Biochem* 268, 2773-2778.
37. Candau, R., Scolnick, D. M., Darpino, P., Ying, C. Y., Halazonetis, T. D., and Berger, S. L. (1997) Two tandem and independent sub-activation domains in the amino terminus of p53 require the adaptor complex for activity, *Oncogene* 15, 807-816.
38. Ohki, R., Kawase, T., Ohta, T., Ichikawa, H., and Taya, Y. (2007) Dissecting functional roles of p53 N-terminal transactivation domains by microarray expression analysis, *Cancer Sci* 98, 189-200.
39. Rajagopalan, S., Sade, R. S., Townsley, F. M., and Fersht, A. R. (2010) Mechanistic differences in the transcriptional activation of p53 by 14-3-3 isoforms, *Nucleic acids research* 38, 893-906.
40. Rajagopalan, S., Andreeva, A., Rutherford, T. J., and Fersht, A. R. (2010) Mapping the physical and functional interactions between the tumour suppressors p53 and BRCA2, *Proceedings of the National Academy of Sciences of the United States of America* 107, 8587-8592.
41. Walker, K. K., and Levine, A. J. (1996) Identification of a novel p53 functional domain that is necessary for efficient growth suppression, *Proceedings of the*

National Academy of Sciences of the United States of America 93, 15335-15340.

42. Muller-Tiemann, B. F., Halazonetis, T. D., and Elting, J. J. (1998) Identification of an additional negative regulatory region for p53 sequence-specific DNA binding, *Proceedings of the National Academy of Sciences of the United States of America* 95, 6079-6084.
43. Dornan, D., Shimizu, H., Burch, L., Smith, A. J., and Hupp, T. R. (2003) The proline repeat domain of p53 binds directly to the transcriptional coactivator p300 and allosterically controls DNA-dependent acetylation of p53, *Mol Cell Biol* 23, 8846-8861.
44. el-Deiry, W. S., Kern, S. E., Pietenpol, J. A., Kinzler, K. W., and Vogelstein, B. (1992) Definition of a consensus binding site for p53, *Nat Genet* 1, 45-49.
45. Qian, H., Wang, T., Naumovski, L., Lopez, C. D., and Brachmann, R. K. (2002) Groups of p53 target genes involved in specific p53 downstream effects cluster into different classes of DNA binding sites, *Oncogene* 21, 7901-7911.
46. Weinberg, R. L., Veprintsev, D. B., Bycroft, M., and Fersht, A. R. (2005) Comparative binding of p53 to its promoter and DNA recognition elements, *Journal of molecular biology* 348, 589-596.
47. Sykes, S. M., Mellert, H. S., Holbert, M. A., Li, K., Marmorstein, R., Lane, W. S., and McMahon, S. B. (2006) Acetylation of the p53 DNA-binding domain regulates apoptosis induction, *Mol Cell* 24, 841-851.
48. Sykes, S. M., Stanek, T. J., Frank, A., Murphy, M. E., and McMahon, S. B. (2009) Acetylation of the DNA binding domain regulates transcription-independent apoptosis by p53, *The Journal of biological chemistry* 284, 20197-20205.
49. Schlereth, K., Beinoraviciute-Kellner, R., Zeitlinger, M. K., Bretz, A. C., Sauer, M., Charles, J. P., Vogiatzi, F., Leich, E., Samans, B., Eilers, M., Kisker, C., Rosenwald, A., and Stiewe, T. (2010) DNA binding cooperativity of p53 modulates the decision between cell-cycle arrest and apoptosis, *Mol Cell* 38, 356-368.
50. Hollstein, M., Sidransky, D., Vogelstein, B., and Harris, C. C. (1991) p53 mutations in human cancers, *Science (New York, N.Y)* 253, 49-53.
51. Hollstein, M., Rice, K., Greenblatt, M. S., Soussi, T., Fuchs, R., Sorlie, T., Hovig, E., Smith-Sorensen, B., Montesano, R., and Harris, C. C. (1994) Database of p53 gene somatic mutations in human tumours and cell lines, *Nucleic acids research* 22, 3551-3555.
52. Hainaut, P., Soussi, T., Shomer, B., Hollstein, M., Greenblatt, M., Hovig, E., Harris, C. C., and Montesano, R. (1997) Database of p53 gene somatic mutations in human tumours and cell lines: updated compilation and future prospects, *Nucleic acids research* 25, 151-157.
53. Hainaut, P., Hernandez, T., Robinson, A., Rodriguez-Tome, P., Flores, T., Hollstein, M., Harris, C. C., and Montesano, R. (1998) IARC Database of p53 gene mutations in human tumours and cell lines: updated compilation, revised formats and new visualisation tools, *Nucleic acids research* 26, 205-213.

54. Liang, S. H., and Clarke, M. F. (2001) Regulation of p53 localization, *Eur J Biochem* 268, 2779-2783.
55. Hupp, T. R., and Lane, D. P. (1994) Allosteric activation of latent p53 tetramers, *Curr Biol* 4, 865-875.
56. Stommel, J. M., Marchenko, N. D., Jimenez, G. S., Moll, U. M., Hope, T. J., and Wahl, G. M. (1999) A leucine-rich nuclear export signal in the p53 tetramerization domain: regulation of subcellular localization and p53 activity by NES masking, *The EMBO journal* 18, 1660-1672.
57. Selivanova, G., Ryabchenko, L., Jansson, E., Iotsova, V., and Wiman, K. G. (1999) Reactivation of mutant p53 through interaction of a C-terminal peptide with the core domain, *Mol Cell Biol* 19, 3395-3402.
58. Ryan, K. M., Phillips, A. C., and Vousden, K. H. (2001) Regulation and function of the p53 tumour suppressor protein, *Curr Opin Cell Biol* 13, 332-337.
59. Kuerbitz, S. J., Plunkett, B. S., Walsh, W. V., and Kastan, M. B. (1992) Wild-type p53 is a cell cycle checkpoint determinant following irradiation, *Proceedings of the National Academy of Sciences of the United States of America* 89, 7491-7495.
60. Kesisis, T. D., Slebos, R. J., Nelson, W. G., Kastan, M. B., Plunkett, B. S., Han, S. M., Lorincz, A. T., Hedrick, L., and Cho, K. R. (1993) Human papillomavirus 16 E6 expression disrupts the p53-mediated cellular response to DNA damage, *Proceedings of the National Academy of Sciences of the United States of America* 90, 3988-3992.
61. Kastan, M. B., Zhan, Q., el-Deiry, W. S., Carrier, F., Jacks, T., Walsh, W. V., Plunkett, B. S., Vogelstein, B., and Fornace, A. J., Jr. (1992) A mammalian cell cycle checkpoint pathway utilizing p53 and GADD45 is defective in ataxia-telangiectasia, *Cell* 71, 587-597.
62. Liebermann, D. A., Hoffman, B., and Steinman, R. A. (1995) Molecular controls of growth arrest and apoptosis: p53-dependent and independent pathways, *Oncogene* 11, 199-210.
63. Oren, M. (2003) Decision making by p53: life, death and cancer, *Cell death and differentiation* 10, 431-442.
64. Yamamoto, H., Ozaki, T., Nakanishi, M., Kikuchi, H., Yoshida, K., Horie, H., Kuwano, H., and Nakagawara, A. (2007) Oxidative stress induces p53-dependent apoptosis in hepatoblastoma cell through its nuclear translocation, *Genes Cells* 12, 461-471.
65. Chylicki, K., Ehinger, M., Svedberg, H., Bergh, G., Olsson, I., and Gullberg, U. (2000) p53-mediated differentiation of the erythroleukemia cell line K562, *Cell Growth Differ* 11, 315-324.
66. Lin, T., Chao, C., Saito, S., Mazur, S. J., Murphy, M. E., Appella, E., and Xu, Y. (2005) p53 induces differentiation of mouse embryonic stem cells by suppressing Nanog expression, *Nature cell biology* 7, 165-171.
67. Bullock, A. N., and Fersht, A. R. (2001) Rescuing the function of mutant p53, *Nature reviews* 1, 68-76.

68. Vassilev, L. T. (2007) MDM2 inhibitors for cancer therapy, *Trends in molecular medicine* 13, 23-31.
69. Vousden, K. H., and Prives, C. (2005) P53 and prognosis: new insights and further complexity, *Cell* 120, 7-10.
70. Cho, Y., Gorina, S., Jeffrey, P. D., and Pavletich, N. P. (1994) Crystal structure of a p53 tumour suppressor-DNA complex: understanding tumourigenic mutations, *Science (New York, N.Y)* 265, 346-355.
71. Kitayner, M., Rozenberg, H., Kessler, N., Rabinovich, D., Shaulov, L., Haran, T. E., and Shakked, Z. (2006) Structural basis of DNA recognition by p53 tetramers, *Mol Cell* 22, 741-753.
72. Vousden, K. H., and Lu, X. (2002) Live or let die: the cell's response to p53, *Nature reviews* 2, 594-604.
73. Martins, C. P., Brown-Swigart, L., and Evan, G. I. (2006) Modeling the therapeutic efficacy of p53 restoration in tumours, *Cell* 127, 1323-1334.
74. Xue, W., Zender, L., Miething, C., Dickins, R. A., Hernando, E., Krizhanovsky, V., Cordon-Cardo, C., and Lowe, S. W. (2007) Senescence and tumour clearance is triggered by p53 restoration in murine liver carcinomas, *Nature* 445, 656-660.
75. Ventura, A., Kirsch, D. G., McLaughlin, M. E., Tuveson, D. A., Grimm, J., Lintault, L., Newman, J., Reczek, E. E., Weissleder, R., and Jacks, T. (2007) Restoration of p53 function leads to tumour regression in vivo, *Nature* 445, 661-665.
76. Bykov, V. J., Issaeva, N., Shilov, A., Hultcrantz, M., Pugacheva, E., Chumakov, P., Bergman, J., Wiman, K. G., and Selivanova, G. (2002) Restoration of the tumour suppressor function to mutant p53 by a low-molecular-weight compound, *Nature medicine* 8, 282-288.
77. Vassilev, L. T., Vu, B. T., Graves, B., Carvajal, D., Podlaski, F., Filipovic, Z., Kong, N., Kammlott, U., Lukacs, C., Klein, C., Fotouhi, N., and Liu, E. A. (2004) In vivo activation of the p53 pathway by small-molecule antagonists of MDM2, *Science (New York, N.Y)* 303, 844-848.
78. Lane, D. (2004) Anthony Dipple Carcinogenesis Award. p53 from pathway to therapy, *Carcinogenesis* 25, 1077-1081.
79. Corcoran, C. A., Huang, Y., and Sheikh, M. S. (2004) The p53 paddy wagon: COP1, Pirh2 and MDM2 are found resisting apoptosis and growth arrest, *Cancer biology & therapy* 3, 721-725.
80. Fakharzadeh, S. S., Trusko, S. P., and George, D. L. (1991) Tumourigenic potential associated with enhanced expression of a gene that is amplified in a mouse tumour cell line, *The EMBO journal* 10, 1565-1569.
81. Roth, J., Dobbelstein, M., Freedman, D. A., Shenk, T., and Levine, A. J. (1998) Nucleo-cytoplasmic shuttling of the hdm2 oncoprotein regulates the levels of the p53 protein via a pathway used by the human immunodeficiency virus rev protein, *The EMBO journal* 17, 554-564.
82. Lohrum, M. A., Ashcroft, M., Kubbutat, M. H., and Vousden, K. H. (2000) Identification of a cryptic nucleolar-localization signal in MDM2, *Nature cell biology* 2, 179-181.

83. Kawai, H., Wiederschain, D., and Yuan, Z. M. (2003) Critical contribution of the MDM2 acidic domain to p53 ubiquitination, *Mol Cell Biol* 23, 4939-4947.
84. Meulmeester, E., Frenk, R., Stad, R., de Graaf, P., Marine, J. C., Vousden, K. H., and Jochemsen, A. G. (2003) Critical role for a central part of Mdm2 in the ubiquitylation of p53, *Mol Cell Biol* 23, 4929-4938.
85. Schlott, T., Reimer, S., Jahns, A., Ohlenbusch, A., Ruschenburg, I., Nagel, H., and Droese, M. (1997) Point mutations and nucleotide insertions in the MDM2 zinc finger structure of human tumours, *J Pathol* 182, 54-61.
86. Tamborini, E., Della Torre, G., Lavarino, C., Azzarelli, A., Carpinelli, P., Pierotti, M. A., and Pilotti, S. (2001) Analysis of the molecular species generated by MDM2 gene amplification in liposarcomas, *International journal of cancer* 92, 790-796.
87. Yu, G. W., Allen, M. D., Andreeva, A., Fersht, A. R., and Bycroft, M. (2006) Solution structure of the C4 zinc finger domain of HDM2, *Protein Sci* 15, 384-389.
88. Haupt, Y., Maya, R., Kazaz, A., and Oren, M. (1997) Mdm2 promotes the rapid degradation of p53, *Nature* 387, 296-299.
89. Honda, R., Tanaka, H., and Yasuda, H. (1997) Oncoprotein MDM2 is a ubiquitin ligase E3 for tumour suppressor p53, *FEBS letters* 420, 25-27.
90. Kubbutat, M. H., Jones, S. N., and Vousden, K. H. (1997) Regulation of p53 stability by Mdm2, *Nature* 387, 299-303.
91. Fang, S., Jensen, J. P., Ludwig, R. L., Vousden, K. H., and Weissman, A. M. (2000) Mdm2 is a RING finger-dependent ubiquitin protein ligase for itself and p53, *The Journal of biological chemistry* 275, 8945-8951.
92. Geyer, R. K., Yu, Z. K., and Maki, C. G. (2000) The MDM2 RING-finger domain is required to promote p53 nuclear export, *Nature cell biology* 2, 569-573.
93. Boyd, S. D., Tsai, K. Y., and Jacks, T. (2000) An intact HDM2 RING-finger domain is required for nuclear exclusion of p53, *Nature cell biology* 2, 563-568.
94. Weber, J. D., Kuo, M. L., Bothner, B., DiGiammarino, E. L., Kriwacki, R. W., Roussel, M. F., and Sherr, C. J. (2000) Cooperative signals governing ARF-mdm2 interaction and nucleolar localization of the complex, *Mol Cell Biol* 20, 2517-2528.
95. Wang, X., Taplick, J., Geva, N., and Oren, M. (2004) Inhibition of p53 degradation by Mdm2 acetylation, *FEBS letters* 561, 195-201.
96. Marine, J. C., and Jochemsen, A. G. (2004) Mdmx and Mdm2: brothers in arms?, *Cell cycle (Georgetown, Tex)* 3, 900-904.
97. Jones, S. N., Roe, A. E., Donehower, L. A., and Bradley, A. (1995) Rescue of embryonic lethality in Mdm2-deficient mice by absence of p53, *Nature* 378, 206-208.
98. Montes de Oca Luna, R., Wagner, D. S., and Lozano, G. (1995) Rescue of early embryonic lethality in mdm2-deficient mice by deletion of p53, *Nature* 378, 203-206.
99. Barak, Y., Juven, T., Haffner, R., and Oren, M. (1993) mdm2 expression is induced by wild type p53 activity, *The EMBO journal* 12, 461-468.

100. Freedman, D. A., and Levine, A. J. (1999) Regulation of the p53 protein by the MDM2 oncoprotein--thirty-eighth G.H.A. Clowes Memorial Award Lecture, *Cancer research* 59, 1-7.
101. Unger, T., Juven-Gershon, T., Moallem, E., Berger, M., Vogt Sionov, R., Lozano, G., Oren, M., and Haupt, Y. (1999) Critical role for Ser20 of human p53 in the negative regulation of p53 by Mdm2, *The EMBO journal* 18, 1805-1814.
102. Moll, U. M., and Petrenko, O. (2003) The MDM2-p53 interaction, *Mol Cancer Res* 1, 1001-1008.
103. Zhang, and Wang, H. (2000) MDM2 oncogene as a novel target for human cancer therapy, *Current pharmaceutical design* 6, 393-416.
104. Bottger, A., Bottger, V., Sparks, A., Liu, W. L., Howard, S. F., and Lane, D. P. (1997) Design of a synthetic Mdm2-binding mini protein that activates the p53 response in vivo, *Curr Biol* 7, 860-869.
105. Chene, P., Fuchs, J., Bohn, J., Garcia-Echeverria, C., Furet, P., and Fabbro, D. (2000) A small synthetic peptide, which inhibits the p53-hdm2 interaction, stimulates the p53 pathway in tumour cell lines, *Journal of molecular biology* 299, 245-253.
106. Zhang, R., Wang, H., and Agrawal, S. (2005) Novel antisense anti-MDM2 mixed-backbone oligonucleotides: proof of principle, in vitro and in vivo activities, and mechanisms, *Current cancer drug targets* 5, 43-49.
107. Tortora, G., Caputo, R., Damiano, V., Bianco, R., Chen, J., Agrawal, S., Bianco, A. R., and Ciardiello, F. (2000) A novel MDM2 anti-sense oligonucleotide has anti-tumour activity and potentiates cytotoxic drugs acting by different mechanisms in human colon cancer, *International journal of cancer* 88, 804-809.
108. Sun, Y. (2003) Targeting E3 ubiquitin ligases for cancer therapy, *Cancer biology & therapy* 2, 623-629.
109. Lohrum, M. A., Ludwig, R. L., Kubbutat, M. H., Hanlon, M., and Vousden, K. H. (2003) Regulation of HDM2 activity by the ribosomal protein L11, *Cancer cell* 3, 577-587.
110. Dai, M. S., and Lu, H. (2004) Inhibition of MDM2-mediated p53 ubiquitination and degradation by ribosomal protein L5, *The Journal of biological chemistry* 279, 44475-44482.
111. Pomerantz, J., Schreiber-Agus, N., Liegeois, N. J., Silverman, A., Alland, L., Chin, L., Potes, J., Chen, K., Orlow, I., Lee, H. W., Cordon-Cardo, C., and DePinho, R. A. (1998) The Ink4a tumour suppressor gene product, p19Arf, interacts with MDM2 and neutralizes MDM2's inhibition of p53, *Cell* 92, 713-723.
112. Zhang, Y., Xiong, Y., and Yarbrough, W. G. (1998) ARF promotes MDM2 degradation and stabilizes p53: ARF-INK4a locus deletion impairs both the Rb and p53 tumour suppression pathways, *Cell* 92, 725-734.
113. Yang, Y., Ludwig, R. L., Jensen, J. P., Pierre, S. A., Medaglia, M. V., Davydov, I. V., Safiran, Y. J., Oberoi, P., Kenten, J. H., Phillips, A. C., Weissman, A. M., and Vousden, K. H. (2005) Small molecule inhibitors of HDM2 ubiquitin ligase activity stabilize and activate p53 in cells, *Cancer cell* 7, 547-559.

114. Wilson, J. M., Henderson, G., Black, F., Sutherland, A., Ludwig, R. L., Vousden, K. H., and Robins, D. J. (2007) Synthesis of 5-deazaflavin derivatives and their activation of p53 in cells, *Bioorganic & medicinal chemistry* **15**, 77-86.
115. Yang, Y., Kitagaki, J., Dai, R. M., Tsai, Y. C., Lorick, K. L., Ludwig, R. L., Pierre, S. A., Jensen, J. P., Davydov, I. V., Oberoi, P., Li, C. C., Kenten, J. H., Beutler, J. A., Vousden, K. H., and Weissman, A. M. (2007) Inhibitors of ubiquitin-activating enzyme (E1), a new class of potential cancer therapeutics, *Cancer research* **67**, 9472-9481.
116. Kussie, P. H., Gorina, S., Marechal, V., Elenbaas, B., Moreau, J., Levine, A. J., and Pavletich, N. P. (1996) Structure of the MDM2 oncoprotein bound to the p53 tumour suppressor transactivation domain, *Science (New York, N.Y)* **274**, 948-953.
117. Oliner, J. D., Pietenpol, J. A., Thiagalingam, S., Gyuris, J., Kinzler, K. W., and Vogelstein, B. (1993) Oncoprotein MDM2 conceals the activation domain of tumour suppressor p53, *Nature* **362**, 857-860.
118. Bottger, V., Bottger, A., Howard, S. F., Picksley, S. M., Chene, P., Garcia-Echeverria, C., Hochkeppel, H. K., and Lane, D. P. (1996) Identification of novel mdm2 binding peptides by phage display, *Oncogene* **13**, 2141-2147.
119. Wasyluk, C., Salvi, R., Argentini, M., Dureuil, C., Delumeau, I., Abecassis, J., Debussche, L., and Wasyluk, B. (1999) p53 mediated death of cells overexpressing MDM2 by an inhibitor of MDM2 interaction with p53, *Oncogene* **18**, 1921-1934.
120. Sakurai, K., Chung, H. S., and Kahne, D. (2004) Use of a retroinverso p53 peptide as an inhibitor of MDM2, *Journal of the American Chemical Society* **126**, 16288-16289.
121. Newman, D. J., Cragg, G. M., and Snader, K. M. (2003) Natural products as sources of new drugs over the period 1981-2002, *Journal of natural products* **66**, 1022-1037.
122. Stoll, R., Renner, C., Hansen, S., Palme, S., Klein, C., Belling, A., Zeslawski, W., Kamionka, M., Rehm, T., Muhlhahn, P., Schumacher, R., Hesse, F., Kaluza, B., Voelter, W., Engh, R. A., and Holak, T. A. (2001) Chalcone derivatives antagonize interactions between the human oncoprotein MDM2 and p53, *Biochemistry* **40**, 336-344.
123. Duncan, S. J., Gruschow, S., Williams, D. H., McNicholas, C., Purewal, R., Hajek, M., Gerlitz, M., Martin, S., Wrigley, S. K., and Moore, M. (2001) Isolation and structure elucidation of Chlorofusin, a novel p53-MDM2 antagonist from a *Fusarium* sp, *Journal of the American Chemical Society* **123**, 554-560.
124. Tsukamoto, S., Yoshida, T., Hosono, H., Ohta, T., and Yokosawa, H. (2006) Hexylitaconic acid: a new inhibitor of p53-HDM2 interaction isolated from a marine-derived fungus, *Arthrinium* sp, *Bioorganic & medicinal chemistry letters* **16**, 69-71.
125. Garcia-Echeverria, C., Chene, P., Blommers, M. J., and Furet, P. (2000) Discovery of potent antagonists of the interaction between human double

- minute 2 and tumour suppressor p53, *Journal of medicinal chemistry* 43, 3205-3208.
126. Banerjee, R., Basu, G., Chene, P., and Roy, S. (2002) Aib-based peptide backbone as scaffolds for helical peptide mimics, *J Pept Res* 60, 88-94.
 127. Majeux, N., Scarsi, M., and Caflisch, A. (2001) Efficient electrostatic solvation model for protein-fragment docking, *Proteins* 42, 256-268.
 128. Zhao, J., Wang, M., Chen, J., Luo, A., Wang, X., Wu, M., Yin, D., and Liu, Z. (2002) The initial evaluation of non-peptidic small-molecule HDM2 inhibitors based on p53-HDM2 complex structure, *Cancer letters* 183, 69-77.
 129. Galatin, P. S., and Abraham, D. J. (2004) A nonpeptidic sulfonamide inhibits the p53-mdm2 interaction and activates p53-dependent transcription in mdm2-overexpressing cells, *Journal of medicinal chemistry* 47, 4163-4165.
 130. Issaeva, N., Bozko, P., Enge, M., Protopopova, M., Verhoef, L. G., Masucci, M., Pramanik, A., and Selivanova, G. (2004) Small molecule RITA binds to p53, blocks p53-HDM-2 interaction and activates p53 function in tumours, *Nature medicine* 10, 1321-1328.
 131. Zhang, R., Mayhood, T., Lipari, P., Wang, Y., Durkin, J., Syto, R., Gesell, J., McNemar, C., and Windsor, W. (2004) Fluorescence polarization assay and inhibitor design for MDM2/p53 interaction, *Anal Biochem* 331, 138-146.
 132. Chen, L., Yin, H., Farooqi, B., Sebt, S., Hamilton, A. D., and Chen, J. (2005) p53 alpha-Helix mimetics antagonize p53/MDM2 interaction and activate p53, *Molecular cancer therapeutics* 4, 1019-1025.
 133. Ding, K., Lu, Y., Nikolovska-Coleska, Z., Wang, G., Qiu, S., Shangary, S., Gao, W., Qin, D., Stuckey, J., Krajewski, K., Roller, P. P., and Wang, S. (2006) Structure-based design of spiro-oxindoles as potent, specific small-molecule inhibitors of the MDM2-p53 interaction, *Journal of medicinal chemistry* 49, 3432-3435.
 134. Lu, Y., Nikolovska-Coleska, Z., Fang, X., Gao, W., Shangary, S., Qiu, S., Qin, D., and Wang, S. (2006) Discovery of a nanomolar inhibitor of the human murine double minute 2 (MDM2)-p53 interaction through an integrated, virtual database screening strategy, *Journal of medicinal chemistry* 49, 3759-3762.
 135. Arkin, M. R., and Wells, J. A. (2004) Small-molecule inhibitors of protein-protein interactions: progressing towards the dream, *Nat Rev Drug Discov* 3, 301-317.
 136. Espinoza-Fonseca, L. M. (2005) Targeting MDM2 by the small molecule RITA: towards the development of new multi-target drugs against cancer, *Theoretical biology & medical modelling* 2, 38.
 137. Krajewski, M., Ozdow, P., D'Silva, L., Rothweiler, U., and Holak, T. A. (2005) NMR indicates that the small molecule RITA does not block p53-MDM2 binding in vitro, *Nature medicine* 11, 1135-1136; author reply 1136-1137.
 138. Owicki, J. C. (2000) Fluorescence polarization and anisotropy in high throughput screening: perspectives and primer, *J Biomol Screen* 5, 297-306.

139. Knight, S. M., Umezawa, N., Lee, H. S., Gellman, S. H., and Kay, B. K. (2002) A fluorescence polarization assay for the identification of inhibitors of the p53-MDM2 protein-protein interaction, *Anal Biochem* 300, 230-236.
140. Vassilev, L. T. (2004) Small-molecule antagonists of p53-MDM2 binding: research tools and potential therapeutics, *Cell cycle (Georgetown, Tex* 3, 419-421.
141. Secchiero, P., Barbarotto, E., Tiribelli, M., Zerbinati, C., di Iasio, M. G., Gonelli, A., Cavazzini, F., Campioni, D., Fanin, R., Cuneo, A., and Zauli, G. (2006) Functional integrity of the p53-mediated apoptotic pathway induced by the nongenotoxic agent nutlin-3 in B-cell chronic lymphocytic leukemia (B-CLL), *Blood* 107, 4122-4129.
142. Coll-Mulet, L., Iglesias-Serret, D., Santidrian, A. F., Cosialls, A. M., de Frias, M., Castano, E., Campas, C., Barragan, M., de Sevilla, A. F., Domingo, A., Vassilev, L. T., Pons, G., and Gil, J. (2006) MDM2 antagonists activate p53 and synergize with genotoxic drugs in B-cell chronic lymphocytic leukemia cells, *Blood* 107, 4109-4114.
143. Tovar, C., Rosinski, J., Filipovic, Z., Higgins, B., Kolinsky, K., Hilton, H., Zhao, X., Vu, B. T., Qing, W., Packman, K., Myklebost, O., Heimbrook, D. C., and Vassilev, L. T. (2006) Small-molecule MDM2 antagonists reveal aberrant p53 signaling in cancer: implications for therapy, *Proceedings of the National Academy of Sciences of the United States of America* 103, 1888-1893.
144. Van Maerken, T., Speleman, F., Vermeulen, J., Lambertz, I., De Clercq, S., De Smet, E., Yigit, N., Coppens, V., Philippe, J., De Paepe, A., Marine, J. C., and Vandesompele, J. (2006) Small-Molecule MDM2 Antagonists as a New Therapy Concept for Neuroblastoma, *Cancer research* 66, 9646-9655.
145. Chene, P. (2004) Inhibition of the p53-hdm2 interaction with low molecular weight compounds, *Cell cycle (Georgetown, Tex* 3, 460-461.
146. Yu, S., Qin, D., Shangary, S., Chen, J., Wang, G., Ding, K., McEachern, D., Qiu, S., Nikolovska-Coleska, Z., Miller, R., Kang, S., Yang, D., and Wang, S. (2009) Potent and orally active small-molecule inhibitors of the MDM2-p53 interaction, *Journal of medicinal chemistry* 52, 7970-7973.
147. Azmi, A. S., Philip, P. A., Beck, F. W., Wang, Z., Banerjee, S., Wang, S., Yang, D., Sarkar, F. H., and Mohammad, R. M. (2010) MI-219-zinc combination: a new paradigm in MDM2 inhibitor-based therapy, *Oncogene*.
148. Azmi, A. S., Philip, P. A., Aboukameel, A., Wang, Z., Banerjee, S., Zafar, S. F., Goustin, A. S., Almhanna, K., Yang, D., Sarkar, F. H., and Mohammad, R. M. (2010) Reactivation of p53 by novel MDM2 inhibitors: implications for pancreatic cancer therapy, *Current cancer drug targets* 10, 319-331.
149. Mohammad, R. M., Wu, J., Azmi, A. S., Aboukameel, A., Sosin, A., Wu, S., Yang, D., Wang, S., and Al-Katib, A. M. (2009) An MDM2 antagonist (MI-319) restores p53 functions and increases the life span of orally treated follicular lymphoma bearing animals, *Mol Cancer* 8, 115.
150. Canner, J. A., Sobo, M., Ball, S., Hutzen, B., DeAngelis, S., Willis, W., Studebaker, A. W., Ding, K., Wang, S., Yang, D., and Lin, J. (2009) MI-63: a

- novel small-molecule inhibitor targets MDM2 and induces apoptosis in embryonal and alveolar rhabdomyosarcoma cells with wild-type p53, *Br J Cancer* 101, 774-781.
151. Shangary, S., Ding, K., Qiu, S., Nikolovska-Coleska, Z., Bauer, J. A., Liu, M., Wang, G., Lu, Y., McEachern, D., Bernard, D., Bradford, C. R., Carey, T. E., and Wang, S. (2008) Reactivation of p53 by a specific MDM2 antagonist (MI-43) leads to p21-mediated cell cycle arrest and selective cell death in colon cancer, *Molecular cancer therapeutics* 7, 1533-1542.
 152. Shvarts, A., Steegenga, W. T., Riteco, N., van Laar, T., Dekker, P., Bazuine, M., van Ham, R. C., van der Houven van Oordt, W., Hateboer, G., van der Eb, A. J., and Jochemsen, A. G. (1996) MDMX: a novel p53-binding protein with some functional properties of MDM2, *The EMBO journal* 15, 5349-5357.
 153. Shvarts, A., Bazuine, M., Dekker, P., Ramos, Y. F., Steegenga, W. T., Merckx, G., van Ham, R. C., van der Houven van Oordt, W., van der Eb, A. J., and Jochemsen, A. G. (1997) Isolation and identification of the human homolog of a new p53-binding protein, Mdmx, *Genomics* 43, 34-42.
 154. Marine, J. C., and Jochemsen, A. G. (2005) Mdmx as an essential regulator of p53 activity, *Biochem Biophys Res Commun* 331, 750-760.
 155. Gu, J., Kawai, H., Nie, L., Kitao, H., Wiederschain, D., Jochemsen, A. G., Parant, J., Lozano, G., and Yuan, Z. M. (2002) Mutual dependence of MDM2 and MDMX in their functional inactivation of p53, *The Journal of biological chemistry* 277, 19251-19254.
 156. Migliorini, D., Danovi, D., Colombo, E., Carbone, R., Pelicci, P. G., and Marine, J. C. (2002) Hdmx recruitment into the nucleus by Hdm2 is essential for its ability to regulate p53 stability and transactivation, *The Journal of biological chemistry* 277, 7318-7323.
 157. Li, C., Chen, L., and Chen, J. (2002) DNA damage induces MDMX nuclear translocation by p53-dependent and -independent mechanisms, *Mol Cell Biol* 22, 7562-7571.
 158. Parant, J., Chavez-Reyes, A., Little, N. A., Yan, W., Reinke, V., Jochemsen, A. G., and Lozano, G. (2001) Rescue of embryonic lethality in Mdm4-null mice by loss of Trp53 suggests a nonoverlapping pathway with MDM2 to regulate p53, *Nat Genet* 29, 92-95.
 159. Finch, R. A., Donoviel, D. B., Potter, D., Shi, M., Fan, A., Freed, D. D., Wang, C. Y., Zambrowicz, B. P., Ramirez-Solis, R., Sands, A. T., and Zhang, N. (2002) mdmx is a negative regulator of p53 activity in vivo, *Cancer research* 62, 3221-3225.
 160. Migliorini, D., Lazzerini Denchi, E., Danovi, D., Jochemsen, A., Capillo, M., Gobbi, A., Helin, K., Pelicci, P. G., and Marine, J. C. (2002) Mdm4 (Mdmx) regulates p53-induced growth arrest and neuronal cell death during early embryonic mouse development, *Mol Cell Biol* 22, 5527-5538.
 161. Danovi, D., Meulmeester, E., Pasini, D., Migliorini, D., Capra, M., Frenk, R., de Graaf, P., Francoz, S., Gasparini, P., Gobbi, A., Helin, K., Pelicci, P. G., Jochemsen, A. G., and Marine, J. C. (2004) Amplification of Mdmx (or Mdm4)

- directly contributes to tumour formation by inhibiting p53 tumour suppressor activity, *Mol Cell Biol* 24, 5835-5843.
162. Ramos, Y. F., Stad, R., Attema, J., Peltenburg, L. T., van der Eb, A. J., and Jochemsen, A. G. (2001) Aberrant expression of HDMX proteins in tumour cells correlates with wild-type p53, *Cancer research* 61, 1839-1842.
 163. Riemenschneider, M. J., Buschges, R., Wolter, M., Reifemberger, J., Bostrom, J., Kraus, J. A., Schlegel, U., and Reifemberger, G. (1999) Amplification and overexpression of the MDM4 (MDMX) gene from 1q32 in a subset of malignant gliomas without TP53 mutation or MDM2 amplification, *Cancer research* 59, 6091-6096.
 164. Laurie, N. A., Donovan, S. L., Shih, C. S., Zhang, J., Mills, N., Fuller, C., Teunisse, A., Lam, S., Ramos, Y., Mohan, A., Johnson, D., Wilson, M., Rodriguez-Galindo, C., Quarto, M., Francoz, S., Mendrysa, S. M., Guy, R. K., Marine, J. C., Jochemsen, A. G., and Dyer, M. A. (2006) Inactivation of the p53 pathway in retinoblastoma, *Nature* 444, 61-66.
 165. Hu, B., Gilkes, D. M., Farooqi, B., Sebt, S. M., and Chen, J. (2006) MDMX overexpression prevents p53 activation by the MDM2 inhibitor Nutlin, *The Journal of biological chemistry* 281, 33030-33035.
 166. Patton, J. T., Mayo, L. D., Singhi, A. D., Gudkov, A. V., Stark, G. R., and Jackson, M. W. (2006) Levels of HdmX expression dictate the sensitivity of normal and transformed cells to Nutlin-3, *Cancer research* 66, 3169-3176.
 167. Bo, M. D., Secchiero, P., Degan, M., Marconi, D., Bomben, R., Pozzato, G., Gaidano, G., Del Poeta, G., Forconi, F., Zauli, G., and Gattei, V. (2010) MDM4 (MDMX) is overexpressed in chronic lymphocytic leukaemia (CLL) and marks a subset of p53wild-type CLL with a poor cytotoxic response to Nutlin-3, *Br J Haematol* 150, 237-239.
 168. Popowicz, G. M., Czarna, A., and Holak, T. A. (2008) Structure of the human Mdmx protein bound to the p53 tumour suppressor transactivation domain, *Cell cycle (Georgetown, Tex)* 7, 2441-2443.
 169. Li, C., Pazgier, M., Yuan, W., Liu, M., Wei, G., Lu, W. Y., and Lu, W. (2010) Systematic mutational analysis of peptide inhibition of the p53-MDM2/MDMX interactions, *Journal of molecular biology* 398, 200-213.
 170. Macchiarulo, A., and Pellicciari, R. (2009) MDM2/MDMX inhibitor peptide: WO2008106507, *Expert Opin Ther Pat* 19, 721-726.
 171. Czarna, A., Popowicz, G. M., Pecak, A., Wolf, S., Dubin, G., and Holak, T. A. (2009) High affinity interaction of the p53 peptide-analogue with human Mdm2 and Mdmx, *Cell cycle (Georgetown, Tex)* 8, 1176-1184.
 172. Pazgier, M., Liu, M., Zou, G., Yuan, W., Li, C., Li, J., Monbo, J., Zella, D., Tarasov, S. G., and Lu, W. (2009) Structural basis for high-affinity peptide inhibition of p53 interactions with MDM2 and MDMX, *Proceedings of the National Academy of Sciences of the United States of America* 106, 4665-4670.
 173. Kallen, J., Goepfert, A., Blechschmidt, A., Izaac, A., Geiser, M., Tavares, G., Ramage, P., Furet, P., Masuya, K., and Lisztwan, J. (2009) Crystal Structures of Human MdmX (HdmX) in Complex with p53 Peptide Analogues Reveal

- Surprising Conformational Changes, *The Journal of biological chemistry* 284, 8812-8821.
174. Engvall, E., and Perlmann, P. (1971) Enzyme-linked immunosorbent assay (ELISA). Quantitative assay of immunoglobulin G, *Immunochemistry* 8, 871-874.
 175. Sigalas, I., Calvert, A. H., Anderson, J. J., Neal, D. E., and Lunec, J. (1996) Alternatively spliced mdm2 transcripts with loss of p53 binding domain sequences: transforming ability and frequent detection in human cancer, *Nature medicine* 2, 912-917.
 176. Brodeur, G. M., Sekhon, G., and Goldstein, M. N. (1977) Chromosomal aberrations in human neuroblastomas, *Cancer* 40, 2256-2263.
 177. Brattain, M. G., Fine, W. D., Khaled, F. M., Thompson, J., and Brattain, D. E. (1981) Heterogeneity of malignant cells from a human colonic carcinoma, *Cancer research* 41, 1751-1756.
 178. Brattain, M. G., Brattain, D. E., Fine, W. D., Khaled, F. M., Marks, M. E., Kimball, P. M., Arcolano, L. A., and Danbury, B. H. (1981) Initiation and characterization of cultures of human colonic carcinoma with different biological characteristics utilizing feeder layers of confluent fibroblasts, *Oncodev Biol Med* 2, 355-366.
 179. Bunz, F., Dutriaux, A., Lengauer, C., Waldman, T., Zhou, S., Brown, J. P., Sedivy, J. M., Kinzler, K. W., and Vogelstein, B. (1998) Requirement for p53 and p21 to sustain G2 arrest after DNA damage, *Science (New York, N.Y)* 282, 1497-1501.
 180. Skehan, P., Storeng, R., Scudiero, D., Monks, A., McMahon, J., Vistica, D., Warren, J. T., Bokesch, H., Kenney, S., and Boyd, M. R. (1990) New colourimetric cytotoxicity assay for anticancer-drug screening, *J Natl Cancer Inst* 82, 1107-1112.
 181. Zabaglo, L., Ormerod, M. G., and Dowsett, M. (2000) Measurement of markers for breast cancer in a model system using laser scanning cytometry, *Cytometry* 41, 166-171.
 182. Saiki, R. K., Gelfand, D. H., Stoffel, S., Scharf, S. J., Higuchi, R., Horn, G. T., Mullis, K. B., and Erlich, H. A. (1988) Primer-directed enzymatic amplification of DNA with a thermostable DNA polymerase, *Science (New York, N.Y)* 239, 487-491.
 183. Lipinski, C. A., Lombardo, F., Dominy, B. W., and Feeney, P. J. (2001) Experimental and computational approaches to estimate solubility and permeability in drug discovery and development settings, *Adv Drug Deliv Rev* 46, 3-26.
 184. Green, M. N., Josimovich, J. B., Tsou, K. C., and Seligman, A. M. (1956) Nitroreductase activity of animal tissues and of normal and neoplastic human tissues, *Cancer* 9, 176-182.
 185. O'Brien, P. J., Wong, W. C., Silva, J., and Khan, S. (1990) Toxicity of nitrobenzene compounds towards isolated hepatocytes: dependence on reduction potential, *Xenobiotica* 20, 945-955.

186. Canman, C. E., Lim, D. S., Cimprich, K. A., Taya, Y., Tamai, K., Sakaguchi, K., Appella, E., Kastan, M. B., and Siliciano, J. D. (1998) Activation of the ATM kinase by ionizing radiation and phosphorylation of p53, *Science (New York, N.Y)* **281**, 1677-1679.
187. Peddibhotla, S., Jayakumar, S., and Tepe, J. J. (2002) Highly diastereoselective multicomponent synthesis of unsymmetrical imidazolines, *Org Lett* **4**, 3533-3535.
188. Murray, J. K., and Gellman, S. H. (2007) Targeting protein-protein interactions: Lessons from p53/MDM2, *Biopolymers*.
189. Shangary, S., and Wang, S. (2009) Small-molecule inhibitors of the MDM2-p53 protein-protein interaction to reactivate p53 function: a novel approach for cancer therapy, *Annu Rev Pharmacol Toxicol* **49**, 223-241.
190. Galipeau, P. C., Cowan, D. S., Sanchez, C. A., Barrett, M. T., Emond, M. J., Levine, D. S., Rabinovitch, P. S., and Reid, B. J. (1996) 17p (p53) allelic losses, 4N (G2/tetraploid) populations, and progression to aneuploidy in Barrett's esophagus, *Proceedings of the National Academy of Sciences of the United States of America* **93**, 7081-7084.
191. Michaelis, M., Rothweiler, F., Klassert, D., von Deimling, A., Weber, K., Fehse, B., Kammerer, B., Doerr, H. W., and Cinatl, J., Jr. (2009) Reversal of P-glycoprotein-mediated multidrug resistance by the murine double minute 2 antagonist nutlin-3, *Cancer research* **69**, 416-421.
192. Cao, C., Shinohara, E. T., Subhawong, T. K., Geng, L., Woon Kim, K., Albert, J. M., Hallahan, D. E., and Lu, B. (2006) Radiosensitization of lung cancer by nutlin, an inhibitor of murine double minute 2, *Molecular cancer therapeutics* **5**, 411-417.
193. Supiot, S., Hill, R. P., and Bristow, R. G. (2008) Nutlin-3 radiosensitizes hypoxic prostate cancer cells independent of p53, *Molecular cancer therapeutics* **7**, 993-999.
194. Arya, A. K., El-Fert, A., Devling, T., Eccles, R. M., Aslam, M. A., Rubbi, C. P., Vlatkovic, N., Fenwick, J., Lloyd, B. H., Sibson, D. R., Jones, T. M., and Boyd, M. T. (2010) Nutlin-3, the small-molecule inhibitor of MDM2, promotes senescence and radiosensitises laryngeal carcinoma cells harbouring wild-type p53, *Br J Cancer* **103**, 186-195.

Appendix I

Potent Isoindolin-1-one compounds and MDM2 protein binding mode prediction

Background

The IC₅₀ evaluation and investigation of cellular effects for the isoindolin-1-one scaffold compounds not only confirmed the inhibitory effect of these compounds on the p53/MDM2 interaction, but also enabled us to examine the correlation between compound structures and their activities. However, further structure design and development based on the isoindolin-1-one scaffold was encumbered with some technical handicaps. Firstly, all the synthesized isoindolin-1-one compounds were racemic mixtures because of their chiral carbons. Although we have already successfully separated some of them, we have not confirmed their solid stereo-structures without their crystal structure analysis data; secondly, so far we still have not obtained the co-crystal structure of an isoindolin-1-one compound binding with MDM2. As a result, it is important for us to predict their binding mode for a better understanding of structure activity relationship of isoindolin-1-one compounds, which benefit further structure design and drug development.

As a result, both docking software and manual docking were applied for binding mode prediction.

Results

1. MDM2 protein structures selection and docking software training

By reviewing all the literature corresponding to MDM2/p53 related co-crystal structure analysis, we have selected 1YCR (MDM2 BOUND TO THE TRANSACTIVATION DOMAIN OF P53), 1RV1 (CRYSTAL STRUCTURE OF HUMAN MDM2 WITH AN IMIDAZOLINE INHIBITOR), 1T4F (MDM2 in complex with an optimized p53 peptide) and 2GV2 (MDM2 in complex with an 8-mer p53 peptide analogue) for docking mode prediction. Then by applying Molegro Virtual Docker software, we have isolated MDM2 protein, p53 peptide, Nutlin-2 optimized p53 peptide, and 8-mer p53 peptide for MDM2 protein work space generating and docking software learning purpose.

The published co-crystal structures of 1YCR, 1RV1, 1T4F and 2GV2 with each correlated MDM2 protein binding pockets were displayed in [Appendix I Figure 1](#) and [Appendix I Figure 2](#). The MDM2 proteins were shown as electrostatic solid protein surfaces, p53 relative peptides or Nutlin-2 compounds were shown as thin sticks with colour coded elements (CPK).

The images in [Appendix I Figure 1](#) display the interaction of ligands with MDM2 proteins. Interestingly, a cofactor $[SO_4^{2-}]$ was used in the generating of 1T4F co-crystal structure, and in the 1RV1 interaction structure image, we can find another Nutlin-2 binding with the MDM2 protein in another position close to the positive charged area near the cofactor functional area of MDM2 in 1RV1, which might indicate that this Nutlin-2 act as an cofactor for crystalisation; furthermore, the extended p53 peptide

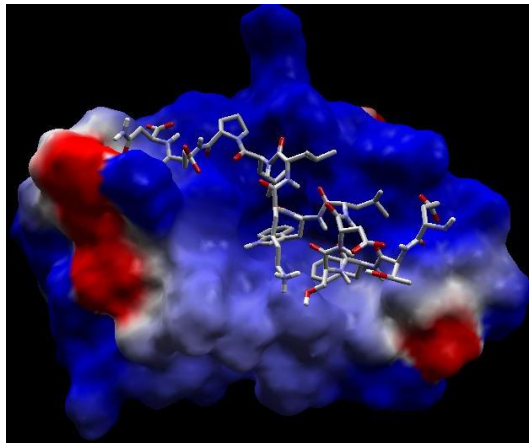
side-chain in 1YCR also formed some H-bond interaction with the positive charged area of MDM2 protein. However, this kind of cofactor effect had not been displayed in 2GV2 co-crystal structure.

On the other hand, the images of 1RV1, 1T4F and 2GV2 co-crystal structures had also displayed the interaction between ligands and water molecules, which may contribute to positioning side chains of ligands into the MDM2 binding pockets and enhancing the binding potency.

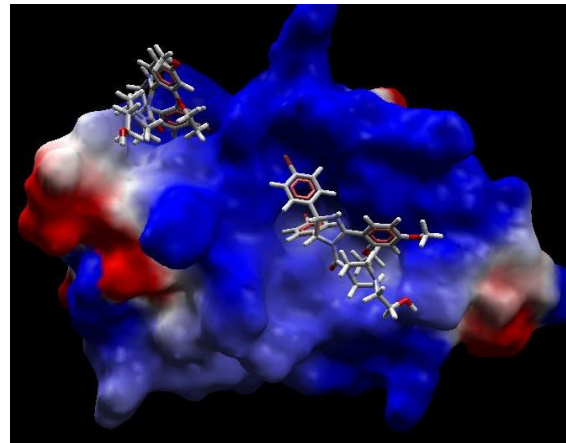
The four images in [Appendix I Figure 2](#) illustrate the shape and depth of the MDM2 protein hydrophobic clefts formed by binding with p53 related peptides or the same position binding with Nutlin-2. These images indicate that the difference of shape and atom characters of ligand can influence the hydrophobic binding pocket of the MDM2 protein. As a result, we have to evaluate and select the most suitable workspace for virtual docking analysis of the isoindolin-1-one scaffold compounds.

Appendix I Figure 1. Reproduction images of published co-crystal structure of 1YCR, 1RV1, 1T4F and 2GV2.

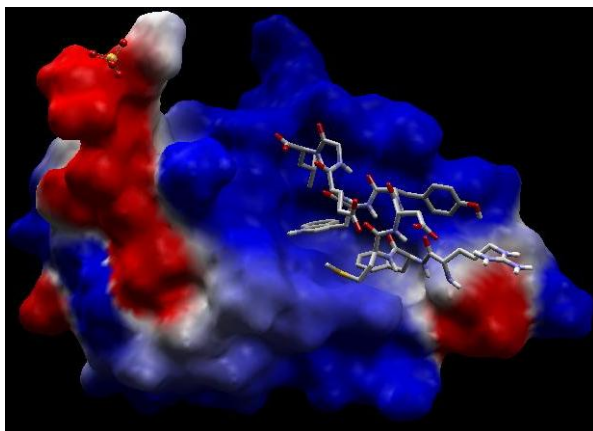
1YCR:



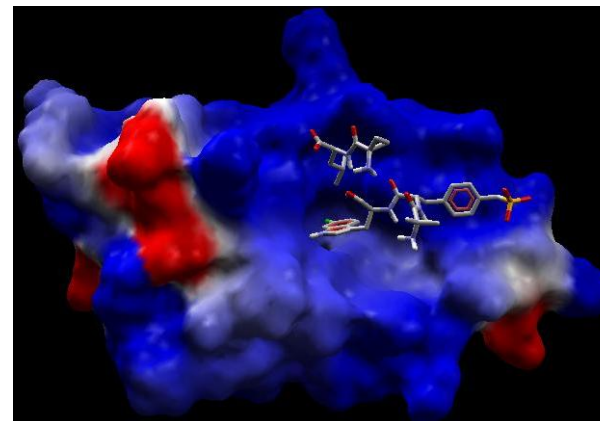
1RV1:



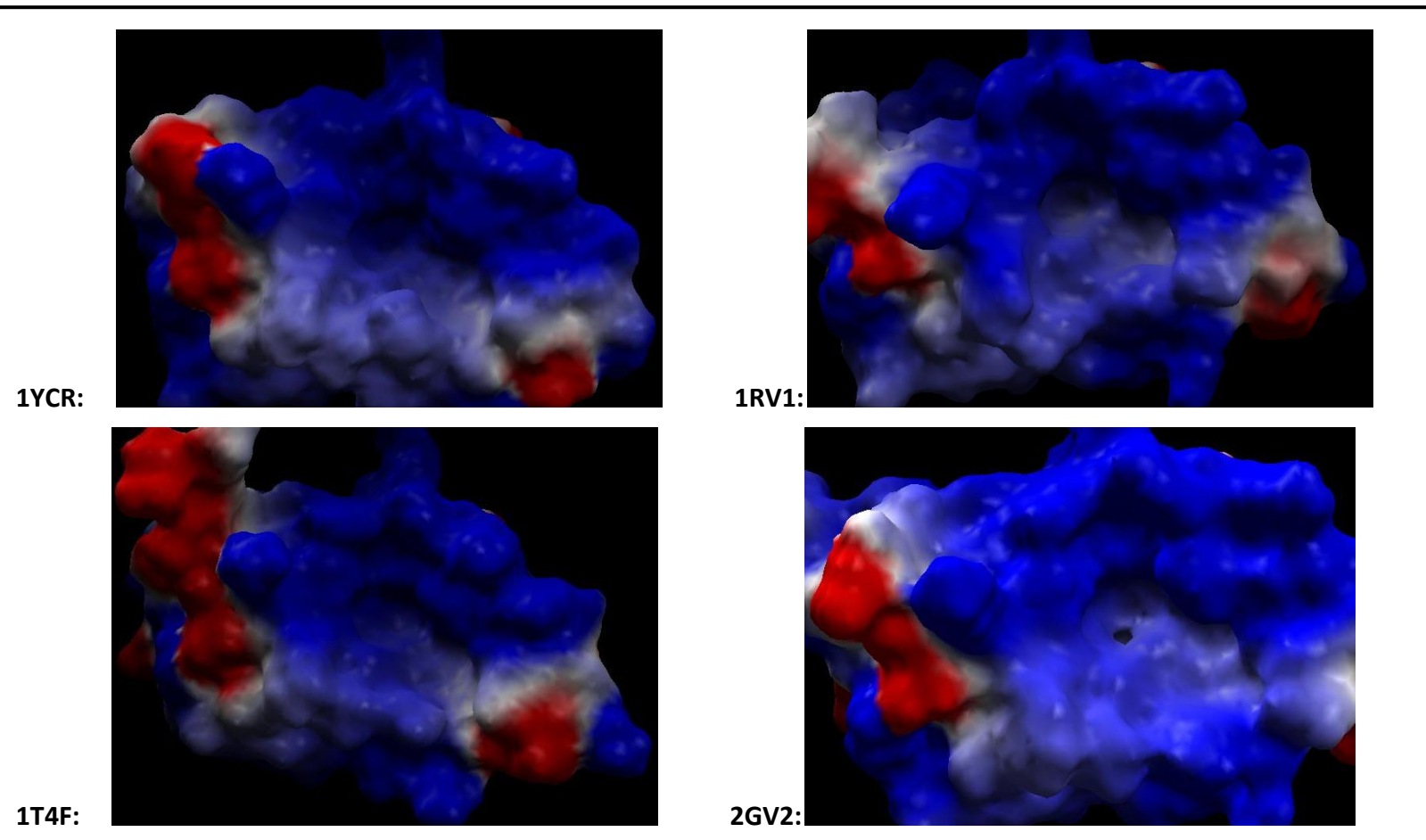
1T4F:



2GV2:



Appendix I Figure 2. Reproduced hydrophobic binding pocket images of MDM2 protein in 1YCR, 1RV1, 1T4F and 2GV2.



2. MDM2 and isoindolin-1-one compounds binding mode prediction and comparison

By using the three MDM2/p53 related co-crystal structure data, we have created three MDM2 protein workspaces and tried to generate MDM2 binding mode models for a progressive series of isoindolin-1-one compounds (NU8260, NU8354, NU8399, NU8406 and NCL-00016149) using Molegro Virtual Docker software (Nutlin-2 was used as positive control for prediction accuracy validation). Then highest ranked docking result of each MDM2 protein workspace was picked out and images were taken for further SAR analysis. Key compound binding modes with every workspace and docking score results were illustrated in [Appendix I Table 1](#).

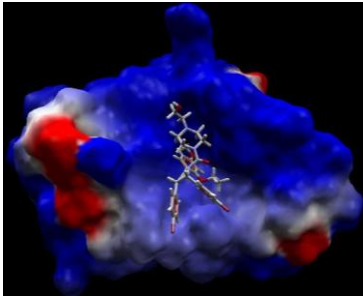
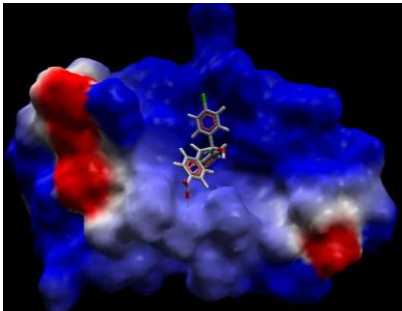
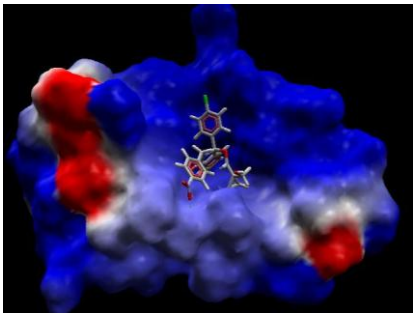
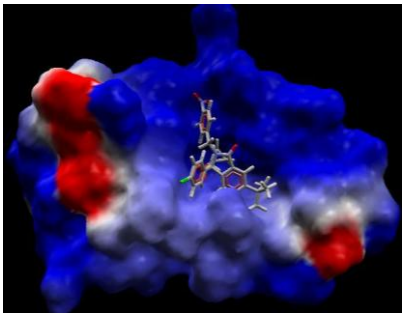
The virtual docking results in [Appendix I Table 1](#) indicate that different workspaces can produce different top scored binding modes for each compound and the water solvent molecules can also affect the binding mode. As a result, we have to consider the docking score together with ELISA IC₅₀ value of each compound to determine the most suitable workspace, and water solution effect to be considered.

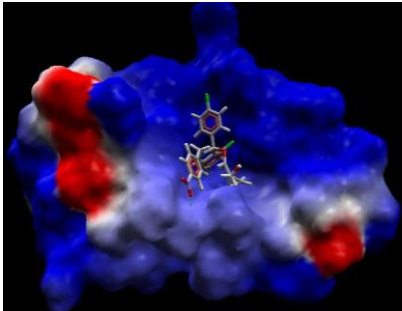
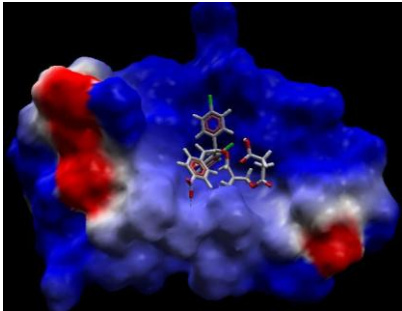
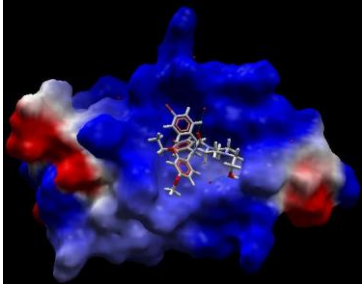
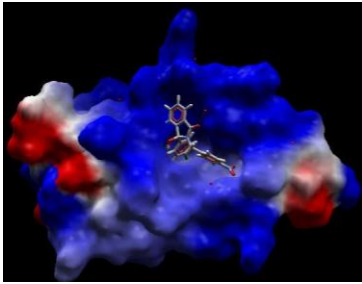
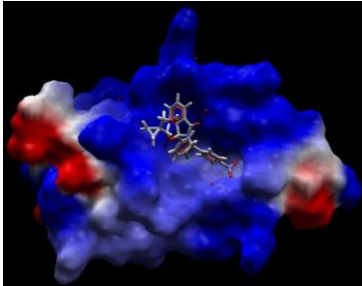
By comparing the scatter charts for correlation of the docking scores with the IC₅₀ values of isoindolin-1-one scaffold key compounds ([Appendix I Figure 3](#)) together with the reproduced Nutlin-2 binding modes ([Appendix I Table 1](#)), it was noted that the docking results generated by using the 1T4F and the 2GV2 workspace including the effect of water molecules produced the more reliable and most favourable binding modes for every compound. Furthermore, some other isoindolin-1-one docking mode

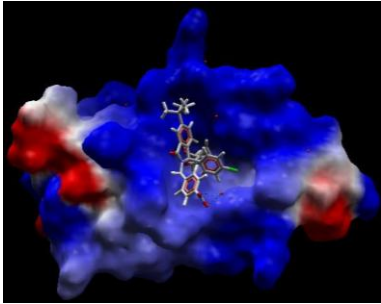
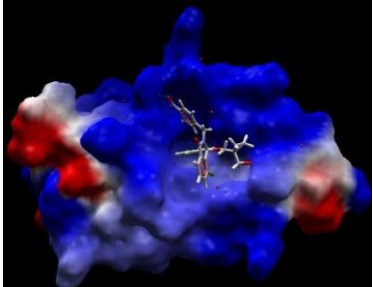
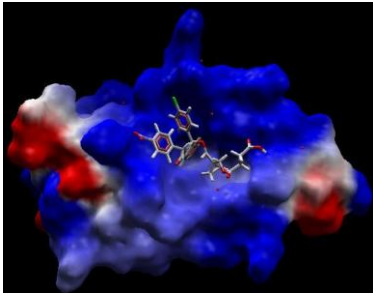
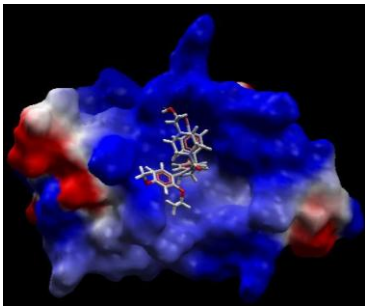
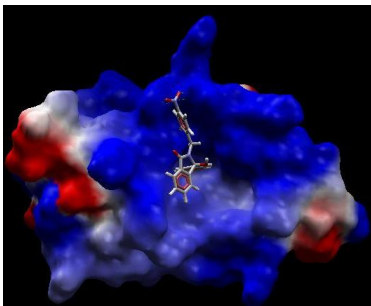
predictions with MDM2 produced by using other workspaces were also produced by using 2GV2 workspace containing solution effect with higher docking energy, which indicated a less favourable binding possibility. As a result, the 2GV2 structure workspace including solvent effect was applied for further binding mode predictions.

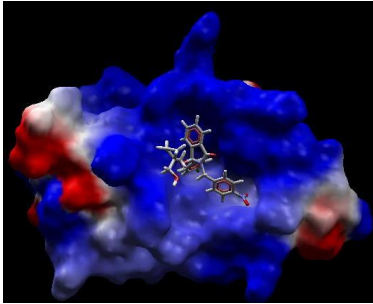
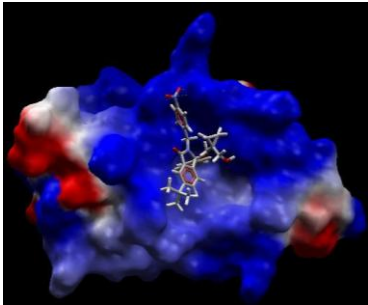
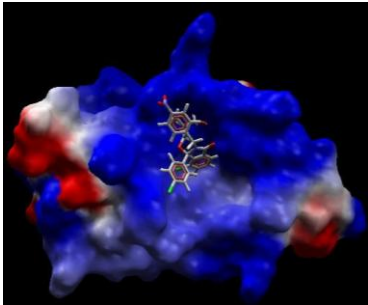
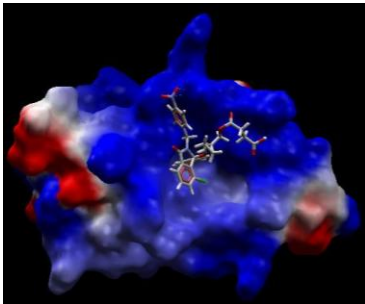
By using the 2GV2 structure incorporating the effect of water molecules, I then generated and compared the binding mode and energy of the key isoindolin-1-one compounds enantiomers ([Appendix I Table 2](#)) for further SAR analysis. It is noted that the docking scores have indicated the same side-chain positions for all the pure enantiomers, i.e. all potent enantiomers have shown the same side-chain orientation (*S*), whereas all the less potent enantiomers have the opposite orientation (*R*), although the binding mode for NU8399 enantiomers are apparently different from the NU8354 and NU8406 enantiomers.

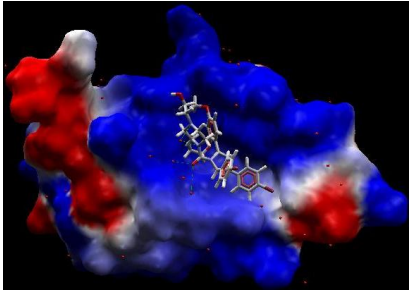
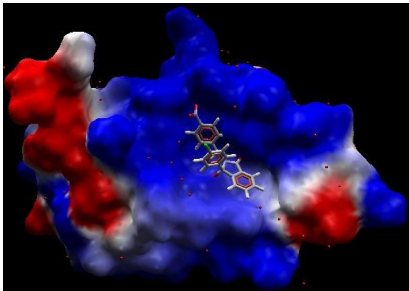
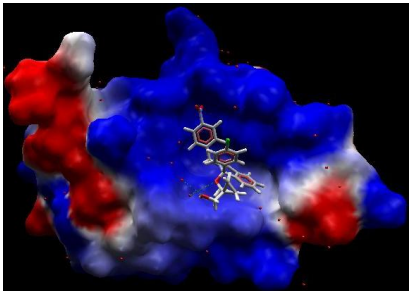
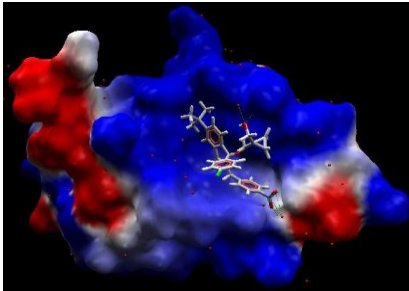
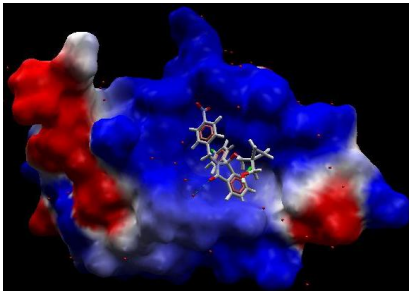
Appendix I Table 1. Virtual docking predicted binding modes and scores of the published MDM2 crystal structures of 1YCR, 1RV1, 1T4F and 2GV2 binding with Nutlin-2 and isoindolin-1-one scaffold key compounds.

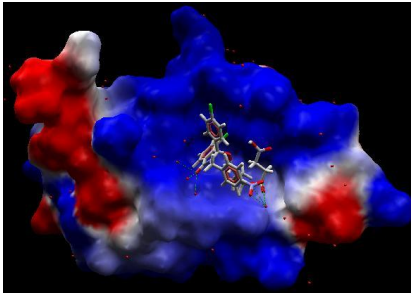
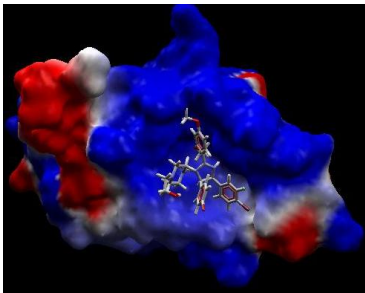
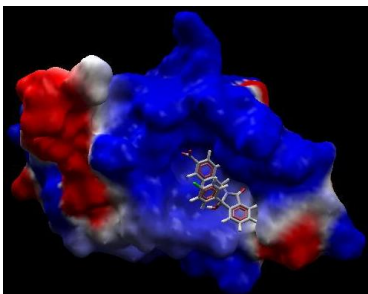
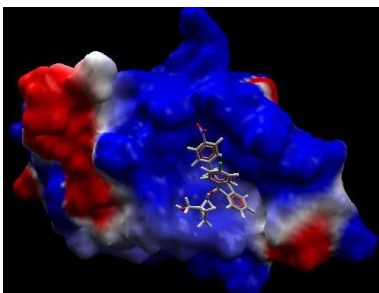
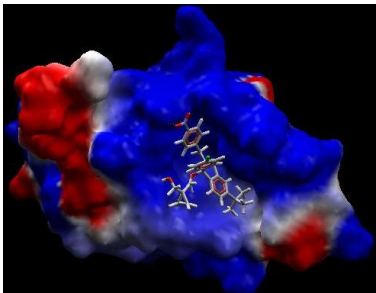
Workspace Name	Compounds Code	Binding Mode	MolDock Score
1YCR	Nutlin-2		-139.654
1YCR	NU8260		-104.358
1YCR	NU8354		-130.448
1YCR	NU8399		-126.237

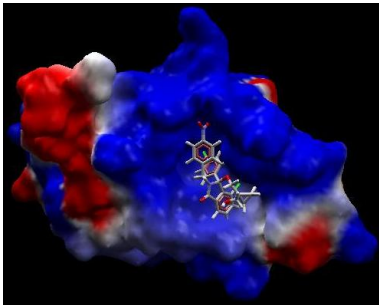
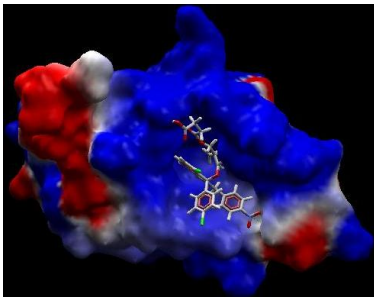
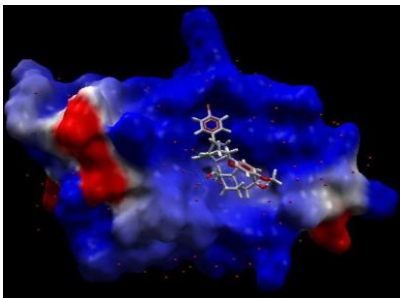
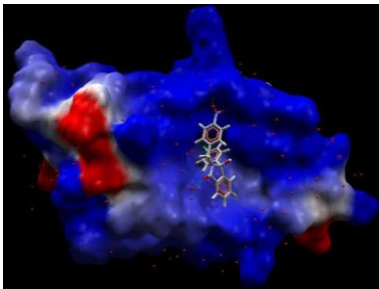
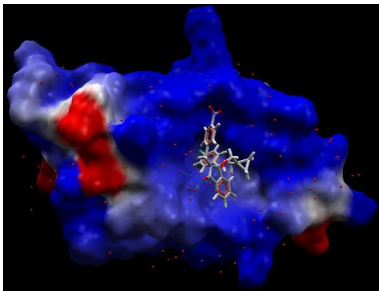
1YCR	NU8406		-133.184
1YCR	NCL-00016149		-146.711
1RV1+H ₂ O	Nutlin-2		-140.733
1RV1+H ₂ O	NU8260		-110.197
1RV1+H ₂ O	NU8354		-130.977

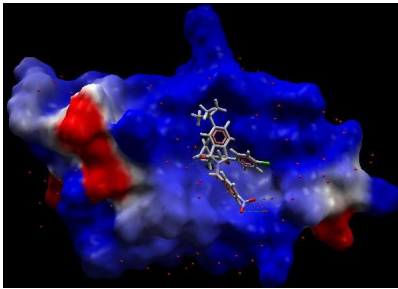
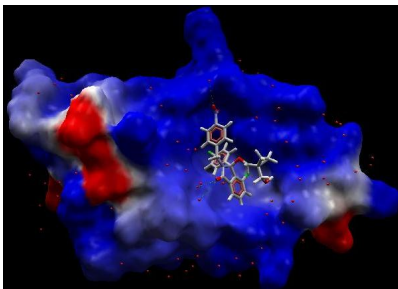
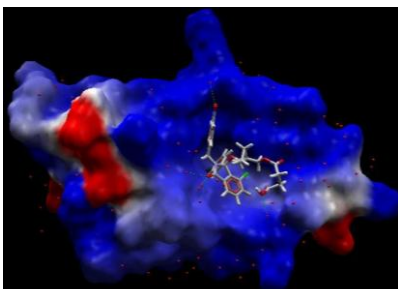
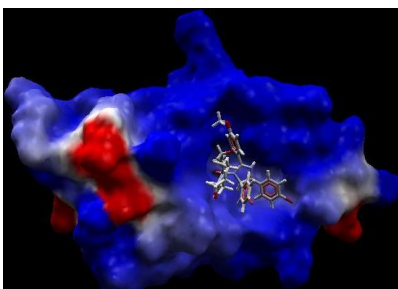
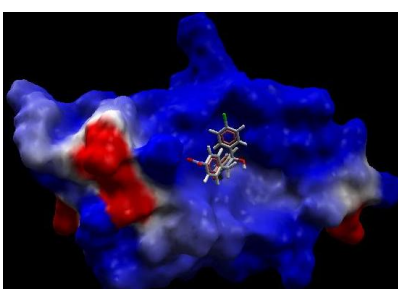
1RV1+H ₂ O	NU8399		-127.134
1RV1+H ₂ O	NU8406		-121.363
1RV1+H ₂ O	NCL-00016149		-137.408
1RV1-H ₂ O	Nutlin-2		-160.626
1RV1-H ₂ O	NU8260		-108.594

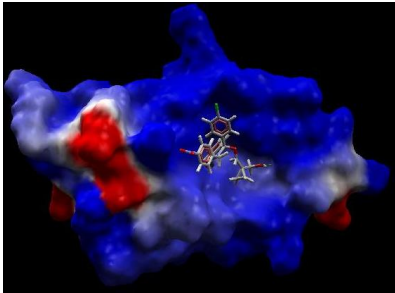
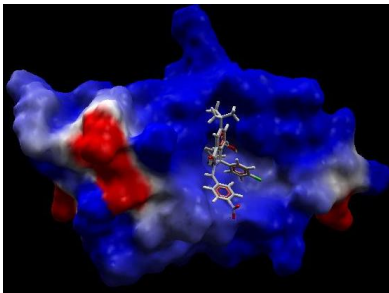
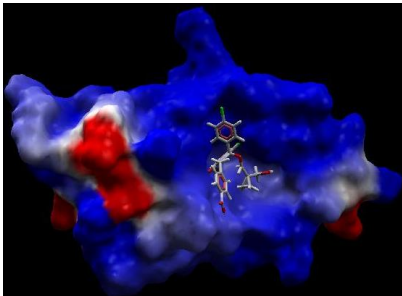
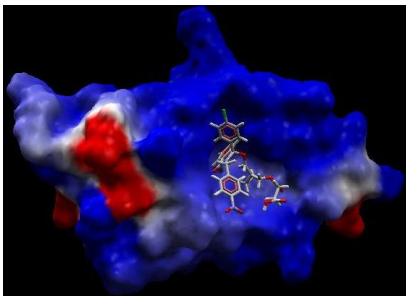
1RV1-H ₂ O	NU8354		-127.019
1RV1-H ₂ O	NU8399		-120.545
1RV1-H ₂ O	NU8406		-134.294
1RV1-H ₂ O	NCL-00016149		-144.844

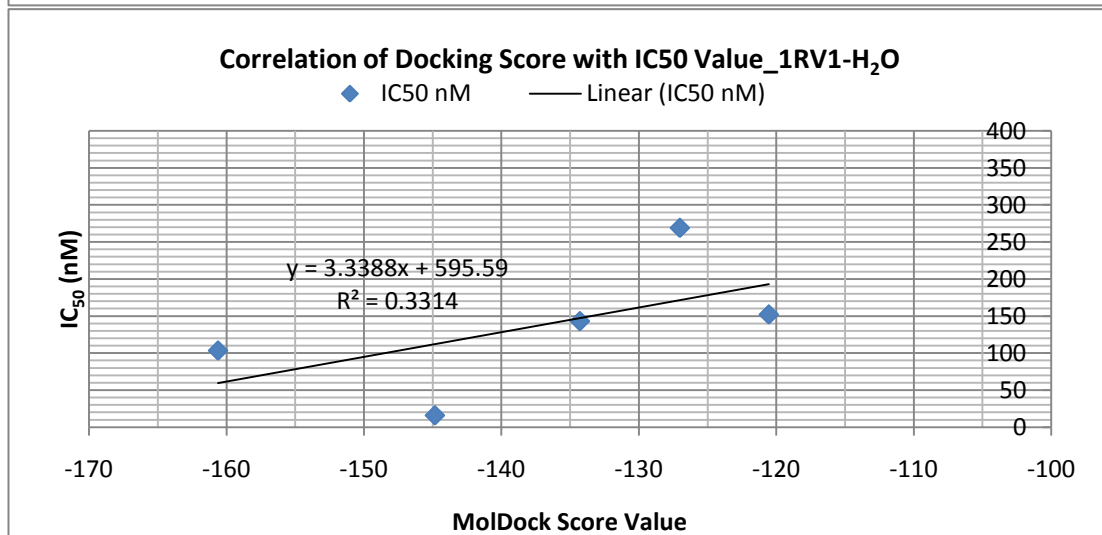
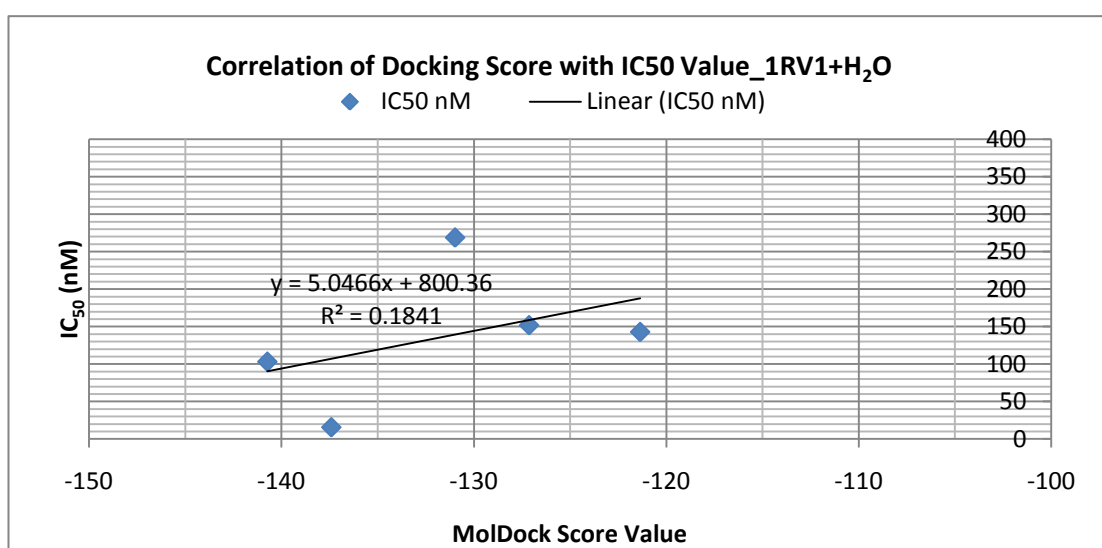
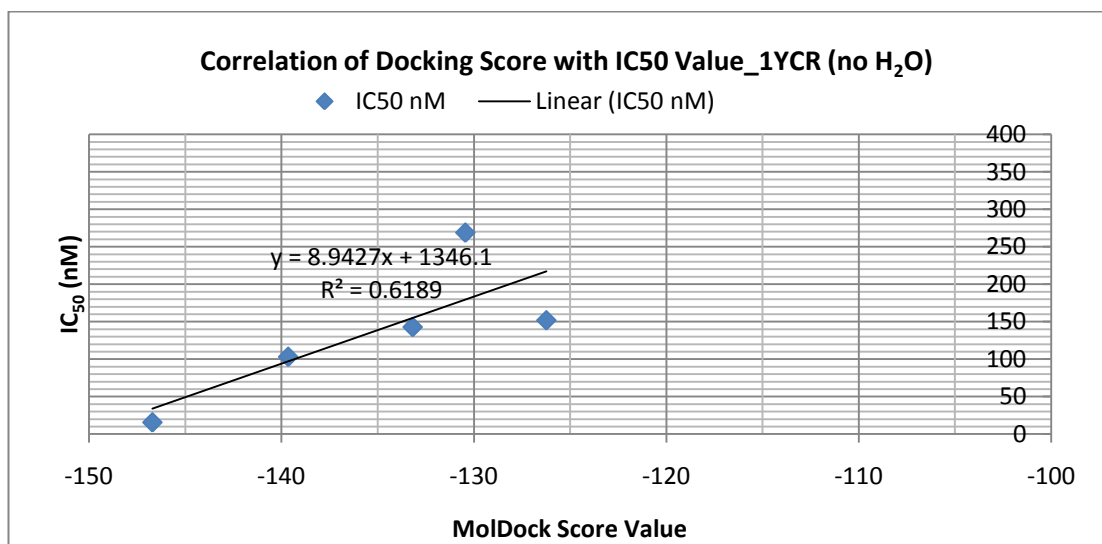
1T4F+H ₂ O	Nutlin-2		-124.839
1T4F+H ₂ O	NU8260		-108.139
1T4F+H ₂ O	NU8354		-108.192
1T4F+H ₂ O	NU8399		-116.788
1T4F+H ₂ O	NU8406		-126.327

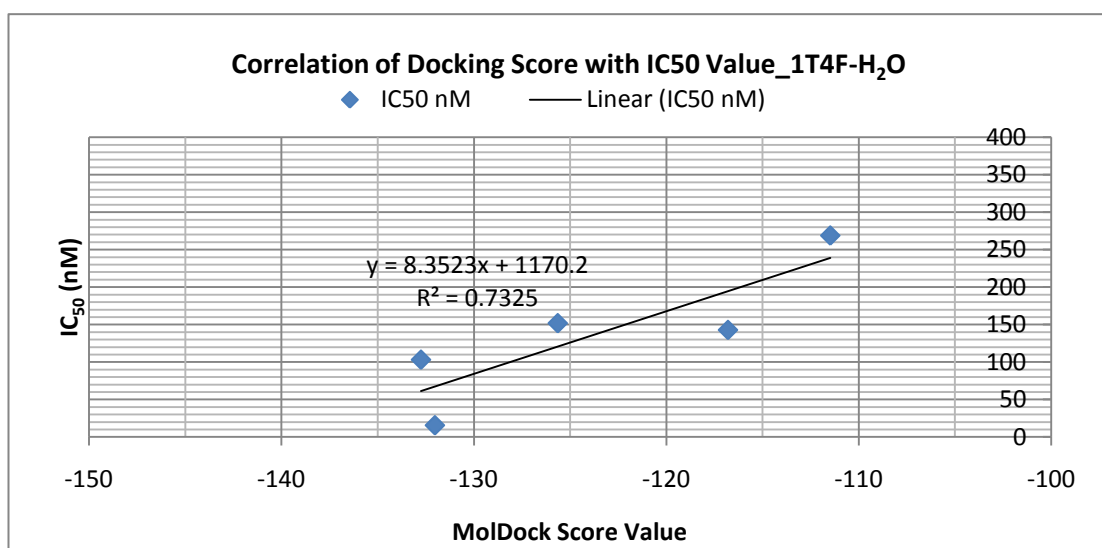
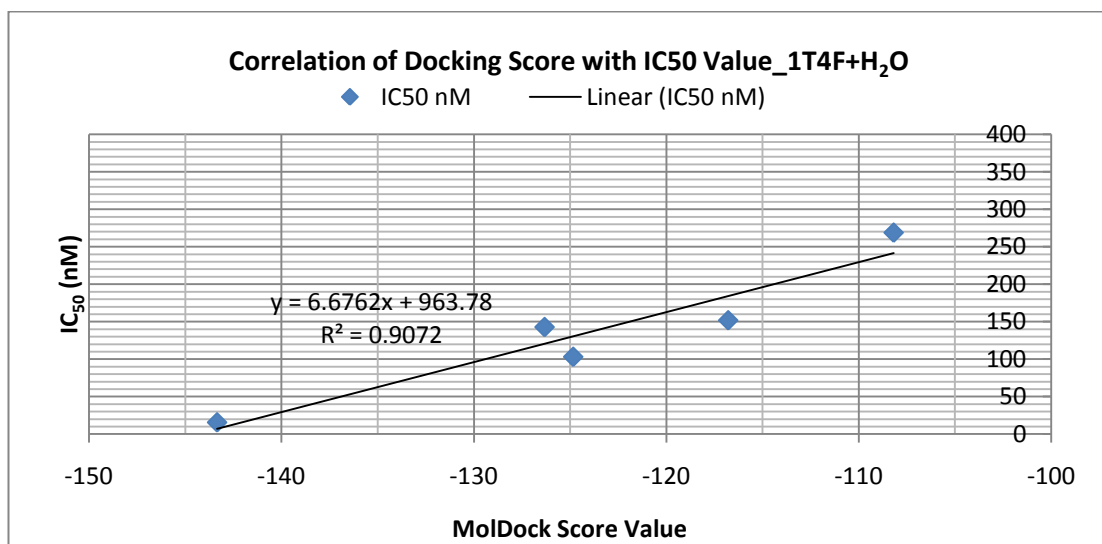
1T4F+H ₂ O	NCL-00016149		-143.341
1T4F-H ₂ O	Nutlin-2		-132.752
1T4F-H ₂ O	NU8260		-100.166
1T4F-H ₂ O	NU8354		-111.486
1T4F-H ₂ O	NU8399		-125.646

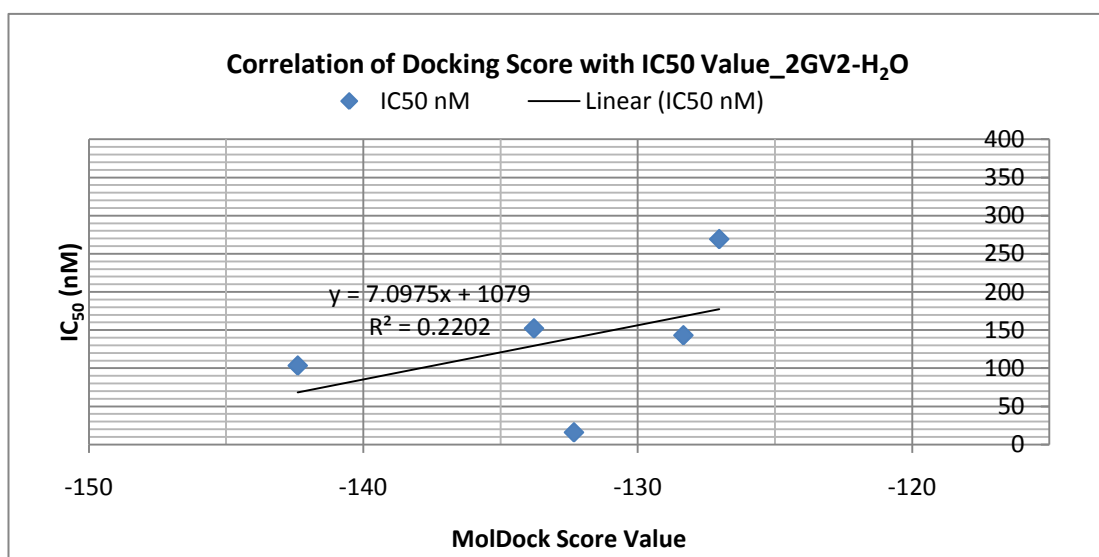
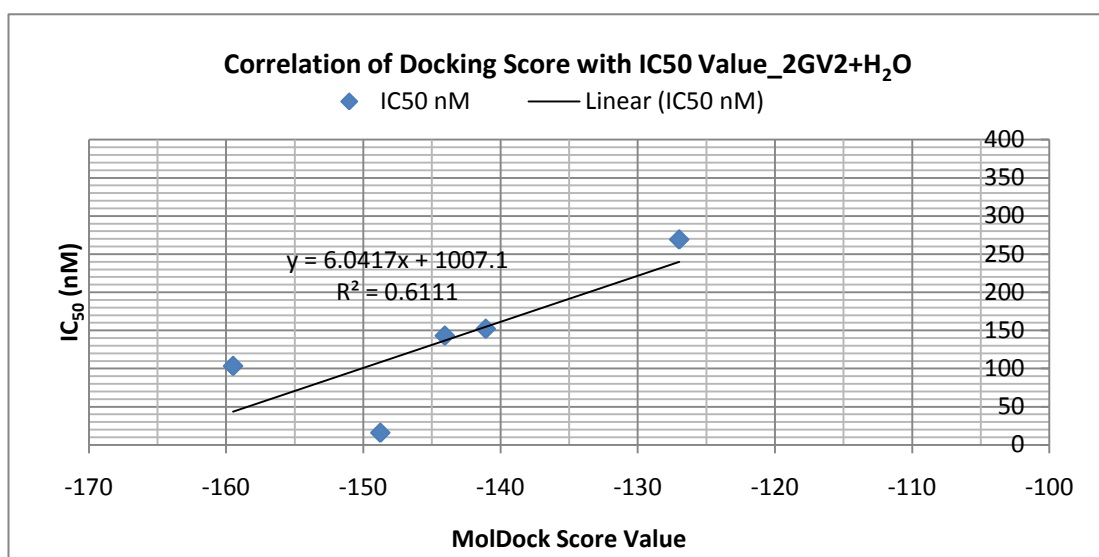
1T4F-H ₂ O	NU8406		-116.801
1T4F-H ₂ O	NCL-00016149		-132.029
2GV2+H ₂ O	Nutlin-2		-159.499
2GV2+H ₂ O	NU8260		-113.140
2GV2+H ₂ O	NU8354		-126.983

2GV2+H ₂ O	NU8399		-141.080
2GV2+H ₂ O	NU8406		-144.067
2GV2+H ₂ O	NCL-00016149		-148.766
2GV2-H ₂ O	Nutlin-2		-142.392
2GV2-H ₂ O	NU8260		-104.355

2GV2-H ₂ O	NU8354		-127.028
2GV2-H ₂ O	NU8399		-133.780
2GV2-H ₂ O	NU8406		-128.333
2GV2-H ₂ O	NCL-00016149		-132.323

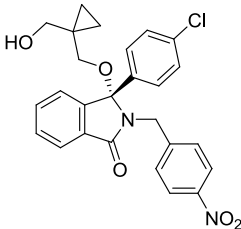
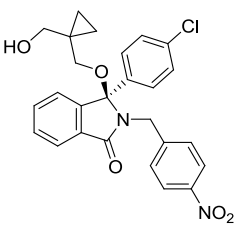
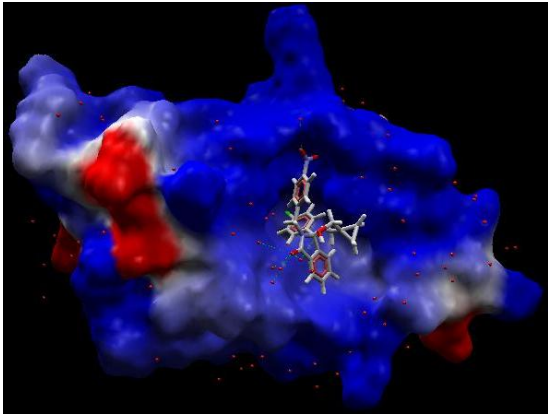
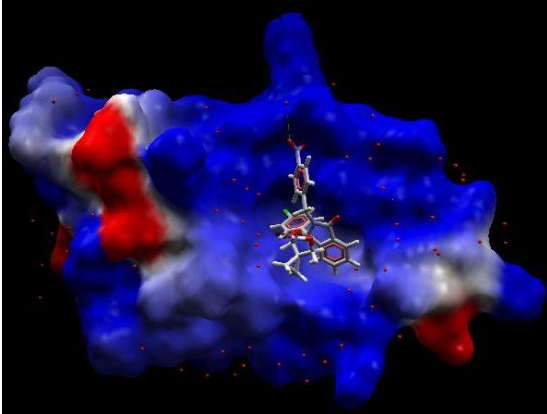


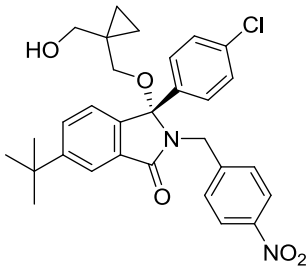
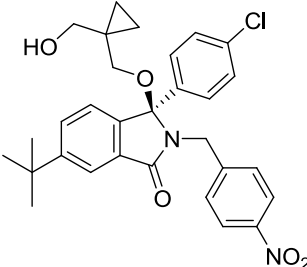
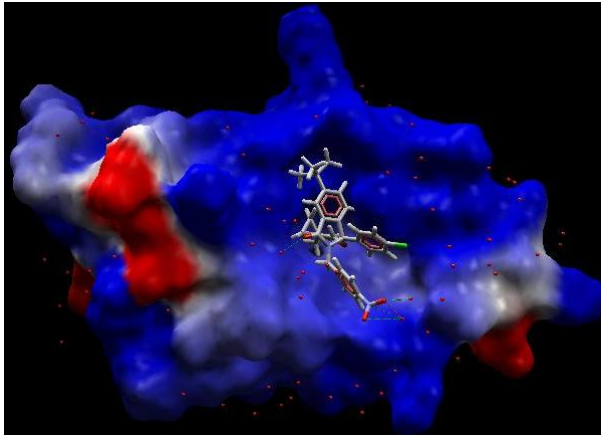
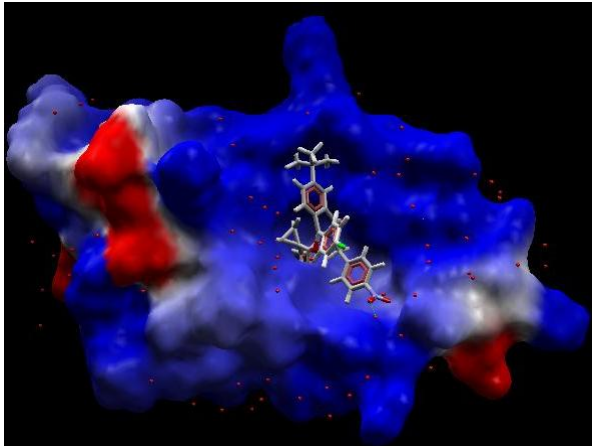


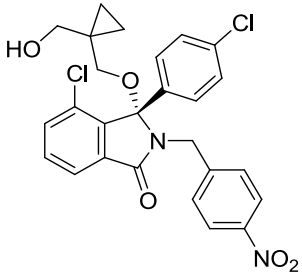
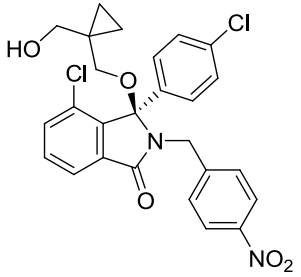
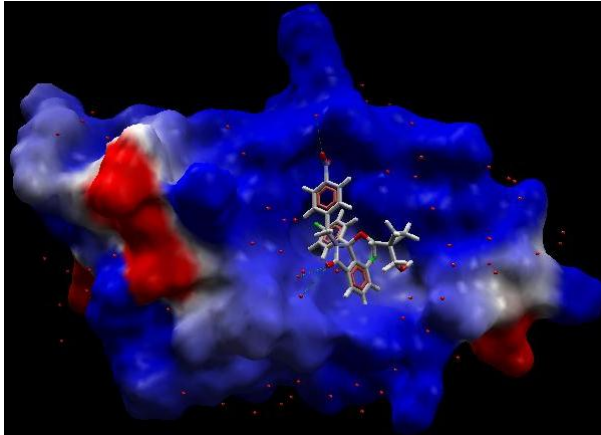
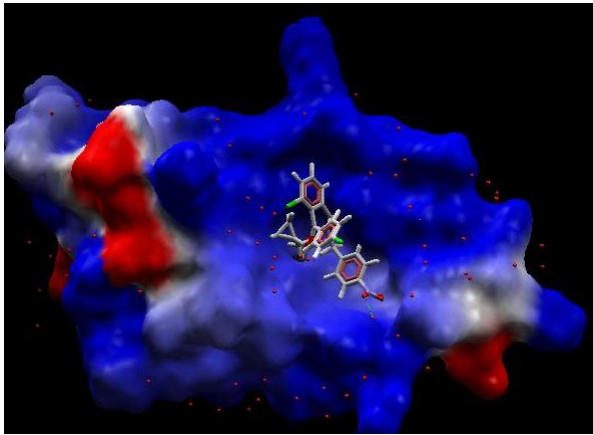


Appendix I Figure 3. Scatter Charts show the correlation of the Docking Scores with the IC₅₀ Values of isoindolin-1-one scaffold key compounds.

Appendix I Table 2. Virtual docking predicted binding modes and scores of isoindolin-1-one enantiomers binding with the 2GV2 MDM2 structure.

Compound Code	NU8354A	NU8354B
Compound Structure		
MolDock Score	-126.983	-111.752
Binding Mode		

Compound Code	NU8399A	NU8399B
Compound Structure	 <p>Chemical structure of NU8399A: A complex molecule featuring a central benzene ring with a tert-butyl group at the 4-position and a carbonyl group at the 1-position. The carbonyl carbon is bonded to a nitrogen atom, which is further bonded to a 4-nitrophenyl group. The carbonyl oxygen is bonded to a 4-chlorophenyl group. A hydroxymethyl group is attached to the 4-chlorophenyl ring via an ether linkage.</p>	 <p>Chemical structure of NU8399B: A complex molecule featuring a central benzene ring with a tert-butyl group at the 4-position and a carbonyl group at the 1-position. The carbonyl carbon is bonded to a nitrogen atom, which is further bonded to a 4-nitrophenyl group. The carbonyl oxygen is bonded to a 4-chlorophenyl group. A hydroxymethyl group is attached to the 4-chlorophenyl ring via an ether linkage.</p>
MolDock Score	-142.407	-122.177
Binding Mode	 <p>MolDock binding mode visualization for NU8399A: A 3D surface representation of the binding pocket, colored by electrostatic potential (blue for positive, red for negative, white for neutral). The molecule is shown as a stick model, with atoms colored by element (carbon in grey, oxygen in red, nitrogen in blue). The molecule is positioned within the binding pocket, showing its interaction with the surrounding environment.</p>	 <p>MolDock binding mode visualization for NU8399B: A 3D surface representation of the binding pocket, colored by electrostatic potential (blue for positive, red for negative, white for neutral). The molecule is shown as a stick model, with atoms colored by element (carbon in grey, oxygen in red, nitrogen in blue). The molecule is positioned within the binding pocket, showing its interaction with the surrounding environment.</p>

Compound Code	NU8406A	NU8406B
Compound Structure	 <p>Chemical structure of NU8406A, a complex molecule featuring a central benzimidazole core. It has a 4-chlorophenyl group, a 4-nitrophenyl group, and a 4-chlorophenyl group attached to the nitrogen. A cyclopropylmethyl group is also present, with a hydroxyl group and a chlorine atom on the cyclopropyl ring.</p>	 <p>Chemical structure of NU8406B, which is identical to NU8406A. It features a central benzimidazole core with a 4-chlorophenyl group, a 4-nitrophenyl group, and a 4-chlorophenyl group attached to the nitrogen. A cyclopropylmethyl group is also present, with a hydroxyl group and a chlorine atom on the cyclopropyl ring.</p>
MolDock Score	-144.067	-113.921
Binding Mode	 <p>MolDock binding mode visualization for NU8406A. The molecule is shown in a 3D representation, with the binding site surface colored in blue (hydrophobic) and red (hydrophilic). The molecule is docked into the binding site, showing its orientation and interactions with the surface.</p>	 <p>MolDock binding mode visualization for NU8406B. The molecule is shown in a 3D representation, with the binding site surface colored in blue (hydrophobic) and red (hydrophilic). The molecule is docked into the binding site, showing its orientation and interactions with the surface.</p>

Appendix II

Western Blotting Reagents and Equipment

1. Electrophoresis buffer (5 litres made with dH₂O)

151.5 g Tris
720.5 g Glycine
50.0 g SDS

2. Blotting buffer (10 litres with dH₂O)

30.3 g Tris
141.4 g Glycine
2 L Methanol

3. SDS loading buffer (10 ml)

2 ml Glycerol
2 ml 10% SDS
2.5 ml 4 x stacking gel buffer
3 ml dH₂O
0.5 ml β-mercaptoethanol (50 ml/ml)
0.25 mg Bromophenol blue (0.5 %)
Aliquot into 1 ml volume eppendorfs and store at -20 °C

4. TBS-Tween (10 x 5 litres made with dH₂O)

300 g Tris
450 g NaCl
25 ml Tween 20
Adjust pH to 7.5

5. SDS (ionic) lysis buffer (20 ml made with dH₂O)

2.5 ml 0.5 M Tris-EDTA pH 6.8
0.4 g SDS
2 ml glycerol

Before loading onto the gel, add 5 % 1:1 β-mercaptoethanol and bromophenol blue.

6. Transfer Buffer

25 mM Tris (Sigma)
192 ml glycerol (Sigma)
20 % v/v Methanol (BDH analytical grade)

7. Equipments for electrophoresis

Novex XL tank (Invitorgen)
gel cassette holder
Power pack

8. Equipments for Western blot

Biorad mini trans-blot holder tank
Transfer tank
Power pack
2 pieces of filter paper (the same size as the gel, Whatman 3MM Chr)
2 glass fibre pads for each gel
1 mini gel holder cassette

Cell Culture Reagents

1. Carnoy's fixative

1:3 ratio of glacial acetic acid (Sigma) and Ethanol (BDH analytical grade)

2. Phosphate Buffered Saline (PBS)

500 ml dH₂O
1 tablet phosphate buffer salt
Solution was sterilized by autoclaving.

3. 0.25 % trypsin-0.02 % EDTA solution

0.02 % EDTA (Sigma) : 0.2 g in 1000 ml PBS
0.25 % trypsin (Sigma, proteomics grade)
dilute stock 2.5 % stock trypsin 1:10 with 0.02 % EDTA solution

Sulphurhodamine B (SRB) colourimetric assay Reagents

- 1. 50 % w/v Trichloroacetic acid (TCA)**
1:1 ratio (w/v) of Trichloroacetic acid (Sigma) and double distilled water
- 2. 0.4 % w/v SRB solution (500 ml solution)**
2 mg Sulphurhodamine B (Sigma)
495 ml dH₂O
5 ml Acetic acid (Sigma)
- 3. 1 % v/v Acetic acid (5 litres solution)**
50 ml Acetic acid (Sigma)
4.95 litres dH₂O
- 4. 10 mM Tris-base (pH 10.5)**
605.7 mg Tris-base (Sigma)
500 ml ddH₂O

Polymerase chain reaction assay Reagents

- 1. 0.5 × Tris Borate EDTA (TBE)**
45.5 mM Tris (Sigma)
45.5 mM Boric Acid (BDH)
1 mM EDTA (Sigma)
- 2. Loading buffer**
25 mg bromophenol blue (Sigma)
4 g sucrose
Add dH₂O to 10 ml
Store at 4 °C to avoid mould growing in the sucrose.
- 3. 10 mg/ml Ethidium Bromide (EtBr)**
10 mg EtBr tablet (Sigma, for molecular biology, 10mg/tablet)
Add dH₂O to 10 ml, the shield from light.

Polymerase chain reaction assay procedure for sequence amplification

For Mutation Specific Primers: Touchdown 63 protocol

	Hotstart	14 cycles			26 cycles			End	
Temperature (°C)	94	94	70	72	94	63	72	72	4
Time (minutes)	10	20 sec	1*	1	20 sec	1	1	5	∞

*- This temperature is optimized based on the primer manufacturer recommend temperature and decreased by 0.5 °C each cycle.

Because of the touchdown PCR protocol was used, the detailed sequence amplification procedure was named 'TD' plus the stabilized cycle annealing temperature.

For Exons 4, 5, 6 and 9: Touchdown 55 standard protocol

	Hotstart	14 cycles			26 cycles			End	
Temperature (°C)	94	94	62	72	94	55	72	72	4
Time (minutes)	10	20 sec	1*	1	20 sec	1	1	5	∞

*-decreases by 0.5 °C each cycle

For Exons 7 and 8: Touchdown 60 standard protocol

	Hotstart	14 cycles			26 cycles			End	
Temperature (°C)	94	94	67	72	94	60	72	72	4
Time (minutes)	10	20 sec	1*	1	20 sec	1	1	5	∞

*-decreases by 0.5 °C each cycle